An evaluation of alternative methodologies for the numerical simulation of solute transport

John Peter Grimm

This thesis is submitted in partial fulfilment of the requirements for the Degree of Doctor of Philosophy

University of Sheffield

Department of Civil and Structural Engineering

July 2003

DECLARATION

I declare that the work in this thesis has been composed by myself and no portion of the work has been submitted in support of an application for another degree or qualification of this or any other university or other institute of learning. The work has been my own except where indicated and all quotations have been distinguished by quotation marks and the sources of information have been acknowledged.

ABSTRACT

The aim of this research was to establish whether it was feasible to use CFD software (in this case Fluent) to predict the transport of a solute through a pipe.

Two approaches were evaluated; the species transport model and the discrete phase (particle tracking) model. The species transport model predictions were found to be sensitive to spatial and temporal disretization scheme, and to the time step. However, the options that result in robust predictions for both the mean travel time and dispersion coefficient were identified. The particle tracking model was found to be computationally efficient and consistent predictions were attainable. However, the prediction of mean travel time was inaccurate, and consequently the model was eliminated from further investigation.

The second half of the thesis focuses on the validation of the species transport modelling approach, with a suitable laboratory data set being identified. The most appropriate modelling options to use in order to represent the experimental flow conditions were identified through consideration of the system being modelled, a grid refinement study and two parametric studies. With the exception of turbulent viscosity, good correlations between measured and simulated flow fields were observed for all of the turbulence model configurations.

The species transport model was utilised to predict solute transport at three flowrates. At each flow rate the measured dispersion was underpredicted. Reanalysis of the laboratory data, and consideration of certain model set-up options (including the turbulent Schmidt number and the upstream boundary conditions) tended to align the simulation results and the experimental data more closely.

With further development, the modelling approach developed within this thesis should enable dispersion coefficients to be identified for a wide range of urban drainage structures. Such predictions are required to enhance urban drainage quality models, and, ultimately, to improve sewer management and pollution control.

ACKNOWLEGEMENTS

I would like to express my deepest gratitude to Dr Virginia Stovin for giving me the opportunity to study for the PhD. I would also like to thank her for giving me the freedom to develop the project and for providing endless advice and encouragement.

Thanks are also due to all my colleagues in the water group. In particular I would like to thank Dr Joby Boxall for his help in identifying an appropriate project. Furthermore, I wish to express my appreciation to Richard Dutton and Klaus Richter for their technical advice and for their assistance on the golf course!

I would also like to thank Dr Ian Guymer for allowing me to use his data and for his constructive criticism.

I would like to acknowledge the financial assistance offered by Yorkshire Water. For obtaining the funding special thanks should go to Prof Saul.

I am also thankful to Dr Robert Harwood of FLUENT for his technical advice.

I would especially like to thank Dr Stella Kythreoti for her continual support during the project. If she had not been there to lift my spirits when I was down I would have never finished.

Finally, but most of all, I would like to thank my family for all their moral and financial support. If they had not encouraged me to study when I was younger I would not have had the opportunity to attend university.

TABLE OF CONTENTS

LIST OF FIGURES

LIST OF TABLES

NOTATION

A	Cross sectional area
c	Concentration
C	Cross sectional averaged concentration
c'	Instantaneous concentration
$\bar{c}$	Time averaged concentration
$C(x_i,t)$	Cross sectional average concentration at location x at time t
C_D	Drag coefficient
C_c	Cunningham correction
C_L	Time scale constant
D	Pipe diameter
D_p	Particle diameter
e_m	Molecular diffusion coefficient
F_D	Drag force on the particle
F_x	Additional forces acting on the particle
g	Gravitational acceleration
J_x	Total flux in the x direction
K	Longitudinal dispersion coefficient
K_i	Dispersion coefficient in the i_{th} direction
k	Generation of turbulent kinetic energy
M	Mass of the tracer in the control volume or mass of tracer introduced
$\dot{m}_{in}$	Mass of tracer entering the control volume
$\dot{m}_{out}$ t	Mass of tracer leaving the control volume
$\delta\dot{m}\|_x$	Net flux of tracer in the x direction
p	Instantaneous static pressure
P	Mean static pressure
Pr_t	Turbulent Prandtl number
r	Distance from the pipe wall
R	Pipe radius
Re	Reynolds number (based on U and D)
R_e	Relative Reynolds number
R^2	Normailised error squared
Sc_t	Turbulent Schmidt number
t	Time
$\bar{t}_i$	Time at the centroid of tracer profile i

T_L	Lagrangian time interval
u	Velocity in x direction
U	Time averaged velocity in the x direction or the cross sectional averaged velocity
$\overline{u}$	Time averaged velocity in the x direction
u'	Fluctuating velocity component in the x direction
u_p	Particle velocity in the x direction
U^*	Shear velocity
U^+	Non dimensional velocity
v	Velocity in y direction
V or $\overline{v}$	Time averaged velocity in the y direction
v'	Fluctuating velocity component in y direction
w	Velocity in z direction
W or $\overline{w}$	Time averaged velocity in z direction
w'	Fluctuating velocity component in z direction
y	Distance from the wall
y^+	Non dimensional distance from the wall
$\overline{u'v'}$	Reynolds shear stress
δ	Boundary layer thickness
$\sigma^2(x_i)$	Temporal variance of the tracer profile at location x
ε	Dissipation rate of turbulent kinetic energy
ε_i	Turbulent diffusion coefficient in the i_{th} direction
ε_m	Turbulent mass diffusivity
ε_t	Turbulent thermal diffusivity
ρ	Fluid density
ρ_p	Particle density
τ_{ij}	Reynolds stresses
τ_0	Wall shear stress
τ_e	Characteristic lifetime of the eddy
κ	Von Kármán's constant
γ	Time integration variable
υ	Kinematic viscosity
μ	Molecular or absolute viscosity
μ_t	Turbulent viscosity

ABREVIATIONS

ADE	Advection-Diffusion Equation
BOD	Biochemical Oxygen Demand
CFD	Computational Fluid Dynamics
CSOs	Combined Sewer Overflows
DHI	Danish Hydraulic Institute
DO	Dissolved Oxygen
DNS	Direct Numerical Simulation
DWF	Dry Weather Flow
HOTs	Higher Order Terms
LES	Large Eddy Simulation
PAH	Polycyclic Aromatic Hydrocarbons
RANS	Reynolds Averaged Navier Stokes
RNG	Renormaization Group
RSM	Reynolds Stress Model
UPM	Urban Pollution Management
USEPA	U.S. Environmental Protection Agency

1 Introduction

The sewerage system transports a wide variety of substances, many of which have a detrimental impact when spilled to the receiving waters. Field observations suggest that many of the polluting substances are transported as dissolved solutes, or as fine suspended material, with the dominant processes on their transport being advection and dispersion.

The quality aspect of sewer discharges has become an important issue in recent years due to the tightening of environmental constraints. Models that predict the transport of pollutants through the sewerage system are therefore being increasingly used. Some of the models transport the pollutants by advection alone, while others also account for the effects of dispersion. Appropriate values must be assigned when dispersion is accounted for, but at present there is only limited guidance for how to obtained them. Simplified assumptions are therefore often made. In some instances laboratory or field measurements are conducted, but these are expensive, time consuming and case specific. It is clear that a versatile approach for determining the dispersive effects of urban drainage structures would be of benefit.

Computational fluid dynamics (CFD) is increasingly being used in the water industry. It has a significant benefit over the other methods in that once a model has been validated it may be used to examine the impact of changes to the geometry or flow rate with comparative ease. CFD has been utilised to model the flow and particle movement through a variety of urban drainage structures including manholes, storage tanks, sewer grit traps and combined sewer overflows (CSOs). Although less well documented, CFD has also been used to model the transport of a solute.

Although there is evidence of the use of CFD in the water industry, the studies that have been undertaken have tended to lack convincing validation, particularly with respect to solute transport. In particular, most of these studies modelled the movement of the solute through relatively complex flows, with any discrepancies between the predicted and measured values being attributed to the complexity of the flow and to the simplifying assumptions that were required. The aim of this study is to determine whether CFD may be used to accurately predict the transport of a solute in a straightforward flow, specifically fully developed pipe flow.

1.1 Aims and Objectives

The aim of the research was to establish whether it was feasible to use commercial CFD software to predict the transport of a solute through a pipe.

The specific objectives for the research were as follows:

- Identify all feasible solute transport modelling approaches within the adopted CFD software.
- Undertake feasibility studies on all identified solute transport modelling approaches to assess their usability and robustness.
- Identify appropriate datasets and undertake validation studies for both the flow field and solute transport predictions.
- Define a methodology and appropriate modelling options to use for the prediction of solute transport through a pipe. Clearly, this objective assumes that one or more of the identified solute transport modelling approaches proves to provide an accurate and robust approach.

1.2 Structure of the thesis

In Chapter 2 a review of the relevant literature is presented. The characteristics of the pollutants that are of interest to the study and the impact they have on the environment when spilled to the watercourse are highlighted in Section 2.2. The advection diffusion equation (ADE) may be used to describe the transport of a solute, with a derivation of the equation presented in Section 2.3. In Section 2.4 the governing equations of fluid dynamics, which are the basis for all CFD code, are presented. Numerical techniques for solving these equations are outlined. In Section 2.4.8 a description of the two transport models that have been utilised to predict the transport of a solute tracer is presented, while details of the Fluent CFD software (Fluent, 1998) that was used during this study are presented in Section 2.4.9. Key studies against which the CFD predictions may be validated are highlighted in Section 2.3.4 and Section 2.5.2.

The feasibility studies that evaluated the species transport model and discrete phase model are presented in Chapters 3 and 4 respectively. Parametric studies that examined the impact of the modelling options on the predictions of solute transport formed a major component of each feasibility study. In Section 4.5 a recommendation is made regarding which of the two models to consider for further investigation.

The data set of Guymer and O'Brien (2000) was identified as appropriate for the validation of the dispersion predictions. The first part of the validation study determined the most appropriate modelling options to use in order to represent the experimental flow conditions.

This was achieved through consideration of the system being modelled, a grid refinement study and two parametric studies. The development of the flow field is reported in Chapter 5.

The species transport model was utilised to predict the transport of a solute at three flow rates. In Section 6.2 a comparison is made between the predictions and the measurements of dispersion. Although the predictions showed the same qualitative features there were significant quantitative differences. Consideration was therefore given to assessing both the accuracy of the measured data and the appropriateness of the modelling assumptions/simplifications that were made. These studies are reported in Section 6.4 to Section 6.7.

The overall conclusions of the study and suggestions for further work are made in Chapter 7

2 Literature review

2.1 Introduction

The engineering stimulus for this research was the need to model the transport of substances through the sewerage system. This is of importance because sewers transport a wide variety of substances, many of which have a detrimental impact when spilled to the receiving waters. Field observations suggest that many of these polluting substances are transported as dissolved solutes, or as fine suspended material. In both cases the dominant transport processes are advection and dispersion, and the effects of gravity (settlement) may be ignored. The characteristics of these pollutants are described in Section 2.2. The transport of these substances may be described by the advection-diffusion equation (ADE), which is derived in Section 2.3. The equation requires coefficients with which to characterise the mixing effects. To date these have been largely identified through laboratory or field measurements.

The specific focus of this study was to determine whether computational fluid dynamics (CFD) could be used to accurately model the transport of a solute, and therefore to identify the ADE coefficients. This is of relevance because CFD is now being used increasingly in the water industry. Section 2.4 describes the fundamental equations of fluid flow that are the basis for all CFD code, the three approaches to solving these equations, and approaches that are available for modelling turbulence. Details of the models that have been used to predict the transport of a solute are highlighted in Section 2.4.8, and in Section 2.4.9 a description is presented of the Fluent CFD software (Fluent, 1998) that was used during this study.

Highlighted in Section 2.4.10.3 are the studies that have used CFD to model the transport of solute tracer. Most of the studies modelled the movement of the tracer through relatively complex flows, with the discrepancies between the predicted and measured values being attributed to the complexity of the flow and to the simplifying assumptions that were required. This study, therefore, aimed to establish whether CFD could be used to accurately predict the transport of a tracer in a straightforward flow. To do this the most basic flow, fully developed flow in a straight pipe, was considered.

Section 2.3.4 and 2.5 highlight key studies against which the CFD model may be validated against

2.2 The characteristics of dissolved and suspended material in the sewerage system

2.2.1 Physical characteristics of suspended sediments

There have been a number of studies, both in the UK and aboard, which have investigated the physical, chemical and biological characteristics of sewer sediments. They have highlighted the spatial variability, both in terms of the position within the sewerage system and between different catchments. These studies have led to attempts to classify sewer sediments according to the source and/or location within the sewerage system (Crabtree, 1989; Ashley and Crabtree, 1992; Verbanck *et al.*, 1994).

Crabtree's (1989) classification did not include sediments that passed through the sewer without depositing, therefore missing out some of the sediments that are of interest to this study. However, Type C sediments were classified as fine grained sediments that were mobile and only deposited in low flow zones. These sediments could be described as moving in suspension under normal flow conditions. Type C sediments had a mean specific gravity of 1.17, with 45 % having a diameter less than 63 microns.

Verbanck *et al.* (1994) proposed a three category classification for combined sewer sediments based on the origin of the sediment. Butler *et al.* (1996) provides a comprehensive summary of studies that have been undertaken, both in the UK and world wide, to determine the physical properties of sewer sediments based on this classification. Using this summary it is possible to determine significant differences in sediment characteristics between regions (e.g. because of catchment slope) and countries (e.g. due to different practices, such as the use of gully pots in UK). Table 2.1 provides a summary of typical UK sewer sediment characteristics based on this classification system. The characteristics of Crabtree's Type C sediments lie somewhere between those of the sanitary and stormwater solids.

Type	Normal Transport mode	Concentration (mg/l)			Median particle size, (μm)			Specific gravity		
		Low	Medium	High	Low	Medium	High	Low	Medium	High
Sanitary solids	Suspension	100	350	500	10	40	60	1.01	1.4	1.6
Stormwater solids	Suspension	50	350	1000	20	60	100	1.1	2.0	2.5
Grit	Bedload	10	50	200	300	750	1000	2.3	2.6	2.7

Table 2.1 Summary of typical UK sewer sediment characteristics (after Butler *et al.*, 1996)

Andoh (1994) calculated the relationship between particle diameter and settling velocity for two values of specific gravity under quiescent conditions, with the comparison presented graphically in Figure 2.1. Figure 2.1 implies that sanitary solids, with the typical properties as indicated in

Table 2.1, would fall at a velocity of approximately one metre per hour. Given that combined sewers are designed to have a minimum flow velocity of between 0.75 and 1 m/s (Ackers *et al.*, 1996) the horizontal component acting on the particle from the flow is clearly much greater than the vertical component causing it to settle. It follows that the influence of gravity on the particle is negligible and it would not be inappropriate to model these particles as neutrally buoyant over short distances or time periods. It may be argued, therefore, that although this research primarily focused on dissolved material, its findings will also be relevant to sanitary solids as well as a proportion of the stormwater solids and Type C sediments.

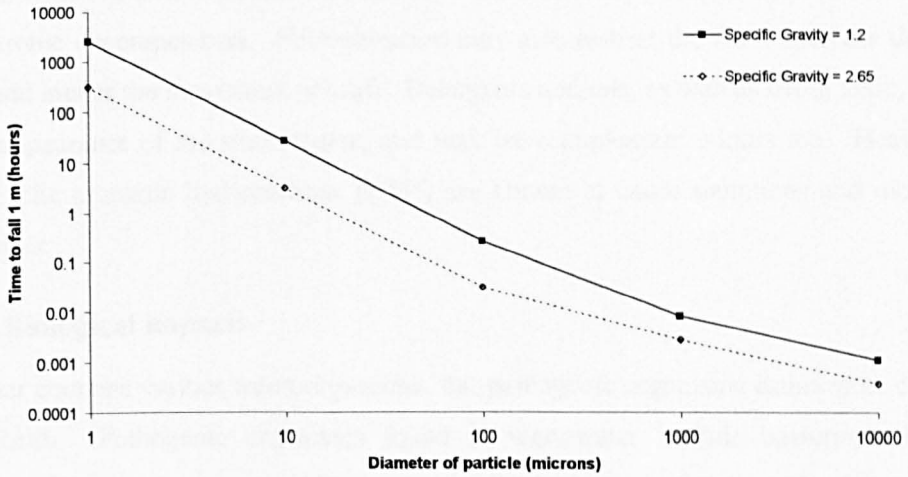

Figure 2.1 The variation in settling velocity with particle diameter and specific gravity (after Andoh, 1994)

2.2.2 Quality impacts of dissolved and suspended material

The flow within the sewerage network originates from domestic, commercial and industrial sources, and from surface runoff during times of rainfall. Although the type and quantity of contaminants found in wastewater will be site specific, it is possible to classify the potential impacts of dissolved and suspended material under the following three categories:

2.2.2.1 Physical impacts

Suspended solids may be kept in suspension by turbulence while in the sewerage system. Once discharged to the watercourse they may eventually settle and form silt or mud. This reduces the channel capacity, which may lead to flooding. It also prevents oxygen exchange to the bed, creating anaerobic conditions.

2.2.2.2 Chemical impacts

Chemically wastewater is composed of organic and inorganic compounds, as well as various gases. Organic matter, such as faeces and vegetable waste, provide nutrients for micro

organisms, creating a biochemical oxygen demand (BOD). When these substances are spilled to the watercourse the concentration of dissolved oxygen (DO) is depleted, which in severe situations can lead to the watercourse becoming devoid of oxygen downstream of an outflow. An oxygen deficiency can asphyxiate aquatic life, creating an imbalance in the ecosystem.

Inorganic compounds include metals, solvents and chemicals. Chemicals such as pesticides, insecticides and herbicides can accumulate in fish and shellfish, poisoning humans, animals and birds that eat them. Nutrients, such as nitrogen and phosphorus, can accelerate the growth of flora in the watercourse, termed eutrophication. This will increase the quantity of rotting vegetation, which in turn increases the release of methane and hydrogen sulphide into the flow from anaerobic decomposition. Eutrophication may also restrict the flow, increase the risk of flooding and hinder the movement of craft. Detergents and oils, as well as being toxic, float and spoil the appearance of the watercourse, and may have unpleasant odours too. Heavy metals and polycyclic aromatic hydrocarbons (PAH) are known to cause mutations and increase the risk of cancer.

2.2.2.3 Biological impacts

Wastewater contains various microorganisms, but pathogenic organisms cause most concern to human health. Pathogenic organisms found in wastewater include bacteria, viruses and protozoa, which can cause typhoid, dysentery, diarrhoea and cholera. Discharge of these pollutants is most significant when the watercourse is used for amenity purposes, or when fished, as marine life can also become contaminated.

2.3 Mixing theory

2.3.1 Mixing in turbulent flows

In order to investigate the transport of solutes and fine particles, it is necessary to understand the fundamental processes of solute mixing. When a tracer is introduced into a flow it is carried with the flow body by a process termed advection. As the tracer moves it will also spread out as a result of differential advection and diffusion, which together are termed dispersion. Differential advection, also sometimes called shear dispersion, is when the tracer is dispersed by variations in the flow velocity. Diffusion can be molecular, where the particles move by Brownian motion, or turbulent, which is the result of short term velocity fluctuations. The processes of differential advection and turbulent diffusion are of a similar order of magnitude, while molecular diffusion is considerably smaller.

Figure 2.2 shows a vertical velocity profile for a turbulent flow in a wide channel with a free surface. It also shows the vertical profile of a tracer being released from an instantaneous line source and at a point downstream. The downstream profile shows that the tracer travels more

slowly near the fixed boundary than at the free surface, creating a profile that is the result of differential advection. The tracer has also spread horizontally, which is primarily the result of turbulent diffusion.

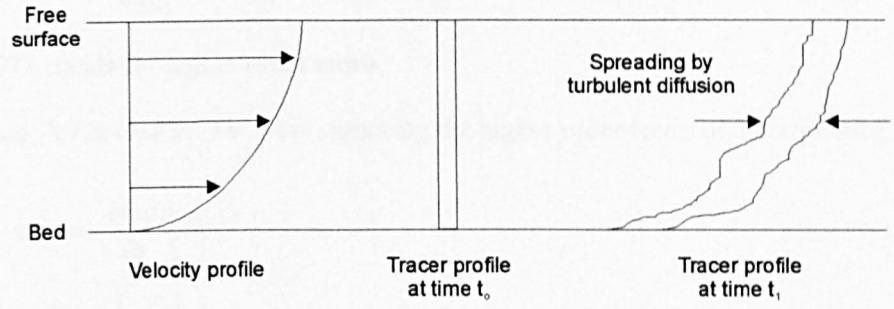

Figure 2.2 The effects of differential advection and turbulent diffusion (after Rutherford, 1994)

2.3.2 Derivation of the advection-diffusion equation

The advection-diffusion equation (ADE) may be used to describe the transport of a solute. The derivation of the equation is presented because it is of fundamental importance to the study. Consider the control volume shown in Figure 2.3. The change in the mass of the tracer with time is given by the mass conservation law:

$$\frac{\partial M}{\partial t} = \Sigma \dot{m}_{in} - \Sigma \dot{m}_{out} \qquad (2.1)$$

where M is the mass of the tracer in the control volume, and $\dot{m}_{in}$ and $\dot{m}_{out}$ are the mass of the tracer entering and leaving the control volume during time δt.

The mass fluxes in and out of the control volume are a function of the advective and diffusive transport, with the diffusive transport described using Fick's first law. The total flux in the x direction is given by (Fischer, 1979):

$$J_x = uc + \left(-e_m \frac{\partial c}{\partial x} \right) \qquad (2.2)$$

where J_x is the total flux in the x direction, u is the velocity in the x direction, c is the tracer concentration and e_m is the molecular diffusion coefficient.

The mass flow rate in the x direction is therefore (inflow defined as positive):

$$\dot{m}\big|_x = \left(uc - e_m \frac{\partial c}{\partial x} \right)\Big|_1 \delta y \delta z - \left(uc - e_m \frac{\partial c}{\partial x} \right)\Big|_2 \delta y \delta z \qquad (2.3)$$

where $\dot{m}\big|_x$ is the mass flow rate in the x direction and locations 1 and 2 are the inflow and outflow faces.

A Taylor series expansion is used to determine $\partial c/\partial x$ and uc at location 2. The general form of the equation is:

$$f(x) = f(x_0) + \left.\frac{\partial f}{\partial x}\right|_{x_0} \delta x + HOTs \qquad (2.4)$$

where *HOTs* stands for higher order terms

Substituting $\partial c/\partial x$ *and* uc *for* $f(x)$, ignoring the higher order terms and rearranging gives:

$$uc|_1 - uc|_2 = \left.\frac{\partial (uc)}{\partial x}\right|_1 \delta x \qquad (2.5)$$

$$-\left.\frac{\partial c}{\partial x}\right|_1 + \left.\frac{\partial c}{\partial x}\right|_2 = \left(\left.\frac{\partial^2 c}{\partial x^2}\right|_1\right)\delta x \qquad (2.6)$$

Thus, for the x direction

$$\dot{m}|_x = -\frac{\partial (uc)}{\partial x}\delta x \delta y \delta z + e_m \frac{\partial^2 c}{\partial x^2}\delta x \delta y \delta z \qquad (2.7)$$

Substituting this result and similar ones for the y and z directions into Equation 2.1, and knowing that the mass of the tracer within the control volume at time t is $M = c\delta x \delta y \delta z$, yields the advection-diffusion equation in three dimensions for a laminar flow.

$$\frac{\partial c}{\partial t} + u\frac{\partial c}{\partial x} + v\frac{\partial c}{\partial y} + w\frac{\partial c}{\partial z} = e_m\left(\frac{\partial^2 c}{\partial x^2} + \frac{\partial^2 c}{\partial y^2} + w\frac{\partial^2 c}{\partial z^2}\right) \qquad (2.8)$$

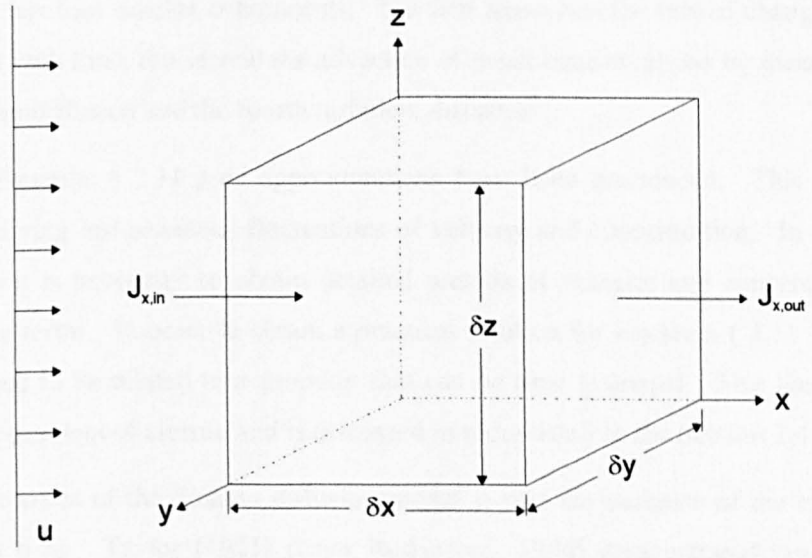

Figure 2.3 Schematic diagram of the control volume

For most practical problems the flow is turbulent and the processes of advection, molecular diffusion and turbulent diffusion need to be considered. Turbulence is characterised by random short term fluctuations about a mean value, which may be described mathematically as:

$$a = \bar{a} + a' \qquad (2.9)$$

where $\bar{a}$ denotes time averaged values and a' denotes instantaneous turbulent fluctuations of the variable.

The description of turbulence may be combined with equation (2.8) to yield the instantaneous turbulent advection-diffusion equation:

$$\frac{\partial(\bar{c}+c')}{\partial t} + (\bar{u}+u')\frac{\partial(\bar{c}+c')}{\partial x} + (\bar{v}+v')\frac{\partial(\bar{c}+c')}{\partial y} + (\bar{w}+w')\frac{\partial(\bar{c}+c')}{\partial z} = e_m\left(\frac{\partial^2(\bar{c}+c')}{\partial x^2} + \frac{\partial^2(\bar{c}+c')}{\partial y^2} + w\frac{\partial^2(\bar{c}+c')}{\partial z^2}\right) \qquad (2.10)$$

By taking ensemble means and considering continuity this may be simplified to (Rutherford, 1994):

$$\left(\frac{\partial \bar{c}}{\partial t}\right) + \left(\bar{u}\frac{\partial \bar{c}}{\partial x} + \bar{v}\frac{\partial \bar{c}}{\partial y} + \bar{w}\frac{\partial \bar{c}}{\partial z}\right) = e_m\left(\frac{\partial^2 \bar{c}}{\partial x^2} + \frac{\partial^2 \bar{c}}{\partial y^2} + \frac{\partial^2 \bar{c}}{\partial z^2}\right) - \left(\frac{\partial(u'c')}{\partial x} + \frac{\partial(v'c')}{\partial y} + \frac{\partial(w'c')}{\partial z}\right) \qquad (2.11)$$

The equation has four bracket components. The first represents the rate of change of the mean concentration with time, the second the advection of mean concentrations by mean velocity, the third molecular diffusion and the fourth turbulent diffusion.

In deriving Equation (2.11) no approximations have been introduced. This has led to an equation involving instantaneous fluctuations of velocity and concentration. In order to solve this equation it is necessary to obtain detailed records of velocity and concentration data to evaluate these terms. In order to obtain a practical solution for Equation (2.11) the turbulent properties need to be related to a property that can be time averaged. This has now become known as the problem of closure and is discussed in more detail in the Section 2.4.4.

One of the features of the Fickian diffusion model is that the variance of the cloud increases linearly with time. Taylor (1921) (from Rutherford, 1994) demonstrated that in stationary homogeneous turbulence the variance of a tracer cloud also increases linearly with time. This suggests that under these conditions the turbulent diffusion may be modelled using Fick's first law. By analogy the turbulent fluxes are:

$$u'c' = -\varepsilon_x \frac{\partial \bar{c}}{\partial x} \quad (2.12)$$

$$v'c' = -\varepsilon_y \frac{\partial \bar{c}}{\partial y} \quad (2.13)$$

$$w'c' = -\varepsilon_z \frac{\partial \bar{c}}{\partial z} \quad (2.14)$$

where ε_x, ε_y and ε_z are turbulent diffusion coefficients.

Equation (2.11) may now be converted to time averaged mean values:

$$\frac{\partial \bar{c}}{\partial t} + \bar{u}\frac{\partial \bar{c}}{\partial x} + \bar{v}\frac{\partial \bar{c}}{\partial y} + \bar{w}\frac{\partial \bar{c}}{\partial z} = (e_m + \varepsilon_x)\frac{\partial^2 \bar{c}}{\partial x^2} + (e_m + \varepsilon_y)\frac{\partial^2 \bar{c}}{\partial y^2} + (e_m + \varepsilon_z)\frac{\partial^2 \bar{c}}{\partial z^2} \quad (2.15)$$

Equation (2.15) contains two separate coefficients for molecular and turbulent diffusion. However, it is commonplace to combine the effects under one term, K. Equation (2.16) is the three dimensional form of the time averaged turbulent advection diffusion equation:

$$\frac{\partial \bar{c}}{\partial t} + \bar{u}\frac{\partial \bar{c}}{\partial x} + \bar{v}\frac{\partial \bar{c}}{\partial y} + \bar{w}\frac{\partial \bar{c}}{\partial z} = K_x \frac{\partial^2 \bar{c}}{\partial x^2} + K_y \frac{\partial^2 \bar{c}}{\partial y^2} + K_z \frac{\partial^2 \bar{c}}{\partial z^2} \quad (2.16)$$

The validity of the model has been questioned. Taylor himself did not go as far as to make the analogy between the molecular and turbulent diffusion coefficients. Fischer *et al.* (1979) argued that although the linear increase in the variance is an essential condition, it is not sufficient on its own to establish the validity of the Fickian model for turbulent diffusion. Despite these doubts, the ADE model has been utilised with great success to address a wide variety of mixing problems.

2.3.3 Longitudinal dispersion

Theoretical and experimental work by Taylor (1953, 1954) in pipe flow indicates that an equilibrium becomes established between the differential advection (which encourages longitudinal dispersion) and turbulent diffusion (which counteracts longitudinal dispersion) at a point downstream of the source. Upstream of this point the shape of the tracer will largely be determined by velocity differences, or differential advection, and this region is termed the advective zone. Beyond this point the region is called the equilibrium zone, where, assuming no change in the cross sectional area or discharge (Rutherford, 1994):

- The tracer will be cross sectionally mixed.
- The longitudinal variance of the tracer concentration will increase linearly with distance, Figure 2.4.
- Any skewness introduced by differential advection in the advective zone or by the initial tracer distribution begins to decay slowly and eventually the tracer distribution will become Gaussian, Figure 2.4.

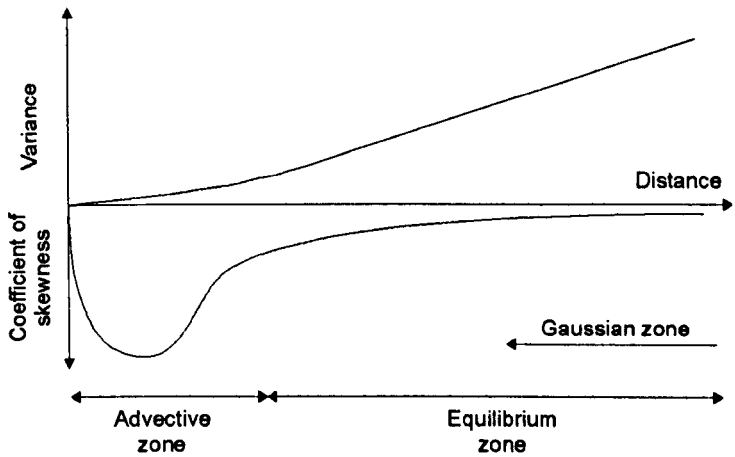

Figure 2.4 Fickian model predictions of how the variance and coefficient of skewness of a concentration profile change with time (after Rutherford, 1994)

When the tracer is in the equilibrium zone it is only possible to determine longitudinal mixing, which is the focus of this study. Longitudinal mixing, or longitudinal dispersion, is shown by a reduction in the peak concentration of a tracer and increasing spread with distance and time, Figure 2.5. Longitudinal dispersion is of importance only for intermittent discharges (short defined in relation to travel time and injection length) because inputs over long durations create constant concentrations downstream.

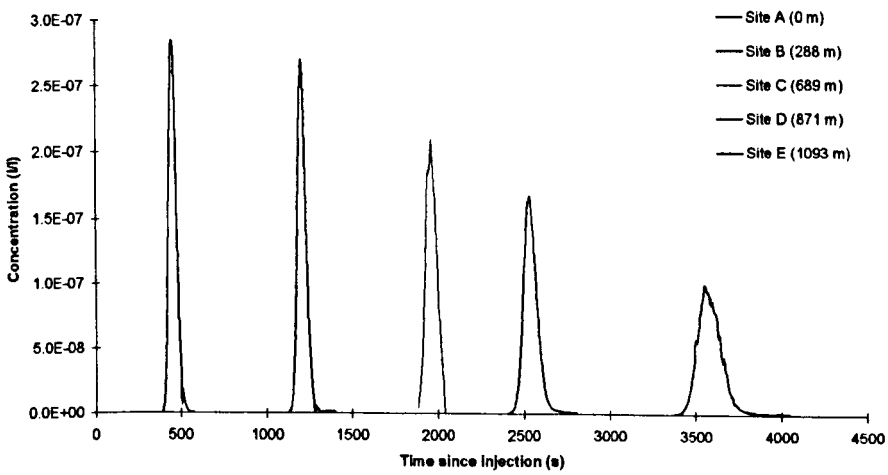

Figure 2.5 Illustration of longitudinal dispersion from a sewer trace (after Boxall *et al.*, 2002)

- The tracer will be cross sectionally mixed.
- The longitudinal variance of the tracer concentration will increase linearly with distance, Figure 2.4.
- Any skewness introduced by differential advection in the advective zone or by the initial tracer distribution begins to decay slowly and eventually the tracer distribution will become Gaussian, Figure 2.4.

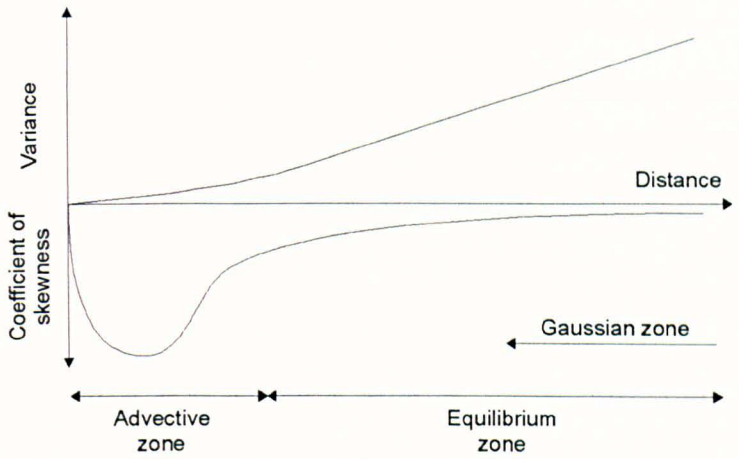

Figure 2.4 Fickian model predictions of how the variance and coefficient of skewness of a concentration profile change with time (after Rutherford, 1994)

When the tracer is in the equilibrium zone it is only possible to determine longitudinal mixing, which is the focus of this study. Longitudinal mixing, or longitudinal dispersion, is shown by a reduction in the peak concentration of a tracer and increasing spread with distance and time, Figure 2.5. Longitudinal dispersion is of importance only for intermittent discharges (short defined in relation to travel time and injection length) because inputs over long durations create constant concentrations downstream.

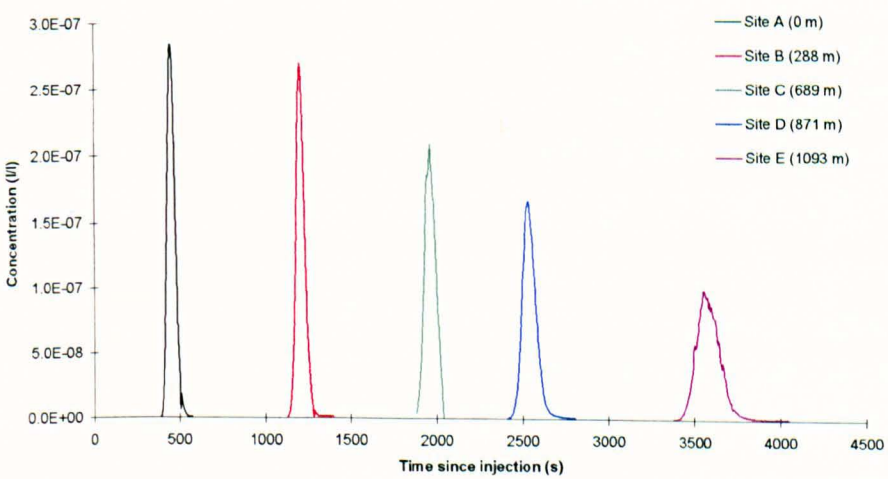

Figure 2.5 Illustration of longitudinal dispersion from a sewer trace (after Boxall *et al.*, 2002)

When the tracer is in the equilibrium zone it is well mixed over the cross section and the transverse concentration gradients become unimportant. Equation (2.16) is still valid under these conditions, however it may be simplified to:

$$\frac{\partial C}{\partial t} + U\frac{\partial C}{\partial x} = K\frac{\partial^2 C}{\partial x^2} \qquad (2.17)$$

where C is the average cross sectional tracer concentration, U is the average cross sectional velocity in the x direction and K is the longitudinal dispersion coefficient.

Equation (2.17) is sometime refereed to as the Fickian model of longitudinal dispersion. No attempt is made to model the variation in the tracer concentration over the cross section and the longitudinal dispersion coefficient includes all the processes that contribute to the tracer spreading longitudinally.

If U and K are constant then the solution to Equation (2.16) for an instantaneous point source (slug injection) is Equation (2.18). It may be used to predict a downstream spatial profile if the upstream profile was an instantaneous injection.

$$C(x,t) = \frac{M}{A\sqrt{4\pi Kt}}\exp\left(-\frac{(x-Ut)^2}{4Kt}\right) \qquad (2.18)$$

where $C(x,t)$ is the cross sectional average tracer concentration, M is the mass of tracer introduced at $x = 0$ and $t = 0$ and A is the cross sectional area.

2.3.3.1 Routing a temporal concentration profile

Equation (2.18) may be used to predict a spatial downstream profile from an instantaneous injection of tracer. However, for most practical situations measurements are made of temporal concentrations as a fixed position. Routing procedures are used to predict a temporal downstream profile from a measured temporal upstream profile. Routing is useful as it can verify velocity measurements and assumed values of the dispersion coefficient. Two alternative temporal routing procedures have been proposed (Rutherford, 1994), but further consideration is only given here to the frozen cloud routing method as it was used in this study.

The frozen cloud routing method relies on the frozen cloud assumption that no longitudinal dispersion occurs during the time taken for the tracer to pass a sampling site. In practice this assumption is incorrect because longitudinal dispersion continually occurs. However, the error is usually small and the approach is considered valid (Rutherford, 1994).

The frozen cloud routing method effectively splits the upstream profile into a series of elements of time Δt. To transport an upstream element downstream, the travel time (the advective

movement downstream) and dispersion coefficient (how much it spreads) are required. By the process of superposition each of the downstream elements is then amalgamated to give a downstream temporal concentration profile. The routing process is illustrated in Figure 2.6 and is described mathematically by Equations (2.19) and (2.20).

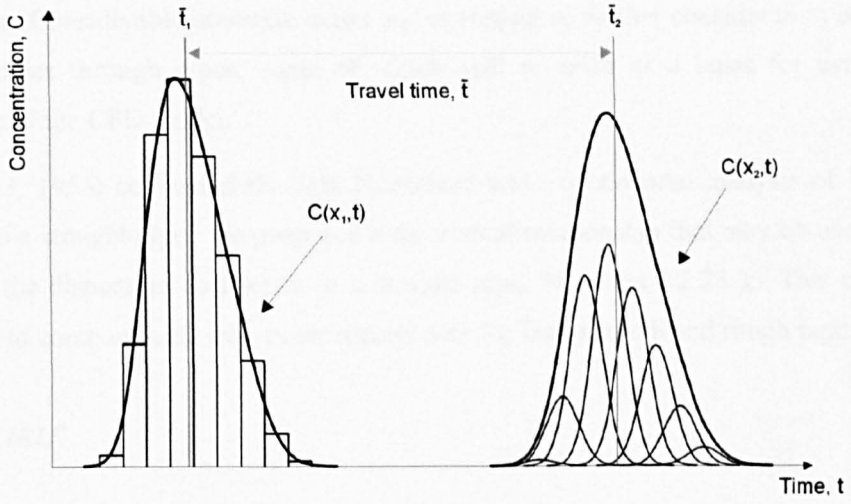

Figure 2.6 Example of the routing procedure

$$C(x_2,t) = \int_{\gamma=-\infty}^{\infty} \frac{C(x_1,t)U}{\sqrt{4\pi K(\bar{t}_2 - \bar{t}_1)}} \exp\left[-\frac{U^2(\bar{t}_2 - \bar{t}_1 - t + \gamma)^2}{4K(\bar{t}_2 - \bar{t}_1)}\right] d\gamma \qquad (2.19)$$

$$\bar{t}_i = \frac{\int_{t=-\infty}^{\infty} tC(x_i,t)\,dt}{\int_{t=-\infty}^{\infty} C(x_i,t)\,dt} \qquad (2.20)$$

where subscript one refers to the upstream profile and subscript two the downstream profile, $C(x_i,t)$ is the predicted temporal concentration, $\bar{t}_i$ represents the time at the centroid of the tracer profile and γ is the time integration variable.

When the tracer is in the equilibrium zone it is possible to calculate a value for the dispersion coefficient between an upstream and downstream temporal concentration profile from:

$$K = \frac{U^2}{2} \frac{\sigma^2(x_2) - \sigma^2(x_1)}{\bar{t}_2 - \bar{t}_1} \qquad (2.21)$$

where σ^2 represents the temporal variance of the profile:

$$\sigma^2(x_i) = \frac{\int_{t=-\infty}^{\infty} (t-\bar{t})^2 C(x_i,t)\,dt}{\int_{t=-\infty}^{\infty} C(x_i,t)\,dt} \qquad (2.22)$$

2.3.4 Previous tracer studies in pipes

Tracers, usually dyes or salts, have been used for many purposes including estimating discharge, monitoring contaminants, detecting leaks and measuring retention times. These studies have occurred in a wide range of flows, such as through ground water, rivers, sewers and power plants. Considerable literature exists on the subject so further consideration is only given to tracer studies through pipes, some of which will be used as a basis for evaluating the performance of the CFD model.

Taylor (1953, 1954) conducted the first theoretical and experimental analysis of longitudinal dispersion in a straight pipe. He proposed a theoretical relationship that may be used to predict a value for the dispersion coefficient in a straight pipe, Equation (2.23). This equation has been shown to compare well with experimental data for both smooth and rough pipes.

$$K = 10.1RU^* \tag{2.23}$$

where R is the pipe radius and U^* is the shear velocity given by Equation (2.24).

$$U^* = \sqrt{(\tau_0 / \rho)} \tag{2.24}$$

where τ_0 is the shear stress at the pipe wall and ρ is the density of the fluid.

Calabrese and Middleman (1979) measured the radial dispersion of three different chemicals in a straight vertical pipe filled with water. Droplets of n-Heptane (ρ = 695 kg/m^3), Butyl Benzoate (ρ = 1000 kg/m^3) and Carbon Tetrachloride (ρ = 1595 kg/m^3) were released from the axis of the pipe in a region where the flow was fully developed. The radial dispersion, $\overline{X^2}$, was measured using at least 300 counts made by photographic observations, Equation (2.25). The results demonstrated that the radial dispersion was governed by particle density, with the effects of particle diameter being almost insignificant.

$$\overline{X^2} = \sum_{i=1}^{n} \frac{X_i^2}{n} \tag{2.25}$$

where n is the number of observations and X_i is the radial displacement of the i^{th} droplet.

A laboratory study by Guymer and O'Brien (2000) determined a relationship between dispersion coefficient and discharge for a straight pipe of fixed diameter over a distance of 2.7 m. Using linear regression analysis the dispersion coefficient was found to equal 3.3 times the discharge (in litres per second), although the R^2 value for relationship was only 0.75. When

compared with the predictions made using Taylor's equation the measured dispersion was 10 % less. This study was used as a basis for validating the CFD model's dispersion predictions. A more detailed description of the laboratory facility, data analysis techniques and results, is presented in Chapter 6.

Boxall *et al.* (2002) presented the results of tracer tests that had been conducted in a sewer during both dry weather flow (DWF) and storm flow. The progress of the tracer was monitored at seven sites. The results highlighted the hydraulic differences, such as increased travel times and dispersion, under storm conditions. It was not possible to compare the results of this study with Taylor's equation as the dispersion coefficient would include the delayed storage effects of ancillary structures, such as manholes, and under DWF conditions the sewer was not flowing full.

2.3.5 Sewer quality modelling

There are a number of computer models which may be used to describe the hydraulics of sewer flow. The aim of these models is to provide insights into the performance of existing sewer networks and to plan sewer rehabilitation and new systems. In recent years the tightening of environmental constraints has meant that intermittent discharges have become an increasing concern. As a result most hydraulic models now offer procedures with which to model water quality parameters. The most widely used models are SWMM, MOUSE and Hydroworks, developed by the US Environmental Protection Agency (USEPA), The Danish Hydraulic Institute (DHI) and Wallingford Software respectively. These are complex models requiring detailed data from the catchment, although they have been shown to simulate the hydraulics of sewer flow accurately. Some more simplistic models have also been produced, such as SIMPOL, which is recommended in the UPM manual (FWR, 1998).

The HydroWorks and SWMM sewer flow quality models assume that all dissolved and suspended sediments are fully mixed, and that their transport is due to advection alone. The effects of dispersion are assumed to be negligible (Herath *et al.* 1999).

The MOUSETRAP model (DHI, 1994) includes an advection dispersion model, with a requirement on the user to input a dispersion coefficient of between 0 m^2/s and 5 m^2/s. Different values of the coefficient may be defined for different system components, although no guidance on suitable values is provided in the documentation.

2.4 Computational fluid dynamics (CFD)

2.4.1 Introduction

"Computational fluid dynamics or CFD is the analysis of systems involving fluid flow, heat transfer and associated phenomena such as chemical reactions by means of a computer based simulation" (Versteeg and Malalasekera, 1999). The use of CFD has grown rapidly over the last decade. This can be attributed to the increased computational power that is now widely available, thus allowing more complex problems to be investigated, and to improvements in the software, both in terms of the algorithms and the user interface. CFD is now used for research and industrial applications associated with a wide range of fluid flows.

CFD represents an additional tool for the investigation of fluid flow. For example, once a numerical model has been validated the effect on the flow pattern of a change in the geometry can be investigated without the need to construct additional physical models. A numerical model also calculates the fluid properties, such as velocity and pressure, at all points defined within the structure. It may not be possible to obtain such complete data sets from physical models or in-situ testing. This demonstrates that CFD may provide benefits in terms of information, time and cost.

Section 2.4.2 describes the fundamental equations of fluid flow that are the basis for all CFD codes, while Section 2.4.3 describes the three approaches that are used to solve these equations. The Reynolds averaging approach is described in more detail in Section 2.4.4, while later sections describe the turbulence models that are used to close these equations.

Additional models have been incorporated into CFD codes to solve transport equations for a chemical species and a discrete phase. These models may be used to track the movement of a tracer, thus providing greater insights into the process of dispersion. Sections 2.4.8 describes these models in more detail.

There are many software packages that have implemented various CFD codes. This study, however, used the Fluent software (Fluent, 1998). This software was chosen because expertise in the use of Fluent exists at the University of Sheffield and because it was already available on the University network. However, the choice of the software is only relevant in terms of the user interface and post processing, as the underlying equations are fundamentally the same. Details of the Fluent software are presented in Section 2.4.9.

CFD has been used increasingly to provide insights into flow patterns, pollutant mixing and sediment transport behaviour of urban drainage structures, such as combined sewer overflows (CSOs) and storage tanks. Details of some of the most relevant studies are presented in Section 2.4.10, including a more detailed discussion of studies that have used CFD to model pipe flow or to predict the movement of a solute.

2.4.2 The governing equations of fluid dynamics

The governing equations of fluid flow are based on the conservation laws of physics:

- Conservation of mass (The continuity equation)
- Conservation of momentum (Newton's second law)
- Conservation of energy (The first law of thermodynamics)

The mathematical statement of these physical principals is the basis for all fluid dynamics code. The equations may be used to describe the movement of fluid exactly, if the temporal and spatial change in the variables can be represented. They were developed by considering the physical principals of flow passing through an infinitesimally small fluid element. A full derivation of the governing equations is not presented, but may be found in many fluid dynamics text books, including Anderson (1995) and Versteeg and Malalasekera (1999). The equations presented here are for a three dimensional compressible flow. The equations relating to the conservation of energy are not included as temperature change is not of interest in this study.

The conservation of mass, or continuity equation, is based on the physical principal that the net mass out of the element is equal to the rate of decrease of mass inside the element:

$$\frac{\partial \rho}{\partial t} + \frac{\partial(\rho u)}{\partial x} + \frac{\partial(\rho v)}{\partial y} + \frac{\partial(\rho w)}{\partial z} = 0 \qquad (2.26)$$

where ρ is the fluid density, t is time and u, v and w are the instantaneous velocities in the x, y and z directions respectively.

The conservation of momentum, or Navier Stokes equations, were developed from Newton's second law of motion. The equations are based on the principal that the rate of increase of momentum on the element is equal to the sum of forces on the element. Equation (2.27) is the Navier Stokes equation for the x direction (with similar equations possible for the y and z directions).

$$\rho\frac{\partial u}{\partial t} + \rho u\frac{\partial u}{\partial x} + \rho v\frac{\partial u}{\partial y} + \rho w\frac{\partial u}{\partial z} = -\frac{\partial p}{\partial x} + \mu\left(\frac{\partial^2 u}{\partial x^2} + \frac{\partial^2 u}{\partial y^2} + \frac{\partial^2 u}{\partial z^2}\right) \qquad (2.27)$$

where p is the instantaneous static pressure, μ is the dynamic viscosity.

2.4.3 Numerical simulation of the governing equations

In low Reynolds number flows (laminar flows) the fluid layers slide smoothly past each other and the molecular viscosity dampens the randomly occurring small scale disturbances making the process predictable. A numerical simulation of the governing equations for this type of flow is relatively simple.

When the Reynolds number increases, the restraining effects of the viscosity are too weak to prevent such disturbances from amplifying, and the velocity and pressure change continuously with time and space. To capture all the length and time scales of turbulence is considerably more difficult. At present there are three numerical techniques to solve the governing equations in turbulent flow; direct numerical simulation (DNS), large eddy simulation (LES) and Reynolds averaging.

Direct numerical simulation (DNS)

The direct numerical simulation (DNS) technique solves the governing equations directly on a fine spatial and temporal grid to resolve all the scales of turbulent motion without assumptions. For high Reynolds number flows the amount of calculation effort required to capture all the temporal and spatial variation in the variables is extremely large and requires phenomenal computational resources. Speziale (1991) (from Versteeg and Malalasekera, 1999) estimated that a DNS of turbulent pipe flow at a Reynolds number of 5×10^5 would require a computer that is ten million times faster than the 1990 Cray supercomputer.

Large eddy simulation (LES)

In large eddy simulations (LES) the governing equations are spatially filtered to separate small scale turbulent motions from large scale turbulent motions. The large scale motions are solved directly using the governing equations, while turbulence models are used to describe the influence of the small scale motions upon the large scale ones. Although providing a saving over the DNS simulation approach, LESs still solve the time dependent governing equations for the large eddies and are therefore too computationally costly to consider for most practical situations.

Reynolds averaging

The Reynolds averaging approach differs from the DNS and LES approaches as no attempt is made to make the simulation time dependent. Instead the governing equations are time averaged by considering the variables as a function of a mean and fluctuating component, Figure 2.7. The time averaged governing equations are used to transport the mean flow quantities, with techniques to model the effects of turbulence. Commonly used turbulence

models include the simple mixing length model developed by Prandtl, the popular k-ε model and the more sophisticated Reynolds Stress Model (RSM).

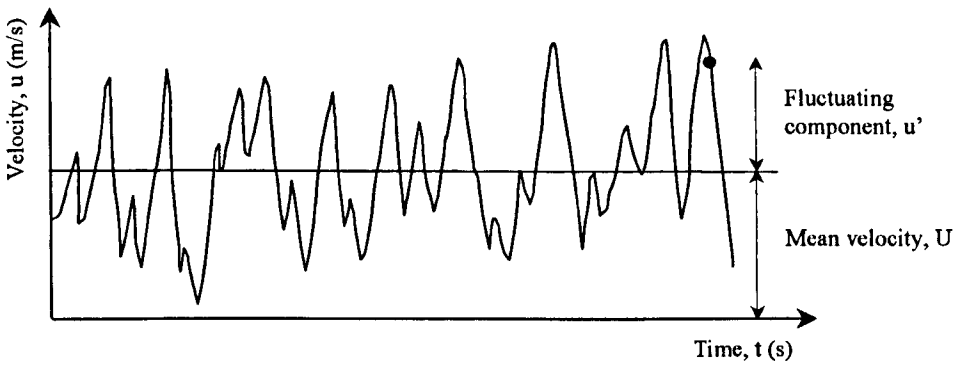

Figure 2.7 A typical point velocity measurement from a turbulent flow

As demonstrated, the DNS and LES of the governing equations for most turbulent flows with typical computational resources is unattainable in the near future. This research therefore used the Reynolds averaging approach.

2.4.4 Reynolds Averaged Navier Stokes Equations (RANS)

In Reynolds averaging the equations are decomposed into the mean (time averaged) and fluctuating components. Mathematically this can be described as:

$$\phi = \Phi + \phi' \qquad (2.28)$$

where Φ is the mean component and ϕ' is the instantaneous fluctuating component.

The time averaged Navier Stokes equation for the x direction is therefore:

$$\rho\frac{\partial U}{\partial t} + \rho U\frac{\partial U}{\partial x} + \rho V\frac{\partial U}{\partial y} + \rho W\frac{\partial U}{\partial z} + \rho\frac{\partial \overline{u'^2}}{\partial x} + \rho\frac{\partial \overline{u'v'}}{\partial y} + \rho\frac{\partial \overline{u'w'}}{\partial z} = -\frac{\partial P}{\partial x} + \mu\left(\frac{\partial^2 U}{\partial x^2} + \frac{\partial^2 U}{\partial y^2} + \frac{\partial^2 U}{\partial z^2}\right) \qquad (2.29)$$

(I) (II) (III)

The process of time averaging has introduced three new terms. These terms are usually placed on the right hand side of the equation to reflect their role as additional turbulent stresses on the mean velocity component U, Equation (2.30):

$$\rho\frac{\partial U}{\partial t} + \rho U\frac{\partial U}{\partial x} + \rho V\frac{\partial U}{\partial y} + \rho W\frac{\partial U}{\partial z} = -\frac{\partial P}{\partial x} + \mu\left(\frac{\partial^2 U}{\partial x^2} + \frac{\partial^2 U}{\partial y^2} + \frac{\partial^2 U}{\partial z^2}\right) - \rho\frac{\partial \overline{u'^2}}{\partial x} - \rho\frac{\partial \overline{u'v'}}{\partial y} - \rho\frac{\partial \overline{u'w'}}{\partial z} \qquad (2.30)$$

Repetition of this process yields the time averaged Navier Stokes equations for the y and z directions:

$$\rho\frac{\partial V}{\partial t}+\rho U\frac{\partial V}{\partial x}+\rho V\frac{\partial V}{\partial y}+\rho W\frac{\partial V}{\partial z}=-\frac{\partial P}{\partial y}+\mu\left(\frac{\partial^2 V}{\partial x^2}+\frac{\partial^2 V}{\partial y^2}+\frac{\partial^2 V}{\partial z^2}\right)-\rho\frac{\partial\overline{u'v'}}{\partial x}-\rho\frac{\partial\overline{v'^2}}{\partial y}-\rho\frac{\partial\overline{v'w'}}{\partial z} \qquad (2.31)$$

$$\rho\frac{\partial W}{\partial t}+\rho U\frac{\partial W}{\partial x}+\rho V\frac{\partial W}{\partial y}+\rho W\frac{\partial W}{\partial z}=-\frac{\partial P}{\partial z}+\mu\left(\frac{\partial^2 W}{\partial x^2}+\frac{\partial^2 W}{\partial y^2}+\frac{\partial^2 W}{\partial z^2}\right)-\rho\frac{\partial\overline{u'w'}}{\partial x}-\rho\frac{\partial\overline{v'w'}}{\partial y}-\rho\frac{\partial\overline{w'^2}}{\partial z} \qquad (2.32)$$

These equations can be written more compactly by using the Cartesian tensor notation:

$$\rho\frac{\partial U_i}{\partial t}+\rho U_j\frac{\partial U_i}{\partial x_j}=-\frac{\partial P}{\partial x_i}+\mu\frac{\partial^2 U_i}{\partial x_j\partial x_j}-\rho\frac{\partial\overline{u'_i u'_j}}{\partial x_j} \qquad (2.33)$$

Equations (2.30), (2.31), (2.32) and (2.33) are called the Reynolds averaged Navier Stokes equations (RANS). They have the same general form as the instantaneous Navier Stokes equations, with the velocities and other solution variables now representing time averaged values. The equations are also exact because no assumptions have been introduced in deriving them. The extra terms that have appeared represent the effects of turbulence and are called the Reynolds stresses.

The Reynolds stresses result from six additional stresses, three normal and three shear stresses:

Normal stresses: $\tau_{xx}=-\rho\overline{u'^2}\quad \tau_{yy}=-\rho\overline{v'^2}\quad \tau_{zz}=-\rho\overline{w'^2}$

Shear stresses: $\tau_{xy}=\tau_{yx}=-\rho\overline{u'v'}\quad \tau_{xz}=\tau_{zx}=-\rho\overline{u'w'}\quad \tau_{yz}=\tau_{zy}=-\rho\overline{v'w'}$

Physically the Reynolds stresses represent the transport of momentum due to turbulent motion. In turbulent flows the normal stresses are always non zero because they contain squared velocity fluctuations. The shear stresses are products of the different velocity components and if they were statistically independent fluctuations the time average of their product would be zero.

The instantaneous Navier Stokes equations form a closed set of four equations with four unknowns. When time averaging all information is lost concerning the instantaneous fluctuations and six additional unknowns (the Reynolds stresses) are obtained to make ten unknowns in total: one mean pressure, three mean velocity components and six Reynolds stresses. The disparity between the number of unknowns and equations makes a direct solution of any turbulent flow problem impossible. Finding additional equations or conditions to make up for this disparity is commonly called 'the problem of closure'. The purpose of a Reynolds

averaging turbulence model is to relate the six Reynolds stresses to the mean flow quantities in some plausible manner, thus providing closure.

2.4.4.1 The k-ε turbulence model

The k-ε model is one type of two equation turbulence model. Although there are many variations of the model, the majority are based on the Boussinesq hypothesis that assumes the Reynolds stresses are proportional to the mean velocity gradient. This hypothesis may be expressed as:

$$\tau_{ij} = -\rho\overline{u_i'u_j'} = \mu_t\left(\frac{\partial U_i}{\partial x_j} + \frac{\partial U_j}{\partial x_i}\right) \qquad (2.34)$$

Unlike the molecular viscosity, μ, the turbulent or eddy viscosity, μ_t, is not a property of the fluid. Its value will vary from point to point in the flow, being largely determined by the turbulence at the position in question. The use of the Boussinesq hypothesis is a step towards a turbulence model, but is not a turbulence model itself, as a way of calculating the turbulent viscosity is still required (Launder and Spalding, 1972).

The k-ε model is used to calculate the turbulent viscosity and hence determine values for the Reynolds stresses. The model uses two transport equations, one for the turbulent kinetic energy, k, and one for the rate of dissipation of turbulent kinetic energy, ε. Exact equations for k and ε can be derived from the Navier Stokes equation, but the ε equation contains complex correlations that are not understood, thus requiring drastic modelling assumptions to make the equation tractable (Rodi, 1993).

The standard k-ε model was published by Launder and Spalding (1972, 1974):

$$\frac{\partial k}{\partial t} + U_j\frac{\partial k}{\partial x_j} = \frac{1}{\rho}\frac{\partial}{\partial x_j}\left(\frac{\mu_t}{\sigma_k}\frac{\partial k}{\partial x_j}\right) + \frac{\mu_t}{\rho}\left(\frac{\partial U_i}{\partial x_j} + \frac{\partial U_j}{\partial x_i}\right)\frac{\partial U_i}{\partial x_j} - \varepsilon \qquad (2.35)$$

$$\frac{\partial \varepsilon}{\partial t} + U_j\frac{\partial \varepsilon}{\partial x_j} = \frac{1}{\rho}\frac{\partial}{\partial x_j}\left(\frac{\mu_t}{\sigma_\varepsilon}\frac{\partial \varepsilon}{\partial x_j}\right) + \frac{C_1\mu_t}{\rho}\frac{\varepsilon}{k}\left(\frac{\partial U_i}{\partial x_j} + \frac{\partial U_j}{\partial x_i}\right)\frac{\partial U_i}{\partial x_j} - C_2\frac{\varepsilon^2}{k} \qquad (2.36)$$

$$\mu_t = C_\mu\rho\frac{k^2}{\varepsilon} \qquad (2.37)$$

where k is the generation of turbulent kinetic energy, ε is the dissipation of turbulent energy and $\sigma_k, \sigma_\varepsilon, C_1, C_2$ and C_μ are model constants.

C_μ	C_1	C_2	σ_k	σ_ε
0.09	1.44	1.92	1.0	1.3

Table 2.2 Values of the constants used in Launder and Spalding's (1974) k-ε model

The equations for k and ε may be expressed in words as:

Rate of change of k or ε	+	Transport of k or ε by convection	=	Transport of k or ε by diffusion	+	Rate of production of k or ε	-	Rate of destruction of k or ε

The constants used in the model represent different types of turbulence. Values were obtained by conducting experiments during which the other types of turbulence were excluded and then optimising for generality (Launder and Spalding, 1972; Rodi, 1993). An example of this is grid turbulence, where diffusion and production terms are zero, so C_2 is the only constant left. The standard values have been used to successfully replicate a number of real fluid flow problems in both two and three dimensions (Launder and Spalding, 1974; Abbot and Basco, 1989; Rodi, 1993; Versteeg and Malalasekera, 1999). The constants are not universal and under certain conditions they require calibration, with the most documented case being an axisymmetric jet (Launder and Spalding, 1974; Rodi, 1993).

The standard k-ε model is the most widely used and validated turbulence model. It has been used successfully with the standard constants for a variety of flow conditions including thin shear layer flows, pipe flows, recirculating flows and confined flows (Launder and Spalding, 1974; Rodi, 1993; Versteeg and Malalasekera, 1999). However, the model has been shown to perform less well in unconfined flows, some swirling flows and flows with rapid strains, such as highly curved boundary layers (Rodi, 1993; Versteeg and Malalasekera, 1999).

Further turbulence models have been proposed as the limitations of the standard k-ε model have become apparent, including the RNG and Realizable models. The RNG k-ε turbulence model was derived from the instantaneous Navier Stokes equations using a mathematical technique called renormalization group (RNG) methods. The model has additional terms and functions in the transport equations for k and ε, and different constants from the standard k-ε model. At low Reynolds numbers a differential equation is used to calculate the turbulent viscosity, which allows the model to better represent low Reynolds number and near wall flows. A more comprehensive description of the RNG turbulence model may be found in Yakhot and Orszag (1986). The model has been shown to perform better than the standard k-ε model for rapidly strained and swirling flows and can improve the modelling of low Reynolds number flows (Fluent, 1998).

The Realizable k-ε turbulence model proposed by Shih *et al.* (1995) differs from the standard k-ε model in that it has different equations for the turbulent viscosity and ε. The Realizable model must satisfy certain mathematical constraints on the Reynolds stresses, consistent with the physics of turbulent flow. The model has been shown to accurately predict the spreading rate of both planar and round jets, and is also likely to have superior performance compared with the standard k-ε model for flow involving rotation, separation and spreading (Fluent,

1998). However, as the model is relatively new the amount of validation data is comparatively small.

The underlying assumption of all the k-ε models is that the turbulent viscosity is isotropic, that is the ratio between the Reynolds stresses and the mean rate of deformation is the same in all directions. This assumption does not affect the calculations in certain instances, such as simple thin shear layer flows, because only the shear stress is important. However, in certain flow situations the assumption of an isotropic eddy viscosity is too crude. For example, it does not produce the turbulence driven secondary motions in square ducts that have been observed in experiments (Rodi, 1993).

2.4.4.2 The Reynolds stress turbulence model

The Reynolds stress turbulence model (RSM) was developed because the Bousinesq hypothesis has been shown to perform badly for complex strain fields, even if the kinetic energy was computed accurately. The RSM model does not use the Bousinesq hypothesis, but instead closes the RANS equations by solving transport equations for each of the Reynolds stresses, plus ε for the dissipation rate. In three dimensions this means solving seven partial differential equations compared to two for the k-ε model.

The exact form of the Reynolds stress transport equations may be derived by taking moments of the exact Navier Stokes equation and Reynolds averaging. There are a number of different forms of the RSM model. However, the model proposed by Launder *et al.* (1975) is the most popular. The equations used in this model are not reproduced here due to their complexity, but may be found in Launder *et al.* (1975) and Rodi (1993). The Reynolds stresses cannot be solved directly and extra models are required for the diffusion, dispersion rate and pressure strain correlation terms. Numerical constants are required to make the equations tractable and these were developed in the same manner as those for the k-ε model.

Rodi (1993) describes how the model has been successfully applied to homogeneous flows, two and three dimensional duct flows and wakes. In particular turbulence driven secondary flows and the effects of strain caused by wall curvature, which cannot be described with two equation models, are well predicted. However, the RSM model may not perform significantly better than the k-ε models for free surface flows, and flows with swirls. As with the k-ε model this can be attributed partly to the closure assumptions, particularly the pressure strain and dissipation rate terms (Rodi, 1993).

The RSM model might not always yield results that are clearly superior to the k-ε models in all cases of flows to warrant the additional computational expense of solving the extra transport equations. The model is also not as well validated as the standard k-ε model, partly due to the

computational cost. However, the RSM model can account for the directional effects of the Reynolds stresses, therefore providing greater potential to accurately predict complex flows.

2.4.5 Discretization

It is not possible for computers to directly solve the governing equations so they are transformed into a numerical analogue of the equation through a process called numerical discretization. Three major numerical discretization schemes exist: the finite difference, finite element and finite volume methods. The main difference between the methods is related to the way in which the simulation is coded, with no significant differences in the results. Details regarding these schemes can be found in many CFD texts including Abbot and Basco (1989), Anderson (1995) and Versteeg and Malalasekera (1999), but further consideration is only given to the finite volume approach as it was used in this study.

The finite volume approach consists of the following steps:

- Division of the domain into discrete control volumes using a computational grid.
- Integration of the governing equations over all the control volumes to construct algebraic equations for the discrete dependent variables such as velocity, temperature and pressure.
- Solution of the algebraic equations by an iterative method.

In each of the cells the fluid properties are stored at the cell centre. However, face values are required for the convection terms and must be interpolated from the cell centred values. This is accomplished through an upwind scheme. Upwinding means that the face value is derived from quantities in the cell upstream, or upwind, relative to the direction of normal flow velocity. Several upwind schemes exist, including first and second order upwind, power law and QUICK. The first order upwind scheme is the most basic of the discretisation schemes as it assumes the face values is identical to the cell centred value. The second order upwind scheme calculates each face value from a Taylor series expansion of the cell centred solution about the cell centriod. The power law scheme interpolates face values from the cell centre using the solution to a one dimensional convection diffusion equation. The QUICK scheme is based on a weighted average of second order upwind and central interpolations of the variable.

When the flow is aligned with the grid the first order scheme is generally acceptable and will give quick convergence. However, when the flow is not aligned the scheme will increase numerical diffusion. Therefore, for complex flows, or flows which do not use structured meshes the use of second order is generally advised (Fluent, 1998). Under certain conditions, such as rotating or swirling flows, the QUICK scheme has been shown to be an improvement over the second order upwind scheme. Versteeg and Malalasekera (1999) provide an example

which shows that the QUICK scheme performs better than the upwind schemes for two dimensional convection diffusion problems. However, there may be stability problems as the coefficient can become negative under certain conditions. There does not appear to be a general consensus of opinion regarding the power law scheme. The Fluent 5 User's Guide (Fluent, 1998) suggests the scheme will typically give the same results as a first order scheme, whereas Shaw (1992) and Versteeg and Malalasekera (1999) suggest that there will be an improvement.

When a segregated solver is used the Navier Stokes and continuity equations are solved sequentially. As most of the terms in the Navier Stokes equations are functions of the velocity components these equations are used to create solutions for the velocity components. However the continuity equation does not contain terms for the fluid pressure. To proceed, the continuity equation is modified to relate pressure to velocity by a process which is commonly referred to as pressure-velocity coupling. There are a number of pressure velocity coupling algorithms, but most are based on the SIMPLE algorithm proposed by Patankar and Spalding (1972). The SIMPLE algorithm uses a relationship between velocity and pressure to enforce mass conservation and obtain a pressure field. A number of variants have been proposed as the limitations of the SIMPLE algorithm have become apparent, including the SIMPLEC, SIMPLER and PISO algorithms.

The SIMPLE algorithm is relatively straightforward and has been used successfully in many types of flows. The SIMPLEC and SIMPLER algorithms require a little more computational time per iteration, but can dramatically reduce the overall time for convergence. However, these algorithms do not provide more accurate results, so if convergence is not limited by the pressure velocity coupling they provide no benefit. For steady state problems the PISO algorithm does not provide any significant benefit over the other algorithms, but is recommended for transient flows (Fluent, 1998).

2.4.6 Meshing

The meshing of a geometry may be considered to be the discretisation of the space in which the flow takes place. When meshing a surface or volume consideration must be given to the requirements of the CFD solver. Some solvers require structured meshes which use *i, j, k* indexing to locate neighbouring cells. More recent solvers are unstructured, thus allowing the use of hexahedral, tetrahedral, pyramid and wedge shaped cells. Hybrid meshes that contain combinations of the above shapes are also possible. Unstructured meshes may be useful as they allow a great deal of flexibility. However, they can increase numerical dispersion.

The shape of the cells has a significant impact on the accuracy of the numerical solution. Skewness is defined as the difference between the cell's shape and the shape of an equilateral cell of equivalent volume. If the cells are highly skewed the accuracy and stability of the

simulation will be reduced. The aspect ratio is a measure of how the cell is stretched. To prevent inaccurate results an aspect ratio of less than 5 to 1 is desirable (Fluent, 1998).

It is usual for a CFD simulation to contain a wide variety of flow features. To make an accurate prediction each one of these will need to be modelled. Extra cells will be required in regions where gradients are large and nonlinear to allow the numerical methods to accurately predict the change. In general the larger the number of cells the better the solution accuracy, however, the finer the mesh the longer the calculation time. For most flows a point will be reached when adding extra cells provides no significant change in the simulation results. This is often referred to as a grid independent solution. A grid independent solution is desirable as it represents the most accurate prediction possible.

2.4.7 Near wall modelling

There are two approaches to modelling the flow close to a wall. In the first approach, the turbulence models do not model the near wall region, instead semi empirical wall functions are used to bridge the gap between the wall and the fully turbulent region. In the second approach the turbulence models are modified to enable the viscous sublayer and buffer layer to be resolved. The difference between the two approaches is shown graphically in Figure 2.8.

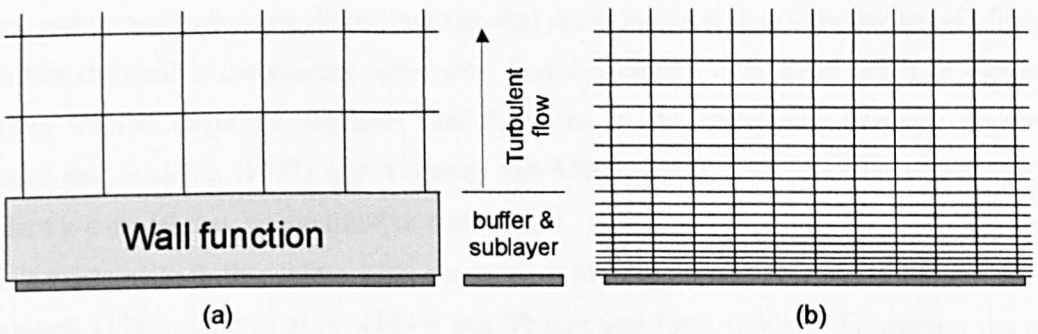

Figure 2.8 Comparison between the near wall modelling techniques. (a) wall functions approach, (b) near wall approach (after Fluent, 1998)

There are two benefits to the use of wall functions. Firstly, as the number of cells used is much fewer they provide a considerable saving of computational resources. Secondly, they allow extra empirical information to be considered, such as a wall roughness. A detailed description of the methodology and equations of the most popular wall function model can be found in Launder and Spalding (1974).

The y^+ value is the non dimensional distance from the wall, Equation (2.38). If wall functions are used it is general desirably for the cell adjacent to a fixed boundary to have a y^+ value of around 30 (Fluent, 1998). However, Tannehill *et al.* (1997) suggests that they are valid in the range $30 < y^+ < 200$, while Versteeg and Malalasekera (1999) claim they may be valid until the

y^+ value exceeds 500. The extent of the near wall region is discussed in more detail in Section 2.5.

$$y^+ = \frac{U^* y}{\upsilon} \qquad (2.38)$$

where y is the distance from the wall and υ is the kinematic viscosity.

The assumptions made with wall functions are that the velocity profile is logarithmic and the turbulence parameters are constant or vary linearly. These assumptions are often adequate for simple flows in pipes and channels, and for high Reynolds number flows. However, they become less reliable when the flow field is different from the idealised conditions assumed in their derivation.

A recent extension of the standard wall function approach is the development of non equilibrium wall functions. Further consideration to the approach is not given here, but may be obtained from Kim and Chohdury (1995).

The universality of wall functions is in doubt, particularly for complex flows. This has led to the development of near wall, or low Reynolds number turbulence models. In these models the transport equations are integrated to the wall allowing the rapid changes in velocity, turbulent kinetic energy and turbulence dissipation rate that occur in this region to be predicted. In order to do this the models incorporate either wall damping effects, or a direct effect of molecular viscosity on the empirical constants and functions in the turbulence transport equations. Launder and Spalding (1974) and Versteeg and Malalasekera (1999) demonstrated how the standard k-ε model may be modified in this manner. A wide range of low Reynolds turbulence models exists, with further information available in Martinuzzi and Pollard (1989), Pollard and Martinuzzi (1989), Hrenya *et al.* (1995) and Thakre and Joshi (2001). To capture the rapid changes that are happening a high grid density is required close to the wall. The general guidance is that the first cell adjacent to the wall should be within the viscous sublayer and that there should be a minimum of ten cells in the near wall region.

The number of mesh points required to resolve all the details in a turbulent boundary layer would normally be prohibitively large, so wall functions are most commonly used. However, wall functions have been shown to be unable to predict rotating or swirling flows, or flows with strong pressure gradients.

2.4.8 Transport models

The transport of a solute has traditionally been modelled using a finite difference or finite volume form of the advection-diffusion equation. Recently particle tracking methods have also been used which are based on the idea that the tracer can be represented by a large number of

discrete particles that are each subjected to advection and dispersion. The underlying principals of each method are presented below.

2.4.8.1 Advection-diffusion equation (ADE) transport model

The transport of a solute may be modelled by the advection-diffusion equation described in Section 2.3.2:

$$\frac{\partial \bar{c}}{\partial t} + \bar{u}\frac{\partial \bar{c}}{\partial x} + \bar{v}\frac{\partial \bar{c}}{\partial y} + \bar{w}\frac{\partial \bar{c}}{\partial z} = (e_m + \varepsilon_x)\frac{\partial^2 \bar{c}}{\partial x^2} + (e_m + \varepsilon_y)\frac{\partial^2 \bar{c}}{\partial y^2} + (e_m + \varepsilon_z)\frac{\partial^2 \bar{c}}{\partial z^2} \qquad (2.39)$$

where $\bar{c}$ is the time averaged concentration, e_m is the molecular mass diffusivity and ε_x, ε_y, and ε_z are the turbulent mass diffusivities in the x, y and z directions.

The molecular mass diffusion coefficient describes the spreading of the tracer due to the random molecular motion of the fluid, called Brownian motion. The coefficient is a property of the fluid and for a given solvent, solute, concentration and temperature the value is constant. Typical values for solutes in water are in the range 0.5 - 2 x10^{-9} m^2/s (Rutherford, 1994).

If the flow is turbulent the mass diffusion will be a function of the molecular and turbulent mass diffusion. The turbulent mass diffusion, unlike the molecular mass diffusion, is not constant. The dimensionless turbulent Schmidt number is used to convert the turbulent viscosity (calculated from the turbulence models) into the turbulent mass diffusivity.

$$\varepsilon_m = \frac{\mu_t}{Sc_t} \qquad (2.40)$$

where ε_m is the turbulent mass diffusivity, μ_t is the turbulent viscosity and Sc_t is the turbulent Schmidt number.

The equations governing turbulent mass diffusivity are analogous to the equations that describe turbulent thermal diffusivity with small temperature differences, Equations (2.41). Therefore, consideration is also given to research that obtained values for the turbulent Prandtl number. The turbulent Prandtl/Schmidt numbers can be deduced from measurements of the mean velocity or concentration profiles, or the radial profiles of the Reynolds shearing stress and the radial turbulent concentration/heat flux.

$$\varepsilon_t = \frac{\mu_t}{\mathrm{Pr}_t} \qquad (2.41)$$

where, ε_t is the turbulent thermal diffusivity and Pr_t is the turbulent Prandtl number.

The first attempt to define the turbulent Schmidt/Prandtl number was made by Prandtl when he took the value to be unity over the whole cross section, but experimental evidence has shown this to be incorrect. Following the approach of Launder (1976), consideration is given to the near wall and core flows separately.

The measurements of Blom (1970) and Baker and Launder (1974) (from Launder, 1976) using a flat plate suggest a value of 0.95 for Pr_t in the near wall region, with a tendency to increase above unity as the wall is approached. Quarmby and Quirk's (1972) (from Launder, 1976) pipe data suggests that the value decreases from 0.85 at $y/R = 0.2$ to only 0.65 at $y/R = 0.05$ (y is the distance from the pipe wall and R is the pipe radius). Koeltzsch (2000) used a flat plate and demonstrated similar results. Rodi (1993) and Schlichting (1997) (from Koeltzsch, 2000) suggested a value of 0.9 for Pr_t and Sc_t in the near wall region. Overall the experimental evidence suggests a value of 0.9 for Pr_t and Sc_t in the near wall region, although it is not clear whether the value increases or decreases very close to the wall.

As with the near wall region there is not an agreement regarding the turbulent Prandtl/Schmidt number away from the wall. Launder (1976) wrote "It does not seem possible to write with any certainty on the variation of the turbulent Prandtl/Schmidt number in fully developed pipe or channel flow. A number of experiments show a gradual reduction in the value towards the centre, while others show quite the reverse". Hinze (1975) used the work of Laufer (1954) to determine a value of 0.625 for Sc_t in the core region of turbulent pipe flow, while Launder (1976) suggests a value of 0.7 is more appropriate. Launder (1976) describes the finding of a conference that found values of Pr_t and Sc_t in the range 0.5 to 1.0.

Reynolds (1975) compares more than thirty ways of predicting turbulent Schmidt/Prandtl numbers. The most quoted of these was developed by Rotta (1964) to describe the variation of Pr_t across a flat plat, Equation (2.42). Values for the constants are taken between 0.9 and 0.95 for A and 0.4 and 0.45 for B. This equation is shown graphically in Figure 2.9.

$$Pr_t = A - B\left(\frac{y}{\delta}\right)^2 \qquad (2.42)$$

where y is the distance from the wall and δ is the boundary layer thickness.

Koeltzsh (2000) used measurements of air flow over a flat plate to demonstrate that Sc_t is not constant, but dependent upon the distance from the boundary. A power series equation to approximate the calculated data is shown graphically in Figure 2.9.

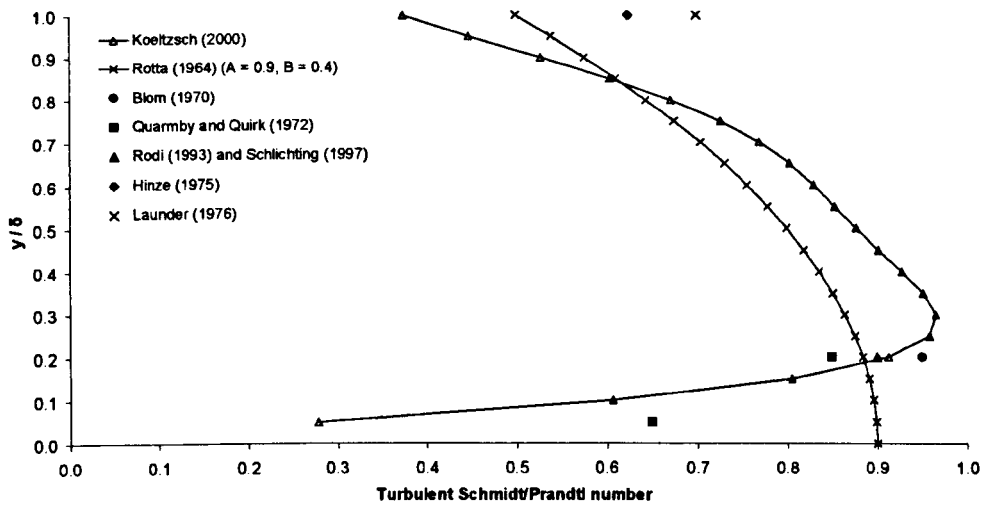

Figure 2.9 Variation in turbulent Prandtl/Schmidt number within the boundary layer

This ADE method performs well for diffusion problems, but can be affected by two types of numerical problems for advection dominated processes. The first type is numerical dispersion, which has an effect similar to that of physical dispersion, but is caused by the truncation error in the Taylor series expansion of the transport equation. This leads to a smearing of concentration fronts that have a sharp leading edge Figure 2.10 (a). The second type of numerical problem is artificial oscillations, Figure 2.10 (b). Artificial oscillations occur in higher order schemes that have been designed to eliminate numerical dispersion. Artificial oscillation is also more severe on steep concentration fronts. Both of these problems can be overcome by refining the grid and time step. However, the increase in computational effort may make this impractical when large complex systems are being studied, or when long term simulations are required.

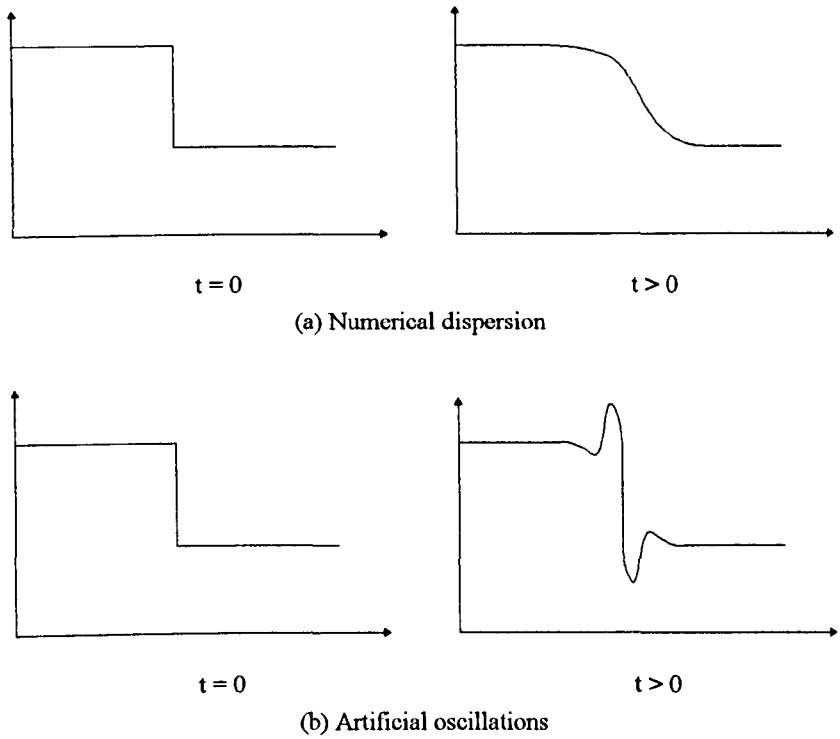

Figure 2.10 Sources of numerical error (after Anderson, 1995)

2.4.8.2 Particle tracking models

Particle tracking models offer an alternative to solving the advection-diffusion equation. The method works by assuming the tracer can be represented by a large number of discrete particles that are each subjected to advection and dispersion. The trajectory of each particle is determined by a force balance calculation that equates the particle inertia with the forces acting on the particle from the continuous phase. Models, such as the random walk model, may be used to include the effects of the instantaneous turbulent fluctuations on the particle trajectories through the use of stochastic methods.

The particle tracking method has a number of potential advantages over the advection diffusion equation transport model:

- When the tracer only occupies a small proportion of the flow domain the particle tracking approach is often more computationally efficient.
- The mass of the tracer must always be conserved locally and globally.
- If the modelling options are chosen correctly it is possible to simulate steep concentration gradients as the method is virtually free from numerical dispersion.

There are many types of particle tracking model available. The equations presented below are for the model contained within the Fluent software (Fluent, 1998), but many of the features are general to all models.

The force balance on a particle in the x direction may be written as:

$$\frac{du_p}{dt} = F_D(u - u_p) + \frac{g_x(\rho_p - \rho)}{\rho_p} + F_x \qquad (2.43)$$

where u is the instantaneous fluid velocity, u_p is the particle velocity, ρ is the fluid density, ρ_p is the particle density, g_x is the gravitational force, F_D is the drag force and F_x are additional forces that may be included. Additional models are available in Fluent 5.5 (Fluent, 1998) to represent the effects of temperature, Brownian motion and the lift due to shear on sub micron particles.

The drag force on the particle, F_D, is related to the size of the particle. For particles greater than one micron the drag force on the particle is represented by Equation (2.44) and for sub micron particles by Equation (2.45).

$$F_D = \frac{18\mu}{\rho_p D_\rho^{\,2}} \frac{C_D R_e}{24} \qquad (2.44)$$

$$F_D = \frac{18\mu}{\rho_p D_p^{\,2} C_c} \qquad (2.45)$$

where μ is the molecular fluid viscosity, D_p is the particle diameter, R_e is the relative Reynolds number, C_D is the drag coefficient and C_c is the Cunningham correction.

The drag coefficient, C_D, is defined by Equation (2.46). When spherical particles are being modelled a_1, a_2 and a_3 are constants (Fluent, 1998). The Cunningham correction, C_c, is defined by Equation (2.47).

$$C_D = a_1 + \frac{a_2}{R_e} + \frac{a_3}{R_e^{\,2}} \qquad (2.46)$$

$$C_c = 1 + \frac{2\lambda}{D_p}\left[1.257 + 0.4\exp\left(-1.1\left(\frac{D_p}{2\lambda}\right)\right)\right] \qquad (2.47)$$

where λ is the molecular mean free path.

The particle Reynolds number, R_e, is defined as:

$$R_e = \frac{\rho D_p |u_p - u|}{\mu} \qquad (2.48)$$

The dispersion of particles due to turbulence in the fluid phase may be modelled using either a stochastic particle tracking model or particle cloud model. The stochastic tracking model, or discrete random walk model, includes the effects of the instantaneous turbulent fluctuations on the particle trajectories through the use of stochastic methods. In the particle cloud model the particles are tracked around a mean trajectory. The concentration of particles within the cloud is represented by a Gaussian probability density function about the mean trajectory. In both models the particles have no direct impact on the generation or dissipation of turbulence on the continuous phase. The particle cloud method was not considered during the study so no further discussion is presented.

Turbulence is modelled as a series of eddies that have a lifetime and associated random velocity fluctuations in the random walk model. The instantaneous fluid velocity is therefore defined as:

$$u_i = \bar{u}_i + u_i' \qquad (2.49)$$

The fluctuating component, u_i', that prevails for the life time of the turbulent eddy is sampled by assuming that they obey a Gaussian probability distribution so that

$$u_i' = \zeta \sqrt{\overline{u_i'^2}} \qquad (2.50)$$

where ζ is a normally distributed random number ranging from zero to one and $\sqrt{\overline{u_i'^2}}$ is the root mean square (rms) of the velocity fluctuations.

When the k-ε models are used the velocity fluctuations are isotropic, so Equation 2.48 is simplified to:

$$\sqrt{\overline{u_i'^2}} = \sqrt{2k/3} \qquad (2.51)$$

To compute a particle trajectory the random fluctuating component has to be kept constant for a certain interval of time, called the characteristic lifetime of the eddy. Fluent 5.5 (Fluent, 1998) provides the option to define the characteristic lifetime of the eddy as constant function, Equation (2.52), or as a random variation around the Lagrangian time interval, T_L, Equation (2.53).

$$\tau_e = 2T_L \qquad (2.52)$$

$$\tau_e = -T_L \log(r) \qquad (2.53)$$

where r is a random number between zero and one.

The Lagrangian time interval is defined as:

$$T_L = C_L \frac{k}{\varepsilon} \qquad (2.54)$$

where C_L is the time scale constant.

The Fluent User's Guide (Fluent, 1998) suggests that the time scale constant be set to 0.15 when using the k-e turbulence model and 0.3 when using the RSM model.

The repeated calculation of a single particle trajectory will show a different direction because of the random nature of the eddy. However, the effects of turbulence may be accounted for by computing the trajectory of a significant number of representative particles.

2.4.9 The Fluent CFD software

Until this point the general principals of CFD have been presented, but now consideration is given to the Fluent CFD software that was used in the study. The Fluent software, from now on referred to as Fluent, is a commercial CFD programme that uses the finite volume based method to solve the governing equations of fluid dynamics. Fluent is capable of modelling fluid flow, heat transfer and chemical reaction in a wide range of situations. A full description of the software may be found in the Fluent 5 User's Guide (Fluent, 1998).

A simulation using Fluent consists of five stages:

- Stage 1 – Importing the grid/mesh

  Fluent, as with all CFD codes, requires a grid, or mesh, upon which to discretize the governing equations. Fluent cannot generate a mesh, but imports ones that have been developed in software such as Gambit (Gambit, 1998), which is supplied with Fluent, or third party CAD software. Fluent can operate in two or three dimensions and supports structured or unstructured meshing techniques.

- Stage 2 – Specification of boundary conditions and material properties

  Once the mesh has been imported the cells that coincide with or touch the outline geometry, termed boundary cells, need to be defined. Fluent offers a wide variety of boundary conditions to suit different types of flows, with typical boundary conditions including

inlets, outlets and walls. Cells inside the domain are given the physical properties of the fluid, such as viscosity and density.

- Stage 3 - Selection of modelling options

  Turbulence may be modelled in Fluent by the Reynolds averaging or LES approaches. If the Reynolds averaging approach is used the software contains three versions of the high Reynolds k-e model: Standard (Launder and Spalding, 1974), RNG (Yakhot and Orszag, 1986) and Realizable (Shih *et al.*, 1995). It also contains the high Reynolds number RSM that is based on the proposals of Launder *et al* (1975). All of these models require the use of wall functions to model the near wall region.

  Fluent also supports two low Reynolds number modelling approaches. In the first approach, called two layer zonal modelling, the high Reynolds number turbulence models are used to predict the turbulent flow. In the viscosity affected near wall region the momentum and k equations are calculated from the high Reynolds number models, but the turbulent viscosity and ε are calculated from new equations. In the second approach, called full low Reynolds number modelling, the turbulence models are altered to allow them to model the viscosity affect region as well as the core. Fluent supports five full low Reynolds number models, including those proposed by Launder and Sharma (1974) and Lam and Bremhorst (1981).

  Fluent offers four schemes with which to discretize the transport equations: first and second order upwind, power law and QUICK. When the segregated solver is used Fluent provides the SIMPLE, SIMPLEC and PISO schemes for pressure-velocity coupling.

- Stage 4 – Simulation

  This study used version 5.5 of the Fluent software. This version supports both segregated and coupled solvers, however, the coupled solver was not considered because it was developed for compressible flows. The segregated solver algorithm solves the governing equations sequentially and segregated from each other. As the governing equations are non linear (and coupled), several iterations of the solution loop must be performed before a converged solution is obtained, this is shown graphically in Figure 2.11.

  The time required for a simulation will depend on a number of factors including the computational power available, the number of cells in the domain and the turbulence model selected.

- Stage 5 - Post processing

  Post processing involves the extraction of the desired flow properties from the computed flow field. This may be through a visual display, such as vectors or contour plots, or in numerical form.

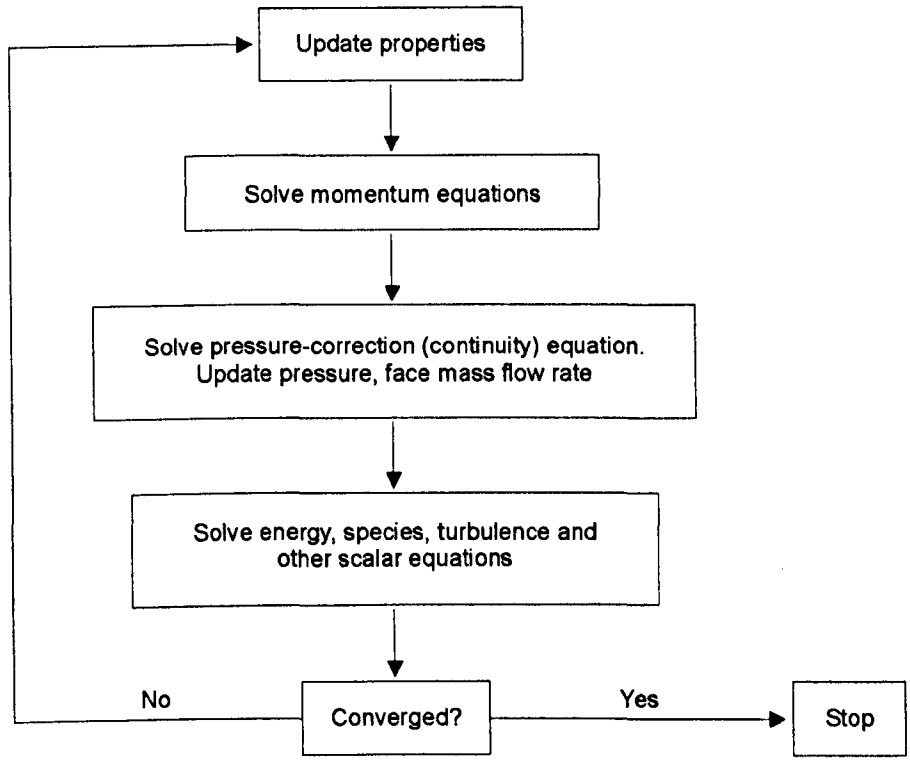

Figure 2.11 Overview of the segregated solution method (after Fluent, 1998)

2.4.9.1 The species transport model

The species transport model may be used to predict the movement of a species with or without chemical reaction. When a non reacting species is transported the advection-diffusion equation presented in Section 2.4.8.1 is used. The model can be incorporated into the simulation process, as illustrated in Figure 2.11, or be used once the flow simulation has been completed, this is often termed cold, or uncoupled, processing.

When using the species transport model the simulation is time dependent. This requires the time dependent equations to be discretized both in time and space, with the spatial discretization being the same as in the steady state case. Temporal discretization involves the integration of every term in the differential equation over a time step Δt. The Fluent 5 User's Guide (Fluent, 1998) suggests that first order accuracy is appropriate for most problems, and is the default setting.

2.4.9.2 The particle tracking model

The particle tracking routine implemented in Fluent is called the discrete phase model. As with all particle tracking routines the particle trajectories are calculated by integrating the force balance on the particle. The particle trajectory is updated in fixed intervals, termed length scales, or when the particle enters a neighbouring cell. The particle tracking routine in Fluent 5.5 allows the movement of the particle to be modelled with a fixed flow field, termed an

uncoupled simulation, or with the effects of the particle on the flow (and visa versa), termed a coupled simulation. The equations used in the discrete phase model are presented in Section 2.4.8.2.

2.4.10 Previous studies using CFD

2.4.10.1 Urban drainage structures

CFD has been used to model a variety of urban drainage structures. Stovin and Saul (1996) and Stovin *et al.* (1999) used the standard k-ε turbulence model to successfully predict the global flow patterns in a variety of storage tank configurations. Stovin and Saul (1998) used a discrete phase model for the prediction of sediment transport and deposition in storage chambers, while Stovin *et al.* (1999) used the same model to replicate the gross solids separation efficiency observed in field scale model storage chambers. Adamsson *et al.* (in press) developed the boundary conditions used by the discrete phase model in the Fluent to include a condition based on bed shear stress. A comparison with experimental storage tank data showed the new boundary condition to be an enhancement over the standard options.

Harwood (1999) used the k-ε turbulence model to predict flow patterns in a single high side weir and a stilling pond CSO, and the Reynolds stress turbulence model to simulate the complex three dimensional flow patterns found in Storm King hydrodynamic separator CSO. A comparison between the velocity and particle movement from the simulated hydrodynamic separator and measurements from a full scale laboratory model demonstrated the CFD predictions replicated both the swirling flow pattern and the retention efficiencies. In a similar study, Tyack and Fenner (1999) used the k-ε RNG turbulence model to predict flow patterns in a Grit King hydrodynamic separator. A comparison with experimental data showed the numerical model approximately predicted the velocity magnitude at two locations.

The research of Buxton (in press) focused on the trapping performance of sewer invert traps. He demonstrated that the choice of turbulence model dramatically affected the predictions of secondary circulations in a trapezoidal channel, and that the sediment retention performance was highly sensitive to the choices made in setting up the discrete phase modelling options.

Asztely and Lyngfelt (1996) used CFD to predict energy losses in different manhole configurations. A number of simplifying assumptions were made including creating a line of symmetry and fixing the free surface. The standard k-ε turbulence model was used to generate the flow field. A good correlation was shown between the CFD predictions of energy loss coefficients and measurements from a physical scale model.

The above examples demonstrate that CFD has been used in a variety of structures connected with the sewerage system. A more detailed review is presented below of studies that have used CFD to investigate the flow in pipes and to model the transport of a tracer.

2.4.10.2 Pipe flow

Martinuzzi and Pollard (1989) used one high Reynolds number k-ε model, one low Reynolds number k-ε model and four algebraic stress models to predict developing turbulent pipe flow in the range $10000 < Re < 380000$. Grid independence was explored, but no consideration was given to the impact of the discretization schemes. A comparison was made with measurements of a number of flow properties including axial velocity, turbulent kinetic energy and Reynolds shear stress. It was found the predictions from the low Reynolds number k-ε model from Lam and Bremhorst (1981) gave the best overall agreement with the experimental data. It was also noted that the use of the low Reynolds number k-ε model proved to be superior to the standard k-ε model, although it required approximately 10 times more CPU time. This study was extend (Pollard and Martinuzzi, 1989) to consider five RSM models. However Lam and Bremhorst's model was still found to give the best results.

Hrenya *et al.* (1995) used ten low Reynolds number k-ε turbulence models to predict fully developed pipe flow. The models predictions were compared with the experimental data of Laufer (1954), Patel and Head (1969), Schildknecht *et al.* (1979) and the DNS simulation data of Eggels *et al.* (1994). The models generally predicted mean axial velocity and Reynolds stress well, but the predictions of turbulent kinetic energy, eddy viscosity and turbulent dissipation rate were less good, with this being most noticeable at low Reynolds number flows. The model developed by Myong and Kasagi (1990) showed the best overall performance as it was the only one that could predict the centreline and peak turbulent kinetic energy to within 15% of the experimental measurements and give a good prediction of the spatial variation in the eddy viscosity.

Thakre and Joshi (2001) extended the study of Hrenya *et al.* (1995) to include three more low Reynolds number k-ε turbulence models, making twelve different versions in total. Although the additional models showed improvement, the model developed by Myong and Kasagi (1990) still performed best overall.

Eggels *et al.* (1994) compared the predictions of a direct numerical simulation (DNS) with measurements of fully developed pipe flow at a Reynolds number of 7000 (*Re* based on centreline velocity). The measurements were carried out using hot wire anemometry (HWA), laser doppler anemometry (LDA) and particle image velocimetry (PIV). A description of the laboratory set up and results can be found in Weiss (1993) and Westerweel (1993). The DNS simulations were performed using Cray computers and required approximately 160 hours of

CPU time and 7.6 Gb of permanent file storage for each simulation. A description of the numerical algorithms and other details of the simulation may be found in Eggels *et al.* (1994).

When the numerical and experimental results were compared the agreement was excellent, particularly for the mean flow and turbulence intensities. For instance, the predicted mean axial velocity and LDA measurements were in agreement to within a few percent over the whole cross section. When a comparison was made between the root mean square (rms) values of the fluctuating velocities an excellent agreement was also found, particularly between the DNS and the LDA data. For higher order statistics the agreement between DNS and experimental data was not as close, but was still very good. The DNS predictions did not replicate the universal velocity profile, but this observation is not unique as Patel and Head (1969) had demonstrated this experimentally.

Eggels (1994) compared the predictions from a LES simulation with experimental data that had been collected by Laufer (1954), Lawn (1971) and Perry (1975). The Reynolds number of the flows used in these experiments was similar to the number used in the simulations. Seven simulations were performed which considered variations to the grid density and model set up options. As with the DNS simulation a Cray computer was used, but the LES simulation required between 10 and 50 percent of the CPU time and file storage capacity. The LES model was shown to be sensitive to set up options, even for mean flow properties such as axial velocity. However, the overall agreement with the experimental data was good.

2.4.10.3 Numerical dispersion studies

CFD has been widely used to investigate dispersion. Considerable research has focused on its use to predict the movement and dispersion of gases and solids from a variety of sources, such as power plants, vehicles and agricultural buildings. Although less well documented, researchers have used CFD to predict neutrally buoyant or suspended contaminant movement through water. A summary of a number of these studies is presented below.

Glekas (1995) and Christodoulou *et al.* (1995) predicted the movement and dispersion of contaminants that were being discharged into the Mediterranean Sea from an outfall pipe connected to the sewage treatment plant in Limassol, Cyprus. Glekas (1995) modelled the process in three dimensions using the standard k-ε turbulence model. No validation was presented for the flow field, but a comparison between numerical and measured concentration distributions at two distances from the shore showed a good agreement considering the simplifying assumptions that were made. The study conducted by Christodoulou *et al.* (1995) modelled the processes using a two dimensional variable depth model. As with the study of Glekes, simplifying assumptions were required for the current and thermal variations. The data presented for the flow field and concentrations of BOD and Nitrogen indicated that the movement of the contaminant was significantly affected by the direction of the wind, with an

easterly wind direction causing the contaminants to be washed into the bay. No validation was presented, although the authors claim the comparison with available current measurements was good.

A number of studies have used CFD to model flow patterns and tracer movement in large volumes of enclosed water such as reservoirs (Ta and Brignal, 1998), ponds (Wood *et al.*, 1998; Shilton, 2000) and lagoons (Salter *et al.*, 2000). These studies were initiated because of concerns about the operating performance, usually in respect to short circuiting effects. The use of CFD in these studies has generally been to investigate the impact on the retention times of using baffles and/or moving the inflow and outflow locations. However, the lack of validation data and the poor reporting of the numerical procedure has limited these studies. The studies by Ta and Brignal (1998) and Salter *et al.* (2000) presented little regarding the numerics and no validation data for the flow or tracer movement. Shilton (2000) provided validation data that showed the CFD velocity predictions were of the same order of magnitude, but no validation data was presented for the tracer movement. Of the four studies considered, Wood *et al.* (1998) provided the most comprehensive details of the numerical model. Validation was not presented for the flow field, but the tracer predictions were compared with experimental data. Various geometric configurations were considered in two dimensions, but the comparison was generally poor. It was suggested that this discrepancy was primarily caused by the two dimensional model's inability to correctly predict the jet from the inlet.

Domgin *et al.* (1997) used CFD to replicate the experiments of Calabrese and Middleman (1979) who measured the radial spreading of chemicals in a straight vertical pipe filled with water. The k-ε turbulence model was used to predict the flow field, but no other information was presented regarding the discretization scheme or mesh. A comparison made between the prediction of turbulent kinetic energy and experimental data showed significant differences. The model's constants were therefore altered to produce a better fit. Three chemicals were used in the study; n-Heptane (ρ = 695 kg/m^3), Butyl Benzoate (ρ = 1000 kg/m^3) and Carbon Tetrachloride (ρ = 1595 kg/m^3). As with the laboratory measurements, the chemicals were released from the centre of the pipe and the radial dispersion recorded. The particle tracking model was used to transport individual droplets of each chemical, using at least 5000 trajectories. The radial dispersion was calculated from Equation (2.25).

The experiments conducted by Calabrese and Middleman (1979) suggested that the size of the chemical droplet did not influence the dispersion, but the CFD results showed a significant change. A comparison between the CFD predictions of radial dispersion and the measured values showed the larger particles produced the same trends as the measured data, but with a constant offset. The authors suggested this offset might be the result of the laboratory injection device disturbing the flow field. The particle tracking model was altered to include extra terms, but these did not affect the numerical predictions significantly.

Hancu *et al.* (2002) reported on a study that used CFD and experimental data to investigate water flow through five partially blocked open channels, and contaminant transport through one of the configurations. The geometry of each channel was carefully meshed to ensure a high resolution in regions that had the largest gradients of fluid velocity, and grid independence was claimed. The contaminant transport was modelled using the advection diffusion equation described in Section 2.4.8. The turbulent Schmidt number was taken as 0.7 throughout, as no significant differences were observed when altering it. No mention is made regarding the choice of time step or temporal discretization scheme. Salt was used as the tracer in the experiments and the same properties and amount were used in the numerical model. The change in concentration of salt with time was measured at the upstream site one hundred seconds after the initial injection. Assumptions were therefore made regarding the concentration in the numerical model during this time.

A visual comparison made between the CFD model and experimental data showed that the numerical model correctly predicted the global features of the flow field, including some of the recirculation effects. Visual data was also presented for predictions of salt concentration for one of the channel configurations. Four snap shots of time are presented that show the build up of contaminant behind the obstruction. Six points within the flow are compared with experimental data between one hundred and seven hundred seconds (approximately half of the peak concentration) after injection. The CFD results show approximately the same change in concentration with time, with the authors attributing some of the differences to the assumptions that were made about the initial injection. Although of interest this study is limited by the lack of numerical comparisons for the flow field, and the assumptions regarding the injection of the salt.

2.5 Fully developed pipe flow

Flow through pipes is of fundamental importance to many fields of engineering. Consequently, a number of experimental studies have been undertaken, with new ones being initiated with improvements in measurement technology. Key studies are presented in Section 2.5.2. These studies, and others on flat plates, have demonstrated that distinct regions exist within the flow. They have been used to develop a number of empirical, or semi empirical, correlations to describe the flow properties. The extent of the regions and equations used to predict the velocity distribution within them is discussed in Section 2.5.1. The equations derived for a flat plate are also presented as the flow in the near wall region is the same. When the data is presented for a flat plate the notation y and δ are used, with y being the distance from the wall and δ being the boundary layer thickness. For pipe flow the boundary layer thickness is the same as the pipe radius.

2.5.1 Pipe flow

Numerous experiments have shown that the flow through a pipe or over a flat plate can be subdivided into three regions; an inner region, an outer or core region, and an overlap region. In the inner region the flow is almost laminar and is dominated by molecular viscosity, while in the outer region the flow is dominated by turbulent shear. The overlap region is between these two layers and the effects of molecular viscosity and turbulence are both important. Many texts describe the processes in each layer, most notably Schlichting (1968) and White (1991).

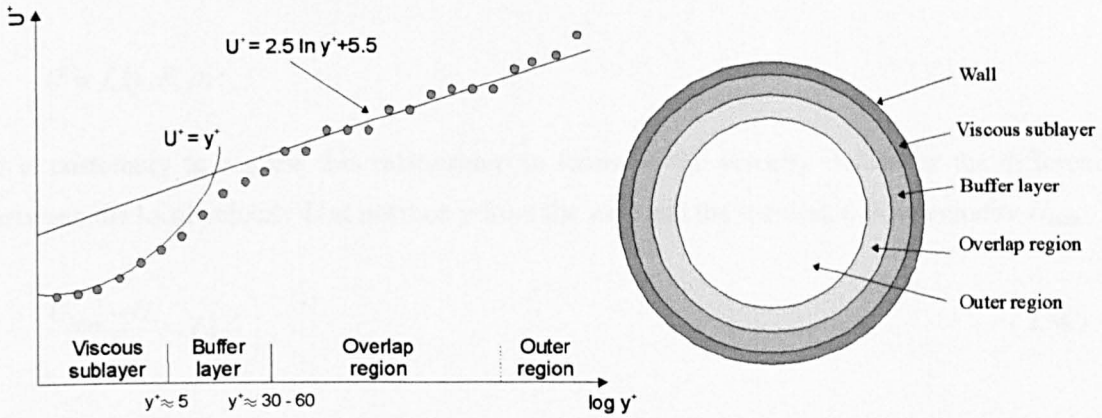

Figure 2.12 Subdivision of pipe flow

2.5.1.1 Inner region

In the inner region the flow is influenced by viscous effects and does not depend on free stream parameters. The velocity depends only upon the distance from the wall (y), the fluid density (ρ) and viscosity (μ), and the wall shear stress (τ_w) (White 1991):

$$U = f_w(y, \rho, \mu, \tau_w)$$

Using dimensional analysis the following equation, which is often referred to as the law of the wall, was derived:

$$U^+ = \frac{U}{U^*} = f_w\left(\frac{\rho U^* y}{\mu}\right) = f_w(y^+) \qquad (2.55)$$

The inner region may be further subdivided into a viscous sublayer and a buffer layer. Within the viscous sublayer the velocity will vary linearly with the distance from the wall, which explains why it is sometimes called the linear sublayer. This layer is extremely thin and will probably only extend to a y^+ value of around five (Schlichting, 1968; White, 1991). Between $5 < y^+ < 30$ (Tennekes and Lumley, 1990; White, 1991) or $5 < y^+ < 70$ (Schlichting, 1968;

Geropp and Odenthal, 2001) the buffer layer exists. In this region the velocity profile is neither linear nor logarithmic, but is instead a smooth merge between the two.

2.5.1.2 Outer Region

In the outer layer, or core region, the wall acts to retard the local velocity below the maximum velocity in a way that is independent of the viscosity, but dependent upon the distance from the wall (y), the wall shear stress (τ_w), the fluid density (ρ) and the boundary layer thickness (δ), which for pipe flow would be the radius (Versteeg and Malalasekera, 1999):

$$U = f_c(y, \delta, \rho, \tau_w)$$

It is customary to express this relationship in terms of the velocity defect, or the difference between the local velocity U at position y from the wall and the maximum flow velocity U_{max}:

$$\frac{U_{\max} - U}{U^*} = f_c\left(\frac{y}{\delta}\right) \qquad (2.56)$$

This formula is called the velocity defect law. At present there is no agreement as to the form of the function f_c. Schlichting (1968) developed the following equation which is widely used:

$$\frac{U_{\max} - U}{U^*} = \frac{1}{\kappa}\ln\left(\frac{y}{\delta}\right) + A \qquad (2.57)$$

The constant κ is referred to as Von Kármán's constant and the value is often taken as 0.4. Schlichting (1968), however, proposed a value of 0.36 and White (1991) 0.41. Schlichting (1968) assumed the other constant A was zero when he favourably compared the results with experimental data. For pipe flow Tennekes and Lumley (1990) demonstrated that a value of -1 was appropriate.

This is not the only form of the velocity defect law. Schlichting (1968) proposed two further methods which he attributes to Von Kármán and Darcy respectively:

$$\frac{U_{\max} - U}{U^*} = -\frac{1}{\kappa}\left\{\ln\left[1 - \sqrt{1 - \frac{y}{\delta}}\right] + \sqrt{1 - \frac{y}{\delta}}\right\} \qquad (2.58)$$

$$\frac{U_{\max} - U}{U^*} = 5.08\left(1 - \frac{y}{\delta}\right)^{\frac{3}{2}} \qquad (2.59)$$

Schlichting (1968) compared equations (2.57), (2.58) and (2.59) with experimental pipe flow data. Equation (2.57) produced the best comparison over the cross section, while Equation (2.59) was only reliable in the region $0.25 < y/\delta < 1.0$.

An alternative approach is to use the empirical power law proposed by Prandtl, and developed using the experimental data from Nikuradse's (1932) pipe flow experiments:

$$\frac{U}{U_{max}} = \left(\frac{r}{R}\right)^{\frac{1}{n}} \qquad (2.60)$$

where r is the distance from the wall and R is the pipe radius

The value of n is not constant and will change according to Reynolds number. For pipe flow Schlichting (1968) demonstrated that if the value of n is correctly calibrated with Reynolds number it will give a good match with experimental data until close to the pipe centre.

More recently Gersten and Herwig (1992) developed a new velocity defect law for pipe flow. When the equation was compared with the LDA velocity measurements of pipe flow, the maximum deviation was 1.5 % (Geropp and Odenthal, 2001).

$$\frac{U_{max} - U}{U^*} = \frac{1}{\kappa}\ln\left[1 + (C-1)\left(\frac{r}{R}\right)^2\right] - \frac{1}{\kappa}\ln\left[1 - \left(\frac{r}{R}\right)^2\right] \qquad (2.61)$$

In this equation r is the distance from the pipe centre. Von Kármán's constant, κ, should be taken as 0.407, and the constant C as 2.09.

2.5.1.3 Overlap region

The inner and outer layers merge smoothly in the overlap region. In this region both the viscous and turbulent effects are important and the velocity varies logarithmically with the distance from the wall, which is why it is often called the log law layer. Schlichting (1968) proposed the following relationship:

$$U^+ = \frac{1}{\kappa}\ln y^+ + B \qquad (2.62)$$

The values most commonly taken for the constants are based on the experiments of Nikuradse, where $B = 5.5$ and $\kappa = 0.4$, although other values have been proposed between $\kappa = 0.36$ to 0.419 and $B = 3.8$ to 5.85 (Datta, 1993).

There is not an agreement over the extent of the log law layer. Versteeg and Malalasekera (1995) suggest a range of $30 < y^+ < 500$, or $2\ \% < y/\delta < 20\ \%$. White (1991) used experimental data to demonstrate a range of $35 < y^+ < 350$ or $2\ \% < y/\delta < 20\ \%$. Alternatively, Datta (1993) suggest for pipe flow the wake is only slight and consequently the log law layer is valid to the pipe axis.

2.5.2 Experimental measurements of pipe flow

Laufer (1954) collected the first complete set of pipe flow data. The tests were conducted in straight brass tube 5 m long with an internal diameter of 247 mm. Measurements were principally taken using a hot wire anemometer (HWA) in fully developed pipe flow corresponding to Reynolds numbers of 50000 and 500000 (Re based on centreline velocity). HWA works by inserting a heated wire into a flow and recording heat loss. The heat loss can then be converted into a fluid velocity in accordance with convective theory. Although the study focused on near wall conditions, measurements of mean velocity, Reynolds shear stress, turbulent dissipation and energy spectra were taken over the cross section.

Lawn (1971) questioned the measurement and analysis technique of Laufer (1954), particularly the assumptions used to determine the dissipation of energy. Laufer only measured five of the contributions to the dissipation rate, and assumed isotropic relations may be used to derive the remainder. This may be valid in the turbulent core, but is not valid in the near wall region. Lawn performed further HWA tests using a pipe 144 mm in diameter and 60 diameters in length. Along with spectral analysis, measurements of the axial velocity and the Reynolds shear stress are presented at five Reynolds numbers ranging from 36700 to 249000. Lawn concluded that although this work was an enhancement of previous studies, particularly with respect to the measurements of the dissipation of energy, further progress was restricted because of the limitations of HWA technology.

Schildknecht *et al.* (1979) used HWA and Pitot tubes to investigate the influence of suction on flow properties in fully developed pipe flow at a Reynolds number of 17250. The pipe was 50 mm in diameter and 9 m long. The effect of suction was investigated on a variety of flow parameters including the mean axial velocity, mean radial velocity, Reynolds shear stress, turbulent kinetic energy and turbulent dissipation rate. Schildknecht *et al.* (1979) also questioned the assumptions Laufer (1954) used to calculate the dissipation of energy. This data set is regarded as the most comprehensive collected using HWA technology.

Durst *et al.* (1995) used laser Doppler anemometry (LDA) measurements to determine mean velocity and turbulence statistics in the near wall region. LDA techniques are not intrusive and therefore useful for measuring flow properties, particularly in the near wall region where the invasive measuring technique of HWA can cause serious errors. Most of the experiments were conducted at a Reynolds number of 7442. The majority of the tests were conducted in the region $0 < y^+ < 300$, although some experiments focused on the near wall region below a y^+ value of 30. This data set is regarded as being the most extensive and accurate for the near wall region.

Eggels *et al.* (1994) reported on the HWA measurements of Weiss (1993) and the LDA and particle image velocity (PIV) measurements of Westerweel (1993) collected at a Reynolds

number of 7000 (based on centreline velocity). The measurements taken using the HWA technique were shown to be accurate to within 1 % for the mean velocity measurements at the pipe centre, and to about 4 % close to the wall. The LDA and PIV experiments were conducted on a pipe 127 mm in diameter, with measurements taken 130 pipe diameters downstream of the inlet. The estimated error for the measured mean velocity was about 0.3 %. There is generally a good agreement between the three measurement techniques. Westerweel *et al.* (1995) extended this work to include measurements taken using digital particle image velocimetry (DPIV).

Geropp and Odenthal (2001) used LDA techniques to measure the change in cross sectional velocity of flow a pipe. The pipe had an internal diameter of 76 mm and a length of 6.08 m. Tests were conducted at Reynolds numbers of 149000 and 186000. Forty five measurement positions were used to develop the profile, at a spacing of 1 mm close to the wall and 2 mm towards the centre of the pipe. For each reading 1000 samples were taken and averaged. Tests showed the total measurement error of the LDA system should be less than 1.5 %. Results from these experiments were used to confirm the velocity profile equation proposed by Gersten and Herwig (1992), Equation (2.61)

2.6 Summary

Although CFD has been used in water engineering applications, the studies that have been undertaken lack convincing validation for the flow field and/or the solute transport predictions. They also lack information on the precise set-up options adopted, and/or sensitivity analysis on the available options.

Given the large range of modelling options embodied in modern CFD codes (see for example the discussion on turbulence modelling approaches) it was felt that there was a need for a comprehensive parametric study on both the flow field and solute transport modelling options. Although the ultimate aim might be to provide a general methodology applicable to the whole range of sewer hydraulic structures, the simplest type of hydraulic structure – a pipe flowing full – was selected as a starting point for the research.

This chapter has also highlighted studies that provide appropriate validation data for both the flow field and the solute transport occurring within a surcharged pipe.

The next two chapters explore the feasibility of using each of the two transport models described in Section 2.4.8, whilst Chapters 5 and 6 focus on validation of the flow field and solute transport predictions respectively.

3 Feasibility study on the species transport model

3.1 Introduction

The aim of this research was to determine whether computational fluid dynamics (CFD) may be used to accurately predict the transport of a solute tracer through a straight pipe. The Fluent CFD software (Fluent, 1998) was used throughout the study, with the reasons for choosing Fluent presented in Chapter 2. The discrete phase model and the species transport model contained within Fluent may be used to predict the transport of a solute. Two feasibility studies were initially conducted to examine the viability of their use. The objectives of the feasibility studies were to determine:

- How to use the models to predict the transport of a solute
- The sensitivity of the predictions to the modelling options selected
- Whether a robust modelling approach was attainable
- Whether the data could be extracted in a form that would allow further analysis
- Whether the available computing resources were sufficient to run the models
- Whether the simulation times were too long to make them viable approaches

This chapter reports on the feasibility study relating to the species transport model, while Chapter 4 reports on the study relating to the discrete phase model.

The predictions obtained from the species transport model are known to be dependent upon the modelling options selected. This includes the schemes to discretize the governing equations, the choice of transport model (reacting or non reacting), the physical properties of the species and the simulation technique. The modelling options that are most relevant to the transport of a non reacting species are described in Section 3.2

A major component of both feasibility studies were two parametric studies that evaluated the impact of the modelling options on the prediction of solute transport. The modelling options considered during the species transport model parametric study were the spatial and temporal discretization schemes, the simulation technique and the available methods for introducing a new species. Consideration was also given to how the transport was affected by a change in the

flow field and whether the predictions were the same in two and three dimensions. The findings of the parametric study are presented in Section 3.3.

Section 3.4 summarises the species transport model feasibility study, including making recommendations of appropriate modelling options to use.

In Chapter 4 a recommendation is made regarding which of the two transport models (i.e. the species transport model or the discrete phase model) to consider for further investigation.

Perhaps the most appropriate method for determining the accuracy of a CFD model is to compare the simulation predictions with measured data. A number of researchers have measured the transport of a solute tracer through a straight pipe, including Taylor (1954) who used the data to verify his theoretical longitudinal dispersion equation, Equation 2.18. This study, however, chose to use the measurements reported by Guymer and O'Brien (2000). This data set was chosen because the measurement technique was more accurate than the one used by Taylor and because flow and tracer data were presented over a range of discharges.

3.2 The species transport model

The transport and mixing of a chemical species may be modelled in Fluent 5.5 by the species transport model. The equations used in the model are analogous to the advection diffusion equation that was described in Chapter 2. Additional models are also available to predict the transport of a species with chemical reactions. The species transport model is described in detail in the Fluent 5 User's Guide (Fluent, 1998) and a summary was presented in Chapter 2. When using the model to predict the movement of a non reacting species the following modelling options are relevant:

Discretization

When performing a time dependent simulation the governing equations must be discretized in both time and space. The segregated solver supports the first and second order implicit formulation, or temporal discretization, schemes. The Fluent 5 User's Guide (Fluent, 1998) suggests that the first order implicit scheme is appropriate for most problems and it is the default setting. The species transport model supports the first and second order upwind, power law and QUICK spatial discretization schemes, with the first order upwind scheme selected by default. The spatial discretization of the species transport equations is similar to that of the flow equations.

Temporal discretization involves the integration of every term in the governing equations over a time step Δt. If the time step is too large the truncation error inherent in the implicit scheme will also be large, however, if the time step is too small it is not computationally efficient. The Fluent 5 User's Guide (Fluent, 1998) recommends the size of the time step be set to at least one order of magnitude less than the smallest time constant in the system being modelled, with this

being deemed to have occurred if ten to twenty iterations are required to obtain convergence at each time step.

Simulation technique

Two methods are available for simulating the transport of a species. The first method solves the species transport equations in isolation, termed cold or uncoupled processing, while the second method solves the equations in conjunction with the flow equations, which from now on will be termed coupled processing.

Species properties

The physical properties of each species and the mixture are required as inputs. This includes specifying the density, molecular weight, absolute fluid viscosity and the molecular diffusion coefficient.

Introduction of the new species

The new species may be introduced from an inlet, or it may be patched directly into the domain. For time dependent simulations the mass fraction of the new species entering the domain from an inlet is required at each time step. This provides the opportunity to introduce a time varying profile.

Mass diffusion

The species transport model contains a mass diffusion term that describes the spreading of the tracer due to molecular and turbulent diffusion. The molecular diffusion term is defined by a molecular mass diffusion coefficient and is specified as a constant throughout the domain. The turbulent diffusion term cannot be specified directly, but is related to the turbulent viscosity by the turbulent Schmidt number. The species transport model in Fluent 5.5 requires a constant value to be specified for the turbulent Schmidt number throughout the domain. The default setting is 0.7, but this may be altered to any non zero value. (It is not possible to alter the turbulent Schmidt number when the k-ε RNG turbulence model is used).

Convergence criteria

If the full processing technique is used the convergence criteria and maximum number of iterations per time step need to be specified for both the discretized flow and species equations. If the simulations are performed using the uncoupled processing technique the convergence criteria is only required for the discretized species equations.

If the residuals drop below the convergence criteria before the maximum number of iterations has been performed, the simulation moves to the next time step. The default setting for the

convergence criteria is 1 $x10^{-3}$, but this may be set to any value, or turned off so that the simulation always performs the maximum number of iterations. More information regarding the residuals may be obtained from the Fluent 5 User's Guide (Fluent, 1998).

3.3 Parametric analysis of the species transport model

3.3.1 Introduction

A parametric study was conducted to determine how the predictions of solute transport were affected by the modelling options selected. Unless otherwise specified the tests were conducted in the pipe described in Section 3.3.2. The modelling options considered during the parametric study were the spatial and temporal discretization schemes, the processing technique and the available methods with which to introduce a new species. The impact of these modelling #options on the prediction of solute transport was considered over a range of time steps. Consideration was also given to assessing how the predictions were affected by changes to the flow field and whether they were the same in both two and three dimensions. Details of modelling options considered in each of the parametric tests are shown in Table 3.1, with the main focus of each test being as follows:

- Parametric test 1: Spatial and temporal discretization scheme
- Parametric test 2: Processing technique
- Parametric test 3: Introduction of the tracer
- Parametric test 4: Flow field
- Parametric test 5: 2D and 3D

In each of the tests the tracer (dye) was introduced into the pipe at, or close to, the inlet. It was then tracked through the pipe until the retained mass fraction was zero. Monitoring positions were created over the cross section of the pipe at the inlet, outlet and at two metre intervals along the length to record the change in the average mass fraction of dye with time, thus creating a series of temporal profiles. Only one simulation was performed for each of the modelling configurations because they are not stochastic and therefore reproduce exactly.

The properties of the new solute species were always specified to be the same as the primary water phase (density 998.2 kg/m^3, molecular weight 18.0152 kg/kgmol and absolute viscosity 1.003 x 10^{-3} kg/m s).

The molecular diffusion coefficient describes how the solute spreads due to molecular diffusion in the primary water phase. The spreading was anticipated to be small as the density of the two fluids was the same, so the value was set to 1 $x10^{-10}$ m^2/s, which is in the range recommended by Rutherford (1994) for a solute in water. At this stage of the investigation the turbulent

Test No	Solver	Mesh	Temporal discretization scheme	Spatial discretization scheme	Processing technique	Convergence criteria	Tracer introduction method	Time steps considered (s)
1	3D	4	First order	First order upwind	Uncoupled	1×10^{-3}	1.2 s slug from the inlet	0.2, 0.1, 0.05, 0.01
	3D	4	First order	Second order upwind	Uncoupled	1×10^{-3}	1.2 s slug from the inlet	0.2, 0.1, 0.05, 0.01
	3D	4	First order	Power Law	Uncoupled	1×10^{-3}	1.2 s slug from the inlet	0.2, 0.1, 0.05
	3D	4	First order	QUICK	Uncoupled	1×10^{-3}	1.2 s slug from the inlet	0.2, 0.1, 0.05
	3D	4	Second order	First order upwind	Uncoupled	1×10^{-3}	1.2 s slug from the inlet	0.2, 0.1, 0.05, 0.01
	3D	4	Second order	Second order upwind	Uncoupled	1×10^{-3}	1.2 s slug from the inlet	0.2, 0.1, 0.05, 0.01
	3D	4	Second order	Power Law	Uncoupled	1×10^{-3}	1.2 s slug from the inlet	0.2, 0.1, 0.05
	3D	4	Second order	QUICK	Uncoupled	1×10^{-3}	1.2 s slug from the inlet	0.2, 0.1, 0.05
2	3D	4	First order	First order upwind	Uncoupled	1×10^{-3}	1.2 s slug from the inlet	0.2, 0.1, 0.05, 0.01
	3D	4	First order	First order upwind	Coupled	1×10^{-6}	1.2 s slug from the inlet	0.2, 0.1, 0.05
	3D	4	First order	Second order upwind	Uncoupled	1×10^{-3}	1.2 s slug from the inlet	0.2, 0.1, 0.05, 0.01
	3D	4	First order	Second order upwind	Coupled	1×10^{-6}	1.2 s slug from the inlet	0.2, 0.1, 0.05
	3D	4	Second order	First order upwind	Uncoupled	1×10^{-3}	1.2 s slug from the inlet	0.2, 0.1, 0.05, 0.01
	3D	4	Second order	First order upwind	Coupled	1×10^{-6}	1.2 s slug from the inlet	0.2, 0.1, 0.05
	3D	4	Second order	Second order upwind	Uncoupled	1×10^{-3}	1.2 s slug from the inlet	0.2, 0.1, 0.05, 0.01
	3D	4	Second order	Second order upwind	Coupled	1×10^{-6}	1.2 s slug from the inlet	0.2, 0.1, 0.05
3	3D	4	First order	First order upwind	Uncoupled	1×10^{-3}	1.2 s slug from the inlet	0.2, 0.1, 0.05, 0.01
	3D	4	Second order	Second order upwind	Uncoupled	1×10^{-3}	1.2 s slug from the inlet	0.2, 0.1, 0.05, 0.01
	3D	4	First order	First order upwind	Uncoupled	1×10^{-3}	5 s slug from the inlet	0.2, 0.1, 0.05, 0.01
	3D	4	Second order	Second order upwind	Uncoupled	1×10^{-3}	5 s slug from the inlet	0.2, 0.1, 0.05, 0.01
	3D	4	First order	First order upwind	Uncoupled	1×10^{-3}	10 s slug from the inlet	0.2, 0.1, 0.05, 0.01
	3D	4	Second order	Second order upwind	Uncoupled	1×10^{-3}	10 s slug from the inlet	0.2, 0.1, 0.05, 0.01
	3D	4	First order	First order upwind	Uncoupled	1×10^{-3}	Skewed profile from the	0.2, 0.01
	3D	4	Second order	Second order upwind	Uncoupled	1×10^{-3}	Skewed profile from the	0.2, 0.01
	3D	4	First order	First order upwind	Uncoupled	1×10^{-3}	Patch method	0.2, 0.01
	3D	4	Second order	Second order upwind	Uncoupled	1×10^{-3}	Patch method	0.2, 0.01

Table 3.1 The modelling options considered during the species model parametric study (continued overleaf)

Test No	Solver	Mesh	Temporal discretization scheme	Spatial discretization scheme	Processing technique	Convergence criteria	Tracer introduction method	Time steps considered (s)
4	3D	1, 2, 3, 4, 5, 6	Second order	First order upwind	Uncoupled	1×10^{-3}	1.2 s slug from the inlet	Time step independence
	3D	1, 2, 3, 4, 5, 6	Second order	Second order upwind	Uncoupled	1×10^{-3}	1.2 s slug from the inlet	Time step independence
5	2D	11, 12, 13, 14	Second order	First order upwind	Uncoupled	1×10^{-3}	1.2 s slug from the inlet	Time step independence
	2D	11, 12, 13, 14	Second order	Second order upwind	Uncoupled	1×10^{-3}	1.2 s slug from the inlet	Time step independence
	3D	1, 2, 3, 4, 5, 6	Second order	First order upwind	Uncoupled	1×10^{-3}	1.2 s slug from the inlet	Time step independence
	3D	7, 8, 9, 10	Second order	Second order upwind	Uncoupled	1×10^{-3}	1.2 s slug from the inlet	Time step independence

Table 3.1 The modelling options considered during the species model parametric study (continued from previous page)

3.3.2 Development of the flow field

The same flow field was used as the basis for the majority of the tests during both the species transport model and discrete phase model parametric studies. The flow field was developed using the general guidelines presented in computational fluid dynamic text books and the Fluent 5 User's Guide (Fluent, 1998). As the purpose of the parametric studies was to assess the transport models, not the accuracy of the flow field predictions, a grid refinement study was not conducted, nor were comparisons made to determine the impact of the different turbulence models or discretization schemes.

The grid, or mesh, was constructed using the mesh generation software Gambit (Gambit, 1998). The diameter of the pipe was set to 88 mm, the same diameter as the pipe used in the experiments of Guymer and O'Brien (2000), and the length to 10 m. The pipe was meshed using the Cooper volume meshing scheme. This scheme treats a volume as a logical cylinder composed of two end faces and a barrel. The scheme projects the mesh from one of the end faces through the volume the other end face. The quad pave scheme was used to mesh one of the end faces. Grid density was controlled by specifying 40 nodal positions evenly around the circumference, which resulted in 145 face elements. Using this face as an input, the Cooper scheme replicated it 1448 times along the length of the barrel at intervals of 6.9 mm, making 209960 elements in total. A cross section through the mesh is shown in Figure 3.1.

Three boundary conditions were specified. One end of the pipe was specified as a velocity inlet, and the other a pressure outlet, while the barrel of the pipe was specified as a wall. The flow was given the properties of water at approximately 20 °C (density 998.2 kg/m^3, molecular weight 18.0152 kg/kgmol and absolute viscosity 1.003 x 10^{-3} kg/m s). Flow entered through the velocity inlet at a constant rate of 0.33 m/s evenly over the face. This is equivalent to 2 l/s or a Reynolds number of 29040 (based on mean velocity and pipe diameter). The turbulence parameters required for the velocity inlet and pressure outlet were based on this velocity. The standard k-ε turbulence model was used. Standard wall functions were used to model the near wall region, and the roughness height was set to 1 x10^{-5} m. The pipe was set to a horizontal position and gravity was modelled accordingly. Second order spatial discretization schemes were used throughout, except for pressure velocity coupling which used the SIMPLE scheme. The simulation was performed using the segregated implicit solver and was not stopped until the residuals became constant.

Figure 3.1 shows how the velocity magnitude changed over the cross section of the pipe with the distance from the inlet. At the inlet the velocity is constant over the face, except for the boundary layer cells as they are computed by the wall functions. Downstream of the inlet the shear stress from the wall retards the flow velocity in this region, so in order to obey continuity the velocity increases in the core. The flow field was found to have become fully developed at a distance of approximately 5 m or 55 D from the inlet.

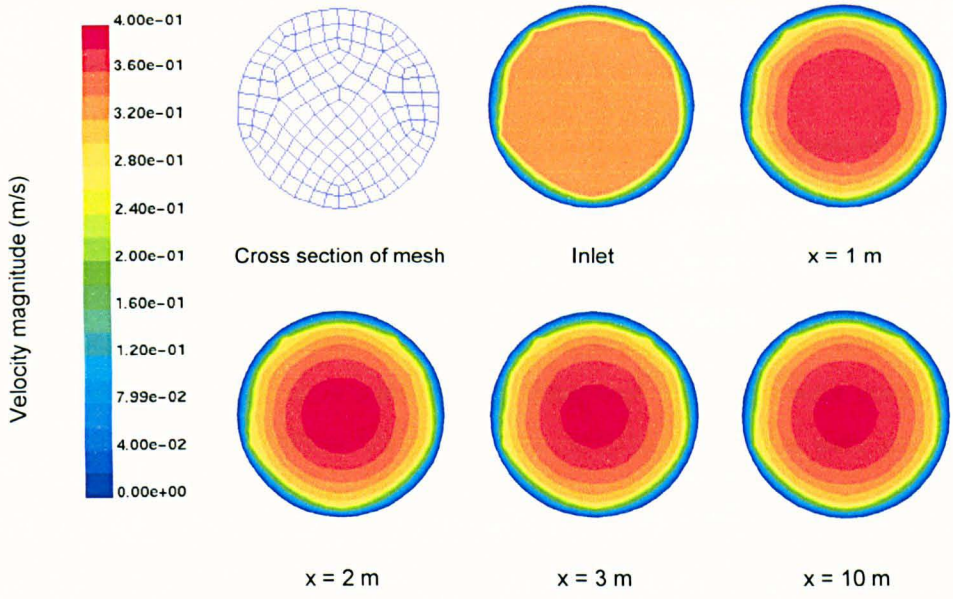

Figure 3.1 A cross section through the mesh and the change in velocity magnitude over the cross section and with distance from the inlet

In the tests reported by Guymer and O'Brien (2000) it was assumed that the flow conditions were fully developed by the first monitoring position. In order to create fully developed flow conditions along the whole pipe length, a second simulation was performed. Values for the three velocity components, the turbulent kinetic energy (k) and the turbulent dissipation rate (ε), were recorded at each cell over the outlet face, creating what is referred to as a profile. These values were then used as new inputs at the velocity inlet. Interpolation was not required as the two face meshes were identical. Apart from this change the second simulation was performed using the same modelling procedure as the first. Post processing showed the flow properties to be constant along the length of the pipe and equal to the values from the profile. The average y^+ value for the boundary layer cell was 58, which is within the recommended guidelines for the use of wall functions. It is this second fully developed flow that was used as a basis for the majority of the species transport parametric studies.

3.3.3 Parametric test 1: Spatial and temporal discretization scheme

3.3.3.1 Test aims and model configurations

The aim of the first series of tests was to assess the sensitivity of the simulation results to the choice of temporal and spatial discretization schemes over a range of time steps. Fluent's segregated solver supports two temporal discretization schemes, first and second order implict, and four spatial discretization schemes, first and second order upwind, power law and QUICK. Every combination of temporal and spatial discretization scheme was tested. When the first and second order upwind schemes were used the following four time steps were considered: 0.2, 0.1, 0.05 and 0.01 seconds. When the Power Law or QUICK schemes were used the 0.01 second time step was not considered. This created 28 separate tests.

A slug of the tracer (dye) was introduced into the primary water phase from the velocity inlet for 1.2 seconds. The movement of the tracer was then simulated until the mass fraction remaining in the pipe was zero. However, for the tests that used the QUICK scheme, trace elements always remained (a mass fraction of approximately 1 $x10^{-11}$). In this case the simulations were stopped when the mass fraction of the dye leaving the pipe was constant for fifty or more iterations.

The simulations were performed using the uncoupled processing technique on the fully developed flow field described in Section 3.3.2. The convergence criteria for the species transport equations were set to 1 $x10^{-3}$, with a maximum of 20 iterations per time step. For most of the time steps convergence was obtained within three iterations. However, the maximum number was required when the dye initially entered the pipe, or at the end of the simulation when low concentrations were left in the pipe. Increasing the maximum number of iterations would not have changed the solution as the residuals normally stabilised to a constant value after approximately 10 iterations.

The amount of CPU time required to complete a simulation was mostly dependent upon the size of the time step, and to a lesser extent upon the choice of temporal or spatial discretization scheme. Key outcomes relating to Parametric test 1 are plotted in Figure 3.8 to Figure 3.15, which have been grouped together at the end of this section.

3.3.3.2 Data analysis

Figure 3.2 shows a typical example of the spatial distribution of the tracer observed from the tests, with the front of the tracer plume shown in the foreground. The mass fraction, or concentration, was lower at the start and end of the plume, with a gradual increase to a peak concentration at the centre. The concentration of the dye was not constant over the cross section. This is in agreement with the work of Sayre (1968) (from Rutherford, 1994) who demonstrated that the concentration does not become uniform over the cross section even when

a tracer is well mixed. This occurs because velocity shear continually creates concentration gradients that are never entirely removed by the turbulent mixing.

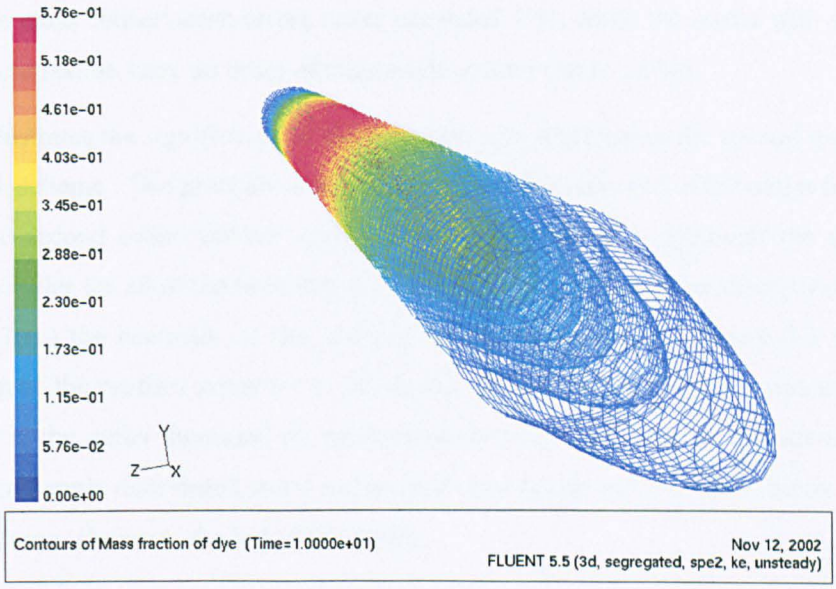

Figure 3.2 An example of the spatial distribution of the tracer

Figure 3.8 shows the temporal profiles recorded at each of the monitoring positions for the tests that used the first order temporal discretization scheme, while Figure 3.9 shows the temporal profiles recorded from the tests that used the second order temporal discretization scheme. In all of the tests the tracer is carried away from the point of discharge by the flow. As the tracer moves downstream the peak mass fraction reduces and the tracer spreads, a process termed longitudinal dispersion. The mean travel time of the tracer was approximately the same in all of the tests, but the amount of longitudinal dispersion was dependent upon the choice of the temporal discretization scheme and the size of the time step.

Moment analysis was used to provide insights into the transport, spread and conservation of the tracer. The results of the moment analysis are presented below.

3.3.3.2.1 Mass

When modelling the transport of a tracer it is usual to first confirm that the mass of the tracer has been conserved. The mass of the tracer at each of the monitoring locations was related to the initial mass of the injection, with the relative mass at each of the locations shown in Figure 3.10. In the majority of the tests the mass of the tracer initially changed before stabilising to a constant value. The distance required for the mass to stabilise was dependent upon the size of the time step, with a longer distance required for larger time steps. For the tests that used the second order temporal discretization scheme with a time step of 0.2 seconds the mass of the tracer did not stabilise. However, the increase in the mass reduced with distance, suggesting that the mass might stabilise over a longer distance. In some instances the mass of the tracer

changed between eight and ten metres. This is a consequence of poor convergence when low concentrations of dye remained in the pipe and is therefore not representative of what happens at this distance. In all cases where the first order temporal discretization schemes were employed the mass conservation errors never exceeded 1 %, while the errors with second order temporal discretization were an order of magnitude greater (up to 12 %).

Figure 3.3 illustrates the significance of the time step size when using the second order temporal discretization scheme. The plots show the temporal profiles recorded at the outlet from the tests that used the second order upwind spatial discretization scheme, although the shape of the profiles are similar for all of the tests that used the second order temporal discretization scheme. In Figure 3.3 (a) the centroids of the profiles are at $t = 0$, while in Figure 3.3 (b) the peak concentration of the profiles are at $t = 0$. When the time step of 0.2 seconds was used the mass of the tracer at the outlet increased by approximately twelve percent. It appears that the extra mass is not uniformly distributed and is not proportional to the concentration, but is added to the start of the plume (shown to the left of the plots).

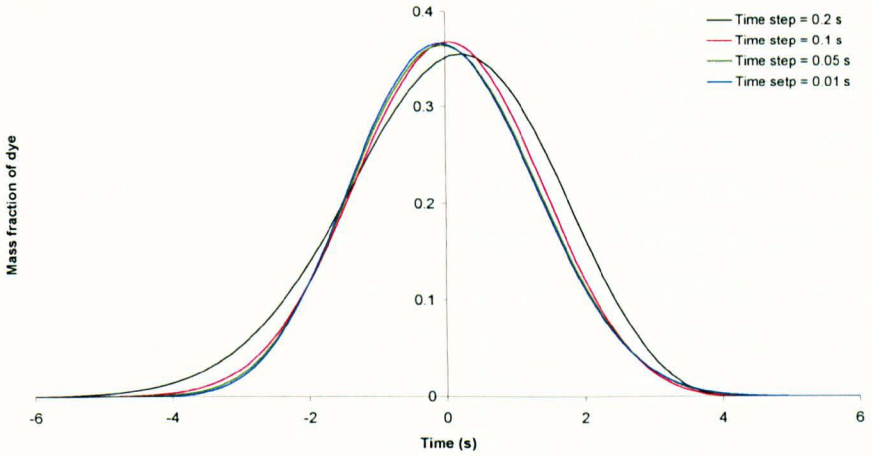

(a) Centroid of the profiles at t = 0.

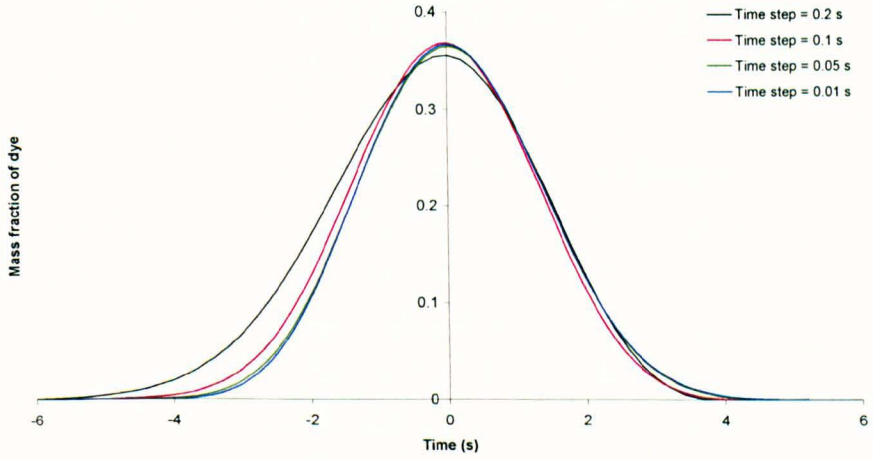

(b) Peak concentration of the profiles at t = 0

Figure 3.3 The temporal profiles recorded at the outlet

The criteria used to determine whether the mass of the tracer was conserved were a stable mass and a difference of less than one percent from the initial injection. This criteria was reached for all of the tests that used the first order temporal discretization scheme, and for the tests that used the second order temporal discretization scheme with a time step of 0.01 or 0.05 seconds. The criteria were not reached for the tests that used the second order temporal discretization scheme with a time step of 0.1 or 0.2 seconds. When the 0.1 second time step was used the mass of the tracer was constant after four metres, but the change was greater than one percent. When the 0.2 second time step was used the mass of the tracer continually increased with distance, with an increase of approximately ten percent from the initial mass at the outlet.

3.3.3.2.2 Mean travel time

The mean travel time of the tracer between each of the monitoring positions is shown in Figure 3.11. As the discharge was constant, and the flow field was fully developed along the length of the pipe, the mean travel time of the tracer should have been constant and equal to the mean travel time of the flow, which was 6.06 seconds between the monitoring positions. The mean travel time of the tracer was, however, not constant and was dependent upon the distance from the inlet, the spatial and temporal discretization schemes, and the size of the time step. The greatest change in the travel time occurred between the inlet to two metres and two to four metres. This change was most likely caused by a combination of the injection method, slight imperfections in the flow field close to the inlet and poor convergence when the tracer was first introduced. Changes in the travel time, either a slight increase or decrease, also occurred along the length of the pipe. These changes were caused by small variations in the flow field.

To determine the accuracy of the predictions, the mean travel time of the tracer was compared to the mean travel time of the flow. The comparison was made between two and ten metres to minimise the imperfections in the flow field close to the inlet and the variations in the flow field along the length of the pipe. The mean travel times of the tracer over this distance are plotted against time step in Figure 3.4. The mean flow rate was 0.33 m/s, resulting in a mean travel time of 24.24 seconds over a distance of eight metres. When the time step was small, 0.05 seconds or less, all of the predictions of mean travel time were similar to the mean travel time of the flow. When the time step was greater than 0.05 seconds the range of the predictions increased and they were generally worse. However, all of the predictions were within one percent of the mean flow and can be considered sufficiently accurate.

It is interesting to note that the predictions of mean travel time are not the same for the tests that used the same temporal or spatial discretization scheme. However, the travel times predicted using the second order upwind and QUICK spatial discretization schemes were almost identical for both of the temporal discretization schemes and across all of the time steps.

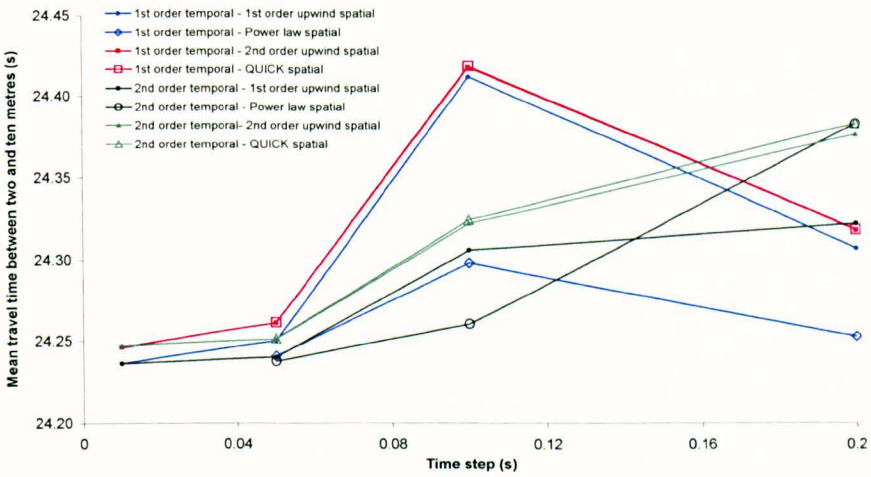

Figure 3.4 Mean travel times between 2 and 10 m (Parametric test 1)

3.3.3.2.3 Temporal variance

The temporal variance of the tracer at each monitoring location is shown in Figure 3.12, and the difference in the temporal variance between monitoring positions in Figure 3.13. When the first order temporal discretization scheme was used, or the second order temporal discretization scheme with a time step of 0.01 or 0.05 seconds, the variance of the tracer increased linearly with distance after two metres from the inlet, therefore following the idealised Fickian model predictions described in Chapter 2. The increase in variance reduced with distance when the second order temporal discretization scheme was used with larger time steps. The author is unaware of any published data showing this under similar flow conditions.

The variance was dependent upon the size of the time step when the first order temporal scheme was used. This is a result of numerical dispersion in the model. The cause of numerical dispersion is discussed in Section 3.3.3.3. Numerical dispersion was less evident in the tests that used the second order temporal discretization scheme, particularly when the time step was 0.1 seconds or less. To further illustrate the significance of the time step on the temporal discretization schemes consider Figure 3.5. The plot shows a cross section through the pipe and the spatial distribution of the tracer at the largest and smallest time steps from two of the tests that used the first order temporal discretization scheme and two of the tests that used the second order temporal discretization scheme. All of the tests show the tracer spreading. When the second order scheme was used, the spread of the tracer was approximately the same for both of the time steps, but when the first order scheme was used the spread of the tracer was different, with considerably more dispersion at the larger time step.

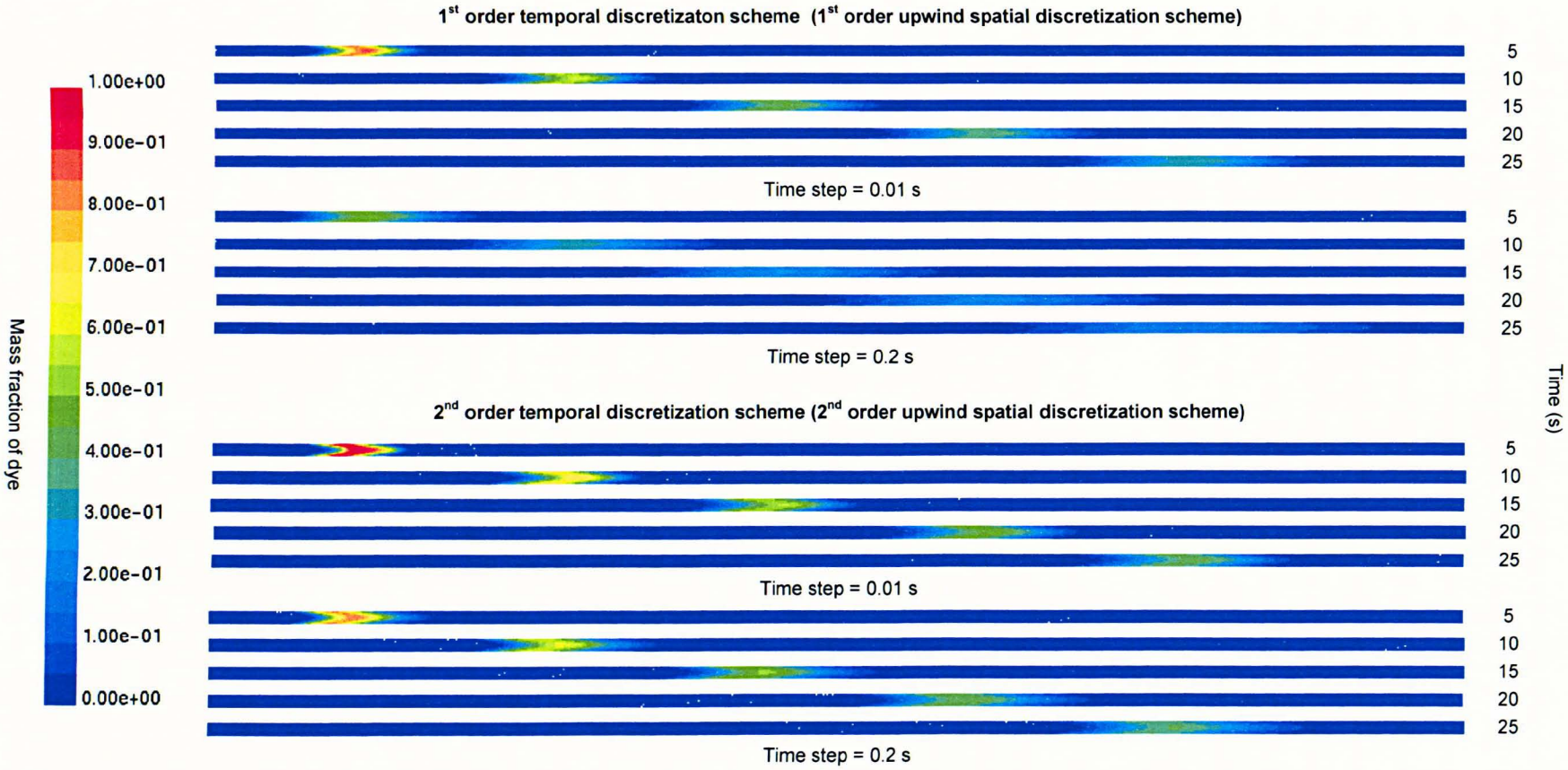

Figure 3.5 A comparison between the spatial distributions of the tracer at different times

3.3.3.2.4 Coefficient of skewness

Figure 3.14 shows the coefficient of skewness of the tracer at each monitoring position. Tests that used the first order temporal discretization scheme, or the second order temporal discretization scheme with a time step of 0.01 or 0.05 seconds showed the same trends. The coefficient initially increased and became positive. A peak value was reached a short distance from the inlet, followed by a continuous reduction, therefore following the idealised Fickian model. When the second order temporal discretization scheme was used with a time step of 0.1 or 0.2 seconds the coefficient initially increased, but was negative. When the time step of 0.1 seconds was used the coefficient remained approximately constant with distance, but when the 0.2 second time step was used the coefficient continually increased with distance, although the rate of increase reduced.

These differences may be attributed to the conservativeness of the modelling configuration. Figure 3.3 shows the temporal profiles recorded at the outlet from two of the tests that used the second order temporal discretization scheme. When the 0.1 and 0.2 second time steps were used the model created extra mass that was added to the front of the tracer plume and it is this that created the negative skewness.

According to the definition of the equilibrium zone proposed in Chapter 2 the tracer entered the zone after two metres from the inlet in all of the tests that used the first order temporal discretization scheme, and in the tests that used the second order temporal discretization scheme with a time step of 0.01 or 0.05 seconds. This was a comparatively short distance as the general guidelines for river flow is 100 - 300 channel widths (Rutherford, 1994). Less distance was needed in the CFD models because the tracer was evenly injected over the cross section, whereas for river studies the tracer usually originates from a single point source, and as a consequence takes longer to become fully mixed. For the remaining tests the criteria for the equilibrium zone was not reached and the movement of the tracer could not, therefore, be accurately modelled using the one dimensional form of the advection diffusion equation, Equation 2.16.

3.3.3.2.5 Longitudinal dispersion coefficient

Figure 3.15 shows the variation in the longitudinal dispersion coefficient between monitoring positions. For all of the tests that used the first order temporal discretization scheme, and for the tests that used the second order temporal discretization scheme with a time step of 0.01 or 0.05 seconds, the dispersion coefficient was constant with distance once the tracer was in the equilibrium zone. To confirm that the calculated values of the dispersion coefficient were accurate the temporal profiles recorded at two metres were routed downstream to ten metres using the constant value of the dispersion coefficient and the frozen cloud assumptions discussed in Chapter 2. The comparison between the predicted and recorded profiles was

excellent, with a typical R^2 value of greater than 0.999. An example is shown in Figure 3.6 (the data presented is for the test that used the second order temporal discretization scheme, second order upwind spatial discretization scheme and a time step of 0.01 seconds).

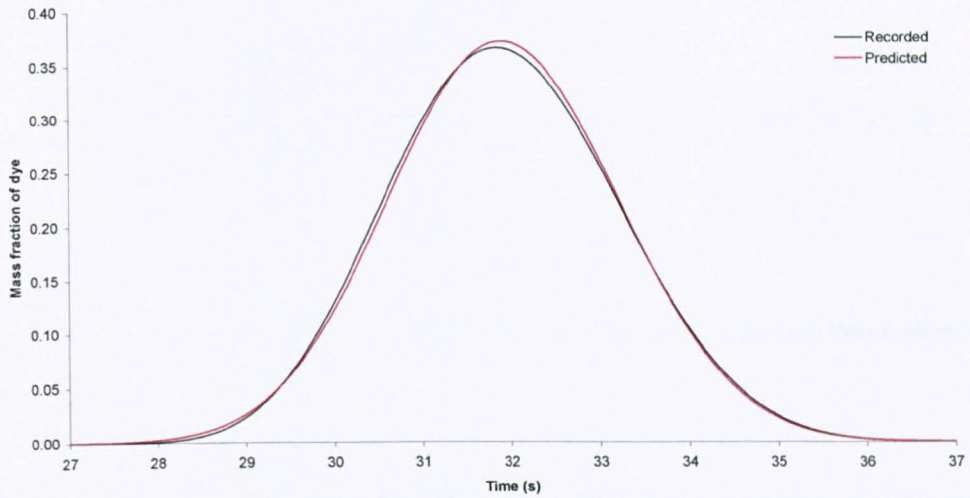

Figure 3.6 An example of the predicted and recorded profiles

The dispersion coefficients obtained from the equilibrium zone are plotted against time step in Figure 3.7. For the tests that used the second order temporal discretization scheme and a time step of 0.1 or 0.2 seconds an average of the values between 6 and 10 m is presented. When the first order temporal discretization scheme was used the value of the coefficient was mostly dependent upon the size of the time step and to a lesser extent upon the spatial discretization scheme. The coefficient increased almost linearly with time step, resulting in approximately three times the amount of dispersion at a time step of 0.2 seconds compared to a time step of 0.01 seconds. This again demonstrates numerical dispersion in the model. The coefficient was independent of the size of the time step and dependent only upon the choice of the spatial discretization scheme when the second order temporal discretization scheme was used with a time step equal to, or below, 0.05 seconds. At larger time steps the coefficient appeared to became dependent upon the size of the time steps as well. However, these values are not true reflections as the criteria to use the one dimensional form of the advection-diffusion equation had not been met.

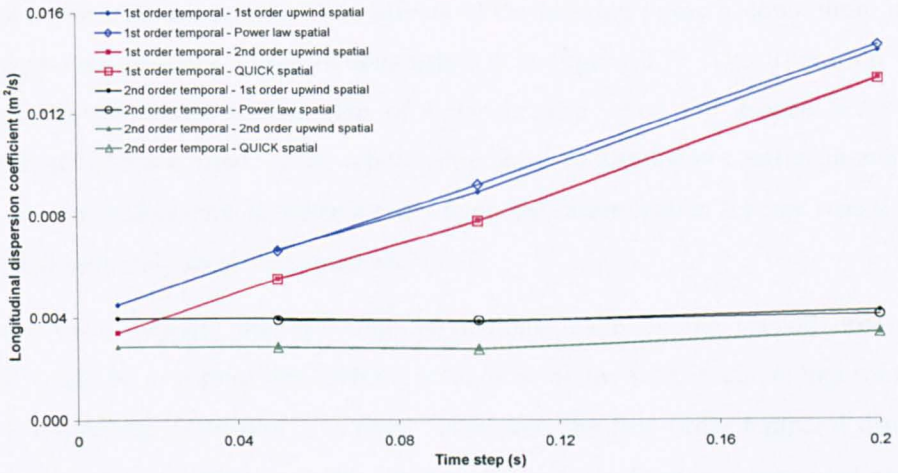

Figure 3.7 Variation in the longitudinal dispersion coefficient with time step (Parametric test 1)

3.3.3.3 Conclusion

In this series of tests the impact of the temporal and spatial discretization schemes on the predictions of solute transport were considered over a range of time steps. Two temporal and four spatial discretization schemes were considered. The tests demonstrated that the choice of the temporal discretization scheme was more significant than the choice of the spatial discretization scheme

The predictions were robust when the first order temporal discretization scheme was used. At every time step the mass conservation criteria was reached, the mean velocity of the tracer was approximately the same as the mean velocity of the flow and the change in the variance and coefficient of skewness with distance followed the idealised Fickian model. However the predictions made by the model suffered from numerical dispersion, shown by a change in the spread of the tracer with time step. This occurred even though the number of iterations used per time step was within the guidelines recommended by the Fluent 5 User's Guide (Fluent, 1998).

The predictions made by the second order temporal discretization scheme were not robust at all of the time steps. When the 0.1 or 0.2 second time steps were used the mass conservation criteria was not reached. Extra mass was added to the start of the tracer plume causing the variance to increase non linearly and the coefficient of skewness to become negative. The model's predictions were robust when the 0.01 or 0.05 second time steps were used, shown by mass conservation, accurate travel time predictions and a linear increase in the variance. The effects of numerical dispersion on the predictions were much less, with time step independence being judged to have occured below 0.05 seconds.

An amount of numerical error must occur in CFD models because higher order terms are missed out when representing the governing equations in a discrete form. The errors that occur are often referred to as truncation errors. Higher order schemes include more higher order terms

which reduces the truncation error. The effects of the missing terms become more significant when the time step is large. This is demonstrated in Figure 3.7. The truncation error was practically removed below a time step of 0.05 seconds when the second order temporal discretization scheme was used. If the relationship between dispersion coefficient and time step continued, the truncation error in the first order temporal discretization scheme would have been present until an infinitely small time step was used.

These observations suggest that only the predictions made by the second order temporal discretization scheme at a time step of 0.05 seconds or below were accurate and robust for the purposes of modelling dispersion in a pipe. However, the first order temporal discretization scheme should not be eliminated at this stage as the poor performance may well reflect other assumptions that have been made in the model set up. For this reason the option is retained for the following two parametric tests.

The tests demonstrated the predictions made by that the first order upwind and the power law spatial discretization schemes, and the second order upwind and QUICK spatial discretization schemes were similar. Therefore to save time and resources only the first and second order upwind schemes were considered further.

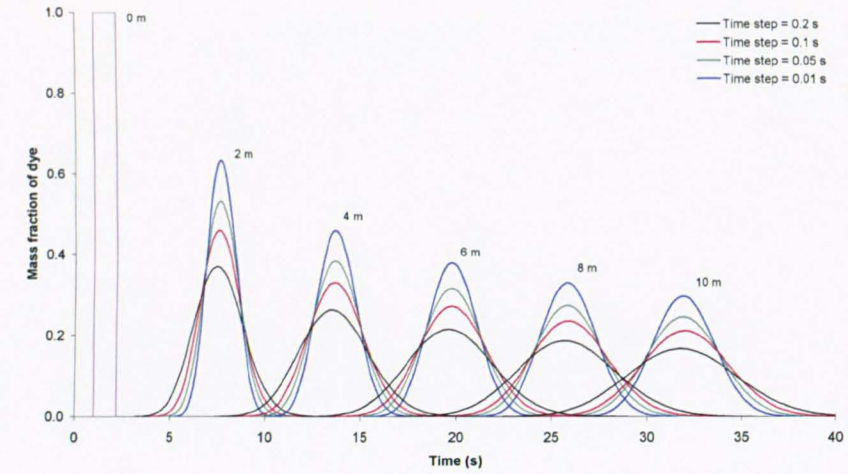

First order upwind spatial discretization

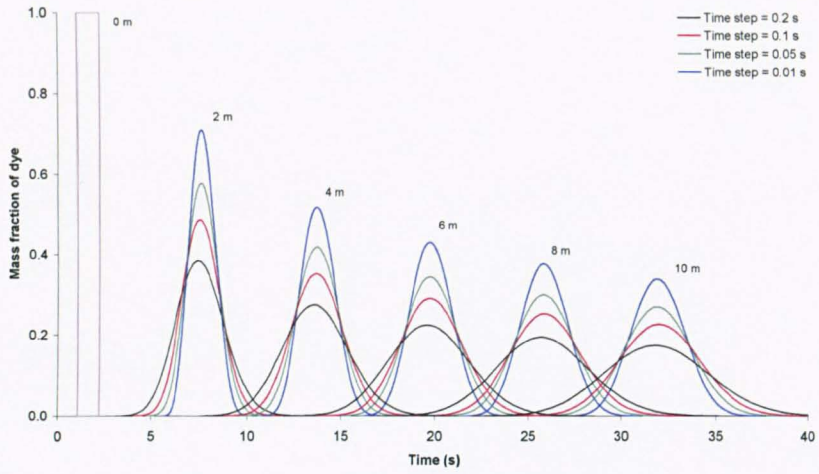

Second order upwind spatial discretization

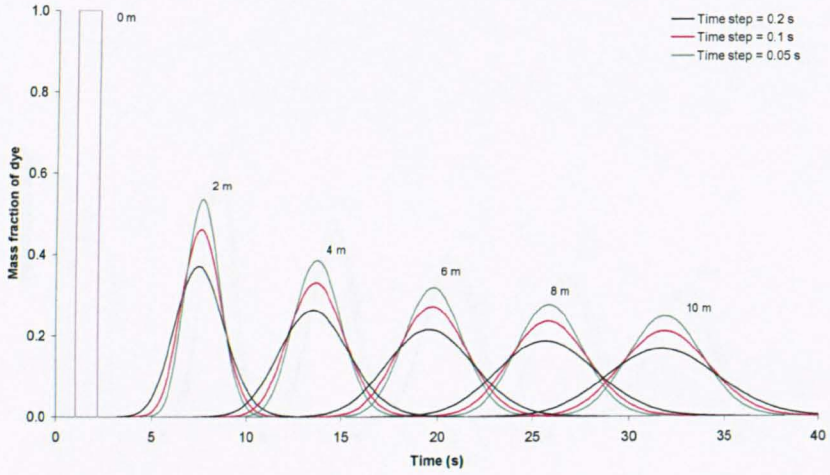

Power law spatial discretization

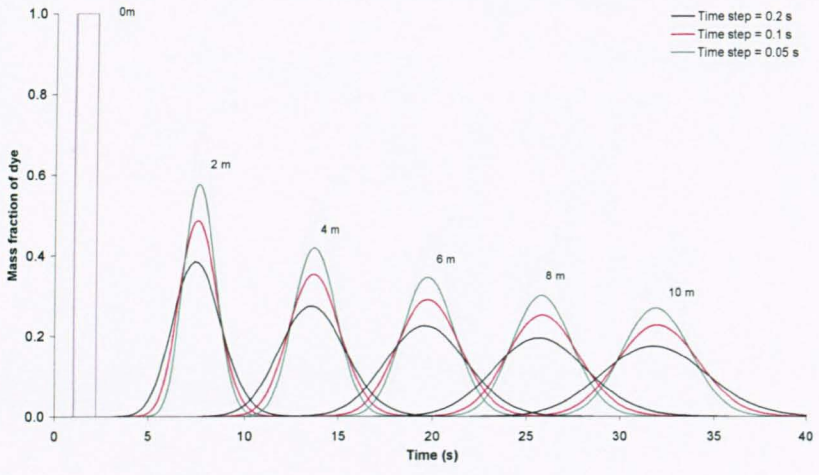

QUICK spatial discretization

Figure 3.8 First order temporal discretization temporal profiles (Parametric test 1)

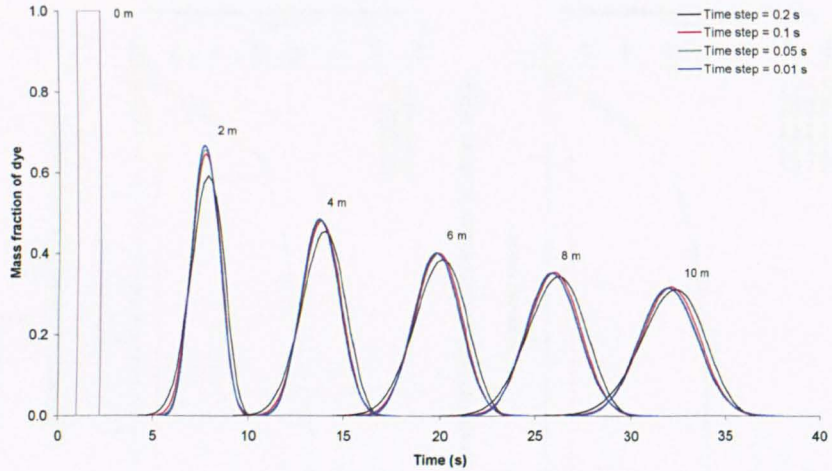

First order upwind spatial discretization

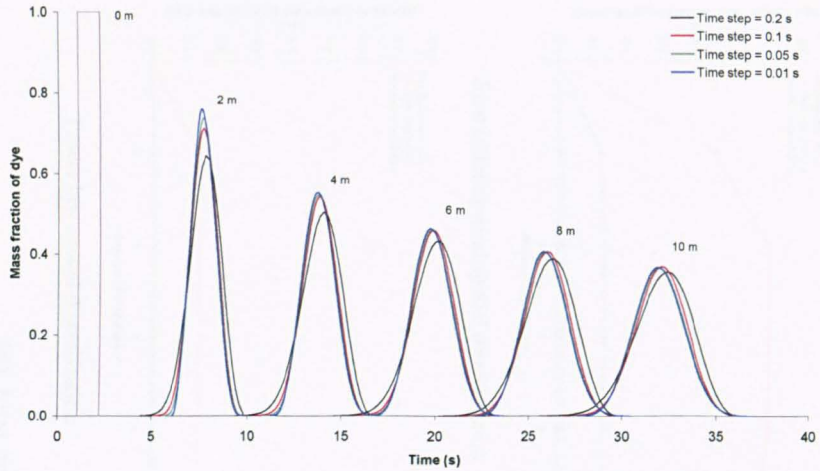

Second order upwind spatial discretization

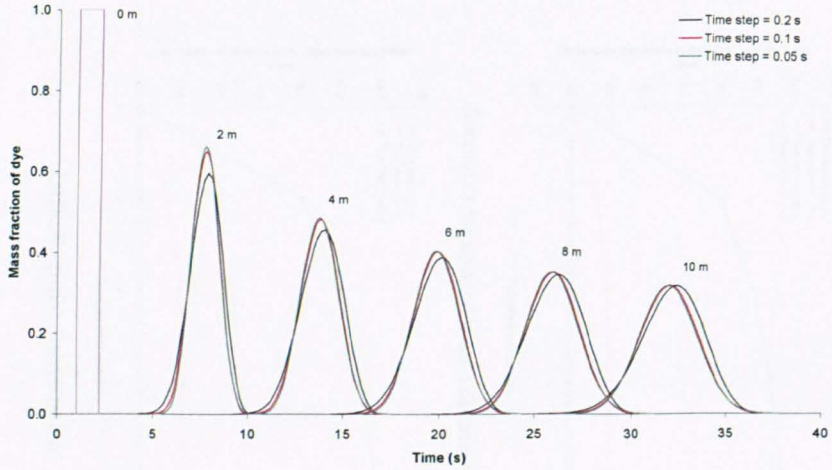

Power law spatial discretization

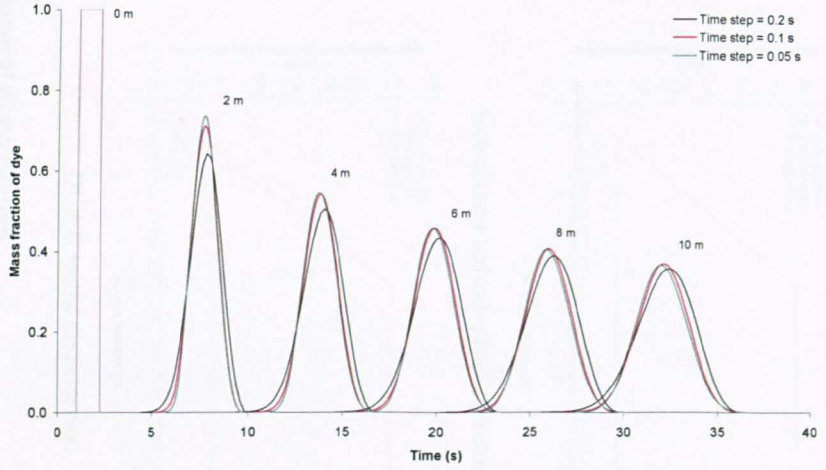

QUICK spatial discretization

Figure 3.9 Second order temporal discretization temporal profiles (Parametric test 1)

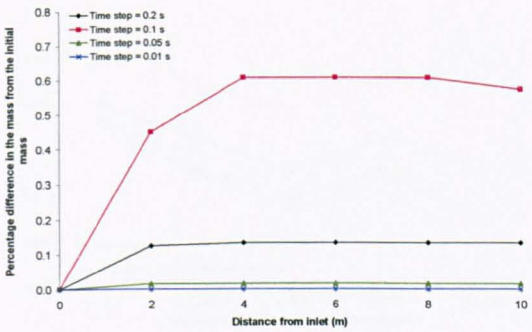

First order upwind spatial discretization

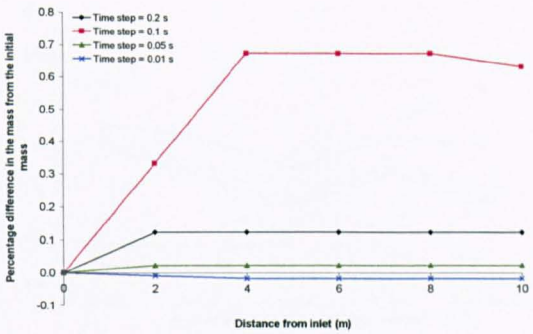

Second order upwind spatial discretization

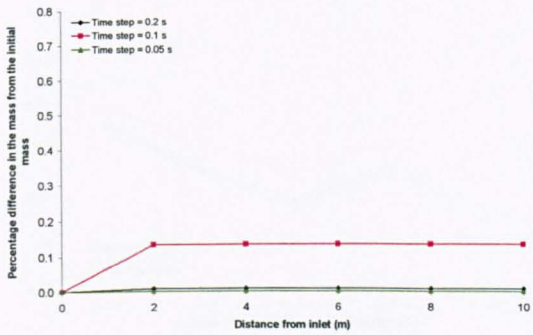

Power law spatial discretization

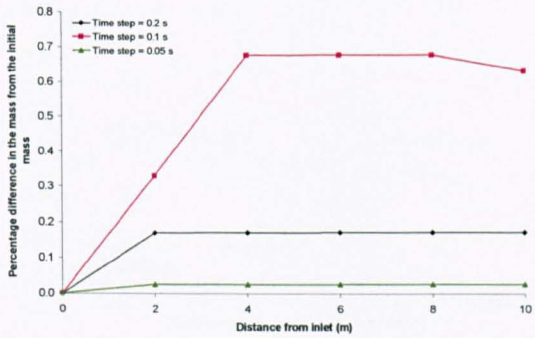

QUICK spatial discretization

(a) First order temporal discretization

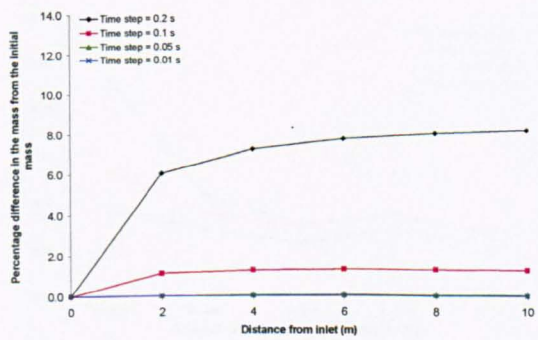

First order upwind spatial discretization

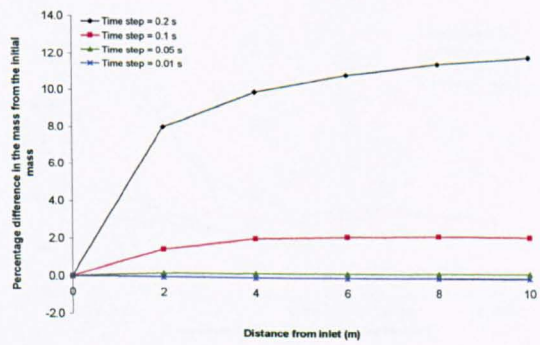

Second order upwind spatial discretization

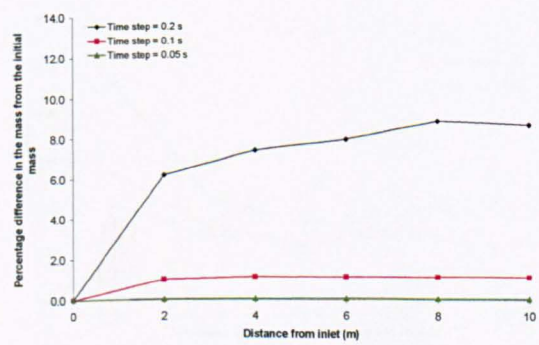

Power law spatial discretization

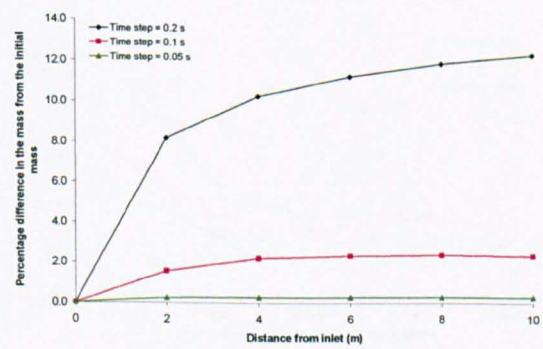

QUICK spatial discretization

(b) Second order temporal discretization

Figure 3.10 Mass (Parametric test 1)

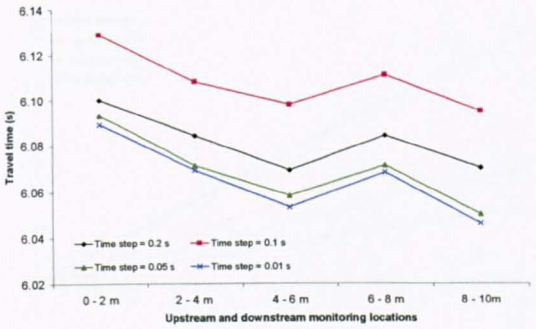

First order upwind spatial discretization

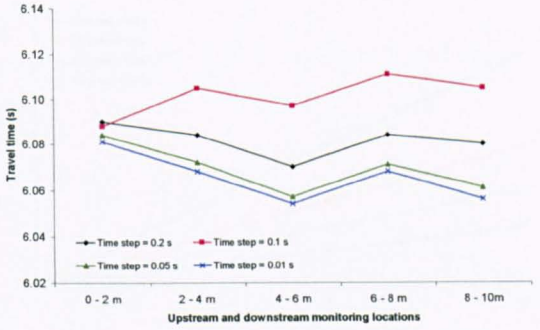

Second order upwind spatial discretization

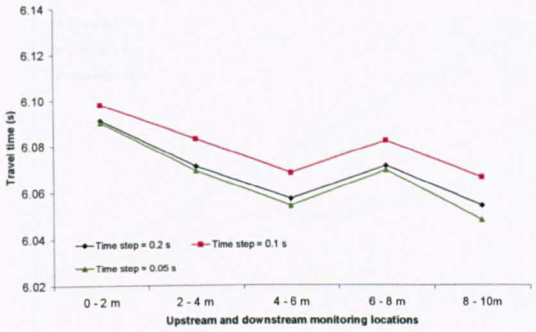

Power law spatial discretization

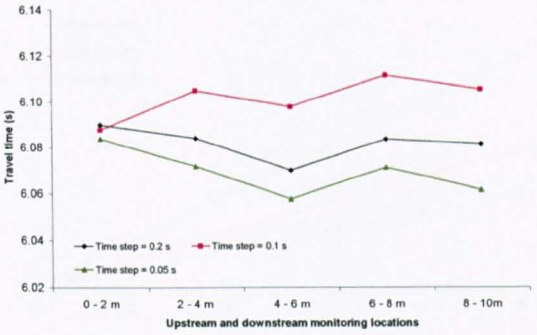

QUICK spatial discretization

(a) First order temporal discretization

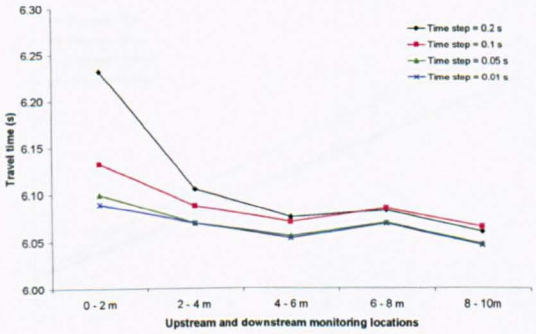

First order upwind spatial discretization

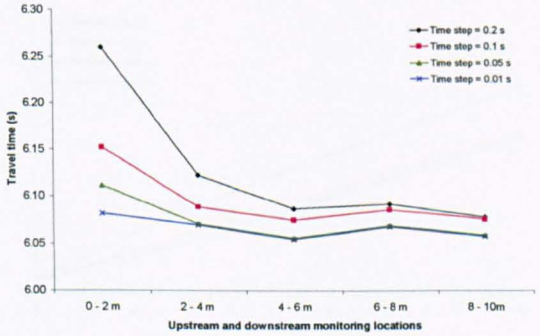

Second order upwind spatial discretization

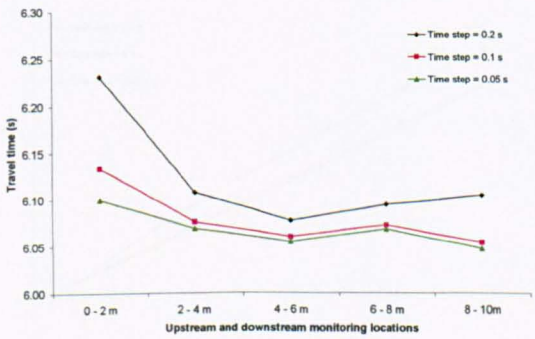

Power law spatial discretization

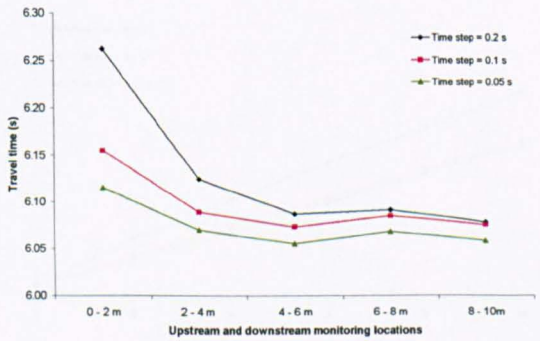

QUICK spatial discretization

(b) Second order temporal discretization

Figure 3.11 Mean travel time (Parametric test 1)

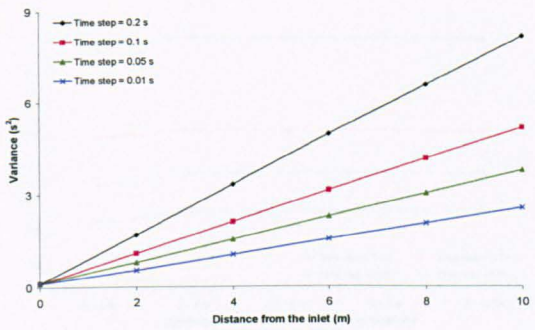

First order upwind spatial discretization

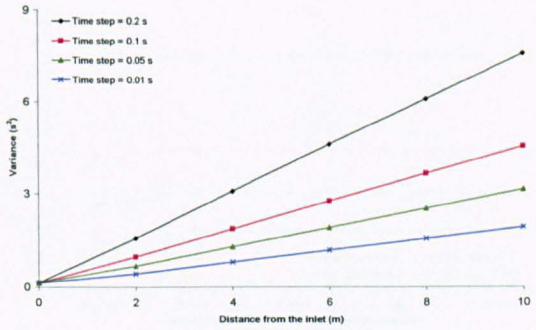

Second order upwind spatial discretization

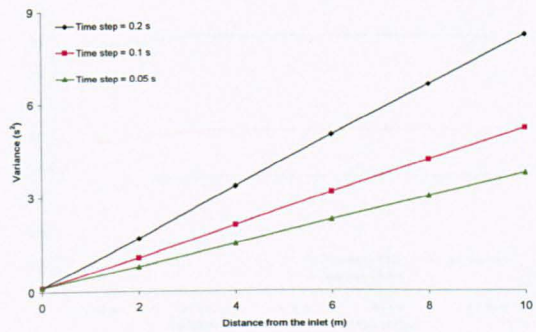

Power law spatial discretization

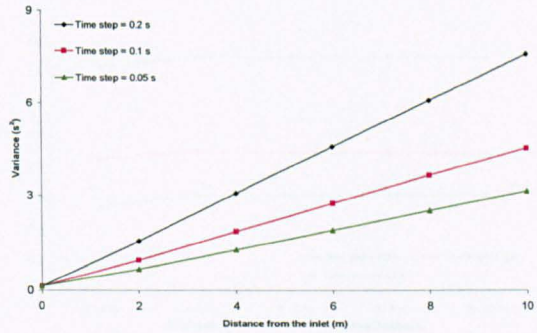

QUICK spatial discretization

(a) First order temporal discretization

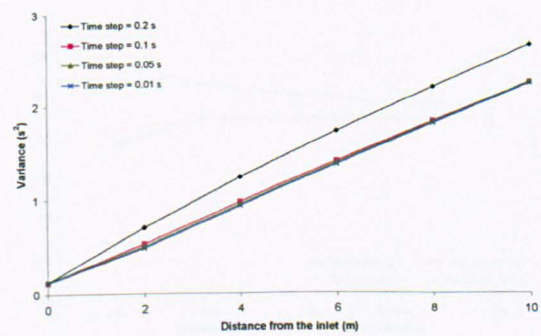

First order upwind spatial discretization

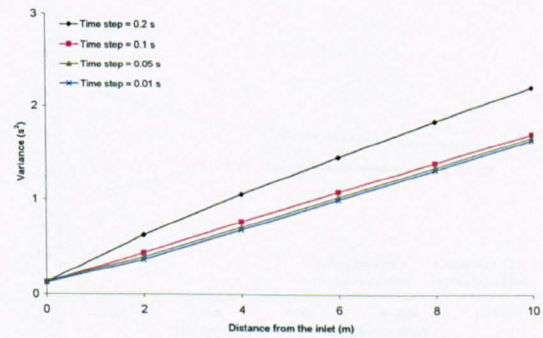

Second order upwind spatial discretization

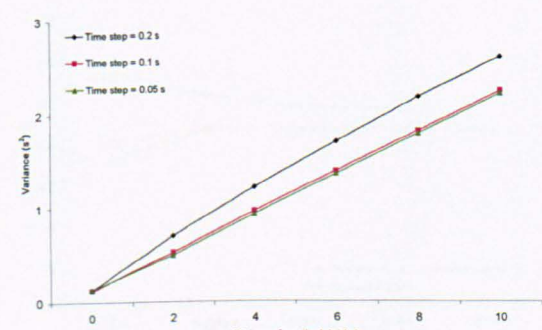

Power law spatial discretization

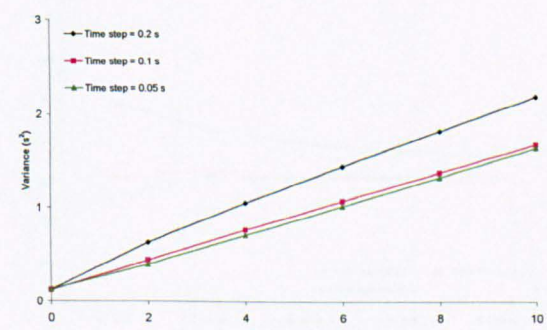

QUICK spatial discretization

(b) Second order temporal discretization

Figure 3.12 Temporal variance (Parametric test 1)

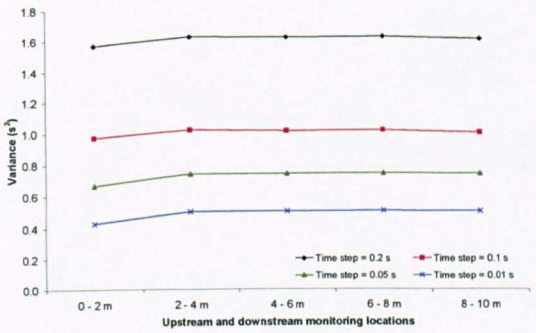

First order upwind spatial discretization

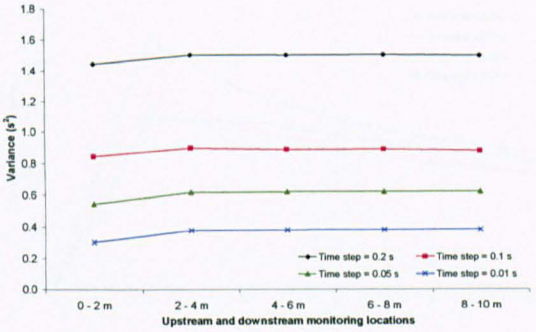

Second order upwind spatial discretization

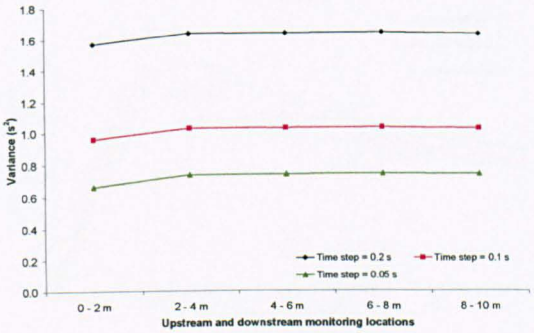

Power law spatial discretization

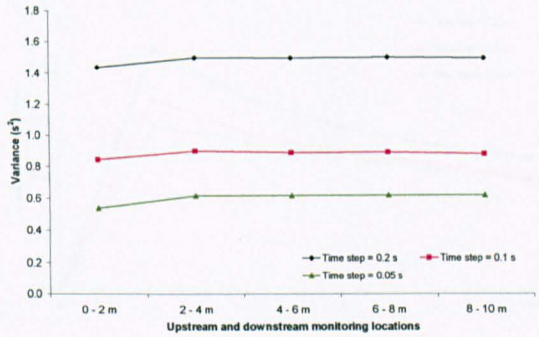

QUICK spatial discretization

(a) First order temporal discretization

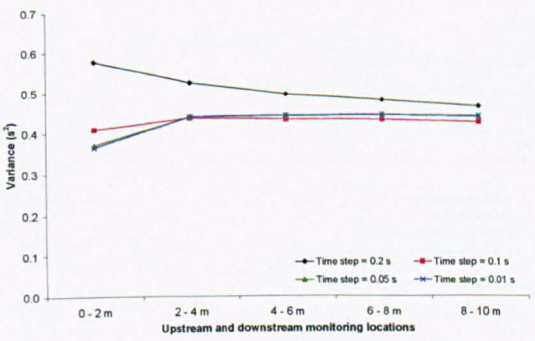

First order upwind spatial discretization

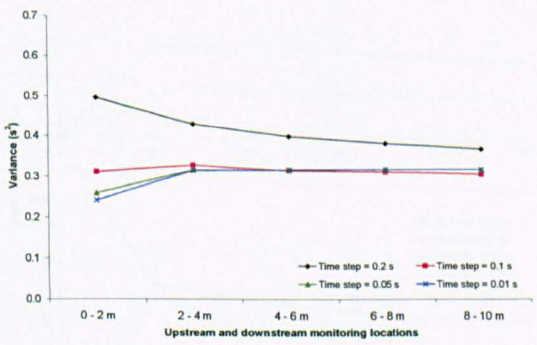

Second order upwind spatial discretization

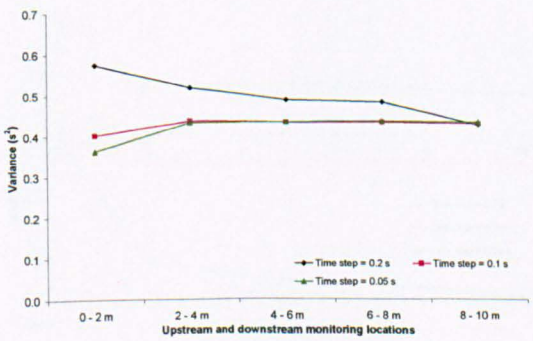

Power law spatial discretization

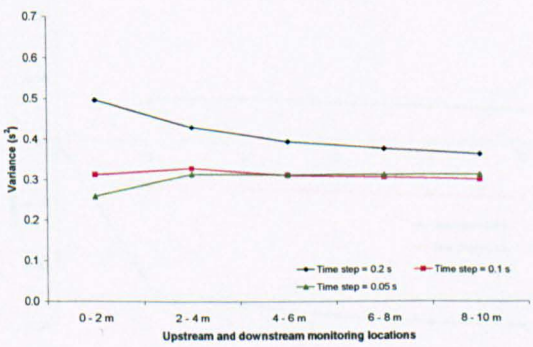

QUICK spatial discretization

(b) Second order temporal discretization

Figure 3.13 Temporal variance (2) (Parametric test 1)

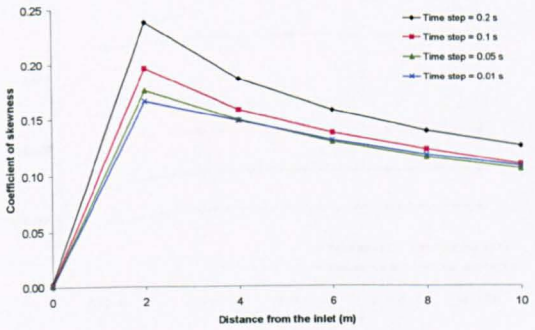

First order upwind spatial discretization

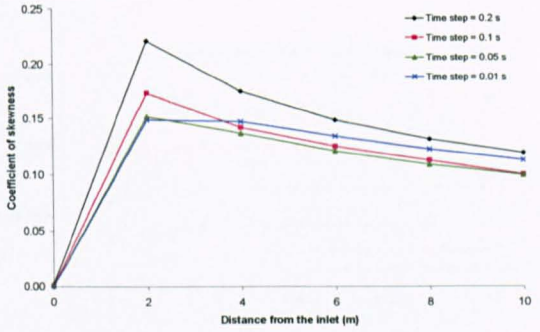

Second order upwind spatial discretization

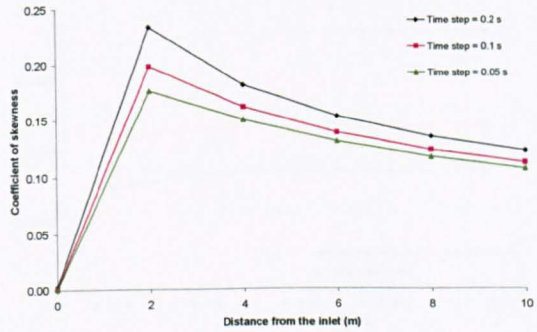

Power law spatial discretization

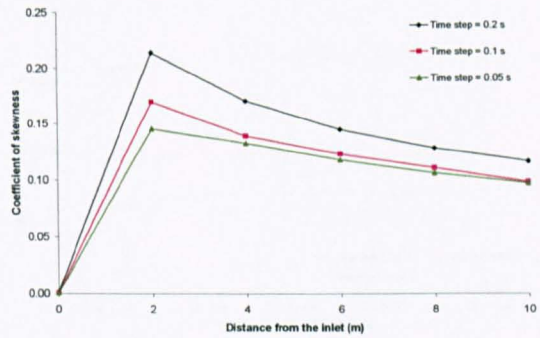

QUICK spatial discretization

(a) First order temporal discretization

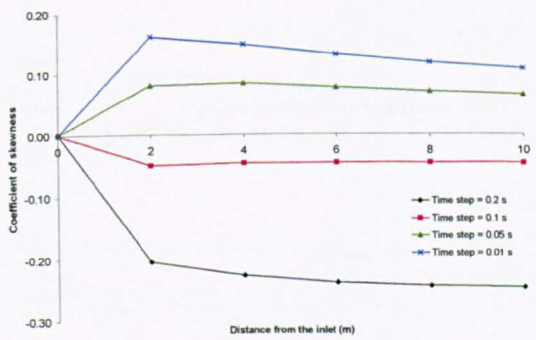

First order upwind spatial discretization

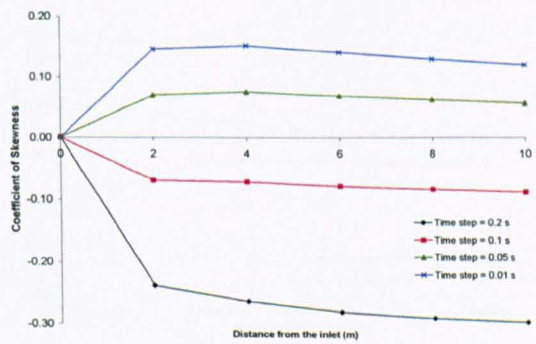

Second order upwind spatial discretization

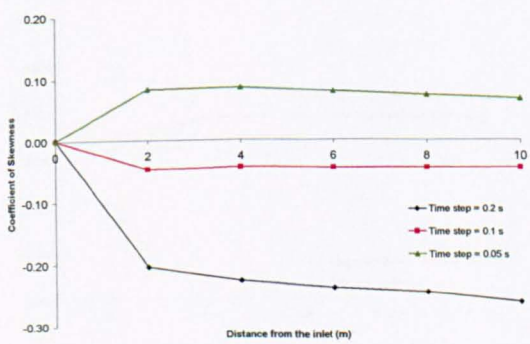

Power law spatial discretization

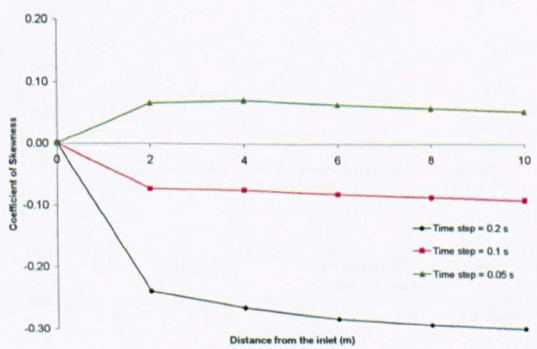

QUICK spatial discretization

(b) Second order temporal discretization

Figure 3.14 Coefficient of skewness (Parametric test 1)

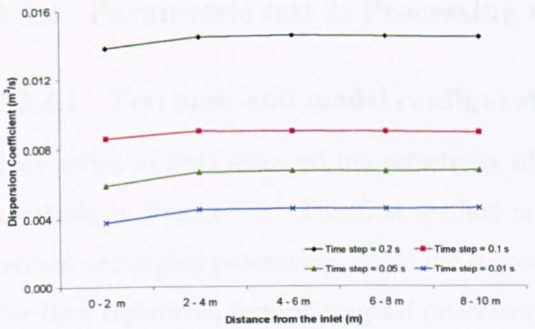

First order upwind spatial discretization

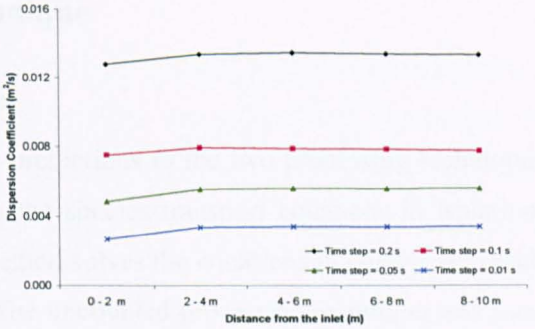

Second order upwind spatial discretization

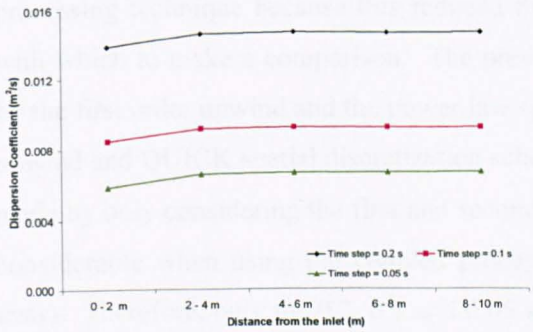

Power law spatial discretization

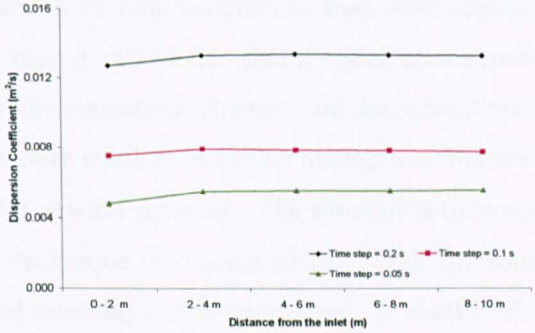

QUICK spatial discretization

(a) First order temporal discretization

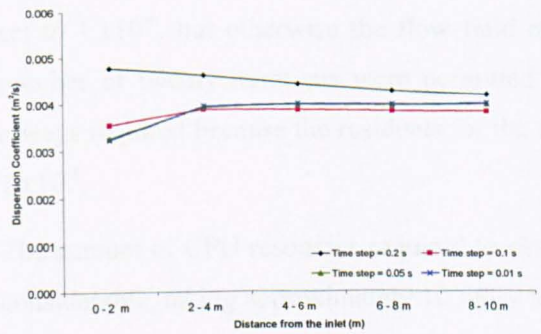

First order upwind spatial discretization

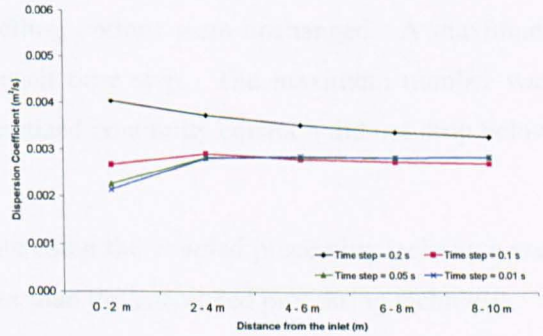

Second order upwind spatial discretization

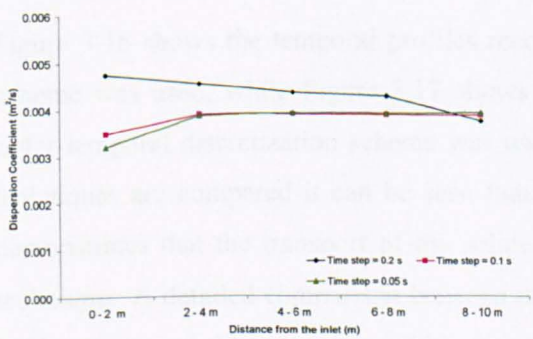

Power law spatial discretization

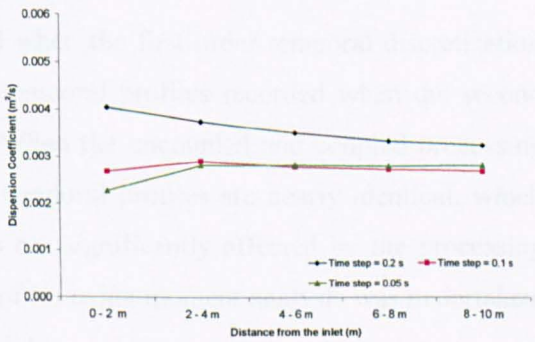

QUICK spatial discretization

(b) Second order temporal discretization

Figure 3.15 Longitudinal dispersion coefficient (Parametric test 1)

3.3.4 Parametric test 2: Processing technique

3.3.4.1 Test aims and model configurations

This series of tests assessed the sensitivity of the predictions to the two processing techniques available in Fluent 5.5. The first method solves the species transport equations in isolation, termed uncoupled processing, while the second method solves the equations in conjunction with the flow equations, termed coupled processing. The uncoupled processing technique was used in Parametric test 1. To save time and resources the same tests were repeated using the coupled processing technique because this reduced the number of new simulations that were required with which to make a comparison. The previous tests demonstrated that the predictions made by the first order upwind and the power law spatial discretization schemes, and the second order upwind and QUICK spatial discretization schemes were similar. A further saving was therefore made by only considering the first and second order upwind schemes. The simulation time was considerable when using the coupled processing technique (in excess of one week for some tests). Therefore, only the 0.2, 0.1 and 0.05 second time steps were considered. In total twelve new simulations were performed.

The flow field used as a basis for both of the simulation techniques is described in Section 3.3.2. In an attempt to obtain a fully converged solution at each time step the convergence criteria was set to 1×10^{-8}, but otherwise the flow field modelling options were unchanged. A maximum number of twenty iterations were permitted at each time step. The maximum number was always required because the residuals for the discretized continuity equation did not drop below 1×10^{-8}.

The amount of CPU resources required to simulate using the coupled processing technique was considerable, taking approximately 10 times longer than the uncoupled processing technique.

3.3.4.2 Data analysis

Figure 3.16 shows the temporal profiles recorded when the first order temporal discretization scheme was used, while Figure 3.17 shows the temporal profiles recorded when the second order temporal discretization scheme was used. When the uncoupled and coupled processing techniques are compared it can be seen that the temporal profiles are nearly identical, which demonstrates that the transport of the solute was not significantly affected by the processing technique. A detailed comparison between the profiles using moment analysis was undertaken, but is not presented because it provides no new insights.

3.3.4.3 Conclusion

There was no significant differences between the predictions of solute transport made using the uncoupled and coupled processing techniques. This occurred because the flow field was fully developed at the start of the test and no flow field modelling options were changed. The small differences between the predictions was most likely to have been caused by the species transport equations being resolved to 1×10^{-8} instead of 1×10^{-3}. Subsequent tests were conducted using only the uncoupled technique as the coupled processing technique required substantially more CPU time.

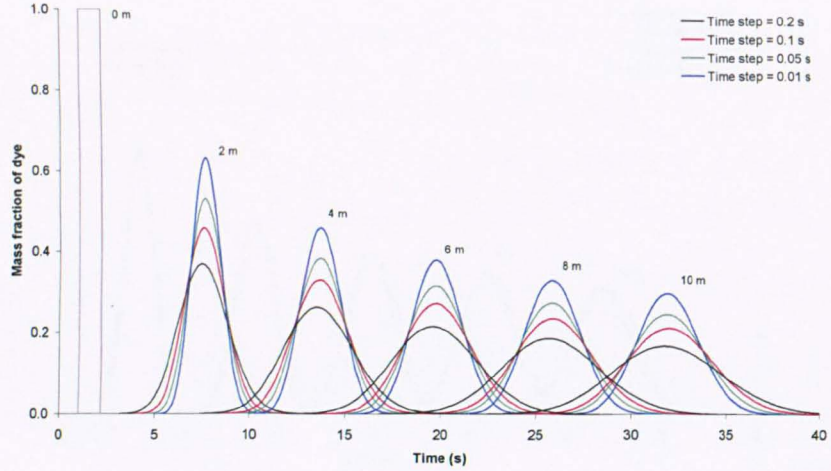

First order upwind spatial discretization – Uncoupled processing technique

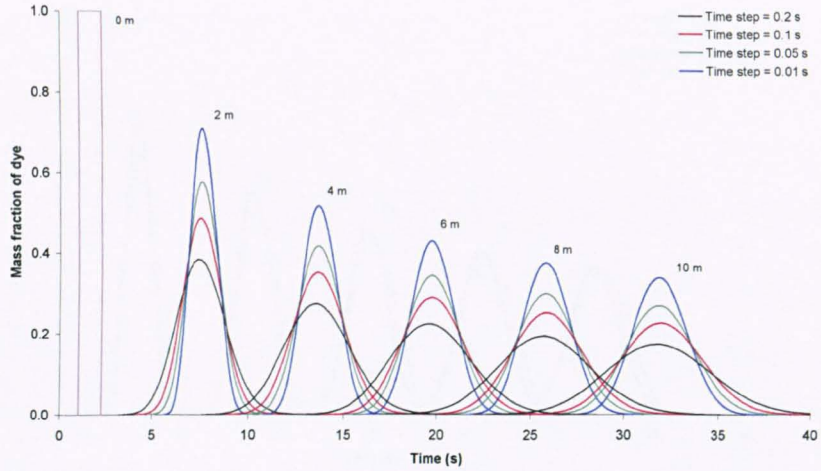

Second order upwind spatial discretization – Uncoupled processing technique

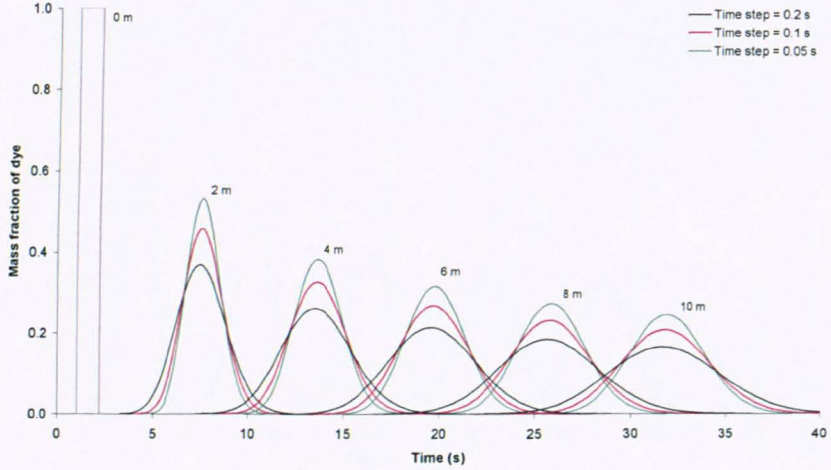

First order upwind spatial discretization – Coupled processing technique

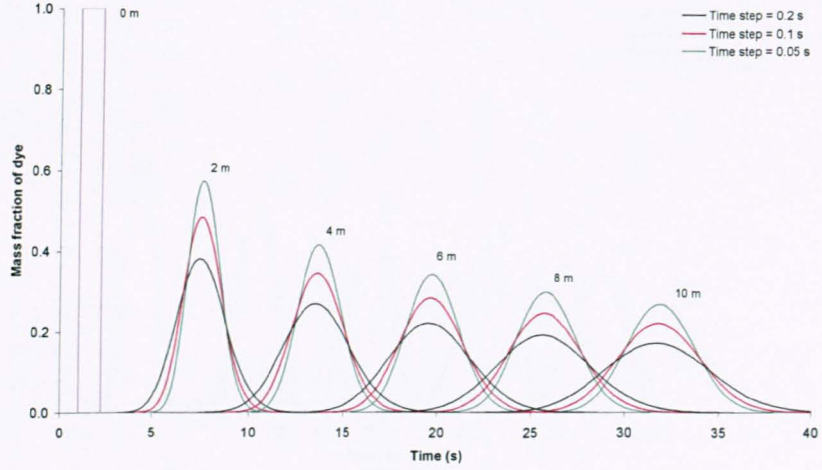

Second order upwind spatial discretization – Coupled processing technique

Figure 3.16 First order temporal discretization temporal profiles (Parametric test 2)

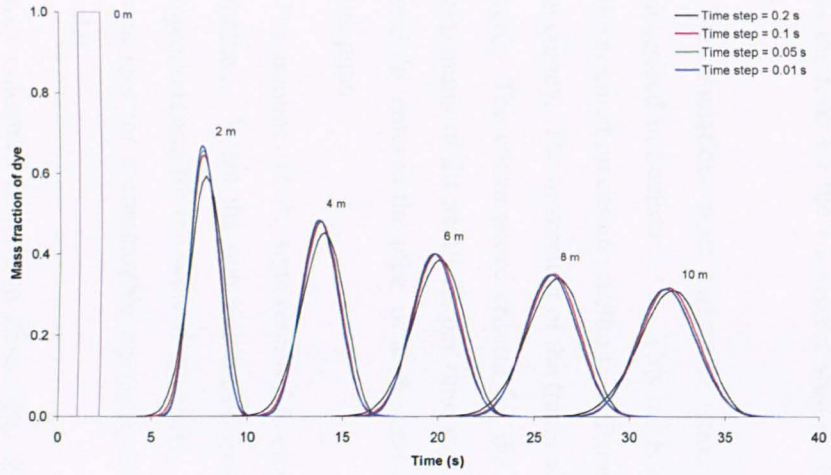

First order upwind spatial discretization – Uncoupled processing technique

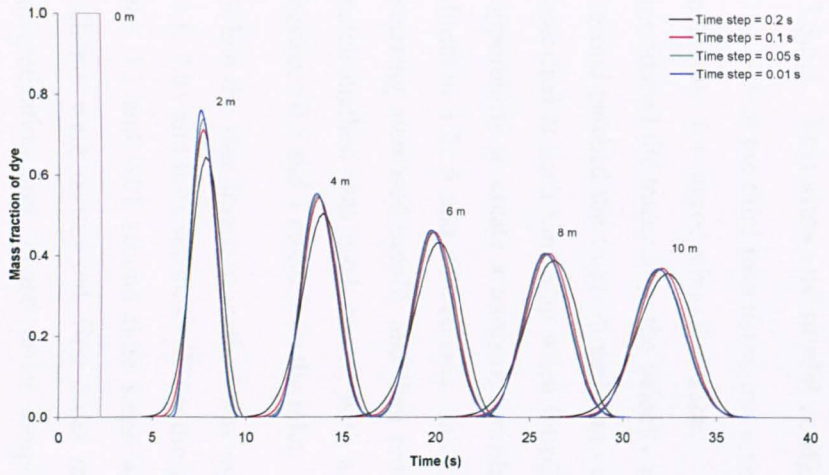

Second order upwind spatial discretization – Uncoupled processing technique

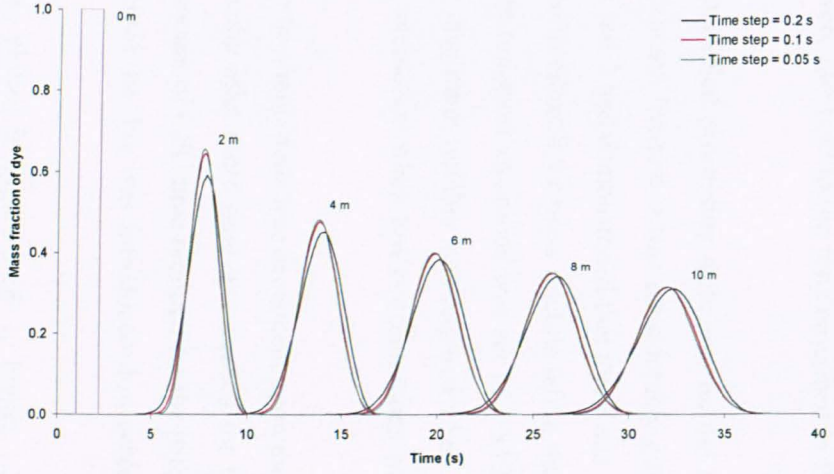

First order upwind spatial discretization – Coupled processing technique

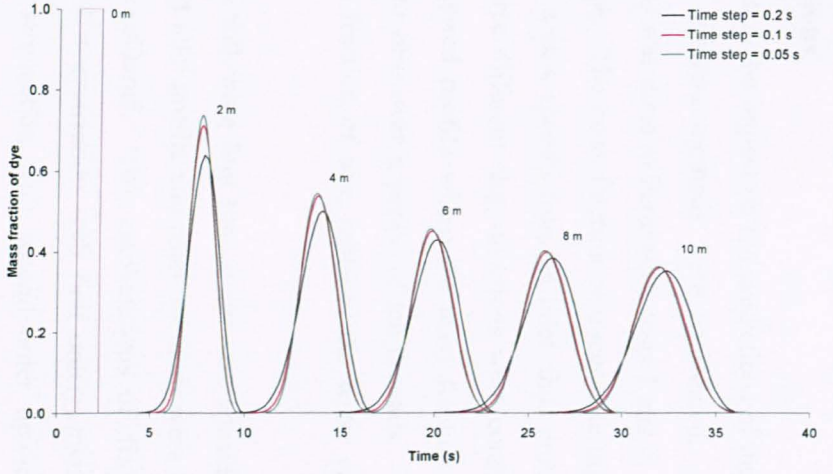

Second order upwind spatial discretization – Coupled processing technique

Figure 3.17 Second order temporal discretization temporal profiles (Parametric test 2)

3.3.5 Parametric test 3: Introduction of the tracer

3.3.5.1 Test aims and model configurations

The aim of the third parametric test was to assess the impact on the predictions of the methods available for introducing the tracer. Two different methods were considered. The first introduced the tracer from the velocity inlet, as was done in Parametric tests 1 and 2, while the second patched the tracer directly into the pipe. The mass fraction of tracer entering must be specified at each time step when introducing a new species from an inlet, thus providing the opportunity to create a temporal profile. Three different slug injections were considered, of duration 1.2, 5 and 10 seconds, and one skewed profile where the mass fraction of tracer entering increased rapidly and then reduced to zero over a period of ten seconds. When the patch method was used, tracer, with a mass fraction of one, replaced the water component between 0.5 and 1 metre from the inlet.

When the slug injection method was used the following four time steps were considered: 0.2, 0.1, 0.05 and 0.01 seconds. When the skewed inlet profile and patch methods were used only the 0.2 and 0.01 second time steps were considered. Two combinations of discretization scheme were considered, first order temporal discretization with first order upwind spatial discretization and second order temporal discretization with second order upwind spatial discretization. This created 32 separate tests. However, only 24 new simulations were required as the tests for the 1.2 second slug injection were identical to the tests described in Parametric test 1.

The simulations were performed using the uncoupled processing technique on the flow field described in Section 3.3.2. This method was chosen because it was considerably quicker than the coupled processing method and Parametric test 2 had demonstrated that there was no loss of accuracy. The movement of the tracer was monitored until the mass fraction left in the pipe was zero. The convergence criteria for the species transport equations was set to 1×10^{-3}, with a maximum of 20 iterations per time step. The maximum number was required when the tracer initially entered the pipe, or at the end of the simulation when low concentrations were left in the pipe.

The amount of CPU time required to complete the simulations was dependent upon the injection method. When the dye was introduced from the inlet more time was needed for the longer injections and for the skewed injection. The amount of CPU time required for the patch method was less for a comparable injection size because the dye was introduced downstream of the inlet.

Key outcomes relating to Parametric test 3 are plotted in Figure 3.18 to Figure 3.25, which have been grouped together at the end of this section.

3.3.5.2 Data analysis

The temporal profiles from the tests that used the 1.2 second slug injection are shown in Figure 3.8 Figure 3.9, while the temporal profiles relating to the other modelling options are shown in Figure 3.18 and Figure 3.19. The shapes of the temporal profiles were very different, reflecting the differences in the type and length of the introduction method. However, all of the tests showed the tracer being transported with the flow and the effects of longitudinal dispersion. Regardless of how the tracer was introduced into the system, all of the tests that used the first order temporal discretization scheme showed signs of numerical dispersion.

3.3.5.2.1 Mass

The mass of the tracer was calculated at each of the monitoring positions and was related to the mass of the initial injection. It was not possible to do this for the tests that used the patched method, so the mass at each monitoring position was related to the mass of the tracer that was calculated at two metres. Figure 3.10 shows the relative mass of the tracer at each of the positions for the tests that used the 1.2 second slug injection, while Figure 3.20 shows the relative mass at each of the positions for the remaining tests. The injection method did not affect whether the mass of the tracer stabilised, with the mass not stabilising for any of the methods when the second order temporal discretization scheme was used with a time step of 0.2 seconds. The method used to introduce the tracer did, however, affect the relative difference in the mass. Consider the mass of the different slug injections. As the length of the injections increased, and as a consequence the mass of the tracer increased, the relative difference in the mass reduced. Therefore, the tests that used the least amount of tracer, namely the 1.2 second slug injection and the patched method, produced the greatest relative errors.

The criteria used to determine if the mass of tracer was conserved were a stabilised mass and a variation of less than one percent from the original mass. This criteria was reached for all the tests with the exception of the ones that used the second order temporal discretization scheme and a time step of 0.2 seconds, and the second order temporal discretization scheme and a time step of 0.1 seconds when the 1.2 second slug injection was used.

3.3.5.2.2 Mean travel time

Figure 3.11 shows the mean travel time of the tracer between the monitoring positions for the tests that used the 1.2 second slug injection, while Figure 3.21 shows the mean travel time for the remaining tests. The travel time was not significantly affected by the method used to introduce the tracer and is therefore not considered further.

3.3.5.2.3 Temporal variance

Figure 3.12 shows the temporal variance of the tracer at each of the monitoring positions for the tests that used the 1.2 second slug injection, while Figure 3.22 shows the temporal variance of

the tracer at each of the monitoring positions for the remaining tests. The initial variance, or spread, of the tracer was dependent upon the shape and size of the introduction method. For instance, the variance for the 10 second slug injection was greater than the variance for the 1.2 second slug injection. When the second order temporal discretization scheme was used the size of the variance at a point downstream was related to the size of the initial injection and the distance from the inlet. When the first order temporal discretization scheme was used the size of the variance at a point downstream was also affected by the size of the time step. This was due to numerical dispersion in the model.

Figure 3.13 shows the difference in the temporal variance between the monitoring positions for the tests that used the 1.2 second slug injection, while Figure 3.23 shows the difference in the temporal variance for the other tests. Although the magnitude of the variance was affected by the introduction method the change in the variance between monitoring positions was not.

3.3.5.2.4 Coefficient of skewness

Figure 3.14 shows the coefficient of skewness of the tracer at each of the monitoring positions for the tests that used the 1.2 second slug injection, while Figure 3.24 shows the coefficient for at each of the monitoring positions for the other configurations. The injection method did not affect whether the tracer became positively or negatively skewed. The exception to this was the test that used the skewed injection profile with the second order temporal discretization scheme and a time step of 0.2 seconds. In this instance the profile became positively skewed. This occurred because the injection profile created a positive skewness that required the tracer to travel for a longer distance to remove. The value of the coefficient was affected by the method used to introduce the tracer and as would be expected the coefficient was greatest for the skewed injection profile. When the slug injection method was used the size of the coefficient reduced as the size of the injection increased.

3.3.5.2.5 Longitudinal dispersion coefficient

Figure 3.15 shows the longitudinal dispersion coefficient between the monitoring positions for the tests that used the 1.2 second slug injection, while Figure 3.25 shows the coefficients for the remaining modelling options. The longitudinal dispersion coefficient was not significantly affected by the method used to introduce the tracer and is therefore not considered further.

3.3.5.3 Conclusion

This series of tests demonstrated that the choice of the introduction method did affect the shape of the temporal profile at each monitoring position, but did not affect the travel time or the amount of longitudinal dispersion between the positions. This was to be expected because the equations governing these processes were the same regardless of the introduction method. It does, however, suggest that the predictions made by the model were robust.

Any introduction method would be appropriate to use in subsequent tests as the mean travel time and longitudinal dispersion coefficient were primarily used to determine the sensitivity of the simulation results to the modelling options selected. Therefore, the 1.2 second slug injection was chosen because it was easy to set up and required the least amount of CPU time to complete a simulation.

This parametric test, and the previous two parametric tests, have demonstrated that the predictions made using the first order temporal discretization scheme generally suffered from excessive numerical dispersion. It is therefore not considered further.

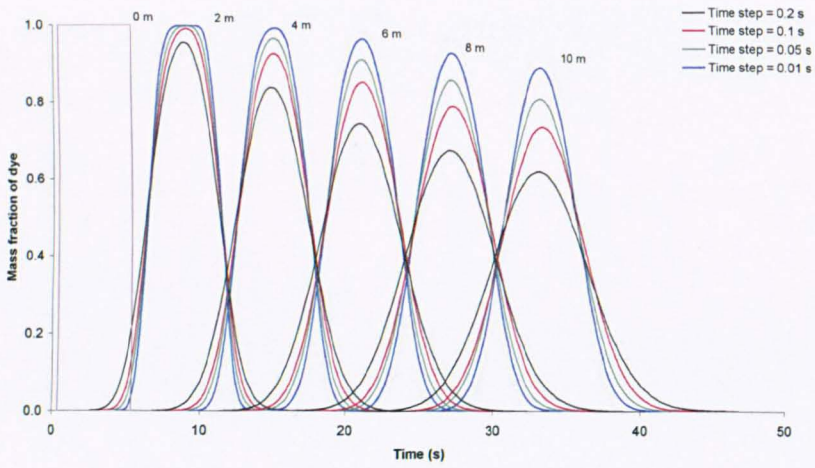

5 second slug injection from the inlet

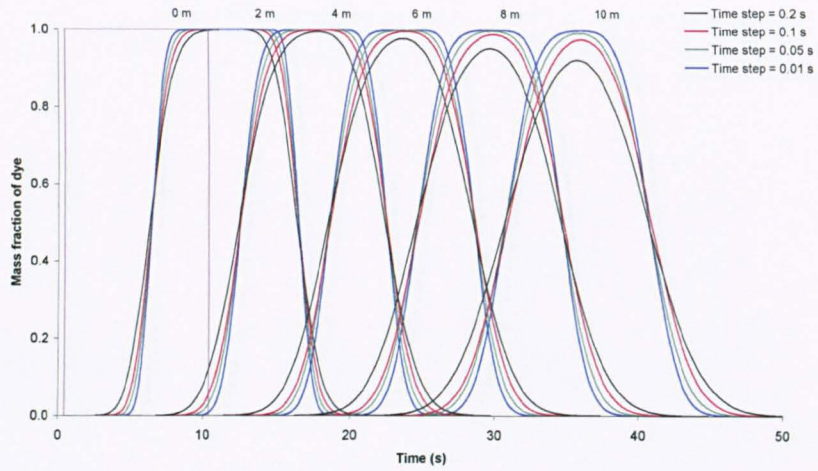

10 second slug injection from the inlet

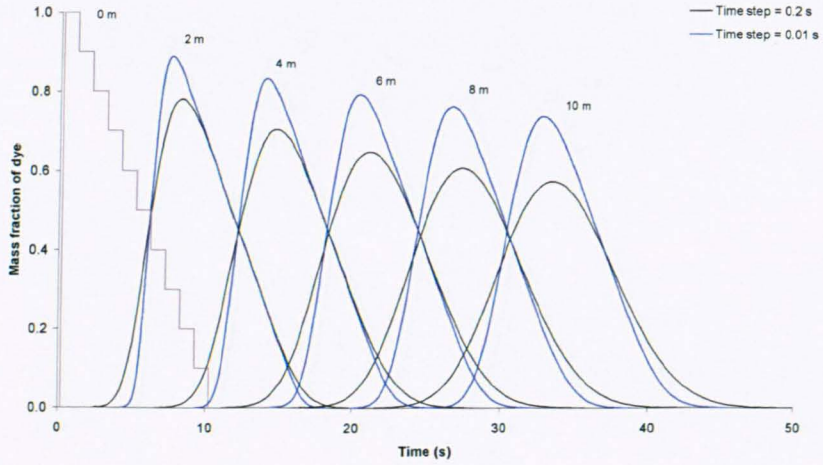

Skewed injection profile from the inlet

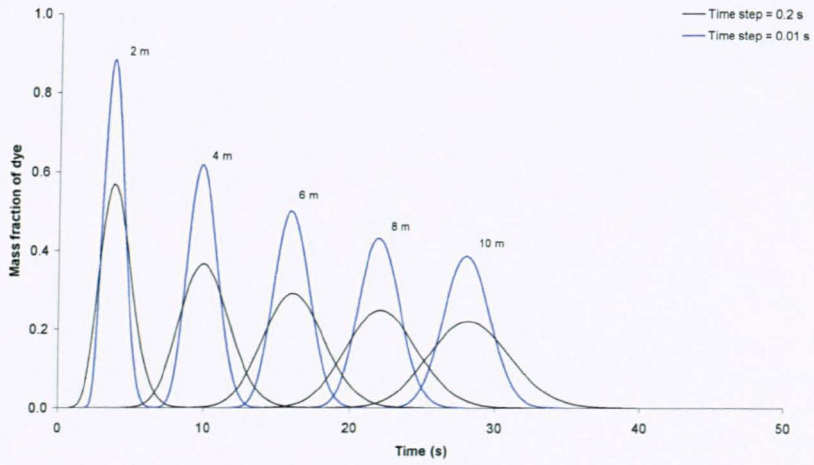

Patched injection method

Figure 3.18 First order temporal discretization temporal profiles (Parametric test 3)

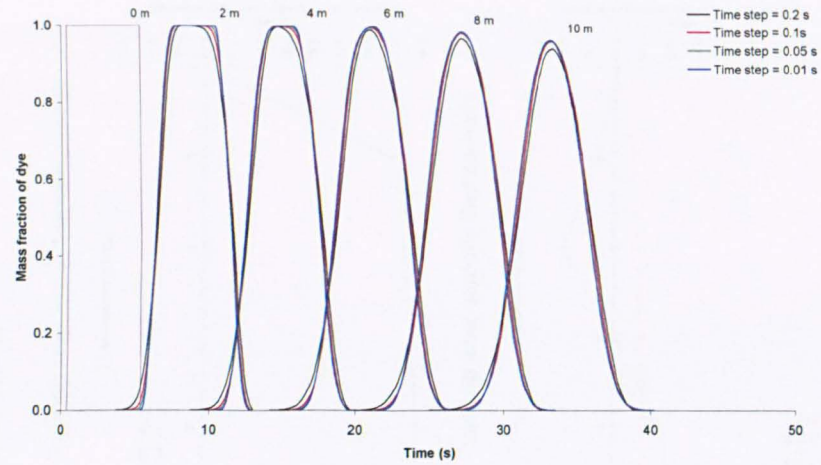

5 second slug injection from the inlet

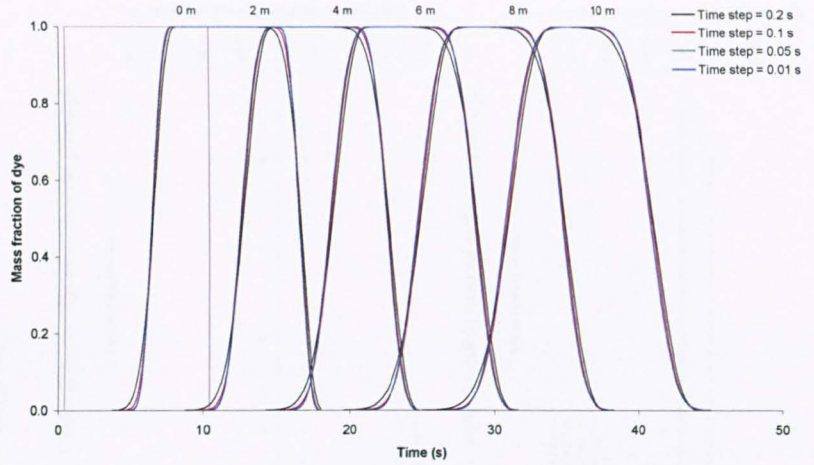

10 second slug injection from the inlet

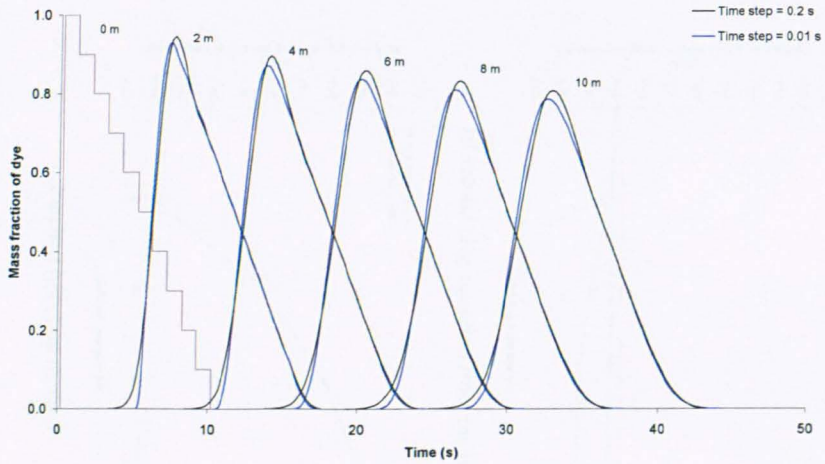

Skewed injection profile from the inlet

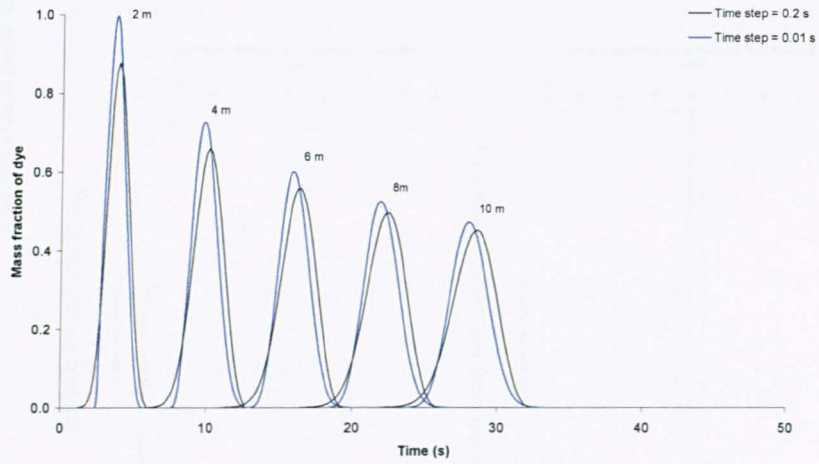

Patched injection method

Figure 3.19 Second order temporal discretization temporal profiles (Parametric test 3)

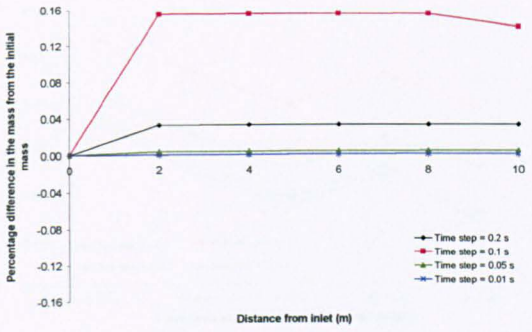

5 second slug injection from the inlet

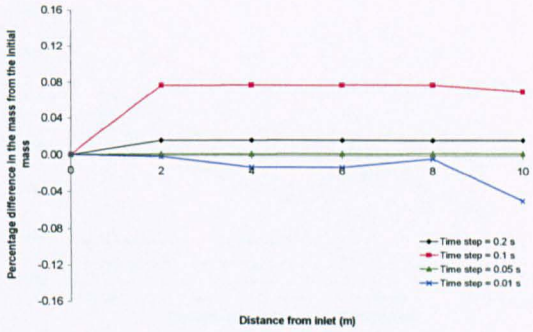

10 second slug injection from the inlet

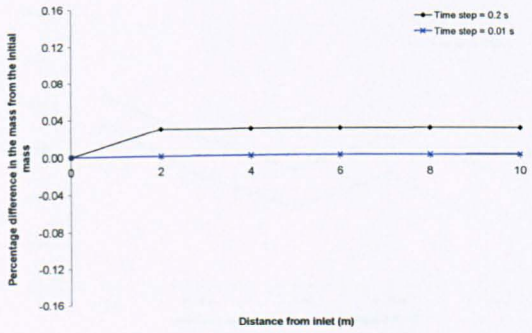

Skewed injection profile from the inlet

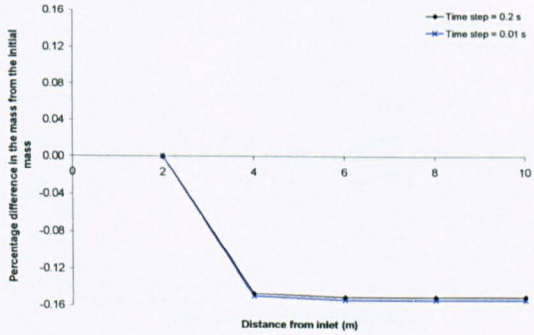

Patched injection method

(a) First order temporal discretization

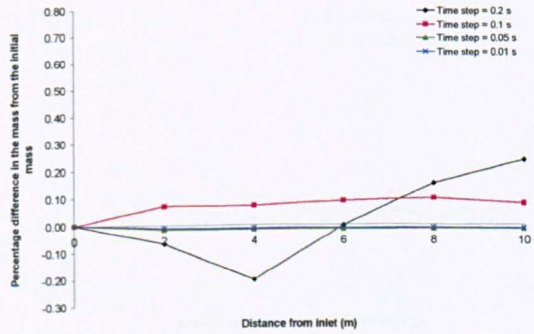

5 second slug injection from the inlet

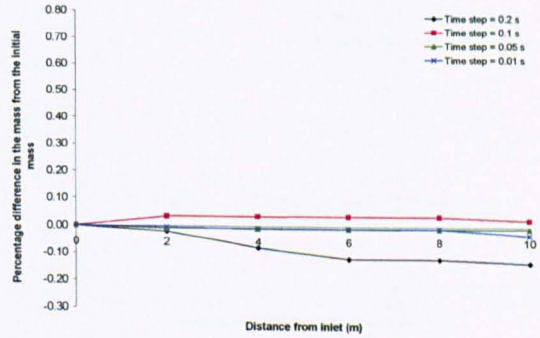

10 second slug injection from the inlet

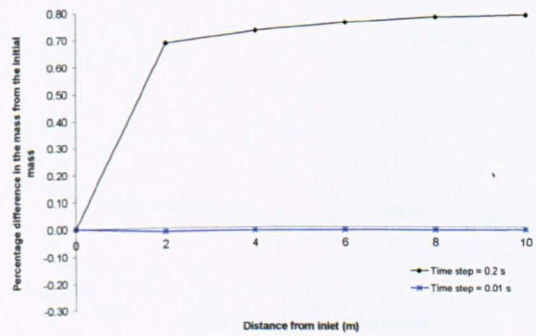

Skewed injection profile from the inlet

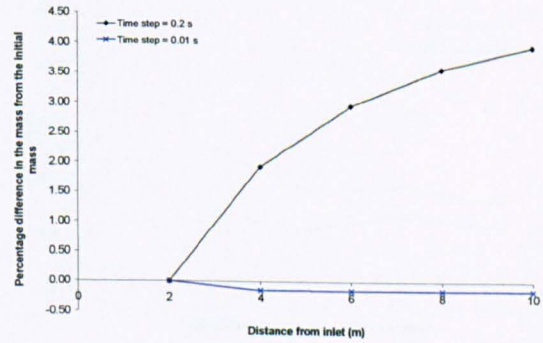

Patched injection method

(b) Second order temporal discretization

Figure 3.20 Mass (Parametric test 3)

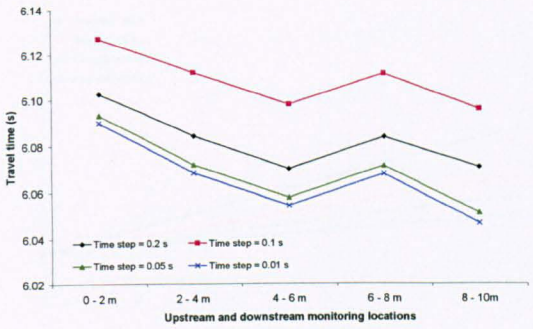

5 second slug injection from the inlet

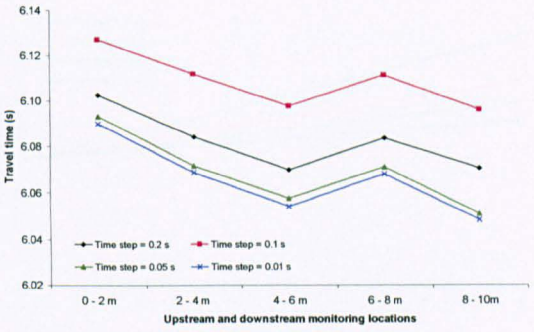

10 second slug injection from the inlet

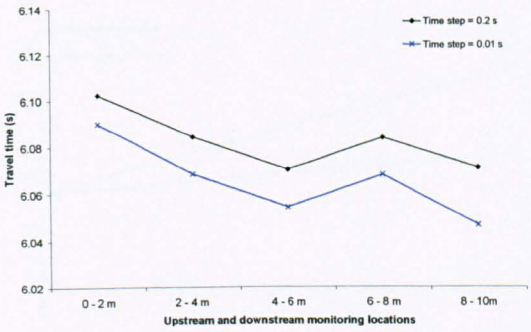

Skewed injection profile from the inlet

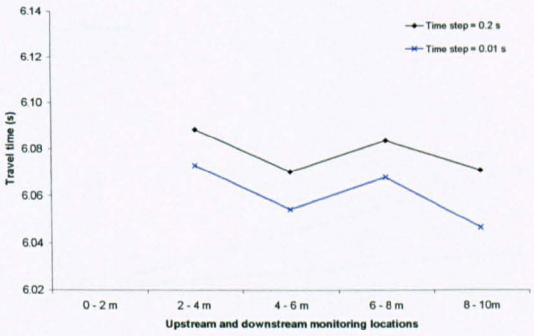

Patched injection method

(a) First order temporal discretization

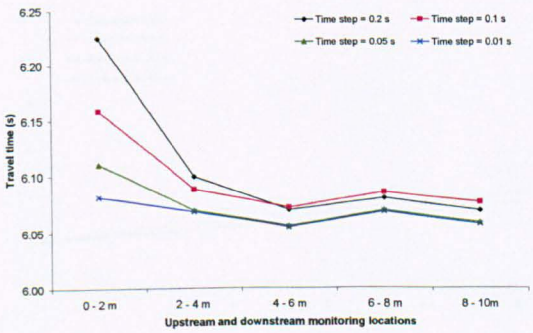

5 second slug injection from the inlet

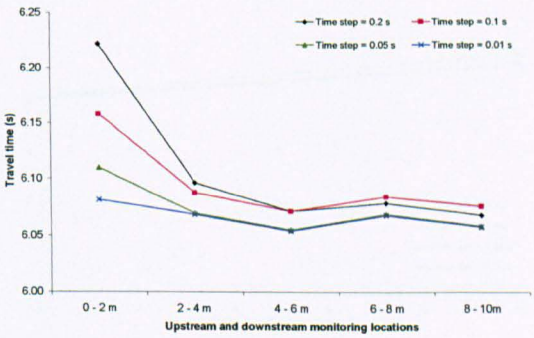

10 second slug injection from the inlet

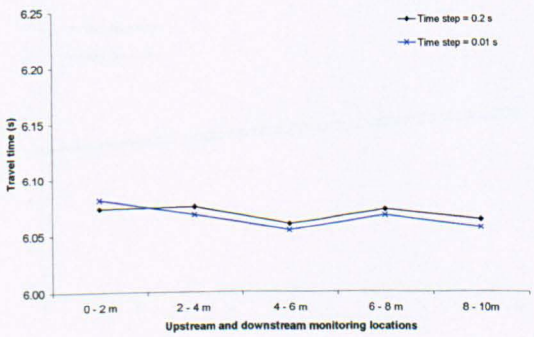

Skewed injection profile from the inlet

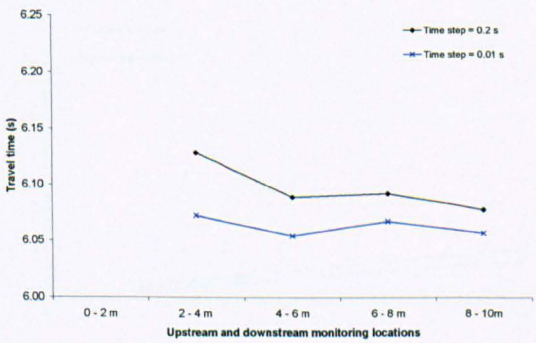

Patched injection method

(b) Second order temporal discretization

Figure 3.21 Mean travel time (Parametric test 3)

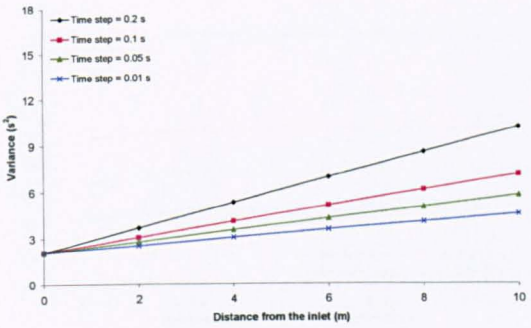

5 second slug injection from the inlet

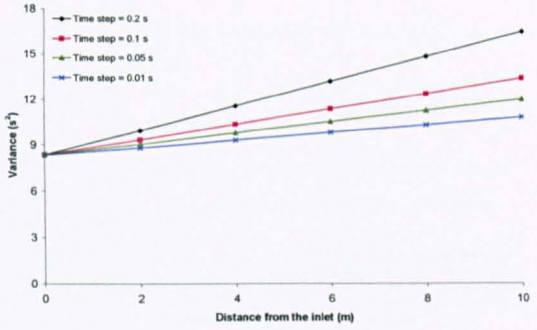

10 second slug injection from the inlet

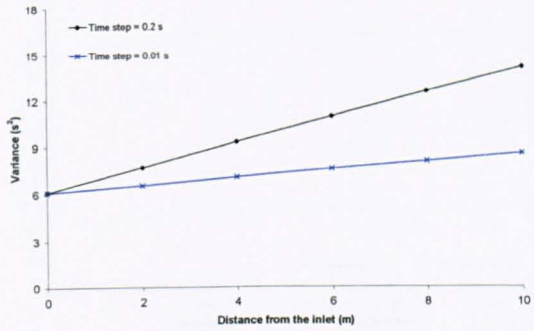

Skewed injection profile from the inlet

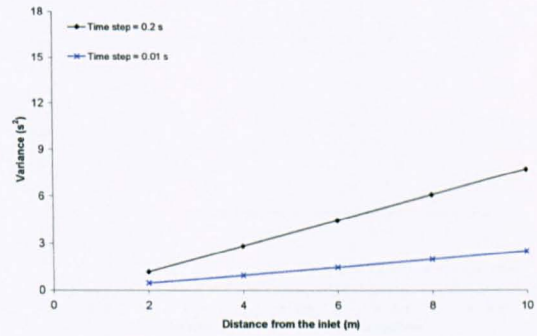

Patched injection method

(a) First order temporal discretization

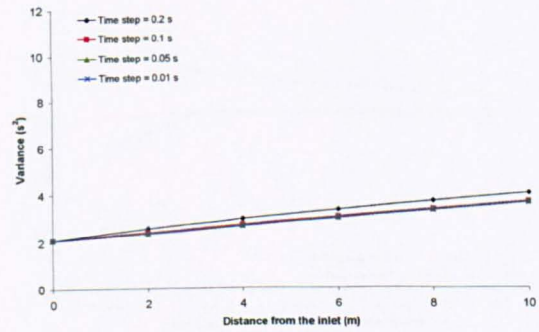

5 second slug injection from the inlet

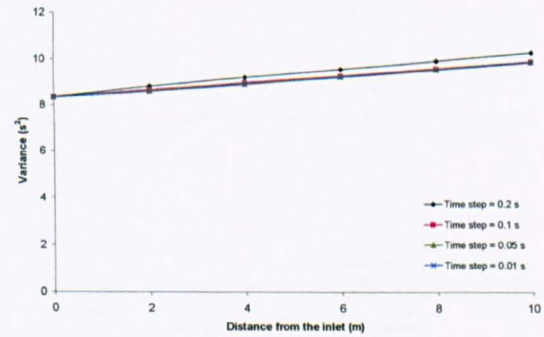

10 second slug injection from the inlet

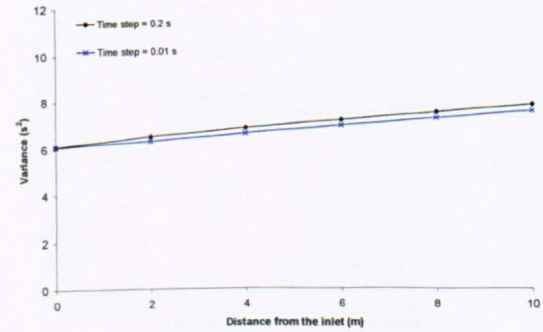

Skewed injection profile from the inlet

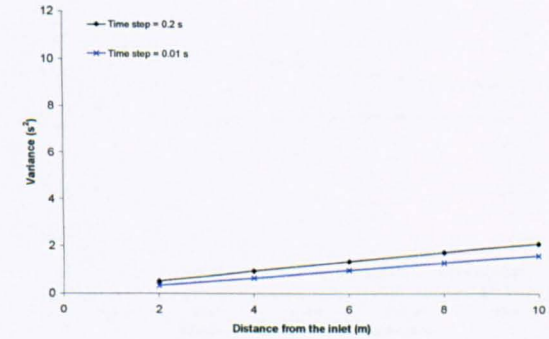

Patched injection method

(b) Second order temporal discretization

Figure 3.22 Temporal variance (Parametric test 3)

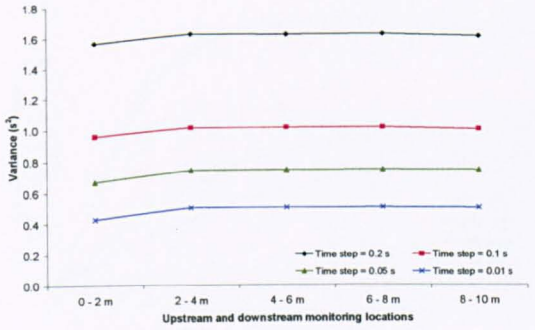

5 second slug injection from the inlet

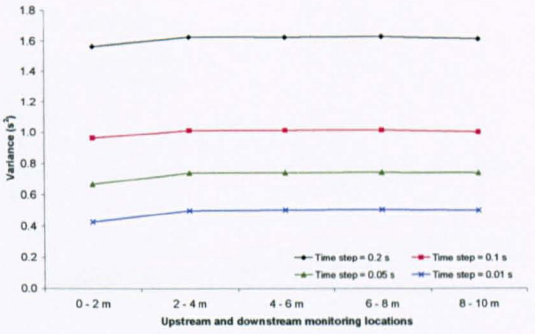

10 second slug injection from the inlet

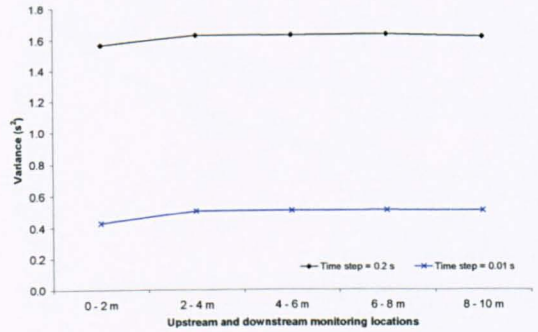

Skewed injection profile from the inlet

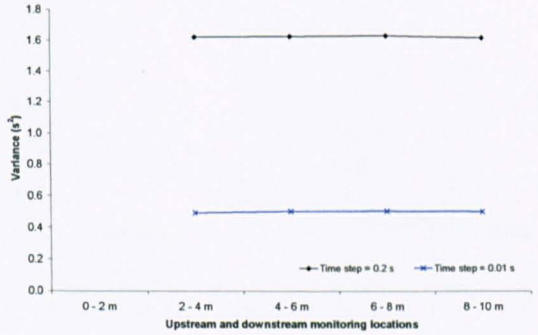

Patched injection method

(a) First order temporal discretization

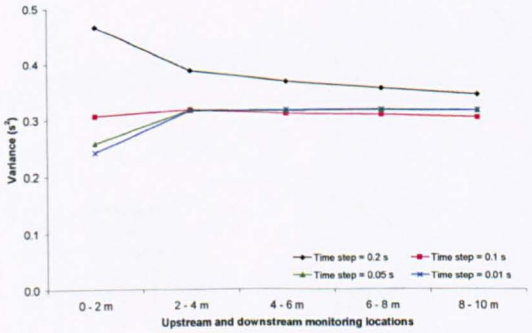

5 second slug injection from the inlet

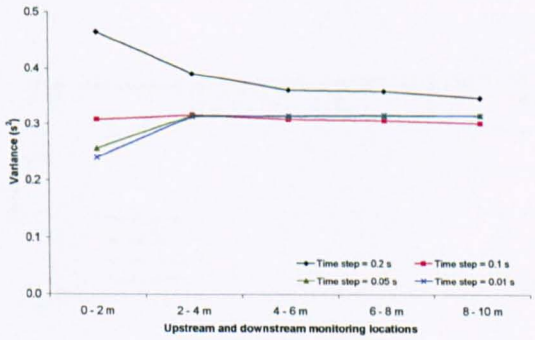

10 second slug injection from the inlet

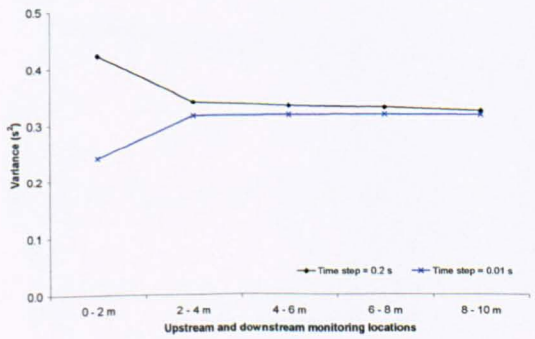

Skewed injection profile from the inlet

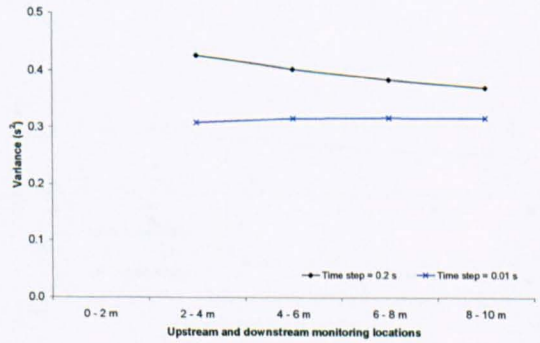

Patched injection method

(b) Second order temporal discretization

Figure 3.23 Temporal variance (2) (Parametric test 3)

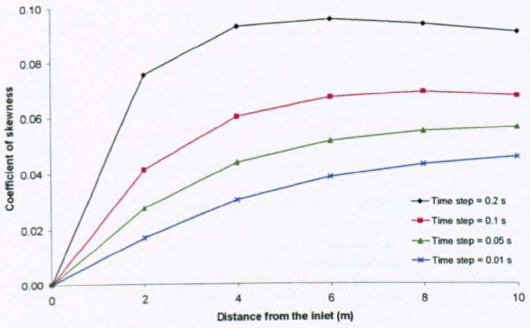

5 second slug injection from the inlet

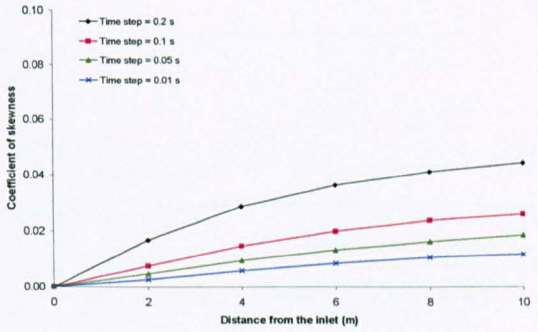

10 second slug injection from the inlet

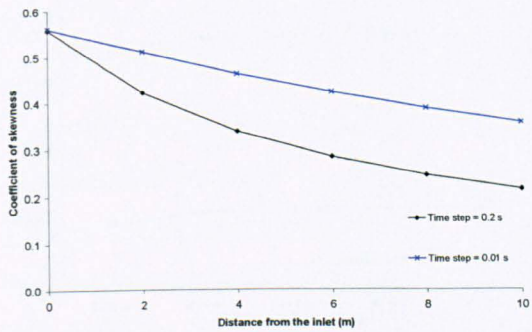

Skewed injection profile from the inlet

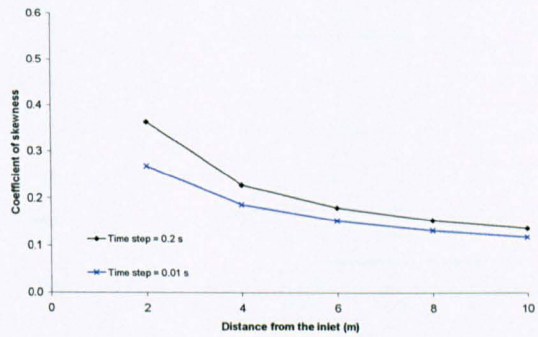

Patched injection method

(a) First order temporal discretization

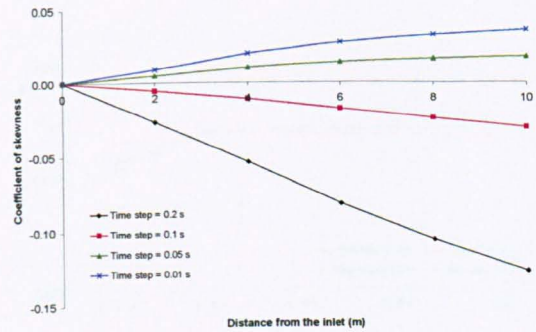

5 second slug injection from the inlet

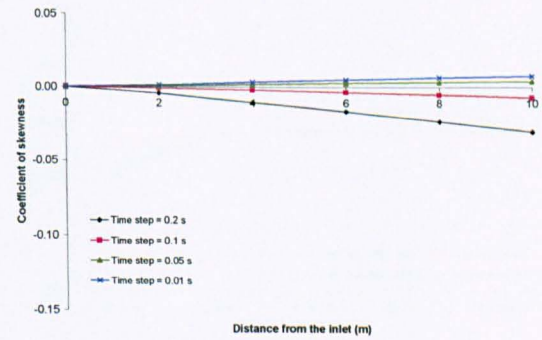

10 second slug injection from the inlet

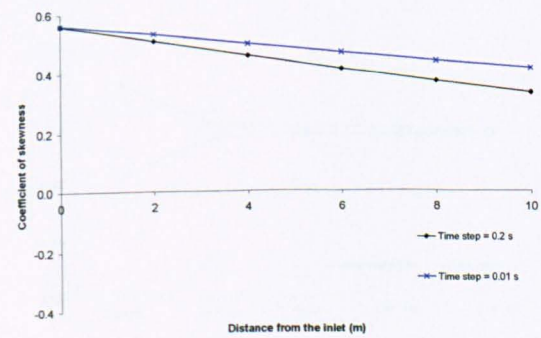

Skewed injection profile from the inlet

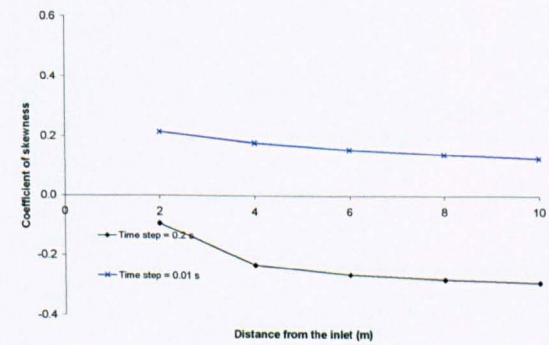

Patched injection method

(b) Second order temporal discretization

Figure 3.24 Coefficient of skewness (Parametric test 3)

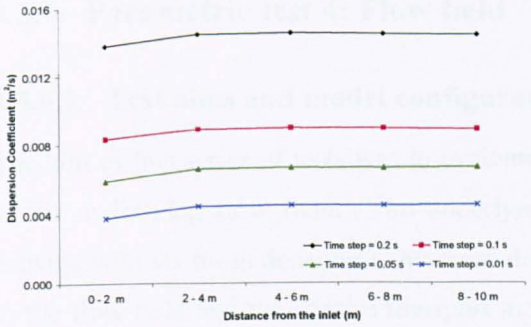

5 second slug injection from the inlet

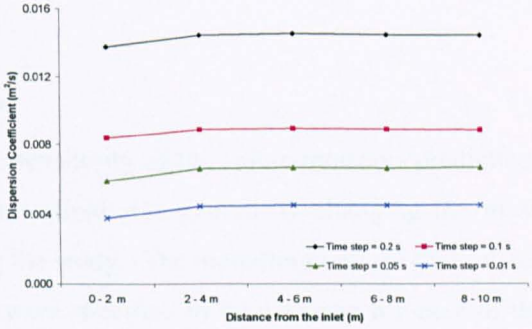

10 second slug injection from the inlet

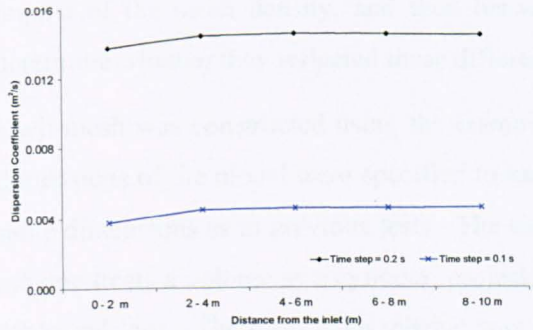

Skewed injection profile from the inlet

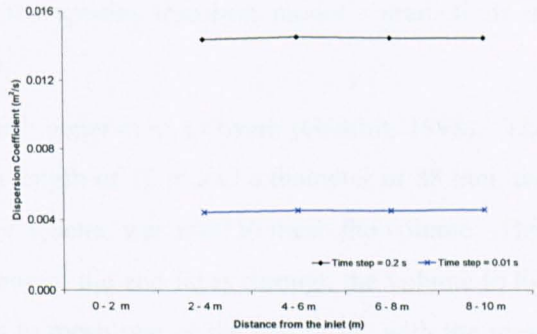

Patched injection method

(a) First order temporal discretization

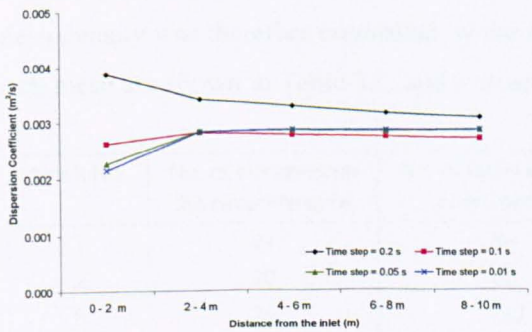

5 second slug injection from the inlet

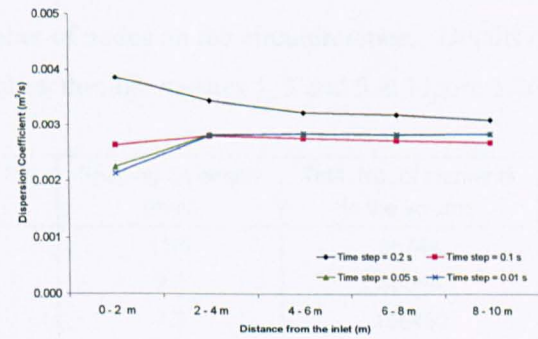

10 second slug injection from the inlet

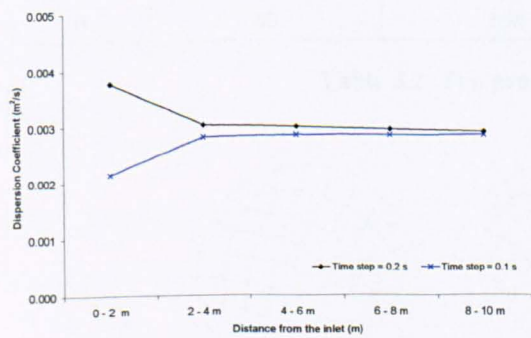

Skewed injection profile from the inlet

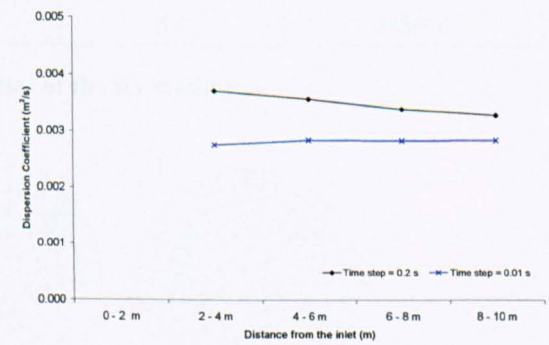

Patched injection method

(b) Second order temporal discretization

Figure 3.25 Longitudinal dispersion coefficient (Parametric test 3)

3.3.6 Parametric test 4: Flow field

3.3.6.1 Test aims and model configurations

The aim of this series of tests was to evaluate the sensitivity of the solute transport predictions to the underlying flow field. The underlying flow field was altered by changing the mesh density, with six mesh densities considered during the study. The modelling options that related to the flow field and the species transport model were specified to be the same for each of the meshes considered. A comparison was initially made between the flow fields to determine the impact of the mesh density, and then between the species transport model's predictions to determine whether they reflected these differences.

Each mesh was constructed using the Gambit mesh generation software (Gambit, 1998). The dimensions of the model were specified to have a length of 10 m and a diameter of 88 mm, the same dimensions as in previous tests. The Cooper scheme was used to mesh the volume. This scheme treats a volume as a cylinder, projecting one of the end faces through the volume to the other end face. The quad pave scheme was used to mesh one of the end faces, with the mesh density controlled by the number of nodes on the circumference. Using this face as the input the Cooper scheme replicated it along the length of the pipe. The interval spacing on the length of the pipe was determined by the Cooper scheme to minimise the aspect ratio. The overall mesh density was therefore controlled by the number of nodes on the circumference. Details of each mesh are shown in Table 3.2, and a cross section through meshes 1, 3 and 5 in Figure 3.26.

Mesh No.	No. of elements on the circumference	No. of faces over the cross section	Spacing on length (mm)	Total No. of elements in the volume
1	24	64	11.5	55744
2	30	88	9.2	95656
3	36	120	7.7	156480
4	40	145	6.9	209960
5	44	178	6.3	283554
6	48	198	5.8	343926

Table 3.2 The properties of the six meshes

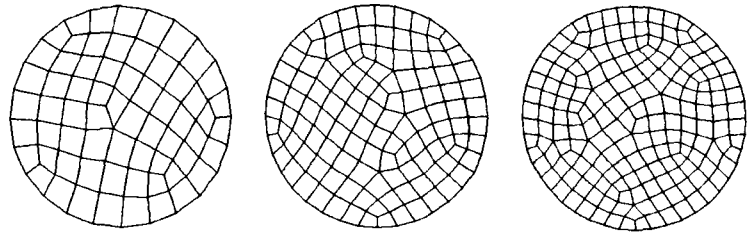

Figure 3.26 Cross sections through meshes 1, 3 and 5

The modelling options that related to the flow field were the same as the modelling options described in 3.3.2. The number of spatial and temporal discretization schemes considered was reduced to save time and resources. Only the second order temporal discretization was considered, as the previous three parametric tests had demonstrated that the first order scheme suffered from considerable numerical dispersion. Only the first and second order upwind spatial discretization schemes were considered as Parametric test 1 had demonstrated that they produced similar results to the power law and QUICK schemes respectively. This resulted in two combinations of spatial and temporal discretization scheme, making twelve tests in total.

The analysis presented in Parametric test 3 demonstrated that the introduction method did not affect the parameters of interest, namely the mean travel time and the longitudinal dispersion coefficient. A slug of the tracer was therefore introduced into the primary water phase from the velocity inlet for 1.2 seconds. The simulations were performed using the uncoupled processing technique. This method was chosen because it was considerably quicker than the coupled processing method and Parametric test 2 had demonstrated that there was no loss of accuracy. The movement of the tracer was simulated until the mass fraction left in the pipe was zero. The convergence criteria for the species transport equations were set to 1 $x10^{-3}$, with a maximum of 20 iterations per time step. The maximum number was required when the tracer initially entered the pipe, or at the end of the simulation when low concentrations were left in the pipe.

Time step independence was determined by using the longitudinal dispersion coefficient as the determining factor. This parameter was selected because it incorporates both the transport and spread of the tracer. An initial time step was selected, the simulation performed, and the longitudinal dispersion coefficient determined from the equilibrium zone. The size of the time step was then reduced (in most cases halved) and the process was repeated. If the value of the coefficients were the same (or a difference of less that 1 %) the process was stopped as time step independence was deemed to have been reached; if they were not the same the process was repeated. Time step independence was determined separately for each of the spatial discretization schemes, but it was found to occur at approximately the same time. Time step independence was reached at 0.05 seconds for meshes one to four and at 0.02 seconds for meshes five and six.

The amount of CPU time required for each simulation was related to mesh density, with more time required as the number of elements in the domain increased.

Key outcomes relating to Parametric test 4 are plotted in Figure 3.28 and Figure 3.30, which are presented at the end of this section.

3.3.6.2 Data analysis

3.3.6.2.1 Flow field

Three flow properties were considered when determining the effect of the mesh density on the flow field: the velocity magnitude, the generation of turbulent kinetic energy (k) and the turbulent dissipation rate (ε). In order to record these properties a monitoring line was created in the flow. When a cell touched the monitoring line the required flow properties were recorded. The monitoring line was created along the pipe radius at a distance of five metres from the inlet. The flow properties recorded along the line are shown in Figure 3.28.

The change in mesh density did not significantly affect the velocity magnitude and ε away from the wall, but it did have a significant impact in the near wall region. For instance, at the wall the value of ε from the finest mesh, Mesh 6, was approximately twice that of the coarsest mesh, Mesh 1. The mesh density had little impact on the turbulent kinetic energy over the entire cross section, although slight variations are evident in the coarsest meshes at a distance of approximately 30 mm from the centre of the pipe

3.3.6.2.2 Temporal profiles

Figure 3.29 shows the temporal profiles recorded at each monitoring position. When the first order upwind scheme was used the difference between the temporal profiles was almost indistinguishable at all of the monitoring positions. When the second order upwind scheme was used the mean travel time of the dye was approximately the same for all of the tests, but the amount of longitudinal dispersion was related to mesh density, with greater dispersion occurring with increased mesh density. The amount of longitudinal dispersion was greater when using the first order upwind spatial discretization scheme for all of the mesh densities considered.

3.3.6.2.3 Mass

The mass of the tracer at each of the monitoring positions was related to the initial mass of the injection, with the relative mass of the tracer at each location showed in Figure 3.30 (a). When the first order upwind scheme was used the mass of the tracer had stabilised by two metres from the inlet in all of the tests. When the second order upwind scheme was used the distance required for the mass to stabilise was related to mesh density, with a longer distance required for the coarser meshes. The relative error in the mass increased between mesh one and four, and then reduced for meshes five and six. This change coincides with a change in the time step and reflects its importance. The criteria used to define mass conservation was a stable mass and a difference of less than one percent from the mass of the original injection. This criteria was reached in all of the tests.

3.3.6.2.4 Mean travel time

The mean travel time of the tracer between the monitoring positions is shown in Figure 3.30 (b). In all of the tests the mean flow velocity was specified to be 0.33 m/s, which equates to a mean travel time of 6.06 seconds between the monitoring positions. There does not appear to be a relationship between the mesh density and the mean travel time as the predictions from all of the meshes were shown to be close to the mean travel time of the flow. This suggests that the mean travel time of the tracer may be accurately modelled by any of the discretization schemes on any of the meshes considered.

3.3.6.2.5 Temporal variance

The temporal variance of the tracer at each monitoring positions is shown in Figure 3.30 (c) and the difference in the temporal variance between the monitoring positions in Figure 3.30 (d). For both of the spatial discretization schemes the variance increased linearly with distance after two metres from the inlet, therefore following the idealised Fickian model. When the first order upwind scheme was used the variance of the tracer was approximately the same at each of the monitoring positions. When the second order upwind scheme was used the variance of the tracer was related to the density of the mesh, with a higher mesh density leading to an increase in the variance. Nevertheless the variance of the tracer was greater at each of the monitoring positions when the first order scheme was used.

3.3.6.2.6 Coefficient of skewness

The coefficient of skewness of the tracer at each of the monitoring positions is shown in Figure 3.30 (e). The skewness of the tracer was always positive when the first order upwind scheme was used. The coefficient reached a peak value downstream of the inlet and then reduced with distance, thus following the Fickian model. The skewness of the tracer was related to mesh density, with an increase in skewness occurring with an increase in mesh density. When the second order upwind scheme was used the same trends were repeated for meshes three to six. Meshes one and two did not follow the idealised model, with the skewness of the tracer becoming negative.

3.3.6.2.7 Longitudinal dispersion coefficient

The longitudinal dispersion coefficients calculated between adjacent monitoring positions are shown in Figure 3.30 (f). In all of the tests the longitudinal dispersion coefficient was constant with distance after two metres from the inlet. The coefficient was approximately the same for all of the meshes when the first order upwind scheme was used. When the second order upwind scheme was used the coefficient was dependent upon the mesh density, with greater longitudinal dispersion occurring as the mesh density increased.

Figure 3.27 compares the longitudinal dispersion coefficients obtained from the equilibrium zone with the number of cells used in the mesh. When the first order upwind scheme was used the coefficient was approximately constant with mesh density, but when the second order upwind scheme was used the coefficient increased with the mesh density. It was previously demonstrated that the flow field was different in each of the meshes. It was only possible to detect these differences when using the second order upwind spatial discretization scheme.

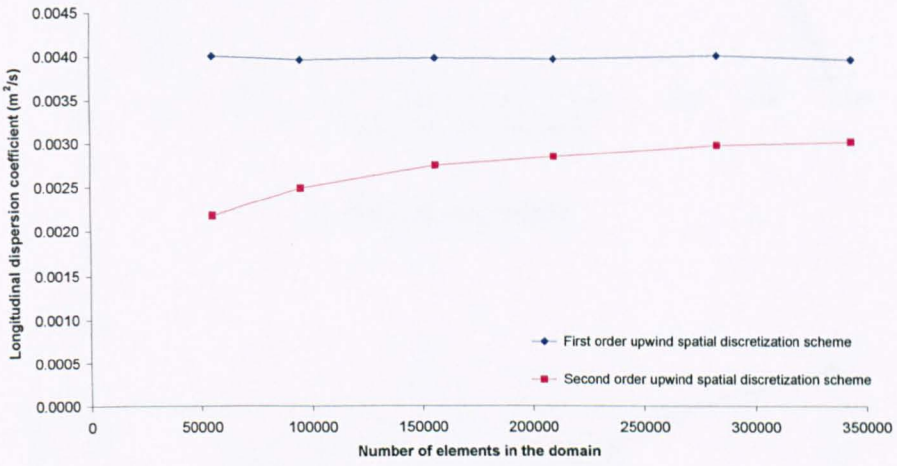

Figure 3.27 Variation in the longitudinal dispersion coefficient with mesh density (Parametric test 4)

3.3.6.3 Conclusion

This parametric study evaluated the sensitivity of the models predictions to the underlying flow field. Six underlying flow fields and two combinations of temporal and spatial discretization scheme were considered. In each of the tests the size of the time step was reduced until the longitudinal dispersion coefficient calculated from the equilibrium zone became independent of the time step.

In all of the tests the mass of the tracer was conserved and the mean travel time was approximately the same as the mean travel time of the flow. The spread of the tracer was not affected by mesh density when the first order upwind scheme was used, but was when the second order scheme was used, with greater dispersion corresponding to an increase in the mesh density.

Analysis of the flow field demonstrated that the near wall flow conditions were sensitive to the density of the mesh. The predictions made using the second order upwind scheme varied in accordance with the mesh density and are therefore judged to be more accurate.

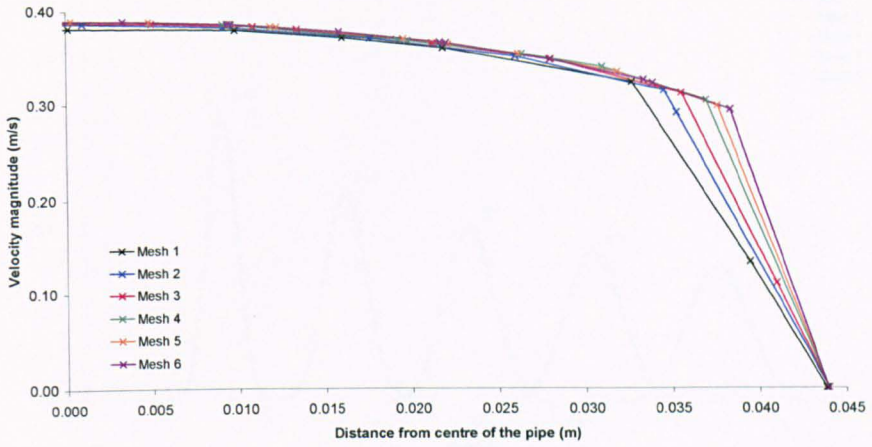

(a) Velocity magnitude

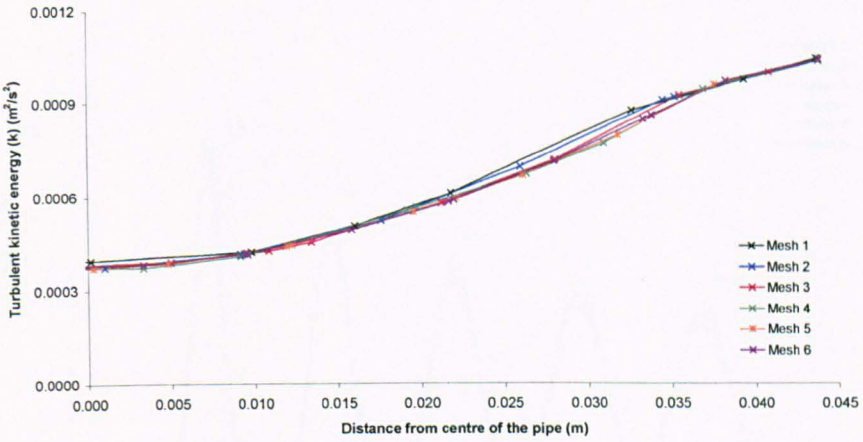

(b) Turbulent kinetic energy (k)

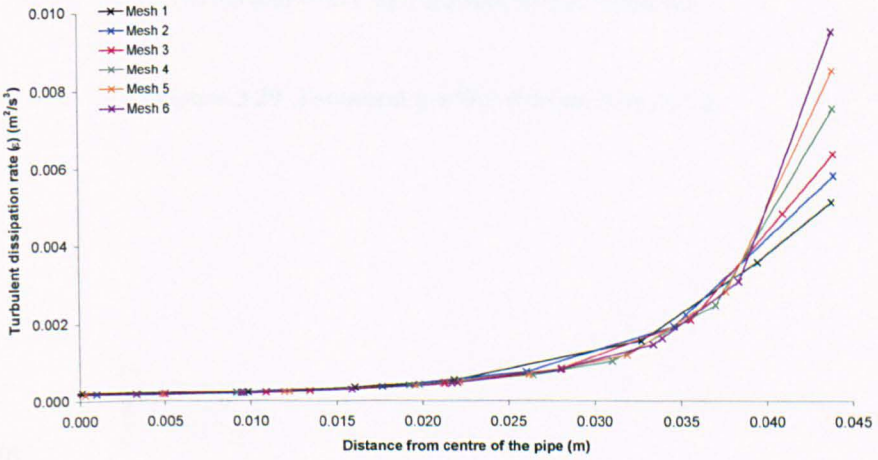

(c) Turbulent dissipation rate (ε)

Figure 3.28 A comparison of predictions made by the different meshes (Parametric test 4)

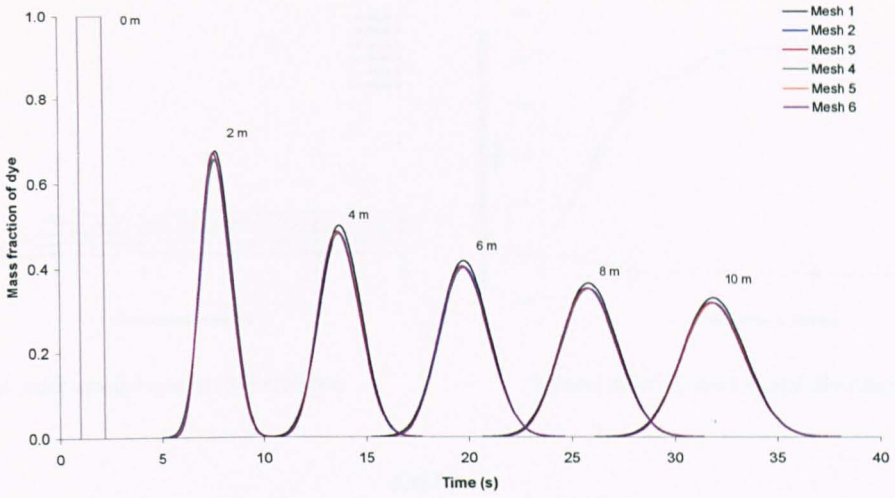

(a) First order upwind spatial discretization

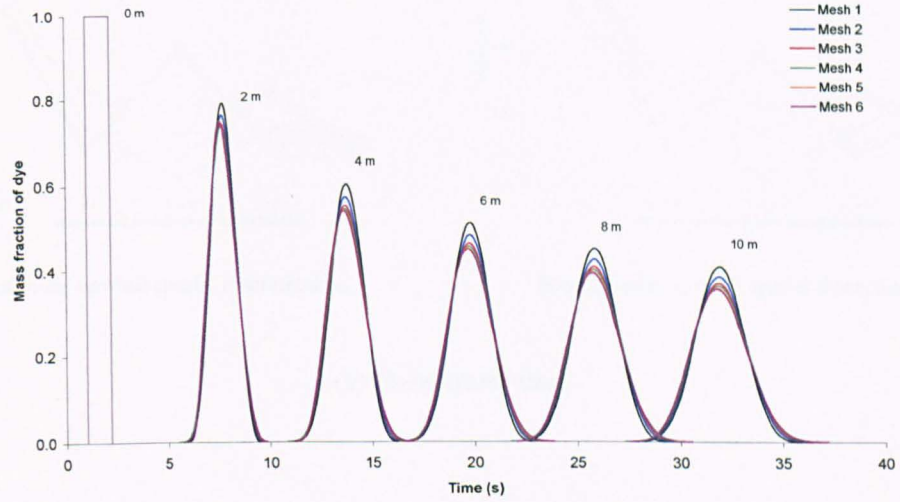

(b) Second order upwind spatial discretization

Figure 3.29 Temporal profiles (Parametric test 4)

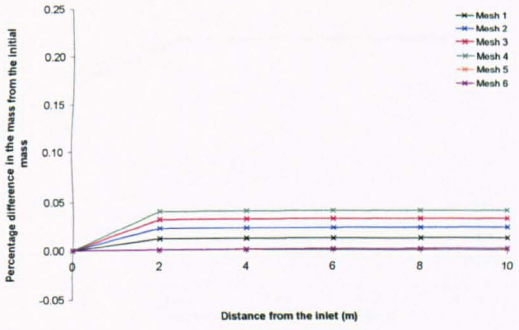

First order upwind spatial discretization

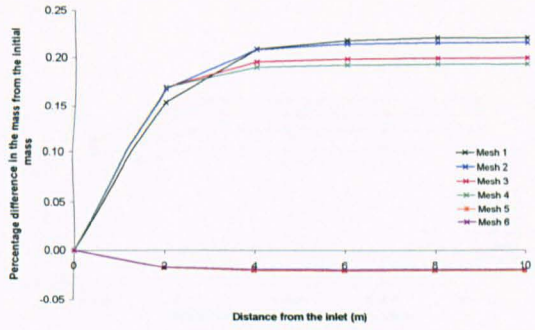

Second order upwind spatial discretization

(a) Mass

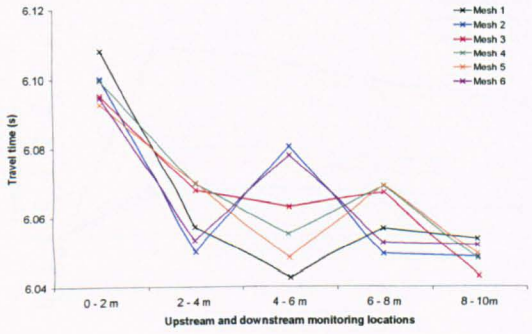

First order upwind spatial discretization

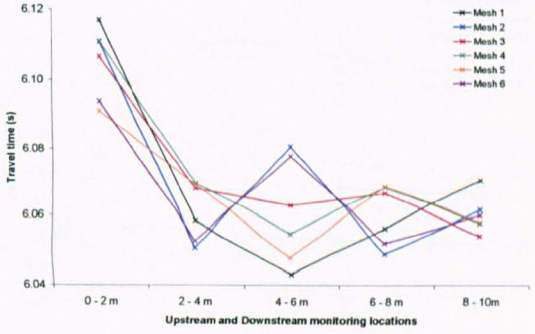

Second order upwind spatial discretization

(b) Mean travel time

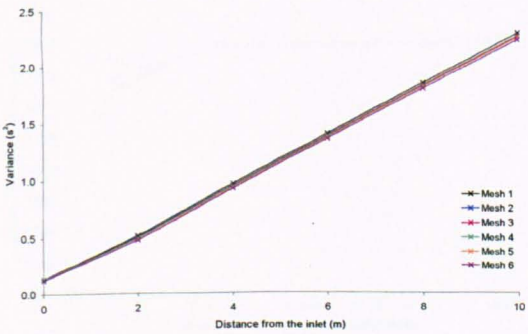

First order upwind spatial discretization

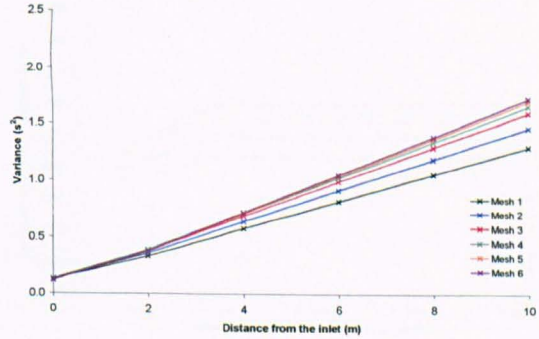

Second order upwind spatial discretization

(c) Temporal variance

Figure 3.30 Moment analysis (Parametric test 4) (continued overleaf)

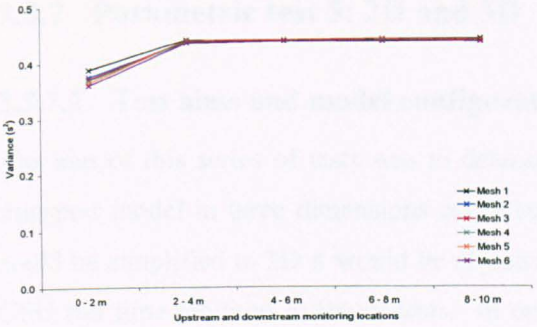

First order upwind spatial discretization

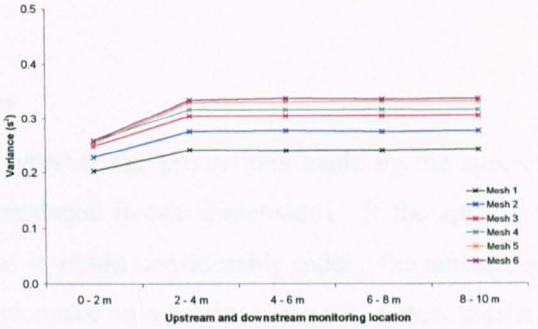

Second order upwind spatial discretization

(d) Temporal variance (2)

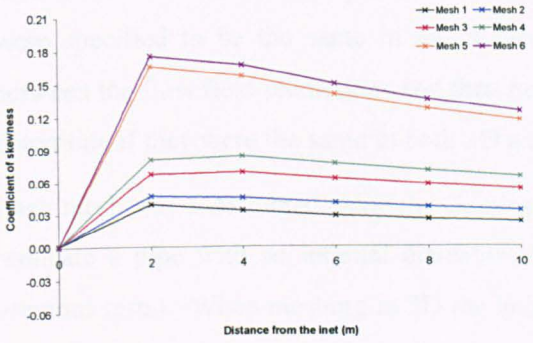

First order upwind spatial discretization

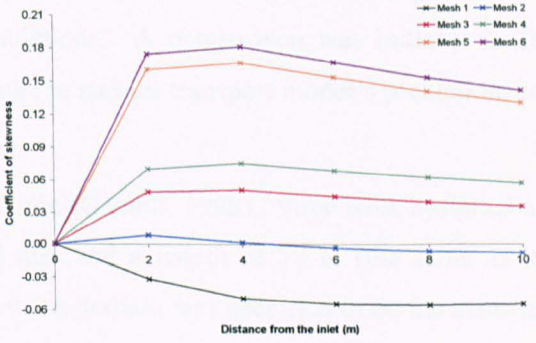

Second order upwind spatial discretization

(e) Coefficient of skewness

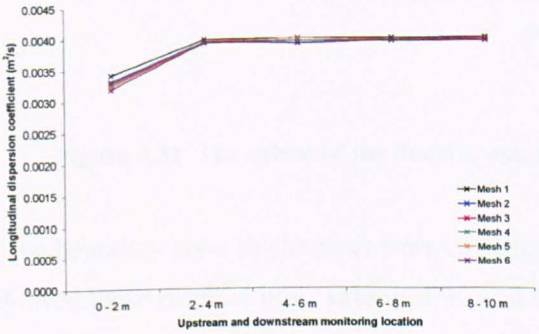

First order upwind spatial discretization

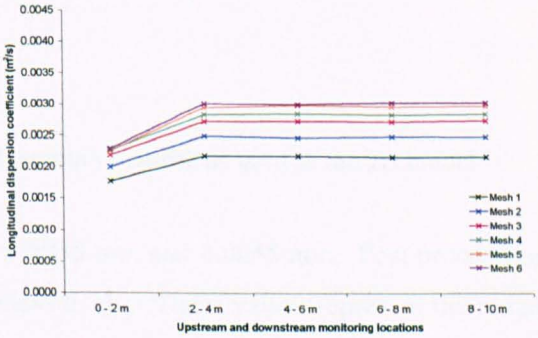

Second order upwind spatial discretization

(f) Longitudinal dispersion coefficient

Figure 3.30 Moment analysis (Parametric test 4) (continued from previous page)

3.3.7 Parametric test 5: 2D and 3D

3.3.7.1 Test aims and model configurations

The aim of this series of tests was to determine whether the predictions made by the species transport model in three dimensions could be reproduced in two dimensions. If the approach could be simplified to 2D it would be of benefit as it would considerably reduce the amount of CPU run time required in future tests. In order to make an accurate comparison new meshes were created in both 2D and 3D. In each of the new meshes the thickness of the cells nearest to the wall of the pipe, called the boundary layer cells, were controlled. This allowed the same boundary layer thickness to be specified in both 2D and 3D. This was done because Parametric test 4 had highlighted the sensitivity of the near wall flow predictions to the size of the boundary layer cells. The modelling options that related to the flow field and species transport model were specified to be the same in all of the simulations. A comparison was initially made between the flow field predictions and then between the species transport model's predictions to determine if they were the same in both 2D and 3D.

Each mesh was constructed using the Gambit software (Gambit, 1998). They were designed to replicate a pipe with an internal diameter of 88 mm and a length of 10 m (the same as in previous tests). When meshing in 2D the height of the domain was specified to be the same as the radius of the pipe, and the width the same as the length of the pipe. The extent of the domain and the boundary conditions used in the 2D model are shown in Figure 3.31.

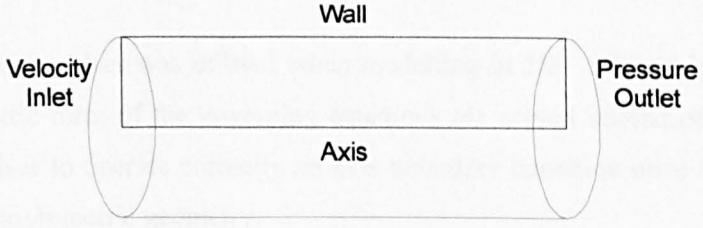

Figure 3.31 The extent of the domain and the boundary conditions used in the 2D model

Two boundary layer thicknesses were considered: 0.0035 mm and 0.0065 mm. Post processing showed these resulted in y^+ values of 30 and 60 respectively. These values represent the range recommended by the Fluent 5 User's Guide (Fluent, 1998) for use with standard wall functions.

Two mesh densities were considered for each boundary layer thickness as this allowed an assessment to be made for grid independence. When meshing in 2D the number of cells could be altered along the radius and the length of the pipe, providing two variables with which to alter the grid density. The Cooper scheme was used to mesh the 3D pipe. As previously discussed, grid density could only be controlled by altering the number of nodes on the circumference.

In total eight different meshes were created, four in 2D and four in 3D. Details of each of the meshes are shown in Table 3.3. A cross section through mesh 7, and part of mesh 11 between the inlet and 55 mm, is also shown in Figure 3.32.

Mesh No.	Solver	Boundary layer thickness (mm)	No. of elements on the circumference	No. of faces over the cross section	Spacing on length (mm)	Total No. of elements
7	3D	3.5	38	174	7.3	239424
8	3D	3.5	44	215	6.3	342495
9	3D	6.5	38	172	7.3	236672
10	3D	6.5	44	228	6.3	363204

Mesh No.	Solver	Boundary layer thickness (mm)	No. of elements on the radius	-	Spacing on length (mm)	Total No. of elements
11	2D	3.5	11	-	3.5	31427
12	2D	3.5	15	-	3.5	42855
13	2D	6.5	6	-	6.5	9228
14	2D	6.5	9	-	6.5	13842

Table 3.3 The properties of each of the meshes

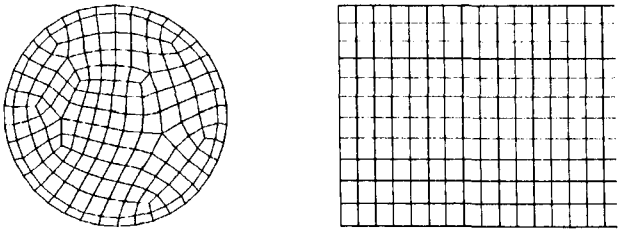

Figure 3.32 A cross section through mesh 7 and part of mesh 11

The 2D axisymmetric solver was utilised when modelling in 2D. When this solver is enabled the 2D axisymmetric form of the governing equations are solved instead of the 2D Cartesian form. For the solver to operate correctly an axis boundary condition must be specified at the centreline of an axisymmetric geometry.

The flow field modelling options that relate to both the 2D and 3D models were the same as those described in Section 3.3.2.

The species transport simulations were performed using the uncoupled processing technique. This method was chosen because it was considerably quicker than the coupled processing method and Parametric test 2 had previously demonstrated that there was no loss of accuracy. Only the second order temporal discretization scheme was used because Parametric tests 1, 2 and 3 had demonstrated that the first order scheme suffered from excessive numerical dispersion. The simulations were conducted using the first and second order upwind spatial discretization schemes in 2D. Simulations were only conducted using the second order upwind scheme in 3D because Parametric test 4 had demonstrated the predictions made by the first

order scheme were insensitive to changes in the flow field close to the wall, thus allowing the data from these tests to be re-used.

In all of the tests a slug of tracer was released from the velocity inlet for 1.2 seconds. The movement of the tracer was then simulated until the mass fraction left in the pipe was zero. The convergence criterion for the species transport equations was set to 1 $x10^{-3}$, with a maximum of twenty iterations per time step. The maximum number was required when the tracer initially entered the pipe, or at the end of the simulation when low concentrations of tracer were left in the pipe.

Time step independence was determined for each mesh and each species transport modelling configuration separately. It was deemed to have occurred when further reduction in the time step did not alter the value of the longitudinal dispersion coefficient obtained from the equilibrium zone. Time step independence was reached by 0.02 seconds in all of the configurations.

It was not possible to made a direct comparison between the length of CPU time required to complete the simulations because the 2D simulations were conducted on a different platform to the one mentioned in Section 3.3.1. However, it was estimated that on the same platform the 2D simulations would have been approximately 7 – 12 times faster.

3.3.7.2 Data analysis

A comparison was first made between the flow fields generated by the 2D and 3D models. If the flow fields were not the same in both models any comparison of tracer movement would have been irrelevant. Three flow field parameters were selected for the comparison, the velocity magnitude, the turbulent kinetic energy (k), and the turbulent dissipation rate (ε). In order to record these properties monitoring lines were created in the flow. When a cell touched the monitoring line the required flow properties were recorded. In 2D one line was created along the radius, while in 3D four lines were created perpendicular to each other and along the radius.

The spatial variation in the three flow properties was the same in both 2D and 3D for the meshes with the same boundary layer thickness. A comparison between the flow properties recorded from mesh 7 (3D) and mesh 11 (2D) are presented in Figure 3.33 as an example. Consideration was therefore given to determining if the species transport model's predictions would also be the same in 2D and 3D.

The temporal profiles recorded during the simulations are shown in Figure 3.34. The profiles for the different mesh densities were the same so only one set is presented. Tests were not conducted using the first order upwind scheme in 3D for the reasons discussed previously. The profiles that are presented relate to Mesh 4 reported in Parametric test 4.

The temporal profiles from the 2D and 3D simulations were the same for both of the boundary layer thicknesses considered and for both of the spatial discretization schemes considered. The temporal profiles were the same for both of the boundary layer thicknesses when the first order upwind scheme was used, again demonstrating the inability of the scheme to detect differences in the flow field close to the wall. The profiles reflected the differences in the boundary layer thickness when the second order scheme was used, with the dispersion being greater when the smaller boundary layer thickness was used.

3.3.7.3 Conclusion

The aim of this series of tests was to determine whether the predictions made using a 3D model could be replicated using a 2D model. The initial comparison made between three flow field properties demonstrated that a 3D flow field could be replicated in 2D. A comparison subsequently made between the recorded temporal profiles demonstrated that the predictions of solute transport made in 3D could also be replicated in 2D.

This study was repeated using the k-ε RNG and RSM turbulence models and the same conclusions were reached.

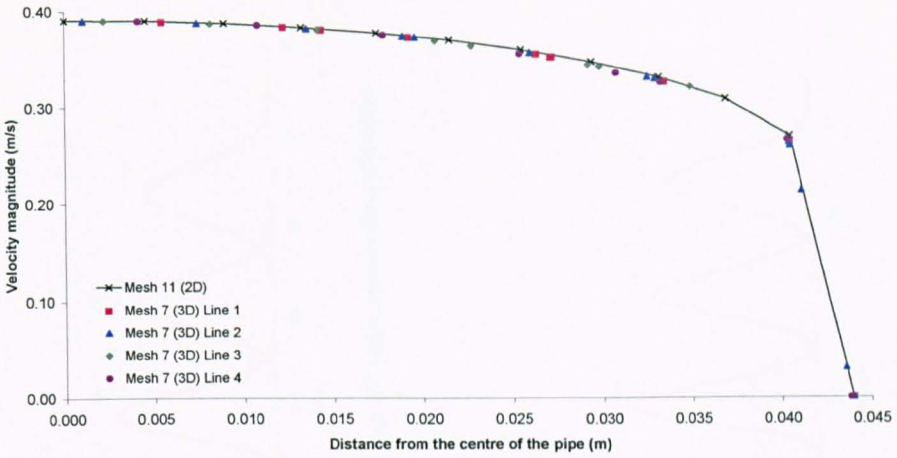

(a) Velocity magnitude

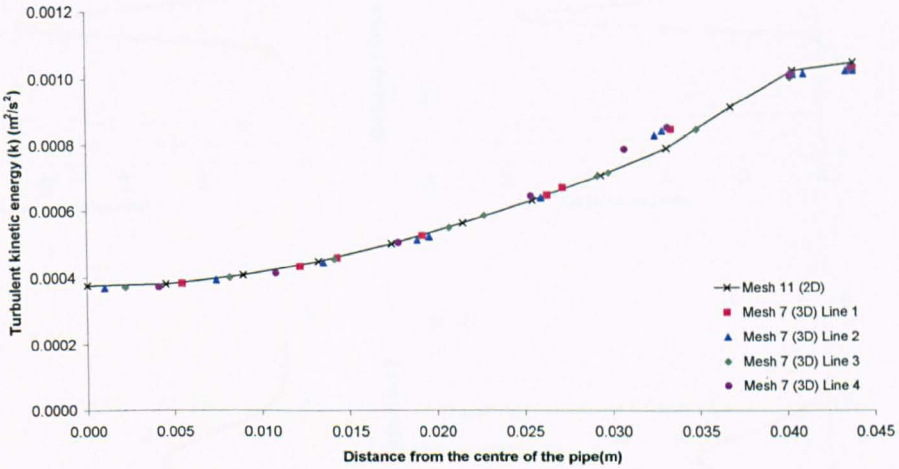

(b) Turbulent kinetic energy (k)

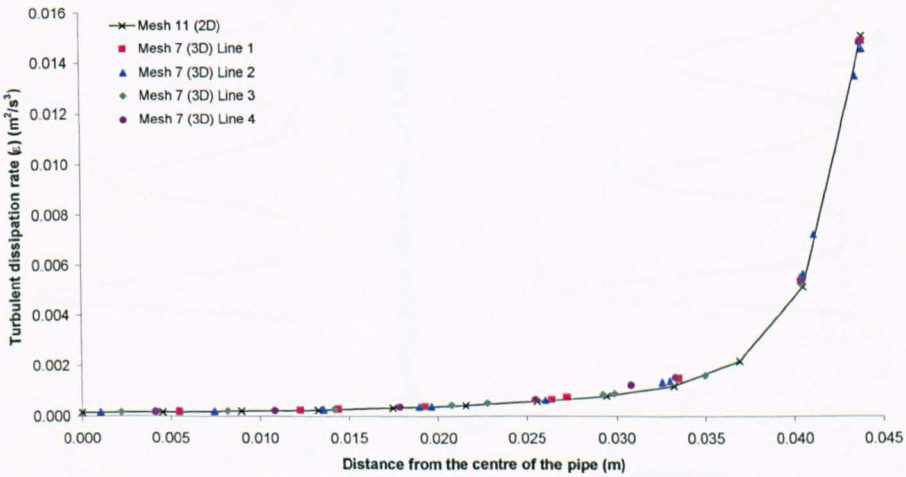

(c) Turbulent dissipation rate (ε)

Figure 3.33 A comparison of the three flow properties obtained using mesh 7 and mesh 11

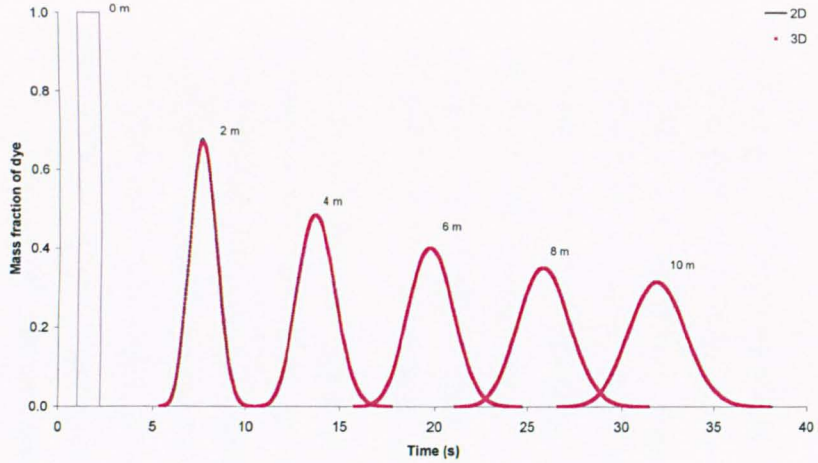

Bounday layer thickness = 35 mm (1st order spatial discretization)

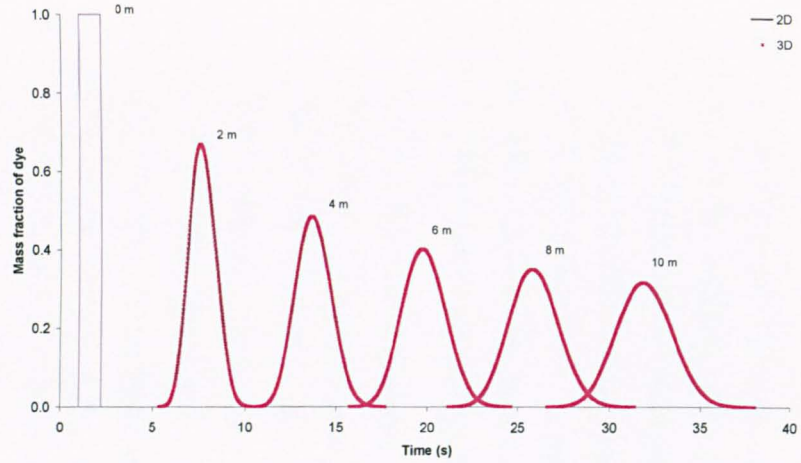

Bounday layer thickness = 65 mm (1st order spatial discretization)

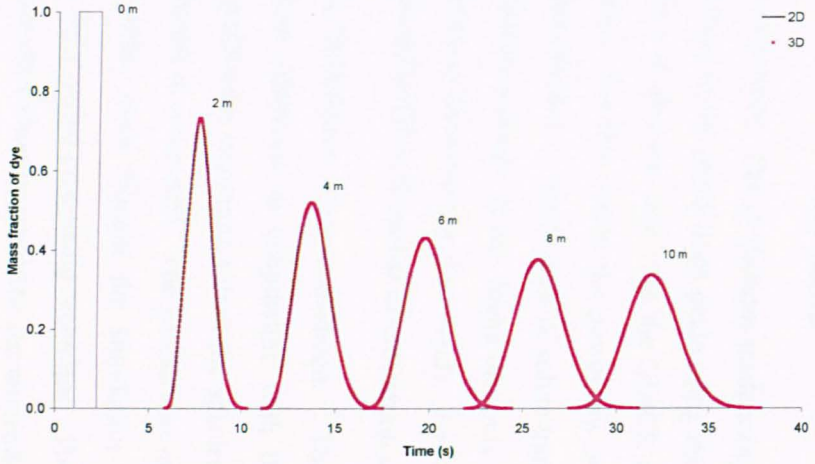

Bounday layer thickness = 35 mm (2nd order spatial discretization)

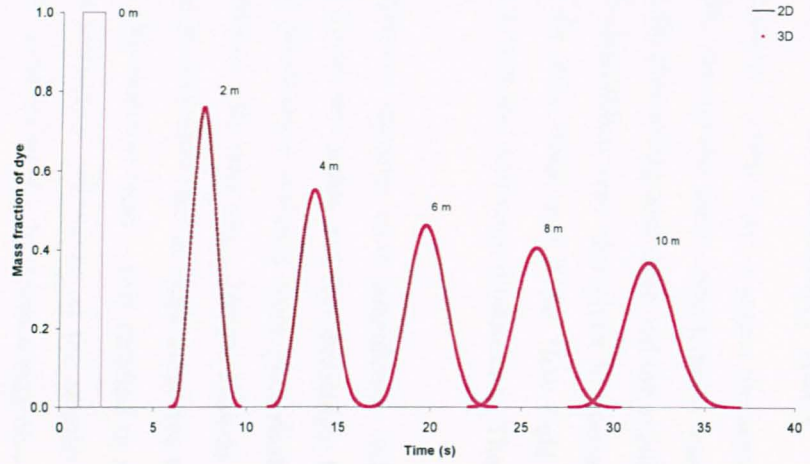

Bounday layer thickness = 65 mm (2nd order spatial discretization)

Figure 3.34 Temporal profiles (Parametric test 5)

3.4 Conclusion of species transport model feasibility study

The aim of the species transport model parametric study was to assess the sensitivity of the predictions to the modelling options selected. During the study consideration was given to the spatial and temporal discretization schemes, the processing technique and the available methods with which to introduce a new species. Consideration was also given to assessing how the predictions were affected by a change in the flow field, and if the flow field and species transport models predictions were the same in both two and three dimensions. The conclusions to the parametric study are highlighted below:

- First and second order temporal discretization schemes were considered. When the first order scheme was used the mass of the tracer was stable and the predictions followed the idealised Fickian model. However the predictions suffered from numerical dispersion, shown by a change in the spread of the tracer with time step. The predictions made using the second order scheme were not robust at each time step as extra mass was added to the start of the tracer plume when the time step was too large. This resulted in a non linear increase in the variance and a negative skewness. However, at the smaller time steps considered the predictions made using the scheme were robust and it was also possible to obtain a time step independent solution. Future tests should, therefore, use the second order temporal discretization scheme, but check for time step independence.

- Four spatial discretization schemes were considered. The predictions made using the power law scheme were found to be almost identical to the predictions made using the first order upwind spatial discrtization scheme. This was also the case with the QUICK and second order upwind spatial discretization schemes. For this reason the power law and QUICK schemes were not considered beyond Parametric test 1. Predictions of solute transport were made using the two schemes on six different flow fields. It was found that only the second order scheme was able to detect the differences between the flow fields. For this reason future tests should use the second order upwind or QUICK spatial discretization schemes.

- The coupled and uncoupled processing techniques were considered. The coupled processing technique solves the fluid flow equations in conjunction with the species transport equations, while the uncoupled processing technique solves the species transport equations in isolation after the flow simulation is completed. The predictions made using both techniques were found to be the same, even thought the simulation time was approximately 10 time longer when using the coupled processing technique. Therefore, if the flow field is steady, the uncoupled processing technique would be recommended.

- It was found that the choice of the introduction method did affect the shape of the temporal profile at each monitoring location, but did not affect the travel time or the amount of dispersion between them. If the shape of the profile is not of interest, a short slug injection

is recommended because the overall simulation time would be less than for a longer injection.

- Both the flow and species transport equations were conducted on equivalent 2D and 3D meshes. It was found that the predictions were the same in both respects. Where possible it would be of benefit to simulate in 2D as the amount of simulation time required is approximately 10 % of the time required for the same 3D simulation.

These tests have demonstrated that the species transport model has the potential to be a good method for predicting solute transport if the modelling options are specified correctly. The data can be extracted from the model in a form that is suitable for analysis, the predictions are sensitive to the underlying flow field and if sought time step independent solutions are possible. Although the run times can be significant (up to 1 week for some of the tests) these can be reduced by using the uncoupled processing technique and simulating in two dimensions. Also, unlike the discrete phase model only one simulation is required for each modelling configuration because stochastic methods are not used.

4 Feasibility study on the discrete phase model

4.1 Introduction

This chapter reports on the second half of a feasibility study that examined the viability of two models that are available in the Fluent software for predicting the transport of a solute. The previous chapter focused on the species transport model, while this chapter considers the discrete phase model.

The transport of a solute tracer in a turbulent flow may be modelled using the discrete phase model by assuming that the tracer can be represented by a large number of discrete particles that are each subjected to advection and dispersion. The predictions obtained when using the discrete phase model are dependent upon the modelling options selected. These include the particle characteristics, the initial conditions, the forces acting on the particle and the response to solid boundaries. The modelling options that are considered most relevant to the transport of a non reacting solute are described in Section 4.2.

A major aspect of the feasibility study was a parametric study that examined the sensitivity of the simulation results to the modelling options selected. The modelling options considered during the parametric study were the injection location, the Saffman lift force, the characteristic eddy lifetime, the diameter of the particles and the length scale. Consideration was also given to how the transport was affected by a change in the flow field and if the predictions were the same in both two and three dimensions. The parametric study is reported in Section 4.3.

Section 4.4 summarises the findings of the discrete phase model feasibility study. This includes recommendations for appropriate default settings and modelling techniques, and suggestions for further investigation.

Section 4.5 summarises the findings of both the discrete phase model and species transport model feasibility studies. A recommendation is also made regarding which of the two transport models to consider for further investigation.

4.2 The discrete phase model

The discrete phase model, more commonly called the particle tracking model, solves transport equations for discrete particles that are dispersed in the continuous phase. The trajectories of the particles are determined by equating the inertia of the particles with the forces acting on

them from the continuous phase. The effects of turbulence on the particle's trajectory may also be modelled through the use of stochastic methods. The discrete phase model is described in detail in the Fluent 5 User's Guide (Fluent, 1998) and a summary is presented in Chapter 2.

A number of inputs are required for the discrete phase calculations. These relate to the physical properties of the particles, the initial conditions, the way in which the particles respond to the boundary conditions, the trajectory calculations and the calculation procedure. Presented below are the inputs that appear most relevant to the transport of a non-reacting solute in a turbulent flow.

Coupling between the discrete and continuous phase

The trajectory calculations are based on the forces acting on the particle from the local fluid phase. Fluent 5.5 can predict the movement of the particles based on a fixed flow field, termed an uncoupled simulation, or to also include the effects of the particle trajectories on the flow, termed a coupled simulation.

Initial conditions

Inputs are required for the initial location, velocity and diameter of the particles. These conditions are defined by creating an injection and assigning the relevant properties. Five injection methods are available in Fluent 5.5, including single and grouped injections. The main advantage of the group method is that a range of initial conditions may be specified. Fluent 5.5 considers the particles in each injection to be of a single material with a single density.

Trajectory calculation

The drag force acting on the particle is included in the force balance calculation. Fluent 5.5 supports three drag laws. The spherical law assumes the particles are smooth spheres, while the non spherical law allows the shape of the particles to be controlled by a shape factor term. The Stokes Cunningham law is used to represent the drag force on sub micron sized particles.

Where relevant, additional forces may be included in the force balance equation, such as the Saffman lift force to represent the effects of shear on sub micron particles, or thermophoretic forces when modelling temperature gradients.

Tracking parameters

The discrete phase model requires the force balance equation to be integrated with respect to time to obtain a particle trajectory. The integration time step, Δt, may be controlled by the length scale, L, Equation (4.1), or the step length factor. The length scale is equivalent to the distance the particle will travel before the trajectory is updated (the trajectory is also updated

when a particle crosses a cell boundary). Smaller values of the length scale may increase the accuracy of the trajectory calculations.

$$\Delta t = \frac{L}{u_p + u_c} \qquad (4.1)$$

where u_p is the velocity of the particle and u_c is the velocity of the continuous phase.

The maximum number of steps defines how many step lengths are considered per track. When the maximum number is exceeded the simulation stops and the particle fate is recorded as incomplete. This prevents a particle from being caught in a recirculating region and being tracked for infinity. The maximum number of steps available is 1 x10^9.

Discrete phase boundary conditions

Discrete phase boundary conditions are only used when a particle comes into contact with a physical boundary such as a wall or outlet. Fluent 5.5 supports three contingencies, reflect, trap and escape. The reflect options sends the particle back into the domain via an elastic or inelastic collision, which is altered via the coefficient of restitution. When a particle comes into contact with the trap and escape boundary conditions the trajectory calculations are stopped at the point of impact and the fate of the particle is reported accordingly.

Stochastic tracking parameters

The dispersion of particles due to turbulence may be predicted using the stochastic random walk model or the particle cloud model. The particle cloud model tracks the statistical evolution of a cloud of particles about a mean trajectory. The concentration of the particles within the cloud is represented by a Gaussian probability density function about a mean trajectory. The initial and maximum cloud diameters are required as inputs.

The stochastic random walk model represents the effects of turbulence as fluctuating velocity components that are discrete functions of time. The random values are kept constant over an integral of time given by the characteristic lifetime of the eddies. The characteristic lifetime of the eddy may be defined as a constant function, or as a random variation about the Lagrangian time integral. The Lagrangian time integral is used in both lifetime equations and is determined by the turbulent kinetic energy (k), the turbulent dissipation rate (ε), and a time scale constant. Little is known about the time scale constant, however the Fluent 5 User's Guide (Fluent, 1998) suggests a value of 0.15 when the k-ε models are used and 0.3 when the Reynolds Stress Model (RSM) is used.

Two identical particles that are released from the same location, but at different times, will not necessarily follow the same path when using stochastic tracking. In order to obtain a

meaningful representation of turbulence a sufficient number of "tracks" must be performed. The number of repeat tracks, or the number of tries, may be specified to any value.

4.3 Parametric analysis of the discrete phase model

4.3.1 Introduction

The aim of the parametric study was to assess the sensitivity of the simulation predictions to a selection of the modelling options. The modelling options considered were regarded as the most relevant for a non-reacting species and were the injection location, the Saffman lift force, the characteristic lifetime of the eddy, the particle diameter and the length scale. Consideration was also given to how the predictions were affected by changes to the flow field and if they were the same in both two and three dimensions. The focus of each test was as follows:

- Parametric test 1: Injection location
- Parametric test 2: Saffman lift force
- Parametric test 3: Characteristic lifetime of the eddy
- Parametric test 4: Length scale
- Parametric test 5: Particle diameter
- Parametric test 6: Flow field
- Parametric test 7: 2D and 3D

The test procedure and analysis techniques were similar to the ones used in the parametric study on the species transport model. In each of the tests the particles were released from the inlet of the pipe and were then tracked through the pipe until exit from the outlet. Monitoring positions were created at two metre intervals along the length of the pipe. The time when each of the particles passed a monitoring position was recorded, thus allowing a series of temporal profiles to be created. Moment analysis was performed on the profiles in an attempt to establish a link between the movement of the particles and the modelling options selected. The equations that were used are presented in Section 3.3.1.

In order to fully assess the impact of the modelling options a full programme of sensitivity tests should have been conducted in which all of the modelling options were altered in relation to each other. Unfortunately the number of tests that would have been required to do this would have been prohibitively large. Instead the modelling options were altered in relation to a set of default modelling parameters. The default parameters are described in Section 4.3.2.

The random walk model was implemented to represent the influence of turbulence on the particle trajectory. In order to obtain a statistical representation of turbulence a sufficient

number of tracks must be performed. The procedure that was used to determine how many repeat tracks were required is reported in Section 4.3.3.

All the simulations were performed using a standard PC running under the Windows 2000 operating system with a 2 GHz Intel Pentium 4 processor and 1048 Mbytes of RAM.

4.3.2 Default parameters

As previously mentioned the modelling options considered during the parametric tests were altered in relation to a set of default values. The default parameter values are specified in Table 4.1, with a further explanation below where required. The options are based on the 3D pipe reported in Section 3.3.2.

- The density of the particles was specified to be the same as the continuous fluid phase, 998.2 kg/m^3, while the diameter was left at the default setting of 1 x10^{-6} m.
- The particles were released from the velocity inlet using a surface injection. This method was chosen because it was anticipated that it would encourage the particles to mix. When a surface injection is used the particles are released from the centre of each cell face in contact with the surface. There are 145 faces in contact with the inlet surface, resulting in a corresponding number of injection positions. The initial velocity of the particles was specified to be zero in all directions. However, the value selected was not important as the velocity of the particles stabilised to the flow velocity a short distance after release (in the order of centimetres).
- The turbulent dispersion of the particles was modelled using the random walk model. The time scale constant used in the model was specified to be 0.15 following the recommendations made in the Fluent 5 User's Guide (Fluent, 1998). The characteristic lifetime of the eddy was defined as a constant function (random eddy set to off). The number of repeat injections was set to 450, creating 65250 (450 x 145 injection positions) individual particle tracks in each simulation. 450 repeat injections were chosen because the data file created by Fluent was the maximum size that could be read into the Microsoft Excel software for analysis. In the following sections each batch of 65250 individual particle tracks is referred to as a 'test'.
- The length scale was left at the default setting of 0.01 m. The maximum number of time steps was specified to 1 x10^5 to ensure that each particle left the domain.

Parameter	Setting / Value
Particle properties	
Density	998.2 kg/m^3
Diameter	1 x10^{-6} m
Boundary conditions	
Inlet	Escape
Outlet	Escape
Wall	Reflect (elastic collision)
Initial conditions	
Type of injection	Surface injection
Location	Velocity inlet
Velocity	Zero in all directions
Trajectory calculations	
Drag law	Spherical
Saffman lift force	Off
Turbulence	
Model	Random walk model
Characteristic eddy lifetime	Constant function
Time scale constant	0.15
Number of repeat injections	450
Tracking parameters	
Length scale	0.01 m
Maximum number of steps	1 x10^5

Table 4.1 Default modelling parameters used in the discrete phase parametric study

4.3.3 Number of stochastic simulations

The random walk model uses stochastic methods to represent the effects of turbulence on the particle trajectory. In order to obtain a statistical representation of the stochastic turbulence a sufficiently large number of particles need to be tracked before reporting final behaviour. If $\bar{x}$ is the sample mean, then the 99 % confidence limits for the true mean of a Gaussian population distribution are defined as:

$$\bar{x} \pm 2.58 \frac{\sigma_p}{\sqrt{n_s}} \qquad (4.2)$$

where σ_p is the standard deviation of the population and n_s is the sample size.

In order to determine representative values for the sample mean and standard deviation twenty repeat tests (each based on 65250 individual particle tracks) were performed using the default modelling configuration shown in Table 4.1 and the flow field reported in Section 3.3.2.

During the species transport model parametric study the concentration of the tracer was recorded directly at every time step for each monitoring position. However, in the case of the particle tracking model some data manipulation was required in order to convert individual

track records into profiles of concentration versus time. This was achieved by disctretizing the time axis into fixed intervals and recording the number of particles passing the monitoring point during each time interval. It was not clear whether the interpretation of the temporal profiles would be sensitive to the time interval selected. For this reason four intervals were initially considered: 0.01, 0.1, 0.2 and 0.5 seconds. An example of the temporal profiles created using each of these intervals is shown in Figure 4.1 (the profiles have been normalised with respect to the 0.01 second sampling interval to ensure that the area under each profile was the same). The profiles from each of the sampling intervals followed the same basic shape, with the start, peak and end at approximately the same time.

Figure 4.2 shows the results of the moment analysis conducted on the profiles shown in Figure 4.1. When the 0.01, 0.1 and 0.2 second sampling intervals were used the predictions were almost identical. When the largest sampling interval (0.5 seconds) was used the predictions differed marginally. As the time required to create and analyse the temporal profiles was approximately the same for all of the sampling intervals it was decided that an interval of 0.1 seconds was appropriate to use. Figure 4.3 shows the temporal profiles calculated at four locations for the first five tests, with the remaining tests omitted for clarity. All the profiles have approximately the same shape, with the differences between them a reflection of the stochastic turbulence. Moment analysis of the temporal profiles was undertaken, with the results for the first ten tests shown in Figure 4.4. The results of the moment analysis are discussed further in Section 4.3.4.

Table 4.2 shows the mean and standard deviation of the predictions of the centroid and the temporal variance that were determined for the twenty repeat tests. Also shown are the number of repeat tests required to achieve a maximum deviation within 1 %, 1.5 % and 2 % from the mean. It was assumed that a maximum deviation of 1.5 % would be acceptable so only one simulation was considered in each of the subsequent parametric tests. This reflects the high number of particle tracks that are incorporated into a single test result.

	Centroid (s)					Variance (s^2)				
	$\bar{x}$	σ_p	n_s			$\bar{x}$	σ_p	n_s		
		($x10^{-3}$)	1 %	1.5 %	2 %		($x10^{-3}$)	1 %	1.5 %	2 %
x = 2 m	6.097	1.353	1	1	1	0.297	1.068	1	1	1
x = 4 m	12.058	2.503	1	1	1	0.698	2.811	2	1	1
x = 6 m	18.015	4.198	1	1	1	1.098	4.550	2	1	1
x = 8 m	23.954	5.506	1	1	1	1.502	5.276	1	1	1
x = 10 m	29.910	6.119	1	1	1	1.906	4.844	1	1	1

Table 4.2 The mean and standard deviation of the twenty repeat tests and the number required to be within 1 %, 1.5 % and 2 % of the mean value

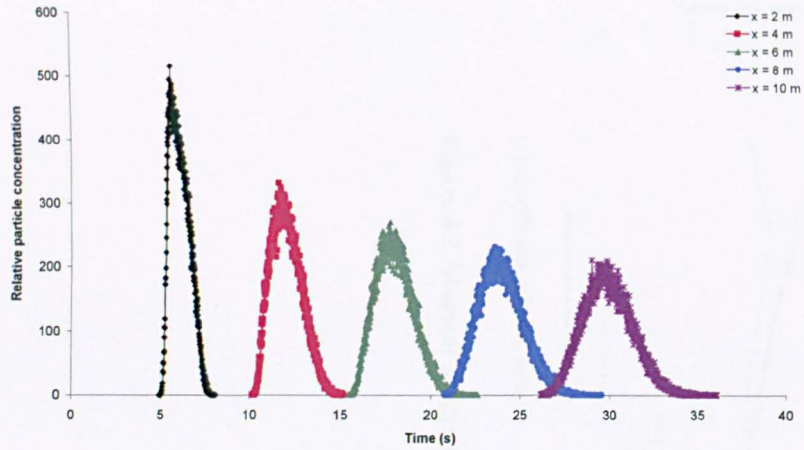

Sampling interval = 0.01 s

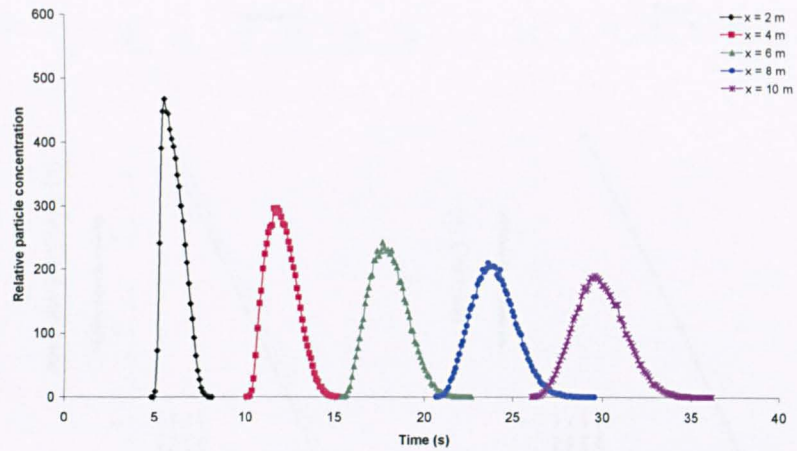

Sampling interval = 0.1 s

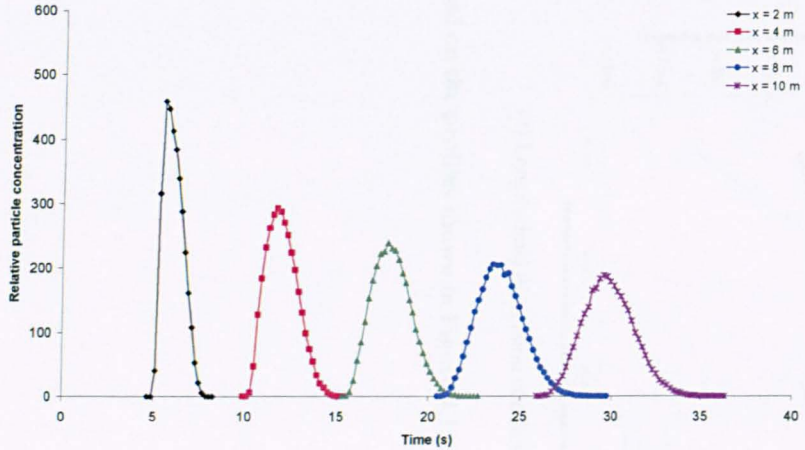

Sampling interval = 0.2 s

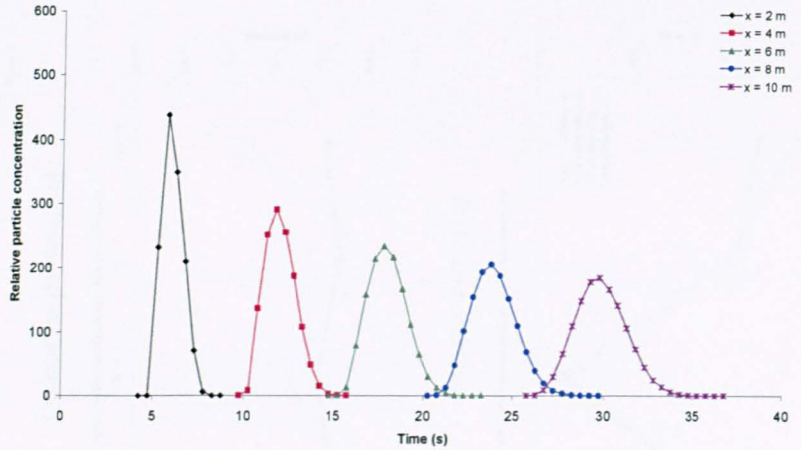

Sampling interval = 0.5 s

Figure 4.1 An example of the temporal profiles calculated using the different sampling intervals

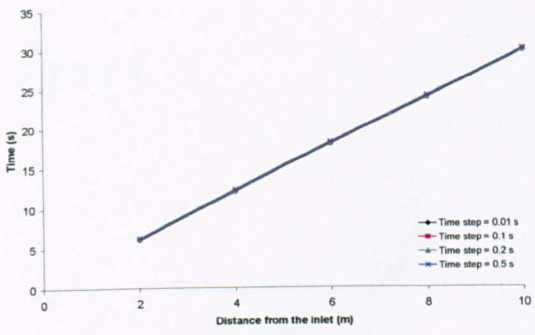

(a) Centriod

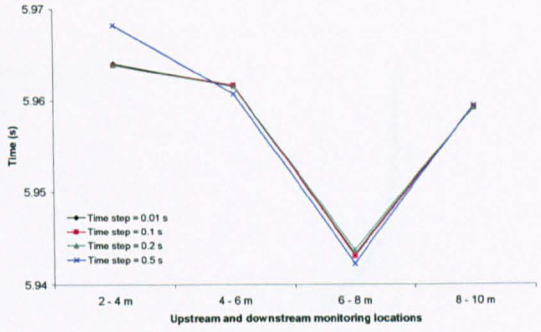

(b) Mean travel time

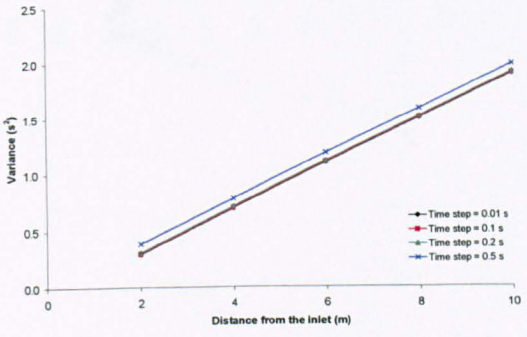

(c) Temporal variance

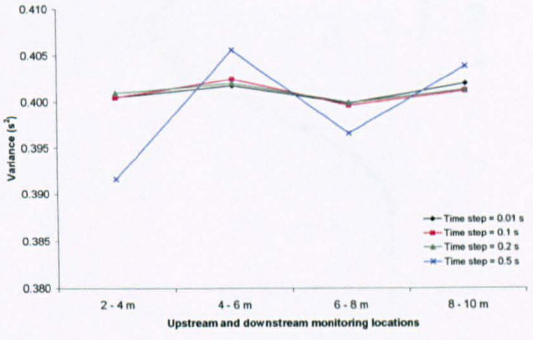

(d) Temporal variance (2)

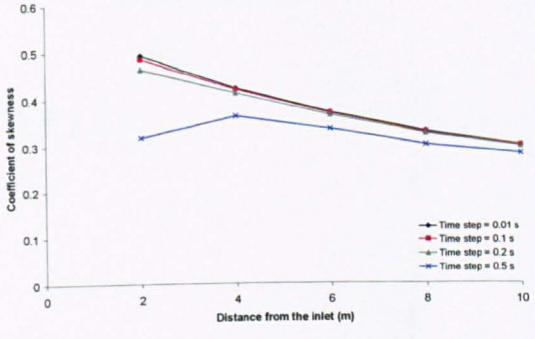

(e) Coefficient of skewness

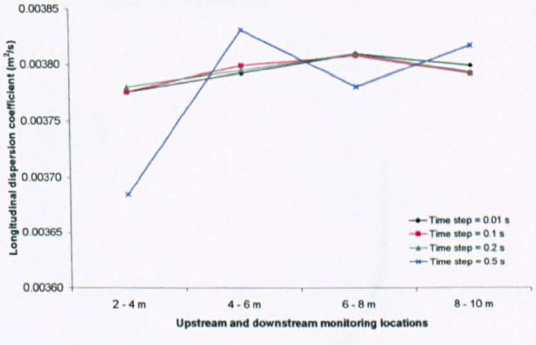

(f) Longitudinal dispersion coefficient

Figure 4.2 Moment analysis conducted on the profiles shown in Figure 4.1

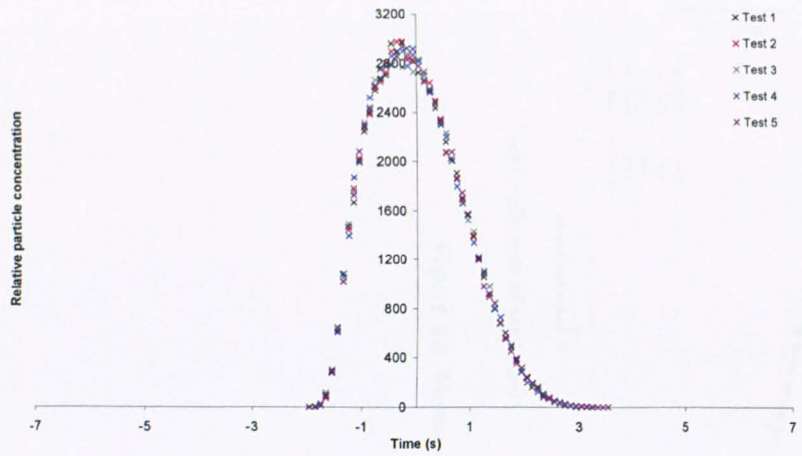

x = 4 m

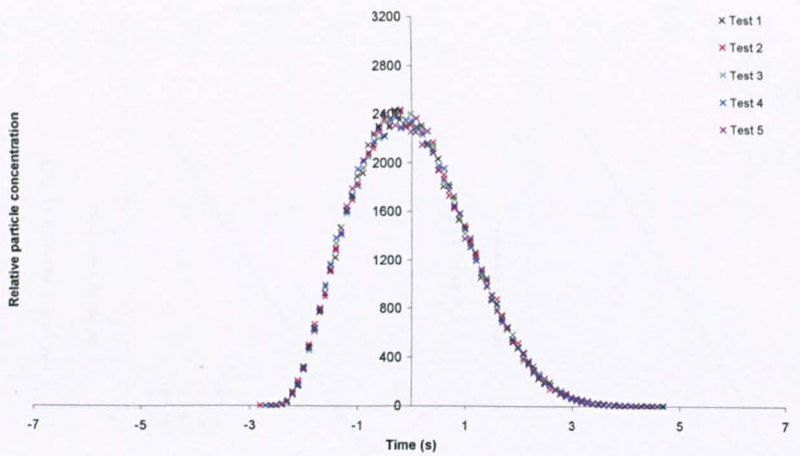

x = 6 m

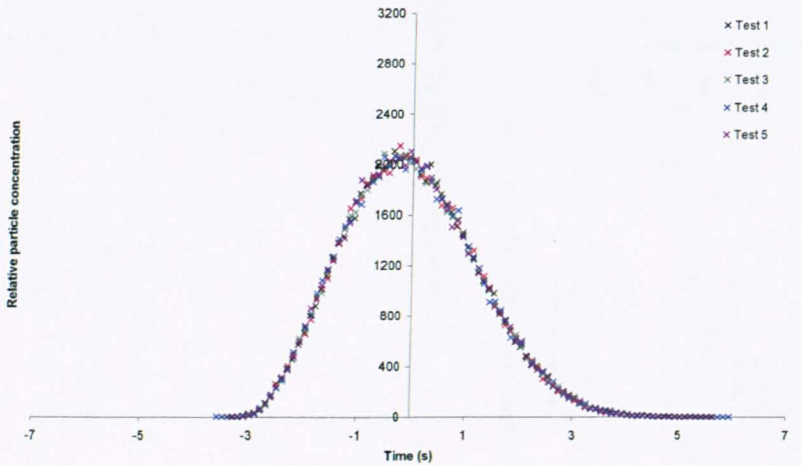

x = 8 m

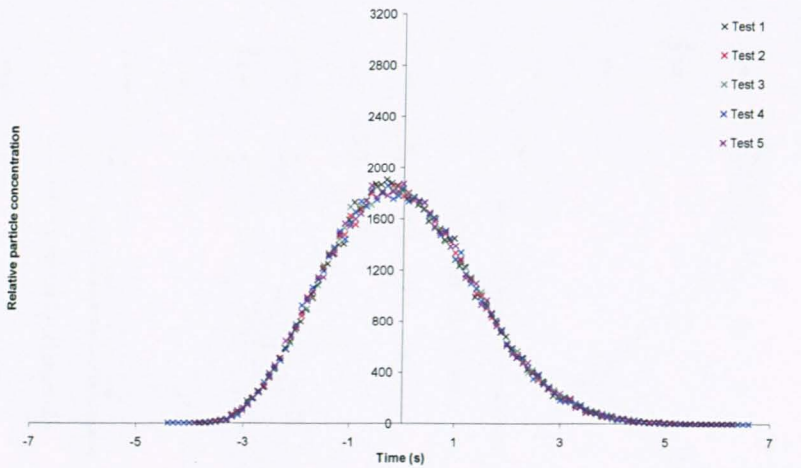

x = 10 m

Figure 4.3 The temporal profiles for the first five repeat tests

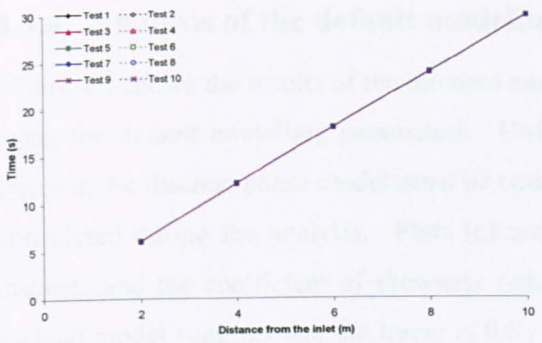

(a) Centriod

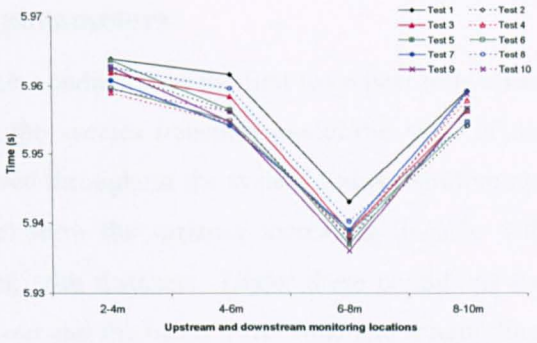

(b) Mean travel time

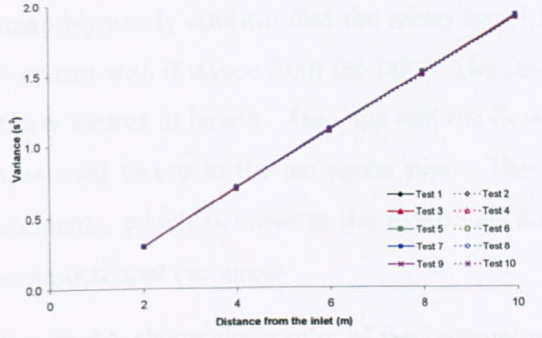

(c) Temporal variance

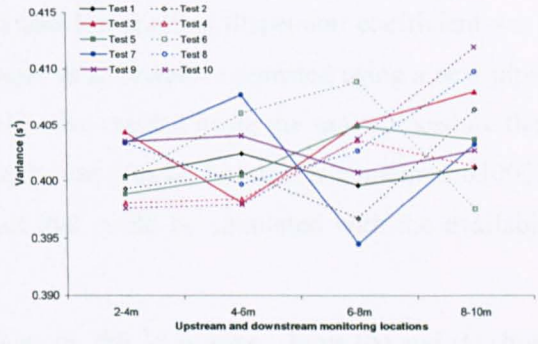

(d) Temporal variance (2)

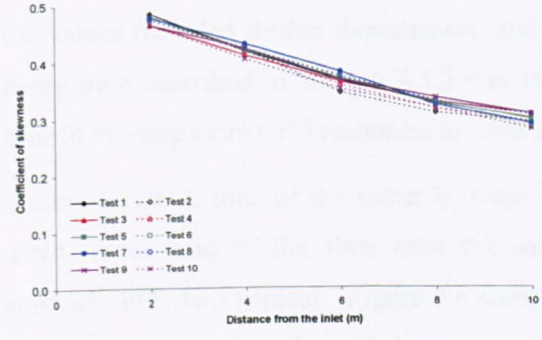

(e) Coefficient of skewness

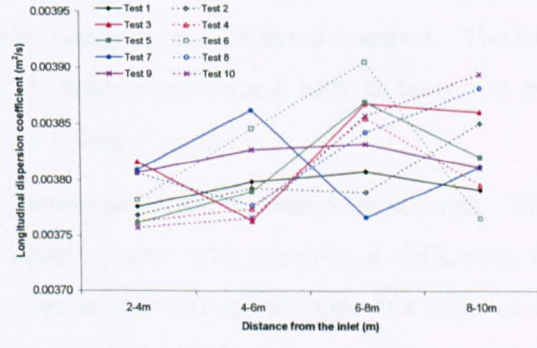

(f) Longitudinal dispersion coefficient

Figure 4.4 Moment analysis on the first ten repeat tests

4.3.4 Analysis of the default modelling parameters

Figure 4.4 shows the results of the moment analysis conducted on the first ten repeat tests when using the default modelling parameters. Unlike the species transport model the mass of the tracer in the discrete phase model must be conserved throughout the system and is therefore not considered during the analysis. Plots (c) and (e) show the variance increasing linearly with distance and the coefficient of skewness reducing with distance. Under these conditions the Fickian model suggests that the tracer is fully mixed and the mean travel time and longitudinal dispersion coefficient between monitoring positions should be constant. Plots (b) and (f) do not unambiguously confirm that the mean travel time and longitudinal dispersion coefficient were constant with distance from the inlet. The same tests were therefore repeated using a new pipe, thirty metres in length. The pipe and the flow field were created using the same procedure that was used to create the ten metre pipe. This length was chosen because it contained 630025 elements, which is close to the maximum number that could be simulated with the available computational recourses.

Figure 4.5 shows the results of the moment analysis on the 30 m pipe. Plots (b) and (f) show the values recorded between the monitoring positions over the first ten metres were typical of the values recorded further downstream, and could therefore be considered constant. The ten metre pipe described in Section 3.3.2 was therefore used in subsequent tests as there was no benefit in using extra CPU resources to simulate over a longer reach.

The mean travel time of the tracer between the monitoring positions was 5.95 seconds. The mean travel time of the flow over the same distance was 6.06 seconds, a difference of approximately two percent. Figure 4.6 shows a cross section through the pipe at a distance of four metres from the inlet and the positions where the first 10000 particles of Test 1 passed through. The particles were not evenly distributed over the cross section, but were more concentrated towards the centre of the pipe. This suggests the mean travel time of the tracer was less than the mean travel time of the flow because the particles were not experiencing enough of the lower flow velocities close to the wall.

Figure 4.7 shows the particle density distribution at three of the monitoring positions. The particle density distribution was higher at the centre of the pipe and lower at the wall of the pipe, again demonstrating the particles were not evenly mixed over the cross section. Although the particles were not evenly mixed, an equilibrium was established in which the distribution was approximately constant with distance. The parametric tests can therefore still demonstrate the impact of the modelling options on the predictions.

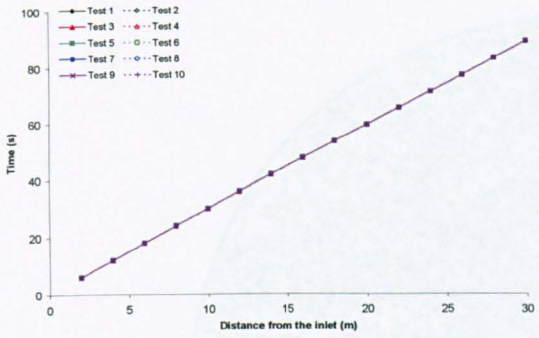

(a) Centriod

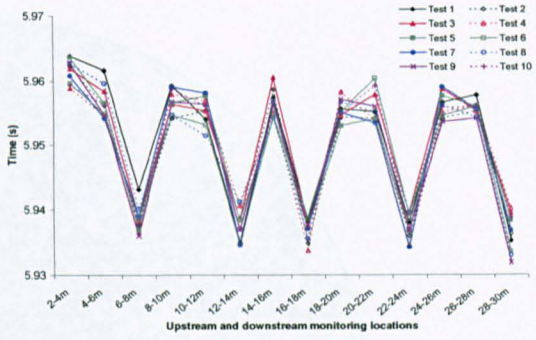

(b) Mean travel time

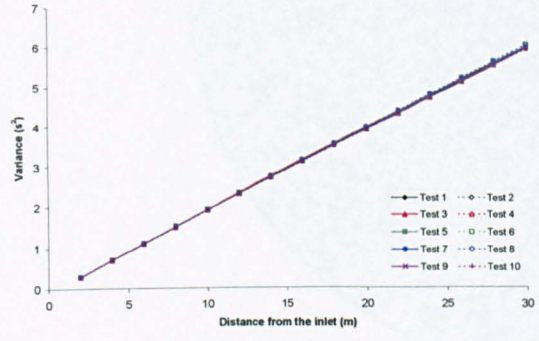

(c) Temporal variance

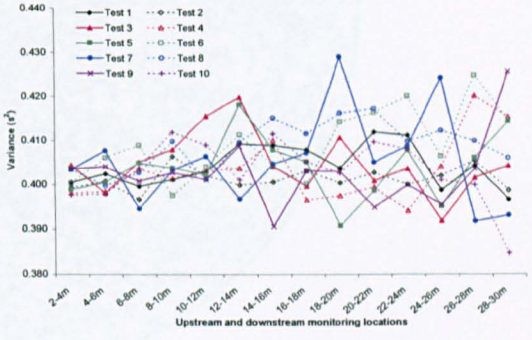

(d) Temporal variance (2)

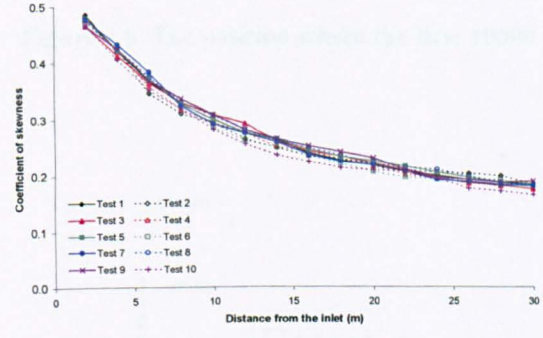

(e) Coefficient of skewness

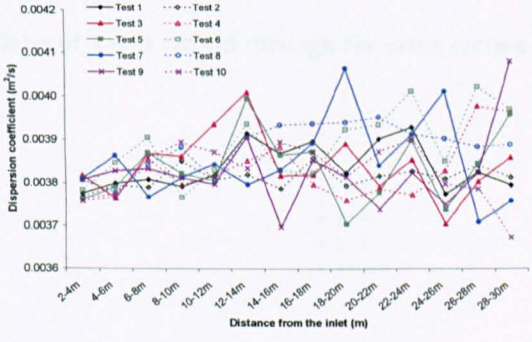

(f) Longitudinal dispersion coefficient

Figure 4.5 Moment analysis on the first ten repeat tests (30 m pipe)

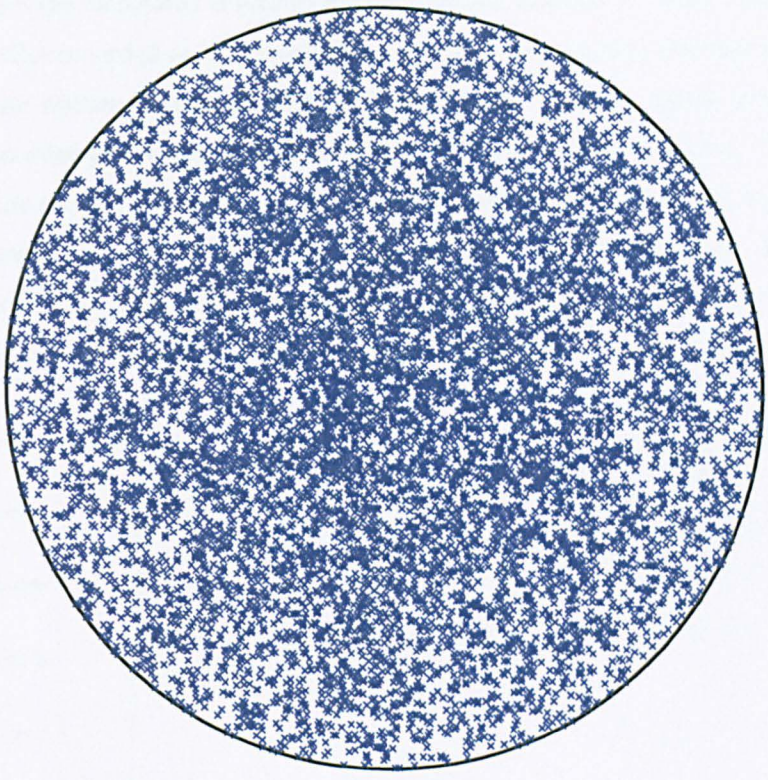

Figure 4.6 The position where the first 10000 particles of Test 1 passed through the cross section

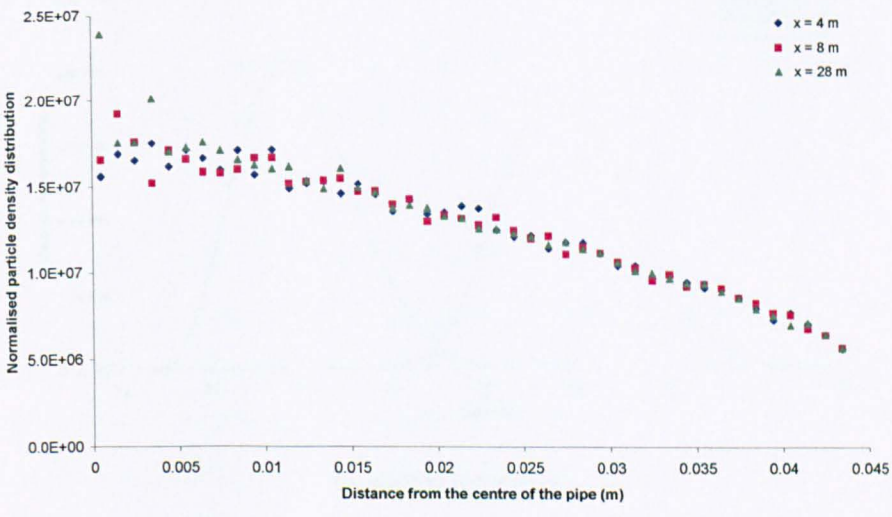

Figure 4.7 Normalised particle density distribution over the cross section

In order to confirm the calculated values of the longitudinal dispersion coefficient were accurate the temporal profiles recorded at 2, 4, 6 and 8 m were routed to the next downstream monitoring position using the routing procedure described in Chapter 2. The comparison between the predicted and recorded profiles was not good close to the inlet, Figure 4.8 (a). This difference occurs because the routing procedure cannot accurately transport a profile that has a steep rising limb. Further away from the inlet the accuracy of the prediction increased, Figure 4.8 (b). Although the accuracy of the dispersion coefficient cannot be demonstrated close to the inlet the parameter is still considered in further investigations as it is believed to be correct.

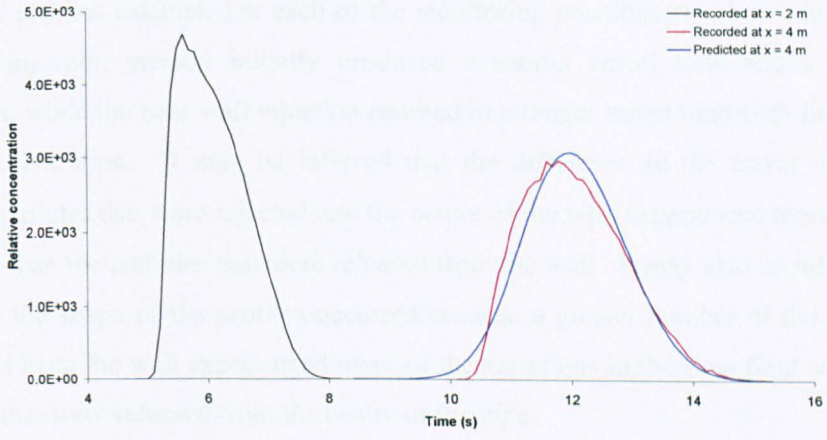

(a) two to four metres

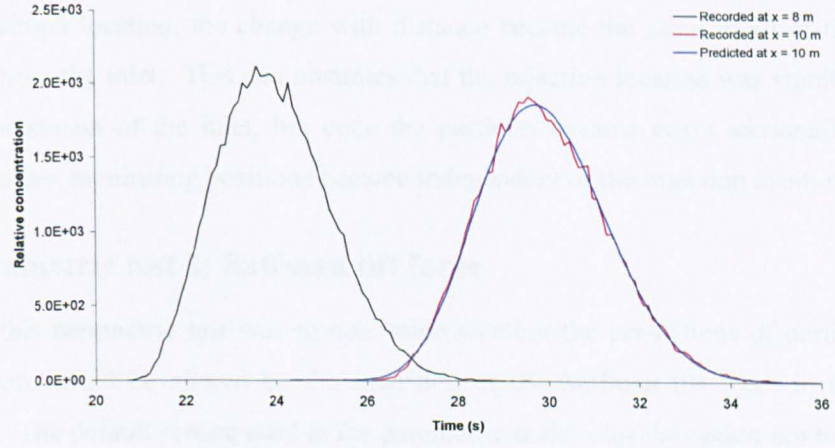

(b) eight to ten metres

Figure 4.8 An example of the recorded and predicted temporal profiles

The key findings of the parametric tests are shown in Figure 4.10 to Figure 4.15. They are grouped together according to the outcome rather than the parametric test. The default modelling options shown in Table 4.1 are represented by the results from Test 1 (Figure 4.3 and Figure 4.4) and are presented in blue.

4.3.5 Parametric test 1: Injection location

The aim of parametric test one was to determine the influence of the injection location on the transport of the particles. Three injection locations were considered; the default setting of an even injection over the inlet surface, and two point injections from the inlet, one from the centre of the pipe and one from the wall of the pipe. When the point injection method was used 65250 repeat injections were performed in order to ensure the total number of particles released in each of the tests was the same. All other modelling options were as the default parameters shown in Table 4.1.

The temporal profiles calculated at each of the monitoring positions are shown in Figure 4.10. The central injection method initially produced a shorter travel time and a higher peak concentration, while the near wall injection resulted in a longer travel time with little impact on the peak concentration. It may be inferred that the difference in the travel time occurred because the particles that were injected into the centre of the pipe experienced more of the faster moving flow than the particles that were released from the wall. It may also be inferred that the difference in the shape of the profiles occurred because a greater number of the particles that were released from the wall experienced more of the variations in the flow field compared with the particles that were released from the centre of the pipe.

Moment analysis was performed on the profiles, with the results shown in Figure 4.11 to Figure 4.15. Although the mean travel time and spread of the tracer particles were initially dependent upon the injection location, the change with distance became the same in all of the tests after four metres from the inlet. This demonstrates that the injection location was significant a short distance downstream of the inlet, but once the particles became cross sectionally mixed the transport between monitoring positions became independent of the injection location.

4.3.6 Parametric test 2: Saffman lift force

The aim of this parametric test was to determine whether the predictions of particle transport and dispersion would be altered by the inclusion of the Saffman lift force in the trajectory calculations. The default setting used in the parametric tests is for the option not to be included, Table 4.1, so a further simulation was performed with the option turned on, but with the remaining modelling options unchanged.

The temporal profiles calculated from both simulations are shown in Figure 4.10. The profiles are almost identical at each monitoring location, with the difference between them partly resulting from the stochastic turbulence. Moment analysis was performed on the profiles, with the results shown in Figure 4.11 to Figure 4.15. The inclusion of the Saffman lift force appears not to significantly affect the transport or dispersion of the tracer particles. Slight variations are shown in the predictions, however these are within the 1.5 % confidence limits.

4.3.7 Parametric test 3: Characteristic eddy lifetime

The aim of this parametric test was to determine whether changing how the characteristic lifetime of the eddy was specified would alter the predictions of particle movement. The characteristic lifetime of the eddy can be defined as a constant or random function. The default setting used in the parametric tests was a constant function, Table 4.1, so a further simulation was performed with the option set to random, but with the other modelling options unchanged.

The temporal profiles calculated from both of the simulations are shown in Figure 4.10. The profiles were very similar, however the peak concentration was less when using the random function. The results of the moment analysis are shown in Figure 4.11 to Figure 4.15. The mean travel time of the particles was not affected when the characteristic lifetime of the eddy was specified as a random function, but the spread was different, with an increase of approximately 6 %.

4.3.8 Parametric test 4: Length scale

The aim of this parametric test was to determine whether the predictions of particle movement were related to the length scale. The length scale is used to determine how far the particle moves before the trajectory is updated. Three different length scales were considered: the default setting used in the parametric tests of 0.01 m, plus 0.001 m and 0.0001 m. When the length scale was 0.001 m and 0.0001 the maximum number of steps was increased to 1 $x10^{6}$, and 1 $x10^{7}$ respectively. This was done to ensure that all the particles left the domain on each track. The remaining modelling options were specified according to the default settings shown in Table 4.1.

The temporal profiles calculated from the three simulations are shown in Figure 4.10. The profiles are almost identical at each monitoring location, with the difference between them partly reflecting the effects of the stochastic turbulence. Moment analysis was performed in an attempt to establish a link between the movement of the tracer and the length scale, with the results shown in Figure 4.11 to Figure 4.15. Altering the length scale did not significantly affect the mean travel time or spread of the tracer particles, with the small variations within the 1.5 % confidence limits.

4.3.9 Parametric test 5: Particle diameter

The aim of parametric test five was to determine whether the predictions of particle transport and dispersion were related to the particle diameter. Five different particle diameters were considered: the default setting used in the parametric tests of 1 $x10^{-6}$ m, plus 1 $x10^{-3}$ m, 5 $x10^{-5}$ m, 5 $x10^{-8}$ m and 1 $x10^{-9}$ m. All the other modelling options were specified according to the default settings shown in Table 4.1. The temporal profiles calculated from the five simulations are shown in Figure 4.10. The profiles relating to the 1 $x10^{-3}$ m particle diameter

were significantly different to the profiles relating to the other particle diameters, with a reduced peak concentration and the centroid offset.

Moment analysis was performed on the profiles, with the results shown in Figure 4.11 to Figure 4.15. The predictions made using all of the particle diameters follow the idealised Fickian model, with the equilibrium zone reached being after two metres from the inlet. The mean travel time of the particles was constant with distance in all of the tests. However, the prediction of mean travel time was slower than the mean travel time of the flow when the 1×10^{-3} m particle diameter was used, whereas the travel time was faster than the mean travel time of the flow when the other particle diameters were used. Likewise the spread of the particles was approximately the same for the smallest four diameters, while the variance was approximately thirty percent greater when the largest particle diameter, 1×10^{-3} m, was used. It may, therefore, be concluded that the predictions of solute transport were dependent upon the particle diameter, however they were constant when the particle diameter was less than 5×10^{-5} m.

4.3.10 Parametric test 6: Flow field

The aim of this parametric test was to determine whether changes to the flow field would affect the transport and dispersion of the particles. The changes to the flow field were caused by using different mesh densities. Three mesh densities were considered, corresponding to Mesh 1, 4 and 6 described in Section 3.3.6. Mesh 1 was the coarsest and Mesh 6 the finest, while Mesh 4 was used in the previous parametric tests. The flow field modelling options were specified to be the same for all the meshes, with details specified in Section 3.3.2. The mean flow rate was the same for all of the meshes, but the flow field close to the wall altered in relation to the mesh density, Figure 3.28.

The modelling options that related to the particle tracking routine were specified to be the same as the default options specified in Table 4.1. The only exception was that the number of repeat tests was altered to ensure the total number of particles released was approximately the same. This resulted in 1019 repeat tracks when Mesh 1 was used (65216 individual particle tracks) and 329 repeat tracks when Mesh 6 was used (65142 individual particles tracks). Figure 4.10 shows the temporal profiles calculated from the different tests. The mean travel time of the particles was approximately the same in all of the tests, but the amount of dispersion was not constant, with less dispersion occurring when the coarsest mesh (Mesh 1) was used.

Moment analysis was performed on the profiles, with the results shown in Figure 4.11 to Figure 4.15. All of the predictions followed the idealised Fickian model, with the equilibrium zone being reached after two metres from the inlet. The mean velocity of the particles was approximately the same for all of the mesh densities, but this was approximately two percent lower than the mean flow velocity. The spread of the tracer was not the same, with greater

dispersion occurring with increased mesh density. This demonstrates that the predictions made by the particle tracking routine were sensitive to changes in the flow field.

4.3.11 Parametric test 7: 2D and 3D

The aim of this parametric test was to determine whether the predictions made by the discrete phase model in three dimensions could be reproduced in two dimensions. If the approach could be simplified to two dimensions it would reduce the computational resources required to run future simulations. A similar comparison was made with the species transport model.

In order to make an accurate comparison it was ensured that the flow field was the same in both two and three dimensions. This was achieved by controlling the thickness of the boundary layer and ensuring grid independence in the core. In the previous study a comparison was made between four flow fields, with the predictions being found to be the same in both two and three dimensions. Therefore, only one flow field was considered in this parametric test to save time. The flow field used corresponds to Mesh 7 (3D) and Mesh 11 (2D), with details regarding the meshing technique and flow field in Section 3.3.7.

The particle tracking modelling options were specified to be the same as the default modelling options specified in Table 4.1. The only option that was altered was the number of repeat tracks as this ensured approximately the same number of particles were released in each test. 5930 repeat tracks were simulated in 2D (65230 individual tracks) and 375 repeat tracks in 3D (65250 individual tracks).

The temporal profiles calculated from the simulations are shown in Figure 4.10. The profiles are very different, with a greater peak concentration and increased skewness associated with the 2D solver. Moment analysis conducted on the profiles is shown in Figure 4.11 to Figure 4.15. The movement of the particles in both 2D and 3D followed the idealised Fickian model, with the equilibrium zone being reached after two metres from the inlet. When modelling in 3D the mean travel times of the tracer particles were approximately two percent lower than the mean flow velocity, and eight percent lower when modelling in 2D. The temporal variance of the tracer increased linearly with distance in both of the simulations, but the variance of the tracer between monitoring positions was not the same, with an increase of approximately 20 % when modelling in 3D. It should be noted that even though the mean travel time and variance were different, the longitudinal dispersion coefficient was approximately the same.

Figure 4.9 shows the normalised particle density distribution at two locations for both the 2D and 3D models. The density distribution is approximately the same, with a greater density at the centre of the pipe. The predictions of particle transport and dispersion should have been the same as the flow field and particle density distribution are the same in both models, but this is not the case. At this stage of the project an explanation cannot be presented to explain why this occurs.

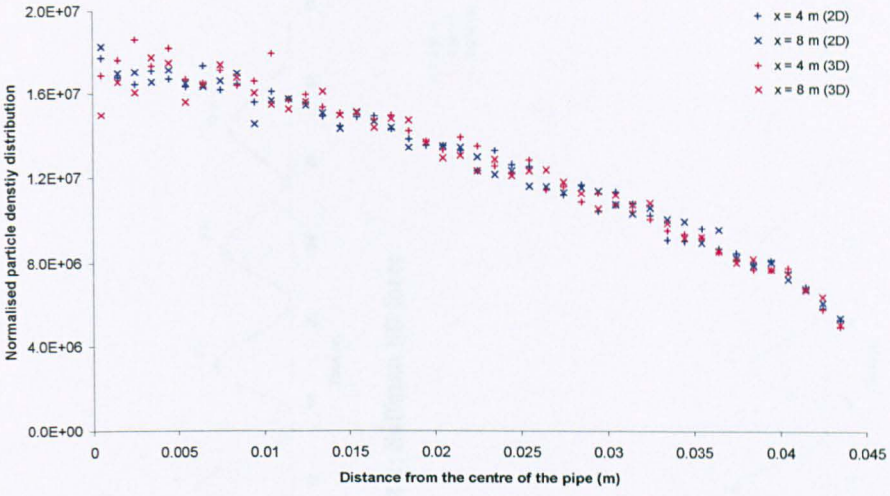

Figure 4.9 Normalised particle density distribution (Parametric test 7)

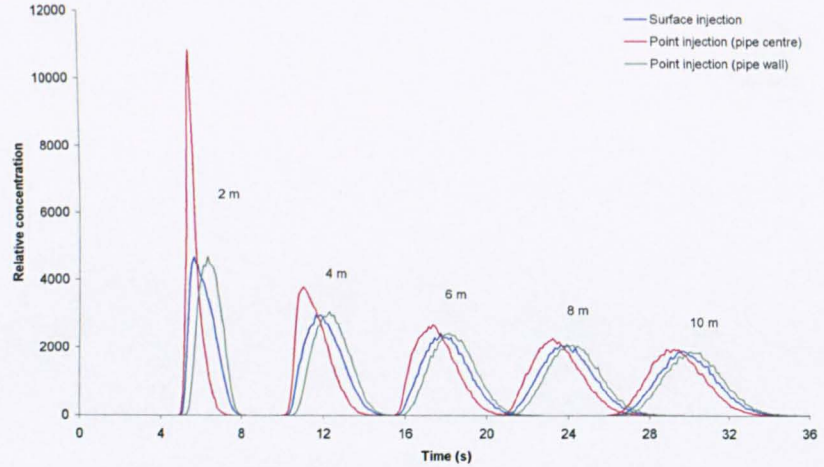

Test 1: Injection location

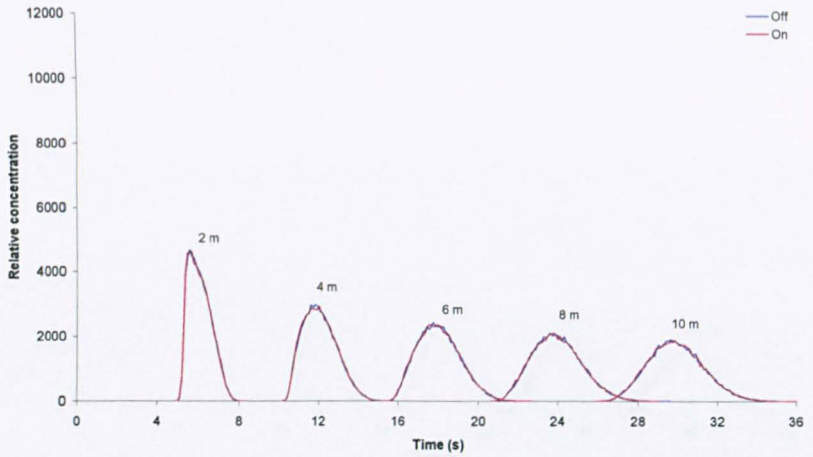

Test 2: Saffman lift force

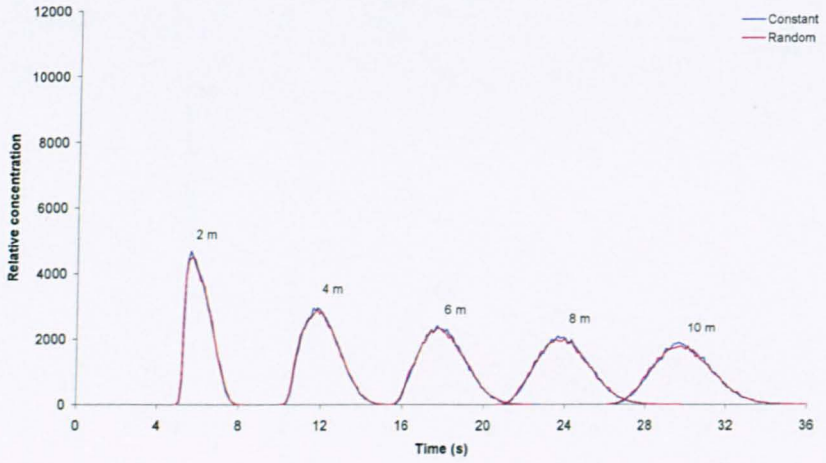

Test 3: Characteristic eddy llifetime

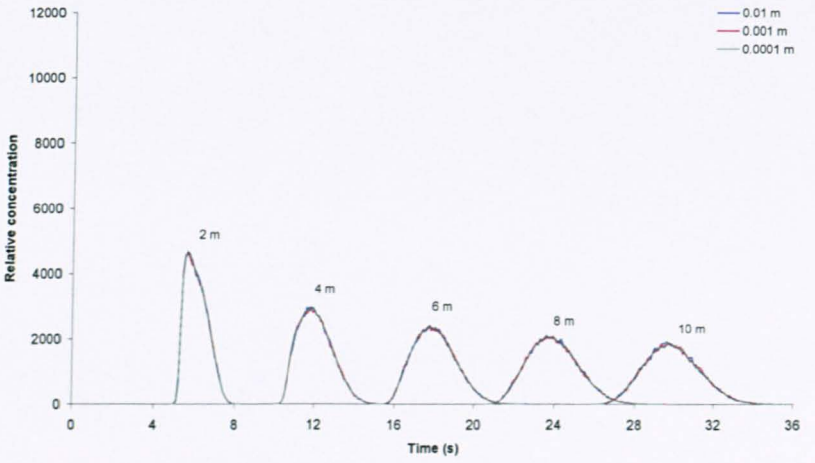

Test 4: Length scale

Figure 4.10 The temporal profiles from each of the parametric tests (continued overleaf)

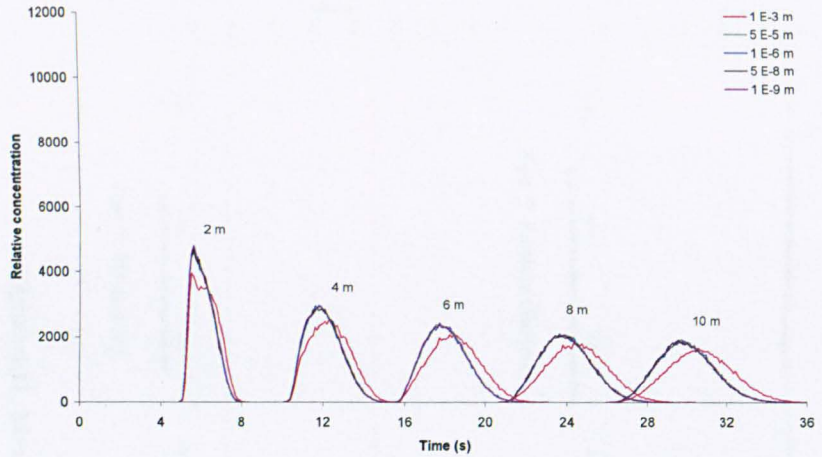

Test 5: Particle diameter

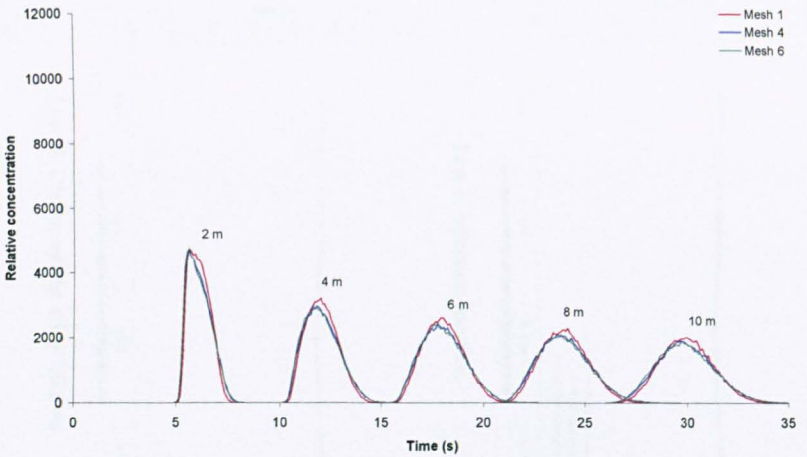

Test 6: Flow field

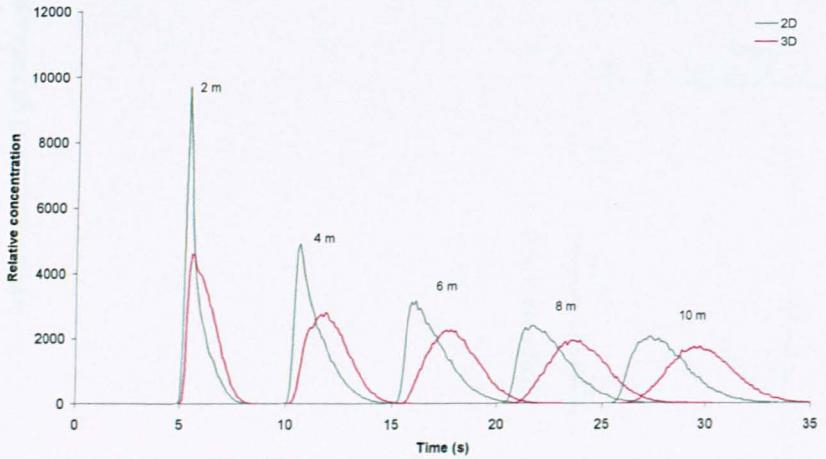

Test 7: 2D and 3D

Figure 4.10 The temporal profiles from each of the parametric tests (continued from previous page)

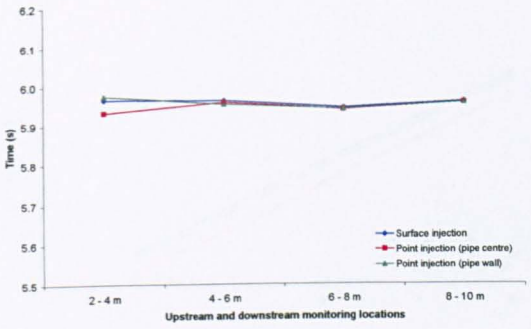

Test 1: Injection location

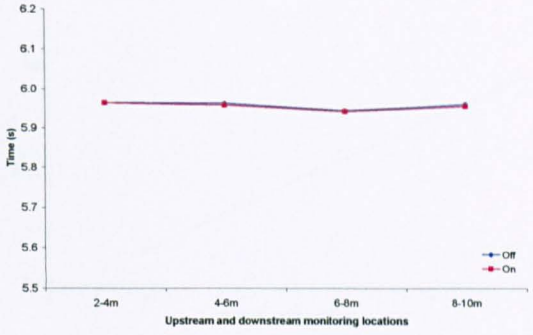

Test 2: Saffman lift force

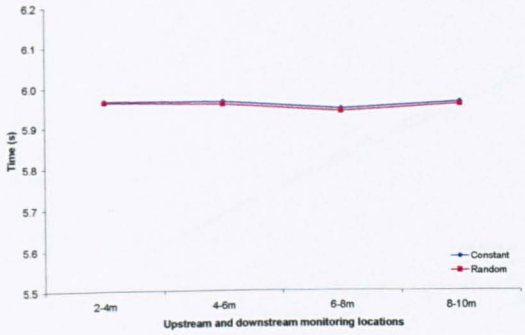

Test 3: Characteristic eddy lifetime

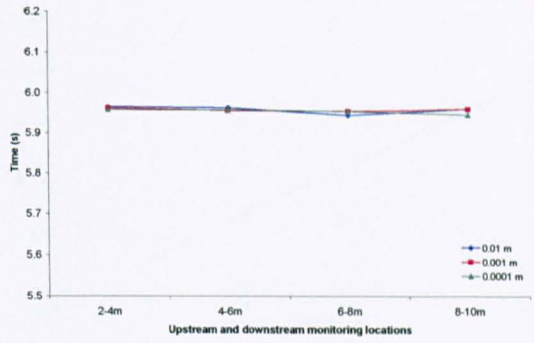

Test 4: Length scale

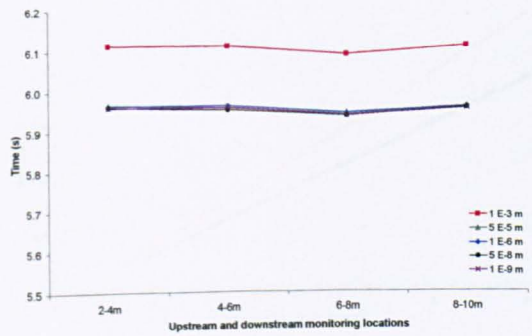

Test 5: Particle diameter

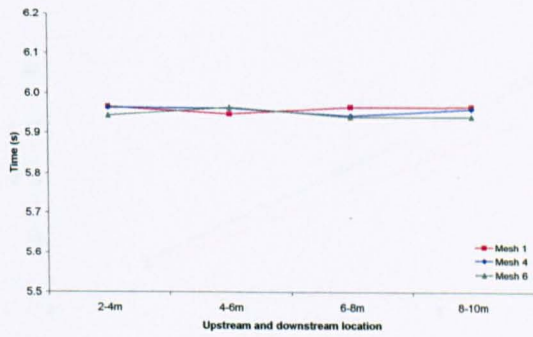

Test 6: Flow field

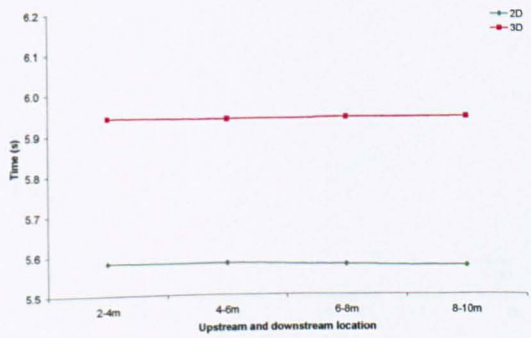

Test 7: 2D and 3D

Figure 4.11 Mean travel time (all parametric tests)

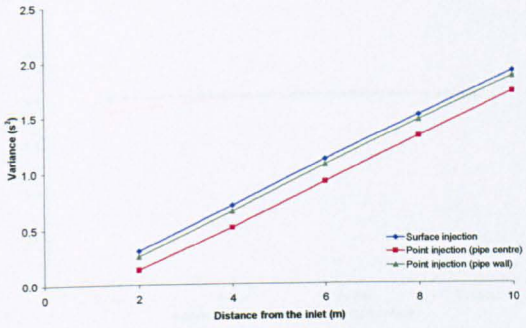

Test 1: Injection location

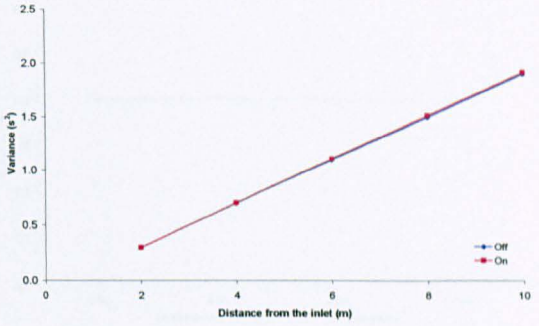

Test 2: Saffman lift force

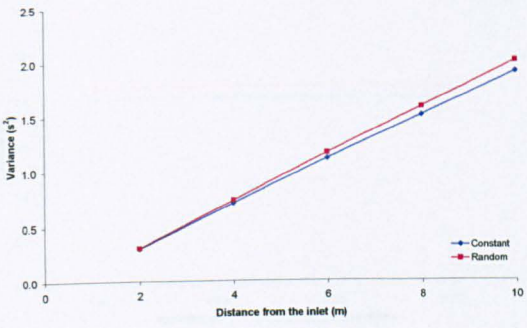

Test 3: Characteristic eddy lifetime

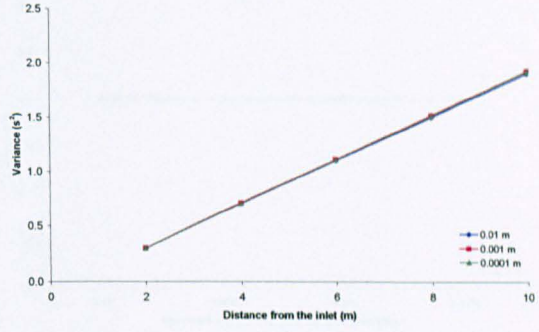

Test 4: Length scale

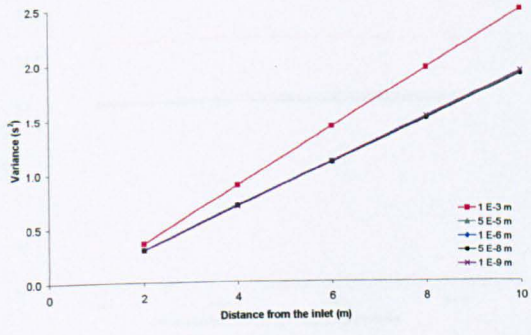

Test 5: Particle diameter

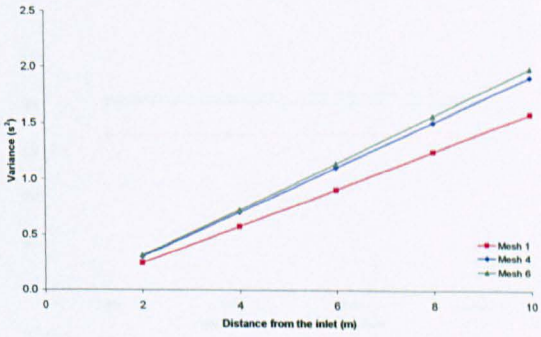

Test 6: Flow field

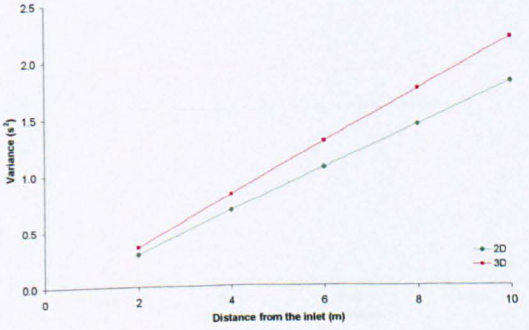

Test 7: 2D and 3D

Figure 4.12 Temporal variance (all parametric tests)

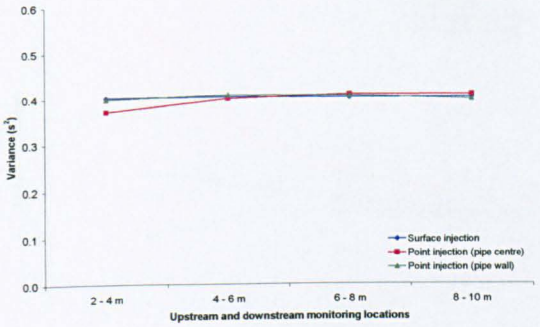

Test 1: Injection location

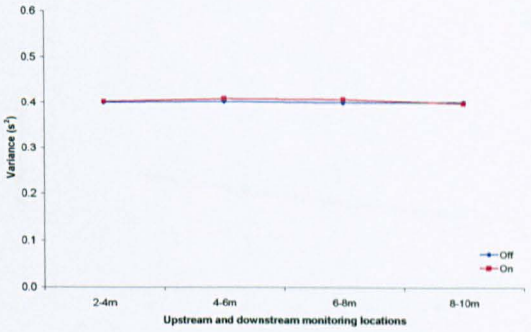

Test 2: Saffman lift force

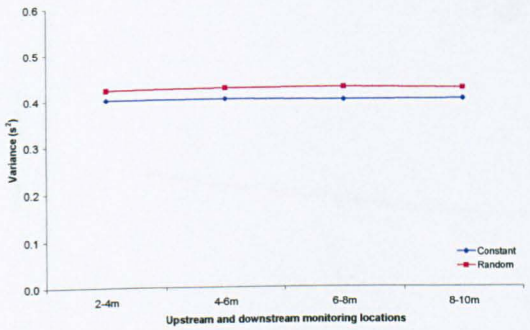

Test 3: Characteristic eddy lifetime

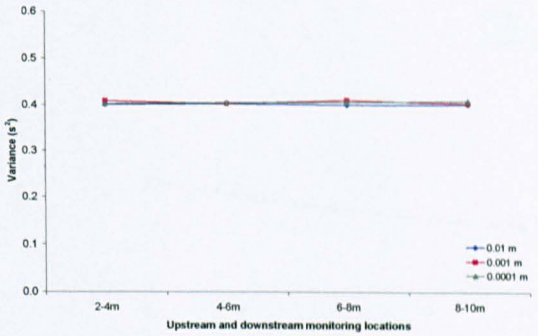

Test 4: Length scale

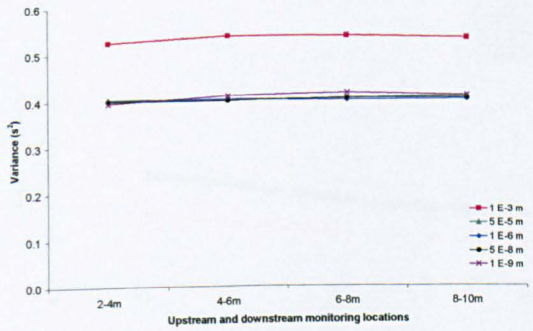

Test 5: Particle diameter

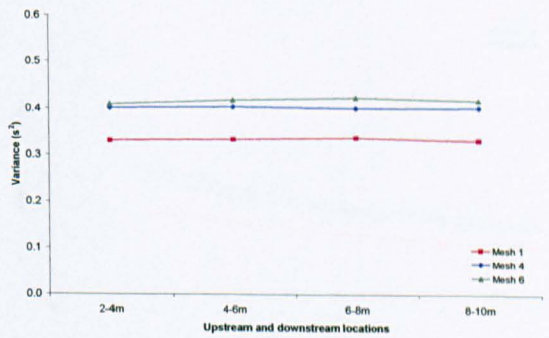

Test 6: Flow field

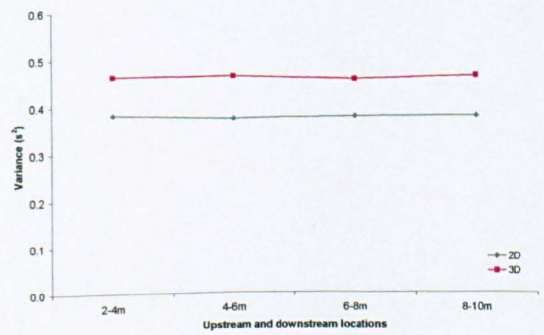

Test 7: 2D and 3D

Figure 4.13 Temporal variance (2) (all parametric tests)

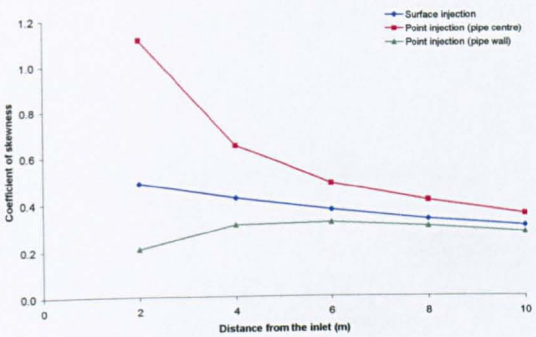

Test 1: Injection location

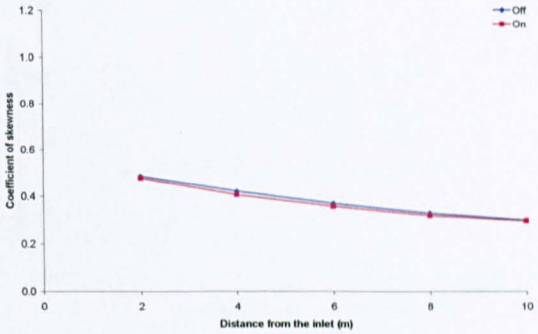

Test 2: Saffman lift force

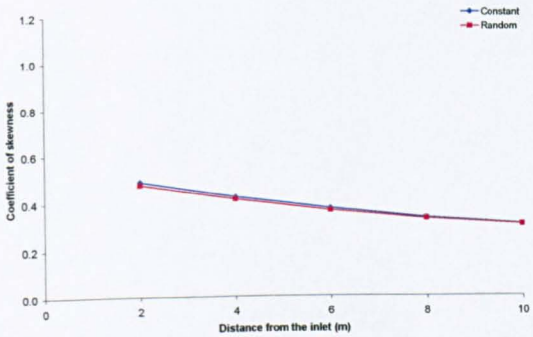

Test 3: Characteristic eddy lifetime

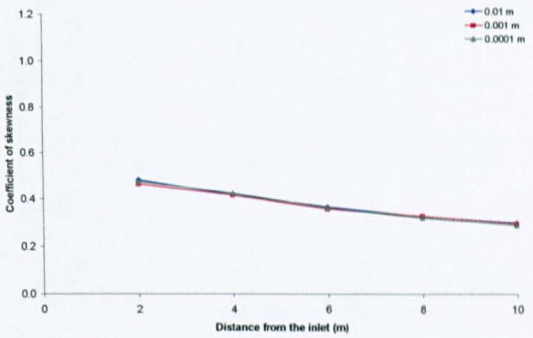

Test 4: Length scale

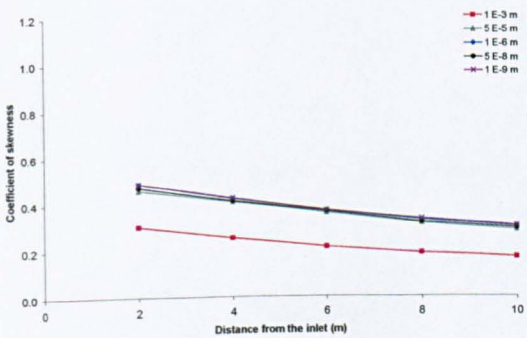

Test 5: Particle diameter

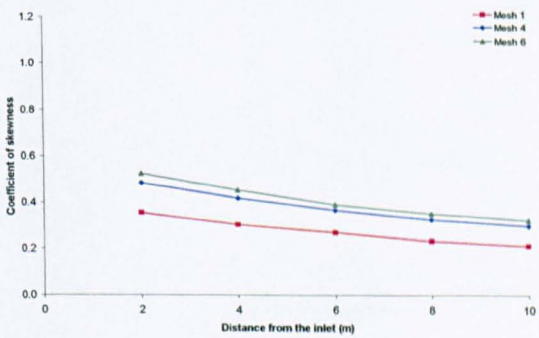

Test 6: Flow field

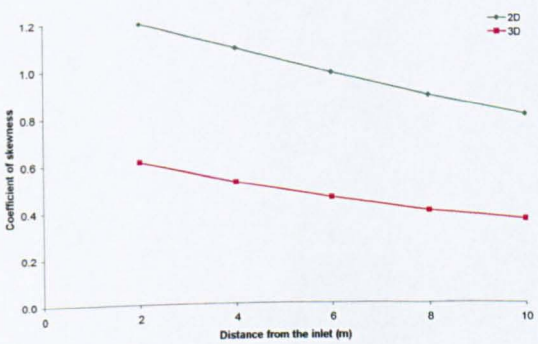

Test 7: 2D and 3D

Figure 4.14 Coefficient of skewness (all parametric tests)

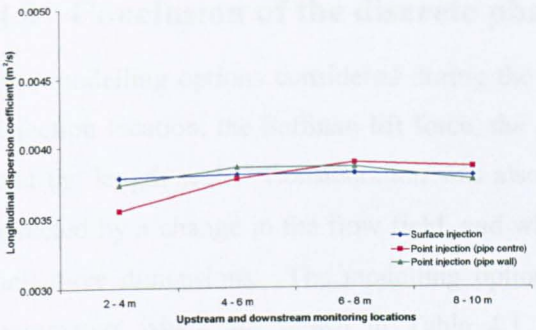

Test 1: Injection location

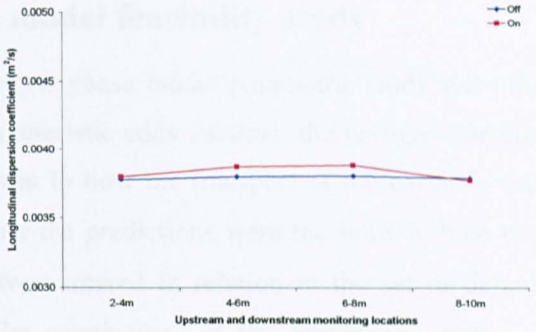

Test 2: Saffman lift force

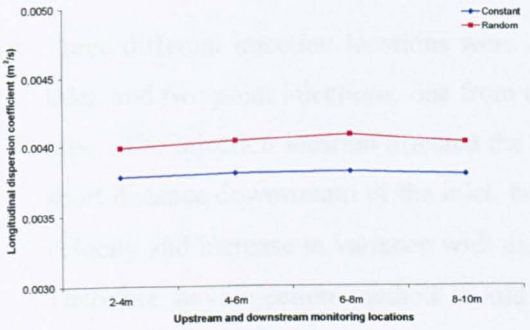

Test 3: Characteristic eddy lifetime

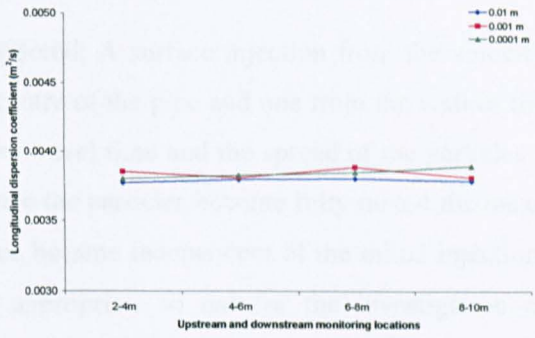

Test 4: Length scale

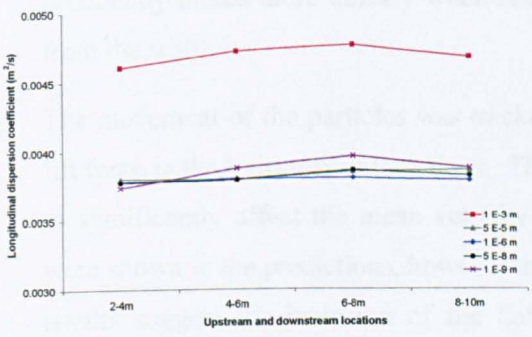

Test 5: Particle diameter

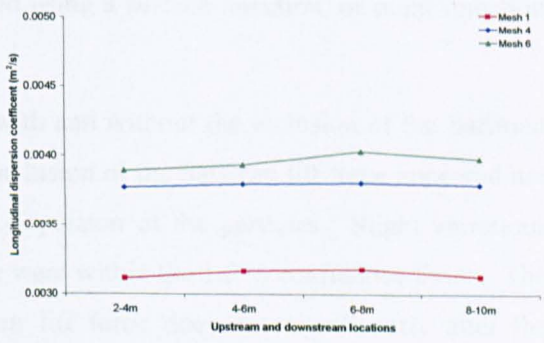

Test 6: Flow field

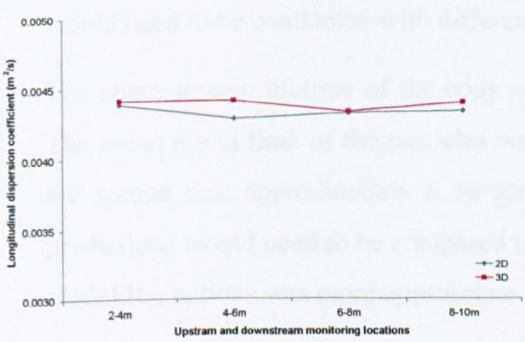

Test 7: 2D and 3D

Figure 4.15 Longitudinal dispersion coefficient (all parametric tests)

4.4 Conclusion of the discrete phase model feasibility study

The modelling options considered during the discrete phase model parametric study were the injection location, the Saffman lift force, the characteristic eddy lifetime, the particle diameter and the length scale. Consideration was also given to how the transport of the particles was affected by a change in the flow field, and whether the predictions were the same in both two and three dimensions. The modelling options were altered in relation to the set of default parameters which are shown in Table 4.1. The conclusions of the parametric study are highlighted below:

- Three different injection locations were considered: A surface injection from the velocity inlet, and two point injections, one from the centre of the pipe and one from the wall of the pipe. The injection location affected the mean travel time and the spread of the particles a short distance downstream of the inlet, but once the particles become fully mixed the mean velocity and increase in variance with distance became independent of the initial injection. Therefore any injection method would be appropriate to use for the investigation of longitudinal dispersion in fully developed flow, although the particles would become cross sectionally mixed more quickly when released using a surface injection, or point injection from the wall.

- The movement of the particles was tracked with and without the inclusion of the Saffman lift force in the trajectory calculations. The inclusion of the Saffman lift force appeared not to significantly affect the mean velocity or dispersion of the particles. Slight variations were shown in the predictions, however these were within the 1.5 % confidence limits. The results suggest the inclusion of the Saffman lift force does not significantly alter the predictions of particle transport under these conditions, although further investigation would need to be conducted with different particle diameters.

- The characteristic lifetime of the eddy can be modelled as a constant or random function. The mean travel time of the particles was the same for both of the modelling options, but the spread was approximately 6 % greater when the random function was used. The predictions would need to be compared to measured data in order to determine which of the modelling options was more appropriate to use.

- Three different length scales were considered: 0.01 m, 0.001 m and 0.0001 m. Altering the length scale did not significantly affect the mean travel time or spread of the particles, with the slight variations within the 1.5 % confidence limits. It would therefore be appropriate to use the 0.01 m length scale in future tests as this would reduce the computational resources required, however further tests would be required to re-establish the value if the flow field or mesh were significantly altered.

- Five particle diameters were considered: 1 $x10^{-3}$, 5 $x10^{-5}$, 1 $x10^{-6}$, 5 $x10^{-8}$ and 1 $x10^{-9}$ m. The mean travel time of the particles was constant with distance in all of the tests, but the travel time was slower when the 1 $x10^{-3}$ m diameter was used. The spread of the particles was approximately the same for the smallest four diameters, while approximately thirty percent more dispersion occurred when the largest particle diameter was used. These results suggest robust predictions are obtained when the particle diameter is less than 5 $x10^{-5}$ m.
- Particles were tracked through three different flow fields. The flow field was the same in the core of the flow, but was different close to the wall. The dispersion predictions altered in relation to the change in the flow field, with greater dispersion occurring when a denser mesh was used.
- A comparison was made between the predictions of particle transport obtained from 2D and 3D models. The flow field was the same in both of the models, but the particle transport predictions were not the same, with the travel time and spread both being different. Further investigation would be required to determine the reason for this.

The discrete phase model has considerable potential as a method for predicting solute transport. The data required for analysis can be collected in a suitable form. Unlike the species transport model the simulations do not require large run times in 3D (see Section 4.5) and the mass of the tracer is inherently conserved throughout the domain. The parametric tests showed the predictions follow the idealised Fickian model and were only sensitive to a few of the set-up parameters, specifically the characteristic lifetime of the eddy and the diameter of the particle. Reassuringly the predictions were sensitive to changes in the flow field.

The discrete phase model also has a number of disadvantages. The model requires more set-up parameters to be specified than the species transport model. The tests conducted during the parametric study were based on a set of default parameters (i.e. it was assumed that the effect of each parameter could be assessed independently). The conclusions reached should therefore be treated with some caution. More repeat simulations may be required to accurately represent the stochastic turbulence for different flow rates. A further limitation of the discrete phase model is the inability to confirm the accuracy of the predicted longitudinal dispersion coefficient with the routing procedure close to the point of release.

Perhaps the issues that most warrant further consideration are the mean travel time of the tracer not being correctly predicted and the predictions of both travel time and dispersion being different when modelling in 2D and 3D.

Although the discrete phase model has shown promise further work would be required to establish correct default parameters and the accuracy of the approach.

4.5 Conclusion of the feasibility study

Two models were used to predict the transport of a neutrally buoyant tracer through a pipe, the species transport model and the discrete phase model, more commonly called the particle tracking model. Indicative run times for generating the flow field and using the two models are shown in Table 4.3. Run 1 refers to the first flow field simulation which developed the flow field, while Run 2 refers to the second simulation which used a 'profile' from the first run to create fully developed flow conditions along the length of the pipe. The tests are based on the Mesh 7 (3D) and Mesh 11 (2D) which were described, along with the flow field modelling options, in Section 3.3.7. The modelling options used for the discrete phase model simulation were described in Section 4.3.11 and the modelling options for the species transport simulation in Section 3.3.7, with the only changes being that just second order spatial discretization and a time step of 0.02 seconds were considered. The simulations were conducted using a Sun V880 SMP server with 8 processors running under Solaris 8.

The discrete phase model was shown to have a number of benefits over the species transport model, with the two biggest benefits being that the mass of the tracer was always conserved and the computational time required to run the simulations in 3D was less than 10 % of the time required to run the species model. However, the model was also shown to have a number of disadvantages, including uncertainties regarding the correct modelling options to use, the incorrect prediction of the mean travel time and the inability to confirm the accuracy of the predicted longitudinal dispersion coefficient close to the point of release. It was also not possible to reproduce the three dimensional predictions in two dimensions.

When the correct modelling options were specified the species transport model was shown to be robust and to provide solutions that were both grid and time step independent. The model has the flexibility to allow a variety of injection profiles to be modelled, and the predictions were shown to be the same in both 2D and 3D.

The aim of the next stage of the project was to identify the most appropriate flow field modelling options to use. This would be done via a series of parametric tests. Table 4.3 shows that it would be beneficial to conduct the simulations in 2D. It was decided, therefore, to just consider the species transport model for further analysis as the predictions made using the model were robust and the same in 2D and 3D.

	2D	3D
Flow field – Run 1	26 mins	208 mins
Flow field – Run 2	18 mins	157 mins
Species transport	37 mins	676 mins
Discrete phase model	48 mins	51 mins

Table 4.3 Indicative run times

5 Development of the flow field

5.1 Introduction

The previous two chapters reported on the feasibility studies that were conducted to examine the ability of the species transport model and the discrete phase model to predict the transport of a solute tracer. The main conclusion of the feasibility study was that it was not appropriate to consider the discrete phase model further at this stage of the investigation because of the limitations identified in Section 4.4.

Although the qualitative characteristics of the species transport model predictions and their robustness were evaluated in Chapter 3, the accuracy of the dispersion predictions was not considered. In order to assess the accuracy of the predictions a comparison needs to be made with measured or theoretical data. As previously mentioned, this study chose to use the measurements of Guymer and O'Brien (2000). In order to make an accurate comparison the flow field in the CFD model must replicate, or at least closely resemble, the flow field from the experiments. The majority of the simulations conducted during the feasibility study used the flow field described in Section 3.3.2. Although the flow field obeyed the generally accepted CFD guidelines, such as for the use of the wall functions, the author was aware of factors omitted from consideration that might affect its accuracy, for example mesh density and turbulence models. At this stage no evaluation of the accuracy of the flow field has been presented.

The aim of the work reported in this chapter was to determine the most appropriate modelling options to use in order to replicate the flow conditions used in the experiments of Guymer and O'Brien (2000). This work is reported in Section 5.3 to Section 5.6.

Chapter 6 reports on the additional species model simulations that were conducted using the flow fields developed with these options, and the comparison between the predicted and measured dispersion coefficients to determine the accuracy of the species transport model predictions.

5.2 Procedure

The aim of the work reported in this chapter was to determine which modelling options to use in order to replicate the flow conditions used in the experiments of Guymer and O'Brien (2000). When developing a flow field a number of modelling options must be defined. These relate to the model geometry, the mesh, the physical properties of the fluid, the boundary conditions and the turbulence models. It was possible to determine some of the options from the experimental configuration and measurements. With the time available it was not possible to consider all of the remaining options in detail. The decision was therefore made to use high Reynolds number turbulence models and standard wall functions because they are more computationally efficient. Consideration was given to developing a grid independent solution and to determining the most appropriate discretization schemes and turbulence models to use. These parameters were selected because they were believed to be the most important options.

The study was conducted in five stages, each subsequent one building upon the last. Stage 1 involved considering the system being modelled and identifying and defining a default set of modelling parameters. Stage 2 was a grid refinement study, undertaken to determine the mesh density at which a grid independent solution occurred. Stage 3 and Stage 4 were parametric studies that determined which discretization schemes and turbulence models were most appropriate to use. Stage 5 concluded the study and identified the most appropriate modelling options to use. The aims and outcomes of each stage are shown in Figure 5.1.

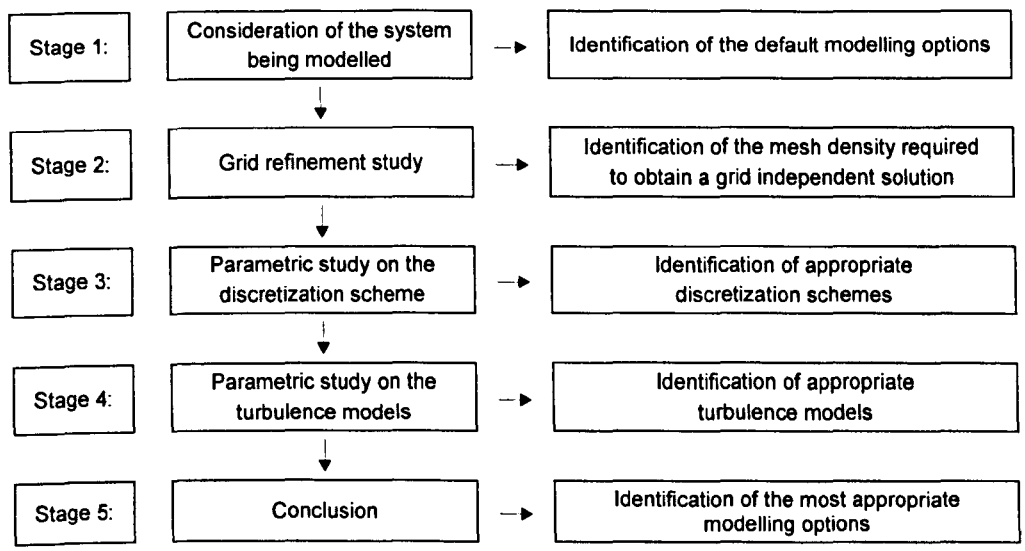

Figure 5.1 The aims and outcomes of each stage of the study

Whenever possible the flow fields were developed and validated using the measurements reported in Guymer and O'Brien (2000). However, other than the discharge the only flow property that was measured was the variation in the head loss with discharge. These parameters alone do not provide sufficient information with which to do this. Where appropriate

consideration was therefore also given to the fully developed pipe flow measurements of Laufer (1954), Lawn (1971) and Schildknecht *et al.* (1979). These data sets were chosen because they include detailed measurements of the spatial flow properties over a range of flow rates. A summary of these experiments is presented in Chapter 2.

5.3 Stage 1: Determining the default modelling options

In order to be able to perform the grid refinement and parametric studies the modelling options relating to the geometry, fluid properties and boundary conditions needed to be defined. Many of the options were determined through consideration of the system being modelled, although simplifications were required. The remaining options were selected using experience, guidance from a variety of sources and by consideration of the resources that were available.

5.3.1 Geometry

The CFD model geometry was based on the experimental straight pipe. Only limited information is presented about the facility in Guymer and O'Brien (2000) and the assumption was therefore made that the flow field was fully developed before the first measurement position. Further consideration is given to this assumption in Chapter 6.

The tests conducted in Chapter 3 demonstrated that the flow field predictions and the species transport model predictions of solute transport were the same in both two and three dimensions when the flow field was fully developed. Therefore all of the simulations reported within this chapter were conducted in two dimensions as this considerably reduced the required run time. The radius of the pipe was specified to be 0.044 m, the same as the pipe used in the experiments of Guymer and O'Brien (2000), and the length to 10 m. This created a length to diameter ratio of 113 which was anticipated to be large enough for the flow field to fully develop before the end of the pipe. The pipe was set to a horizontal position and gravity was modelled accordingly.

5.3.2 Fluid properties

The flow was given the properties of water at approximately 20 °C, with the density being specified as 998.2 kg/m^3 and the absolute fluid viscosity as 1.003 x 10^{-3} kg/m s.

5.3.3 Turbulence models

The Reynolds number of the lowest flow rate considered, 2 l/s, was greater than 20000, demonstrating that the flow was fully turbulent. In order to model these effects, turbulence models were used. At this stage of the investigation all of the simulations were performed using high Reynolds number turbulence models and wall functions. High Reynolds number models were considered because they are more computationally efficient than the low Reynolds number models. For instance, simulations reported by Martinuzzi and Pollard (1989) in fully developed

turbulent pipe flow demonstrated that the run time required when using high Reynolds number models was between five and ten times less than the run time required when using the low Reynolds number models, with only minimal loss of accuracy. The parametric study that considered the accuracy of the turbulence models is reported in Section 5.6, while a comparison is made between high and low Reynolds number turbulence models in Chapter 6.

5.3.4 Boundary conditions

The boundary conditions were specified as follows:

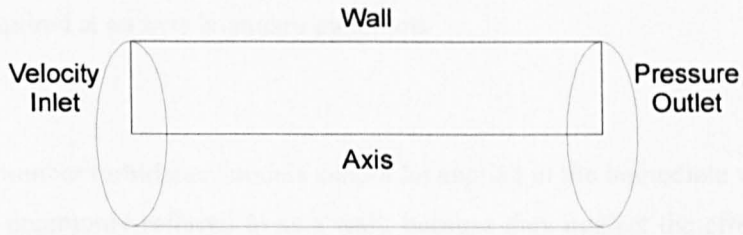

Figure 5.2 The model boundary conditions

5.3.4.1 Inlet

The inlet to the domain was specified as a velocity inlet. Inputs are required for the inflow velocity magnitude and turbulence levels. Guymer and O'Brien (2000) presented measurements of solute transport at seven flow rates between 2 and 10.3 litres per second. During the present study only three flow rates were considered, two, five and ten litres per second. These flow rates were chosen because they allow the accuracy of the species transport model to be assessed over a range of flow rates, whilst minimising the number of simulations required. The inflow discharge was modelled as a uniform mean velocity.

The turbulence levels may be specified in a number of different ways. This study, however, chose to specify the turbulence quantities in terms of the turbulence intensity and hydraulic diameter. Turbulence intensity is the ratio of the root mean square (rms) of the velocity fluctuations to the mean flow velocity. Following recommendations made in the Fluent 5 User's Guide (Fluent, 1998) the turbulent intensity was determined from Equation (5.1) and the hydraulic diameter was specified to equal the pipe diameter, 0.088 m.

$$I = 0.16\,Re^{-1/8} \qquad (5.1)$$

where I is the turbulent intensity and Re is the Reynolds number of the flow.

5.3.4.2 Outlet

The outlet from the domain was defined as a pressure outlet. Inputs are required for the static pressure and the turbulent backflow conditions. The static pressure provides a reference location for the reporting of pressure change within the domain, but does not affect the other flow properties. The parameter was therefore set to zero. The turbulent backflow properties were specified to be the same as the turbulent properties at the inlet.

5.3.4.3 Axis

No inputs are required at an axis boundary condition.

5.3.4.4 Wall

High Reynolds number turbulence models cannot be applied in the immediate vicinity of a solid boundary, more commonly referred to as a wall, because they neglect the effects of molecular viscosity. In order to avoid modelling these viscous effects, wall functions are used to bridge the gap between the wall and the fully turbulent region. Wall functions are a collection of empirical formulas and functions that represent flow properties close to the wall. Two types of wall function are available in Fluent 5.5 (i.e. standard and non equilibrium), but consideration was only given to the standard function that is based on the proposal of Launder and Spalding (1974). More information regarding wall functions is presented in Chapter 2.

Wall functions only operate in the cells nearest to the wall, called the boundary layer. The size of the cells should be determined by considering the extent of the viscous affected region. Figure 2.11 shows the viscous affected region extending to a y^+ value of between 30 and 60, although this is only a general rule as the extent of the region is dependent upon a number of factors including pressure gradient and Reynolds number. More specifically the measurements of Lawn (1971) and Schildknecht *et al.* (1979) in fully developed turbulent pipe flow show the viscous region extending to a y^+ value of approximately 30. It was not possible to determine the extent of the viscous affected region from the measurements of Guymer and O'Brien (2000) so it was assumed to have extended to a distance of $y^+ = 30$ from the wall.

When using wall functions the roughness height may be specified as an input. When a roughness height is specified the wall functions are modified to incorporate the changes to the flow field. The method used to modify the near wall flow field was developed using Nikuradse's (1932) measurements of flow in pipes that were artificially roughened with tightly packed uniform sand grains. The roughness height in the model is equivalent to the height of a sand grain. For other types of roughness an equivalent roughness height should be estimated.

The roughness height of the pipe was not measured in the laboratory experiments, but an estimate was made by calculating the head loss for a range of roughness heights and making a comparison with the measured head loss. The head loss was calculated using the Darcy-

Weisbach equation, Equation (5.2). The pipe friction factor, λ, was determined from the Colebrook-White equation, Equation (5.3), for a range of roughness heights and flow rates. Figure 5.3 shows a comparison between the best fit equation used to represent the measured head loss and the different calculated head losses. A roughness height of 8 $x10^{-5}$ m corresponded best to the measured data over the range of flow rates considered. This value is higher than the typically quoted value of 3 $x10^{-6}$ m for a Perspex pipe (Chadwick and Morfett, 1994). This is likely to have occurred because of increased roughness at the joints of the pipes and tappings into the pipe.

$$h_f = \frac{\lambda L U^2}{2gD} \qquad (5.2)$$

where, h_f is the head loss and λ is the pipe friction factor.

$$\frac{1}{\sqrt{\lambda}} = -2log\left(\frac{k_s}{3.7D} + \frac{2.51}{Re\sqrt{\lambda}}\right) \qquad (5.3)$$

where, k_s is the wall roughness height.

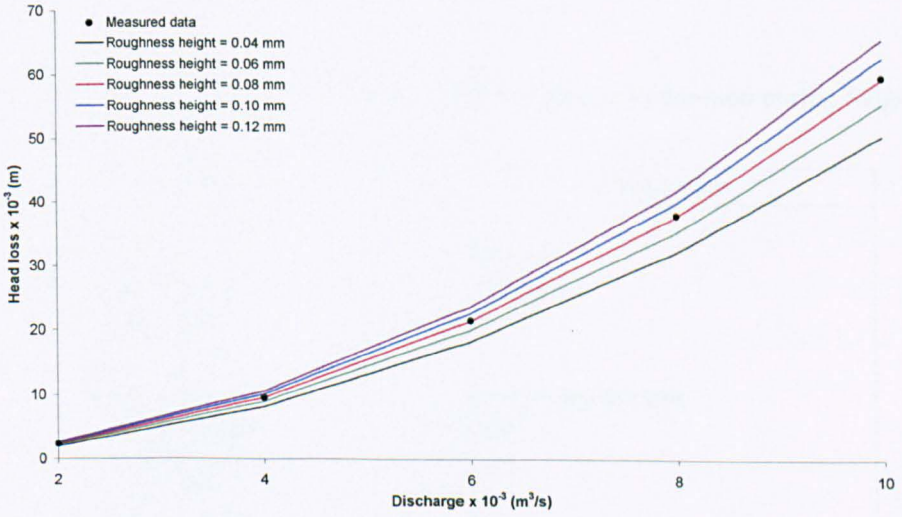

Figure 5.3 A comparison between the measured and calculated head loss

When a roughness height is specified a roughness constant must also be specified. The default value of 0.5 was specified because it was not possible to determine this parameter from the data available.

5.3.5 Solver

The 2D axisymmetric solver was used. When this solver is enabled the 2D axisymmetric form of the governing equations are solved instead of the 2D Cartesian forms. For the 2 l/s flow rate the 2D single precision solver was found to be adequate. For the larger flow rates the double precision solver was required to ensure the flow rate remained constant on the second simulation (see below).

5.3.6 Simulation procedure

Two flow simulations were performed. The first flow simulation was used to create a fully developed flow profile. The second used the fully developed flow properties as input parameters, thus creating fully developed flow conditions along the length of the pipe. This procedure was followed because it created the conditions required for the subsequent tracer tests. For both runs the simulations were not stopped until the residuals became constant, as is generally accepted to indicate the best possible prediction.

The majority of the simulations were performed using a standard PC running under the Windows 2000 operating system with a 2 GHz Intel Pentium 4 processor and 1048 Mbytes of RAM.

Table 5.1 summarises the default flow field modelling options determined during Stage 1.

Parameter	Setting / Value
Fluid	
Density	998.2 kg/m^3
Absolute viscosity	1.003 kg/m s
Boundary conditions	
Wall	
Model	Standard wall functions
Roughness height	8 x10^{-5} m
Roughness constant	0.5
Inlet	
Q = 2 l/s	Vel = 0.33 m/s - Turb Int = 4.4 %
Q = 5 l/s	Vel = 0.82 m/s - Turb Int = 4.0 %
Q =10 l/s	Vel = 1.64 m/s - Turb Int = 3.6 %
Hydraulic diameter	0.088 m
Outlet	
Pressure	0 Pa
Turbulent intensity	As above
Hydraulic diameter	0.088 m

Table 5.1 The default flow field modelling options

5.4 Stage 2: Grid refinement study

In order to obtain the most accurate solution possible a grid refinement study was conducted. A grid refinement study involves refining the grid or mesh (cells becoming smaller and the total number increasing) and examining the changes that occur to the solution. These changes occur because the spatial discretization errors are reduced as the mesh is refined (excluding computational round off error). When further refinement to the mesh produces no changes to the solution grid independence is reached. In practice a truly grid independent solution is rarely reached so grid independence is claimed when further refinement to the mesh yields only small, insignificant, changes to the solution.

A grid refinement study was performed at each of the three flow rates considered because a grid independent solution is not independent of flow rate. For each flow rate six meshes were considered, with the density controlled so the first mesh was relatively coarse and the subsequent ones progressively finer. Each of the meshes were constructed using the mesh generation software Gambit (Gambit, 1998). The model geometry and boundary conditions are described in Section 5.3.1 and Section 5.3.4. The work reported in Stage 1 suggested that the wall functions should extend to a y^+ value of 30 in order for them to correctly model the viscous affected region. The size of the boundary layer cell to achieve this was determined from Equation 2.33. The mesh density away from the wall was varied by changing the number of elements on the radius and altering the mesh spacing on the length to minimise the maximum aspect ratio. A low aspect ratio was desirable as large aspect ratios affect the accuracy and convergence of the simulation. The spacing of the nodes on the radius was determined to ensure the ratio of any two succeeding interval lengths was constant, while the spacing on the length was fixed. For illustrative purposes Mesh GR 1, GR 4 and GR 6 are shown in Figure 5.4.

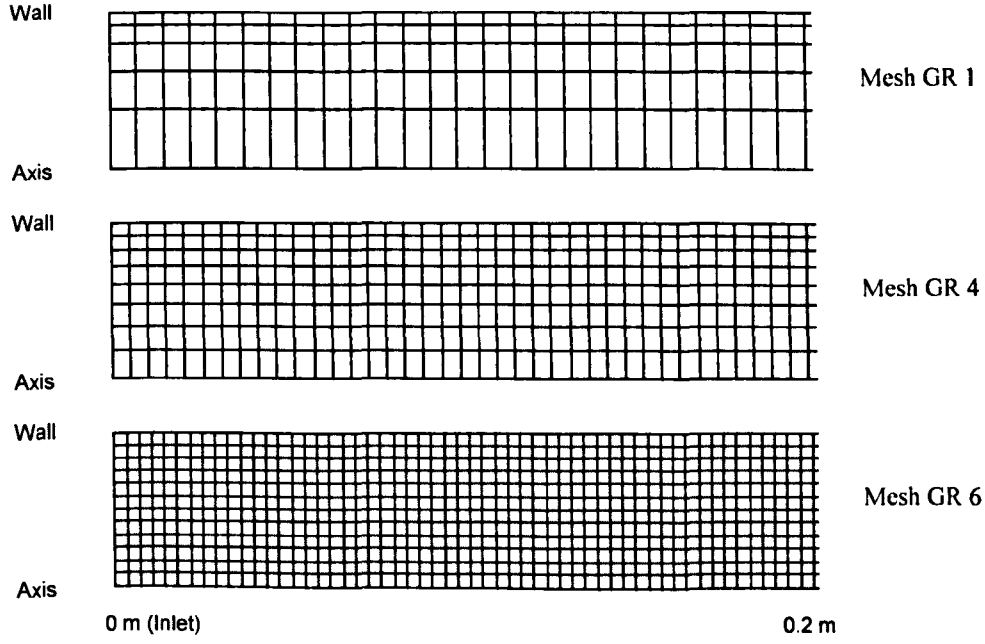

Figure 5.4 Three of the meshes considered during the study

Discharge: 2 l/s					
Mesh	Boundary layer thickness (m)	No. of elements on the radius	Spacing on the length (m)	Total No. of elements	Max. aspect ratio
GR 1	0.0035	5	0.0076	6580	2.18
GR 2	0.0035	6	0.0066	9090	1.93
GR 3	0.0035	7	0.0059	11865	1.70
GR 4	0.0035	8	0.0052	15384	1.55
GR 5	0.0035	10	0.0044	22730	1.26
GR 6	0.0035	12	0.0036	33336	1.07

Discharge: 5 l/s					
Mesh	Boundary layer thickness (m)	No. of elements on the radius	Spacing on the length (m)	Total No. of elements	Max. aspect ratio
GR 7	0.0015	8	0.0044	18184	2.94
GR 8	0.0015	10	0.0038	26320	2.53
GR 9	0.0015	12	0.0032	37500	2.21
GR 10	0.0015	14	0.003	46662	2.00
GR 11	0.0015	16	0.0026	61536	1.73
GR 12	0.0015	18	0.0024	75006	1.59

Discharge: 10 l/s					
Mesh	Boundary layer thickness (m)	No. of elements on the radius	Spacing on the length (m)	Total No. of elements	Max. aspect ratio
GR 13	0.0008	12	0.0028	42852	3.50
GR 14	0.0008	14	0.0025	56000	3.13
GR 15	0.0008	16	0.0023	69568	2.88
GR 16	0.0008	18	0.0021	85716	2.63
GR 17	0.0008	20	0.0019	105260	2.43
GR 18	0.0008	22	0.0018	122232	2.25

Table 5.2 Details of the meshes considered during the grid refinement study

In addition to the default set of modelling options shown in Table 5.1 the flow field was developed using the standard k-ε turbulence model and second order discretization schemes throughout, except for the pressure velocity coupling which used the SIMPLE scheme.

Grid independence was determined by comparing three flow properties and assessing the mesh density at which the changes to the solution became insignificant. The three flow properties considered were the velocity magnitude, the turbulent viscosity and the turbulent kinetic energy. Figure 5.5 shows the spatial variation of these properties for each of the meshes considered at the 2 l/s flow rate. Cell centred values are presented because they do not require interpolation and are therefore most fundamental representation of the flow field. A grid independent solution was determined to have occurred for the velocity magnitude when Mesh GR 1 was used, and for the turbulent viscosity and the turbulent kinetic energy when Mesh GR 6 and Mesh GR 5 were used respectively. Therefore Mesh GR 6 was deemed to have given an overall grid independent solution. A similar process was repeated for the other flow rates, with Mesh GR 10 yielding a grid independent solution for the 5 l/s flow rate and Mesh GR 15 for the 10 l/s flow rate.

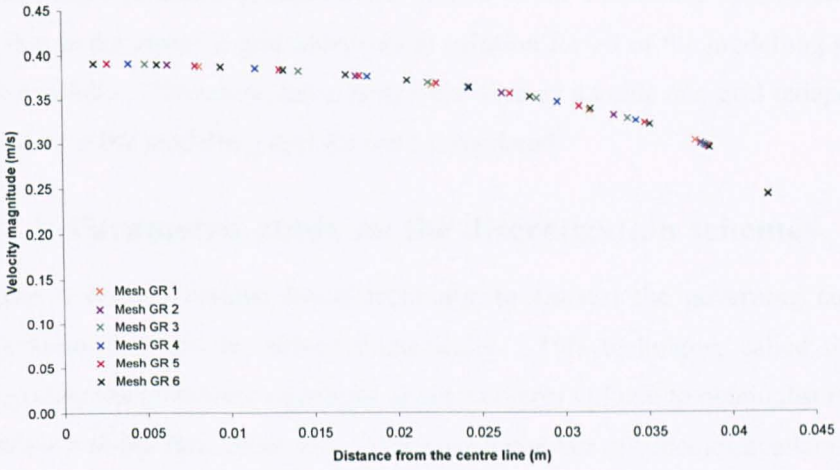

(a) Velocity magnitude

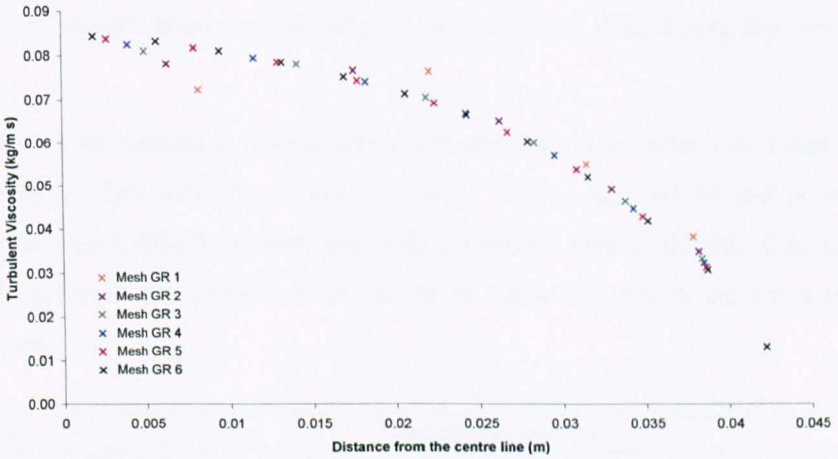

(b) Turbulent viscosity

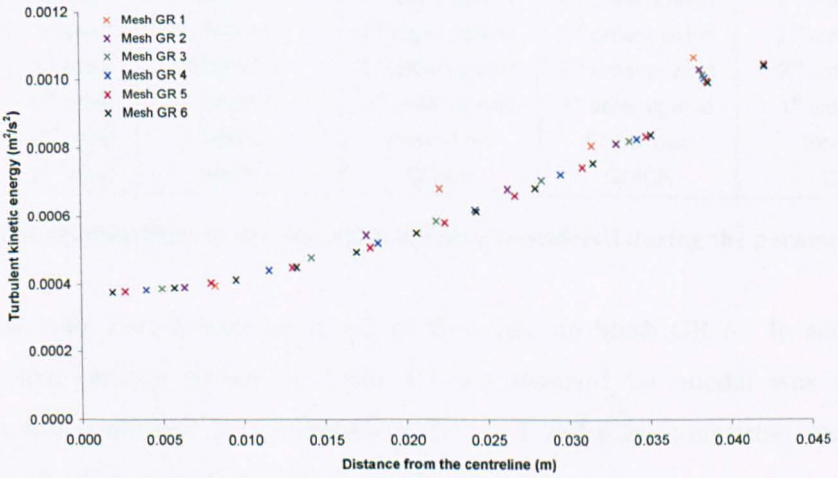

(c) Turbulent kinetic energy

Figure 5.5 Comparison of the flow field predictions

The grid independent solutions presented are limited to the modelling options considered. It was not possible to determine a grid independent solution for all of the modelling permutations with the time available. Therefore, these tests were used as a guide and grid independence was reconfirmed when other modelling options were considered.

5.5 Stage 3: Parametric study on the discretization schemes

Fluent 5.5 uses a control volume based technique to convert the governing equations into algebraic equations that can be solved numerically. This technique, called discretization, involves integrating the governing equations about a control volume to obtain discrete equations that represent each of the flow processes. There are a number of schemes available with which to discretize the governing equations. The work reported in Chapter 3 demonstrated that the choice of the spatial and temporal discretization schemes was significant when discretizing the advection-diffusion equation. A parametric study was therefore conducted to determine the most appropriate spatial discretization schemes to use when discretizing the governing flow equations.

A complete list of the available discretization schemes is not presented, but can be obtained from the Fluent 5 User's Guide (Fluent, 1998). To consider all of the permutations of discretization scheme would have been impossible with the time available. Consideration was therefore only given to the combinations shown in Table 5.3, which are for a two equation turbulence model.

Combination	Discretization scheme				
	Pressure	Pressure velocity coupling	Momentum	Turbulent kinetic energy	Turbulent dissipation rate
DS 1	2nd order	SIMPLE	2nd order upwind	2nd order upwind	2nd order upwind
DS 2	Standard	SIMPLE	2nd order upwind	2nd order upwind	2nd order upwind
DS 3	Linear	SIMPLE	2nd order upwind	2nd order upwind	2nd order upwind
DS 4	Presto	SIMPLE	2nd order upwind	2nd order upwind	2nd order upwind
DS 5	2nd order	SIMPLE-C	2nd order upwind	2nd order upwind	2nd order upwind
DS 6	2nd order	SIMPLE	1st order upwind	1st order upwind	1st order upwind
DS 7	2nd order	SIMPLE	Power Law	Power Law	Power Law
DS 8	2nd order	SIMPLE	QUICK	QUICK	QUICK

Table 5.3 The combinations of discretization schemes considered during the parametric study

The parametric tests were conducted at a 2 l/s flow rate on Mesh GR 6. In addition to the default modelling options shown in Table 5.1 the standard k-ε model was used. Grid independence was confirmed for combinations DS 1, 3 and 6 by comparing the predictions made using Mesh GR 6 with the predictions made using a denser mesh

The main conclusion from this study was that the predictions of fully developed turbulent flow were not significantly affected by the choice of discretization scheme. For instance, the maximum difference in the prediction of static pressure along the length of the pipe was less

than 0.01 % between combinations DS 1 and DS 4. As the choice of discretization scheme was not found to be significant, combination DS 1 was used in subsequent tests.

5.6 Stage 4: Parametric study on the turbulence models

"In general, analyses of turbulence modelling for pipe flow applications are notably lacking in the literature" (Hrenya *et al.* 1995). The majority of the work that has been conducted to date used low Reynolds number turbulence models (Martinuzzi and Pollard, (1989); Hrenya *et al.*, (1995); Thakre and Joshi, (2001)). The purpose of this parametric test was to test the predictive capabilities of the high Reynolds number turbulence models contained within the Fluent software for the case of fully developed turbulent pipe flow.

The Fluent software contains three versions of the high Reynolds number k-ε turbulence model and one version of the high Reynolds number Reynolds stress model (RSM). Additional modelling options are also available for each turbulence model. With the time available it was not possible to consider all of the additional options, so consideration was only given to the options that appeared most relevant. Details of the configurations considered during the study are shown in Table 5.4, with a description of the additional modelling options considered in Section 5.6.1. Further information regarding the turbulence models and the additional modelling options are presented in the Fluent 5 User's Guide (Fluent, 1998) and a summary is presented in Chapter 2.

Model configuration	Turbulence model	Additional modelling options			
		Differential viscosity model	Wall B.C. from k equation	Quadratic pressure strain model	Wall reflection effects
K-E 1	k-ε Standard				
K-E 2	k-ε RNG	Off			
K-E 3	k-ε RNG	On			
K-E 4	k-ε Relizable				
RSM 1	RSM		Off	Off	Off
RSM 2	RSM		On	Off	Off
RSM 3	RSM		Off	Off	On
RSM 4	RSM		On	Off	On
RSM 5	RSM		On	On	
RSM 6	RSM		Off	On	

Table 5.4 The turbulence modelling options considered during the parametric study

5.6.1 Additional modelling options

Differential viscosity model

When the k-ε RNG model is used the turbulent viscosity may be modelled using a high or low Reynolds number form of the equation. When the low Reynolds number form of the equation is used low Reynolds number and near wall flows are better modelled (Fluent, 1998). The low Reynolds number form is enabled when the differential viscosity model is turned on.

Wall boundary conditions for the Reynolds stresses from the k equation

The Reynolds stresses at the wall adjacent cells may be solved using a transport equation for turbulent kinetic energy or by the wall shear stress. The near wall Reynolds stresses are solved using the transport equation when the option is turned on.

Quadratic pressure strain model

The pressure strain term may be modelled using the linear pressure strain model proposed by Gibson and Launder (1978) among others, or by the quadratic pressure strain model proposed by Speziale *et al.* (1991). The quadratic pressure strain model has been shown to give superior flow predictions in a variety of simple shear flows (Fluent, 1998). The quadratic pressure strain model does not require correction to account for wall reflection effects so the option to include the wall reflection term is removed when the model is selected.

Wall reflection effects on Reynolds stresses

Wall reflection effects may be included in the pressure-strain term if the linear pressure strain model is used. The wall reflection term is responsible for the redistribution of normal stresses near to the wall and has the effect of dampening the normal stress perpendicular to the wall while enhancing the stresses parallel to the wall (Fluent, 1998).

5.6.2 Modelling configuration

Three flow rates were considered during this analysis because the studies mentioned previously had noted that the accuracy of the turbulence models was partly dependent upon the flow rate. The flow rates considered during the study were 2 l/s (Re = 29040), 5 l/s (Re = 72160) and 10 l/s (Re = 144320) (Reynolds numbers based on mean velocity and pipe diameter). With the time available it was not possible to consider all of the configurations shown in Table 5.4 at the three flow rates. Therefore, all of the configurations were considered at 2 l/s, and only K-E 1, K-E 2 and RSM 4 (the default setting) at the higher flow rates. The default values were used for the model constants. Further information regarding the constants may be found in the Fluent 5 User's Guide (Fluent, 1998).

Following the grid refinement study, meshes GR 6, GR 10 and GR 15 were selected. Following the first parametric study second order discretization schemes were used throughout, except for the pressure velocity coupling which used the SIMPLE scheme. Grid independence was confirmed for all of the predictions.

5.6.3 Flow field validation

Other than the discharge, the only flow property measured by Guymer and O'Brien was the variation in the head loss with discharge. These parameters alone do not provide sufficient information with which to determine the accuracy of the predicted flow field. Where

appropriate, consideration was therefore also given to the fully developed pipe flow measurements of Laufer (1954), Lawn (1971) and Schildknecht *et al.* (1979). These data sets were chosen because they include detailed measurements of fully developed turbulent pipe flow over the whole cross section. The data by Laufer was collected at two Reynolds numbers, approximately 40000 and 400000 when converted to mean flow rate, and the data of Schildknecht *et al.* at a Reynolds number of 17250. Measurements of the turbulent dissipation rate were compared with the data of Lawn (1971) (Re = 90000) because the measurement and analysis techniques used were regarded as being more rigorous. More information regarding these experiments is presented in Chapter 2.

In order to enable qualitative comparisons to be made between these experimental data sets and the model results, the experimental data was digitised from published graphs. The data presented is estimated to be accurate to within approximately 1 %.

The Reynolds numbers of the simulations did not exactly correspond to the Reynolds number used in the experiments of Laufer (1954) Lawn (1971) or Schildknecht *et al.* (1979). The accuracy of the simulations could, however, still be established using this data. This is made possible because the properties of different flows will show similar trends when non dimensionalized if the Reynolds number is of the same order of magnitude. Nevertheless, where possible, two experimental data sets were used for comparison, one at a higher Reynolds number and one at a lower Reynolds number as this allowed the accuracy of the predictions to be better determined.

5.6.4 Data analysis

Model predictions of the mean axial velocity, turbulent kinetic energy, turbulent viscosity, dissipation rate of turbulent kinetic energy, Reynolds shear stress and the Reynolds normal stresses are compared with the experimental measurements in Figure 5.7 to Figure 5.14. Cell centered values are presented for the predictions as they do not require interpolation and are therefore the most fundamental representation of the numerical flow field. In order to allow a comparison to be made the predicted flow properties were non-dimensionalised using the friction velocity, U^*. The friction velocity was determined from Equation (5.4).

$$U^* = \sqrt{\frac{\tau_o}{\rho}} \qquad (5.4)$$

where the shear stress, τ, was determined from Equation (5.5).

$$\tau_o = \frac{D}{4}\frac{dP}{dl} \qquad (5.5)$$

The turbulent viscosity, μ_t, cannot be directly measured and was determined using the measurements of the axial velocity and Reynolds stress via Equation (5.6). Likewise the turbulent kinetic energy, k, was determined using the measurements of the fluctuating velocity components via Equation (5.7).

$$\overline{uv} = -\mu_t \frac{dU}{dr} \qquad (5.6)$$

$$k = \frac{u'^2+v'^2+w'^2}{2} \qquad (5.7)$$

where $\overline{uv}$ is the Reynolds shear stress, U is the mean axial velocity and u', v' and w' are the axial, radial and tangential fluctuating velocity components respectively.

A comparison was also made with the head loss measurements of Guymer and O'Brien (2000) This is reported in Section 5.6.4.7.

In Figure 5.7 to Figure 5.14 all the data are plotted as a function of r/R in which r represents the distance from the centreline of the pipe and R is the pipe radius (i.e. r/R = 1.0 corresponds to the wall).

5.6.4.1 Axial velocity

The predicted axial velocity profiles are compared with the experimental data in Figure 5.7. The predictions made by all the turbulence models showed the same trends as the experimental data, with a low velocity near to the wall and a peak velocity at the centre of the pipe. There was however a larger than expected variation in the predictions depending upon the turbulence model. For instance there was a 12 % variation in the predictions of peak velocity at 2 l/s.

The predictions made by the four k-ε turbulence models may be considered accurate over the whole cross section as they are contained within the experimental data sets. The accuracy of the RSM predictions was dependent upon the additional models selected. When the near wall Reynolds stresses were determined from the wall shear stress (RSM 1, 3, 6) there was an under prediction of the experimental data near to the wall. Unless these configurations included wall reflection effects there was also a significant underprediction in the core of the pipe. Of the six RSM modelling configurations considered only RSM 4 and 5 can be considered accurate over the whole cross section.

At the higher flow rates the predictions made by the modelling configurations can be considered accurate as they were contained within the experimental data set over the whole cross section.

5.6.4.2 Turbulent kinetic energy

The turbulent kinetic energy predictions are compared with experimental data in Figure 5.8. The characteristic turbulent kinetic energy profile consists of a rapid increase from zero at the wall of the pipe to a peak value at a distance of $20 < y^+ < 40$ (r/R $\approx$ 0.96). The turbulent kinetic energy then reduces in the form of an exponential decay to a minimum value at the centre of the pipe.

With the exception of the realizable model (K-E 4) the predictions made by the k-ε models in the central region of the pipe over estimated the turbulent kinetic energy. Closer to the wall the predictions were approximately accurate for all the modelling configurations, although the peak intensity was under predicted. The inclusion of the low Reynolds number effects of the turbulent viscosity did not significantly change the predictions made by the RNG model.

Away from the wall the Reynolds stress model predictions were primarily determined by the selection of the wall reflection effects modelling options, with the predictions being more accurate when the effects were not included (RSM 1, 2, 5, 6). Nearer to the wall the predictions were primarily determined by how the wall boundary conditions were modelled, with an under prediction of the peak intensity when the near wall Reynolds stresses were modelled using the transport equation for k (RSM 2, 4, 5), and perhaps an over prediction when the wall shear stress was used (RSM 1, 3, 6). The specification of the quadratic pressure strain model did not appear to be significant.

All of the models could be considered to have predicted the turbulent kinetic energy quite well. Of the k-ε models the relizable model, K-E 4, most closely represented the experimental data, but it is less clear which Reynolds stress modelling configuration was best.

At the higher flow rates the predictions made at the centre of the pipe were very similar, with an over prediction of the experimental measurements. There was a noticeable difference in the predictions nearer to the wall, but it was not possible to determine which model was most accurate from the measurements presented.

5.6.4.3 Turbulent viscosity

The distributions of turbulent viscosity are shown in Figure 5.9. Considerable differences exist between the predicted values of turbulent viscosity, and also between the predicted and measured values.

The predictions made by all of k-ε models were similar to the experimental data close to the wall, but away from the wall there was a significant variation. The predictions made by the relizable k-ε model (K-E 4) differed most from the calculated values, with an expected over prediction of 100 % at the centre of the pipe. The predictions made by the RNG models (K-E 2, 3) most closely represent the measured data, with the inclusion of the differential

viscosity making an improvement to the predictions. The predictions made using the RNG model were also different to the predictions made using the other turbulence models as they showed the maximum turbulence viscosity occurring away from the centre of the pipe. This is in agreement with the experimental data.

All of the RSM modelling configurations predicted the turbulent viscosity increasing from the wall to the centre of the pipe. Near to the wall the predictions were similar to the experimental data. Away from the wall all of the models over predicted the measured data. The predictions were improved when the quadratic pressure strain model was used (RSM 5, 6) and were made worse when the wall reflection effects were included (RSM 3, 4).

In general the predictions were not in good agreement with the experimental data. Of the models considered the k-ε RNG models (K-E 2, 3) and the RSM models that used the quadratic pressure strain model (RSM 5, 6) produced the best comparison with experimental data, while the k-ε relizable model (K-E 4) produced the worst comparison.

At the higher flow rate the relative performance of the three models did not change. The k-ε RNG models (K-E 2) best represented the experimental data, while the standard k-ε model (K-E 1) produced the worst fit.

5.6.4.4 Turbulent dissipation rate

In Figure 5.10 the turbulent dissipation rate predictions are compared with the experimental data of Lawn (1971). It should be noted the accuracy of the experimental data is limited because measurements were not made of all the turbulent correlations necessary to define the dissipation rate.

The qualitative features of the predictions were the same as the measurements, with a rapid increase in the dissipation rate close to the wall. However all of the models under predicted the dissipation rate at the centre of the pipe and over predicted the dissipation rate close to the wall.

The predictions made by the k-ε models were basically the same over the cross section. With the exception of RSM 3 the predictions made by the RSM models were the same in the core of the flow. Close to the wall the models which used the wall shear stress to determine the near wall Reynolds stresses (RSM 1,3,6) showed a greater over prediction than the models which used the transport equation for k.

At the higher flow rates the relative performance of the models did not change.

5.6.4.5 Reynolds shear stress

The Reynolds shear stress predictions were compared with experimental data in Figure 5.11. The Reynolds stresses, $\overline{uv}$, could not be determined directly when the k-ε models were used and was therefore calculated using Equation (5.6).

Away from the wall of the pipe all of the predictions were almost indistinguishable from the measured data. Close to the wall the predictions made by the k-ε models were greater than the measured data, while the predictions made using the RSM model were determined by the method used to model the near wall Reynolds stresses. The predictions more closely represented the measured data when they were determined from the *k* equation.

At the higher flow rates the same trends were repeated for the three turbulence models considered.

5.6.4.6 Reynolds normal stresses

The calculated Reynolds normal stresses are compared with the measured fluctuating velocity components in Figure 5.12 to Figure 5.14 (The Reynolds normal stresses are the same as the velocity fluctuations). It is not possible to determine the Reynolds normal stresses for the k-ε models because they use the Bousinesq assumption.

The predictions of axial normal stress, u', showed the same trends as the experimental data. However, u' is over predicted in the centre of the pipe by the models that included wall reflection effects (RSM 3, 4), while close to the wall the experimental data was under predicted when the near wall Reynolds stress was determined by the transport equation for *k* (RSM 2, 4, 5). The experimental data is best represented by RSM 1 and RSM 6.

The predictions of radial normal stress, v', away from the wall were determined by the method used to represent the pressure strain term and by the modelling of wall reflection effects. At the centre of the pipe the experimental data was under predicted when the quadratic pressure strain model was used (RSM 5, 6), while between r/R = 0.3 and 0.95 the data was under predicted when the wall reflection effects were included (RSM 3, 4). Close to the wall the predictions were more accurate when the near wall Reynolds stress were determined using a transport equation for k (RSM 1, 5, 6). The experimental data is best represented by RSM 2.

The predictions of the tangential normal stress, w', are in reasonable agreement with the experimental data in the core of the flow, but do not predict the rapid decline close to the wall. The wall reflection effects modelling option dominates the predictions, but it is unclear which option is best to use.

5.6.4.7 Headloss

In Figure 5.6 a comparison is made between the predicted headloss and the best fit equation which represents the measured headloss in the study of Guymer and O'Brien (2000). The values presented for the predicted headloss refer to models K-E 1, K-E 2 and RSM 4, as a comparison can be made over a range of discharges. The predicted and experimental values are close at 2 and 5 l/s, but differ at the higher discharge. This may be the result of the extra complexity required to model the flow field at a higher discharge. If this is correct it is perhaps

surprising that the standard k-ε model (K-E 1) performs better than the more complex Reynolds stress model (RSM 4).

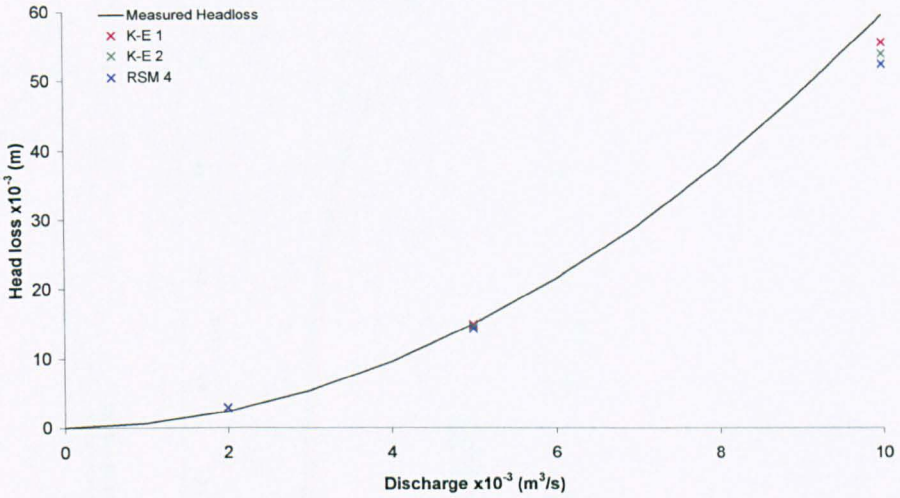

Figure 5.6 A comparison between the predicted and measured headloss

5.6.5 Conclusion

During the study the ability of 10 different modelling configurations to predict the fully developed turbulent pipe flow were examined. All of the configurations were considered at a flow rate of 2 l/s, and three of the configurations at two higher flow rates.

In general the predictions were in reasonable agreement with the experimental data. The only exception to this was the turbulent viscosity, where most of the predictions showed both qualitative and quantitative errors.

With the exception of the Reynolds stress there was a considerable difference in the predictions made by the different models. It was not possible to determine the superiority of one type of turbulence model. This demonstrates the extra computational expense required to solve the extra partial differential equations when using the RSM model does not necessarily lead to improved predictions.

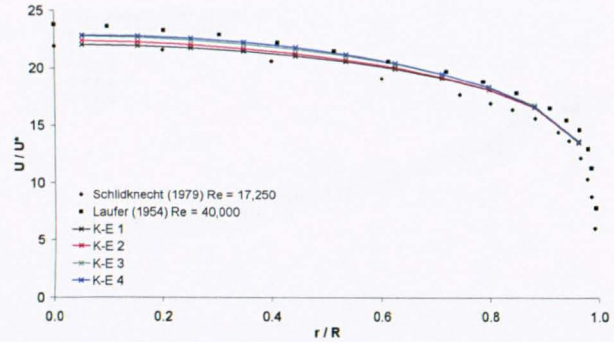

Q = 2 l/s
(Re = 29040)

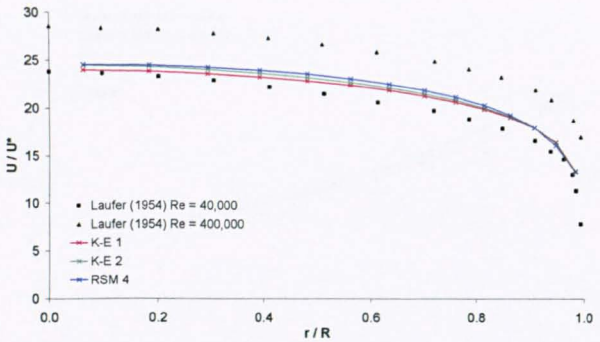

Q = 5 l/s
(Re = 72160)

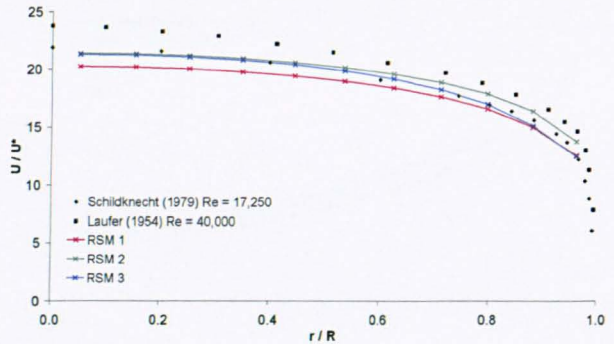

Q = 2 l/s
(Re = 29040)

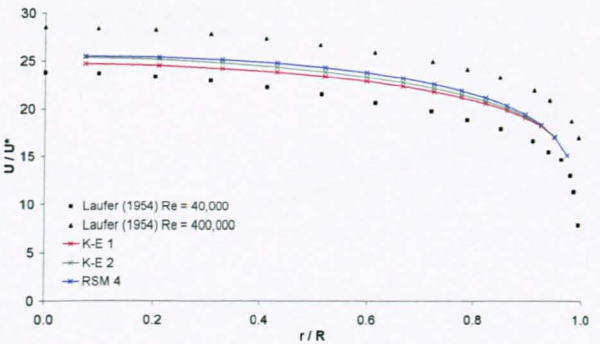

Q = 10 l/s
(Re = 144320)

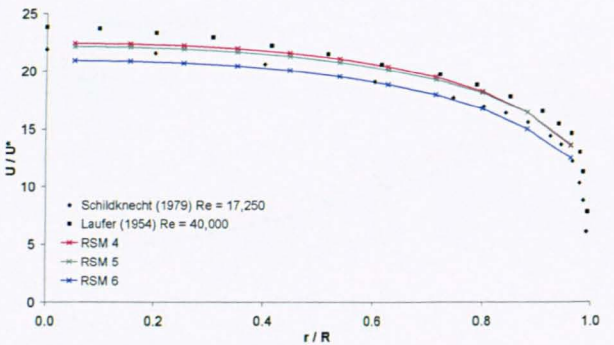

Q = 2 l/s
(Re = 29040)

Figure 5.7 Predicted and measured mean axial velocity

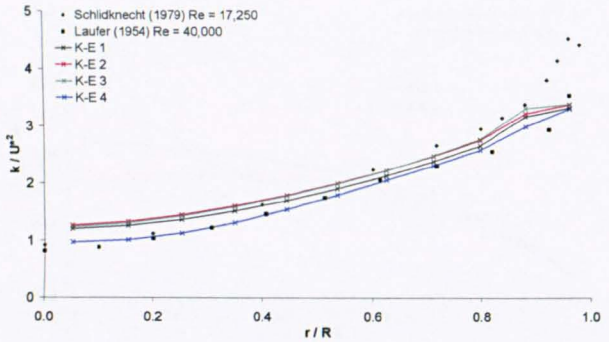

Q = 2 l/s
(Re = 29040)

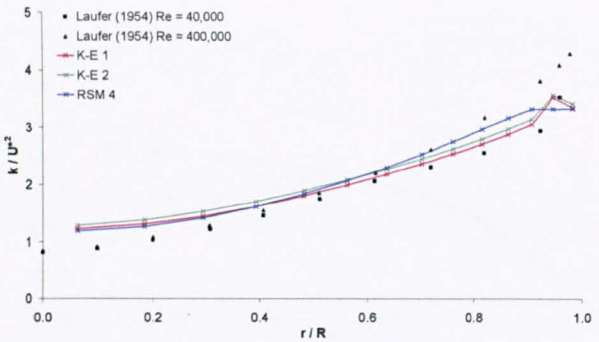

Q = 5 l/s
(Re = 72160)

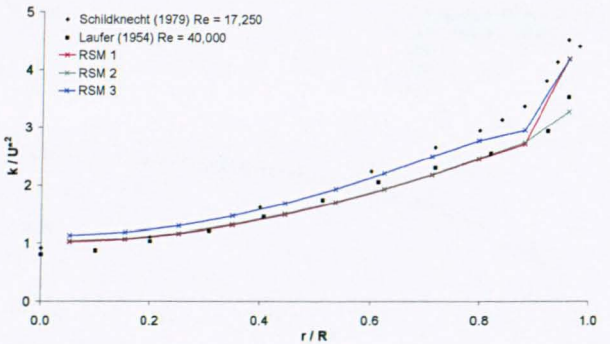

Q = 2 l/s
(Re = 29040)

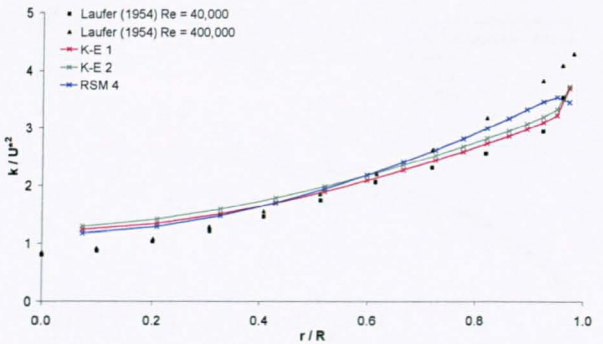

Q = 10 l/s
(Re = 144320)

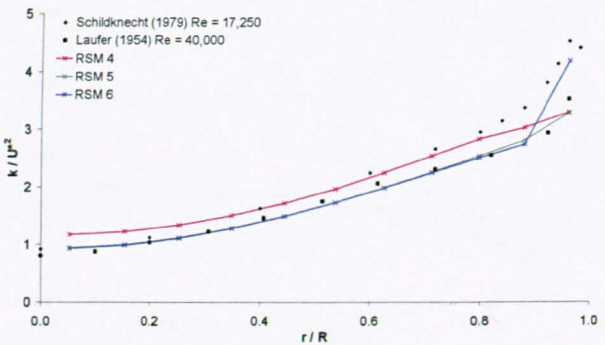

Q = 2 l/s
(Re = 29040)

Figure 5.8 Predicted and measured turbulent kinetic energy

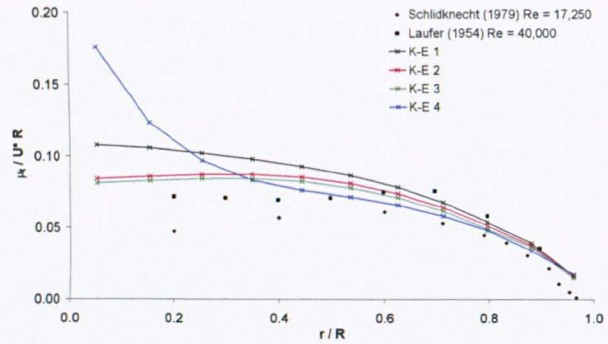

Q = 2 l/s
(Re = 29040)

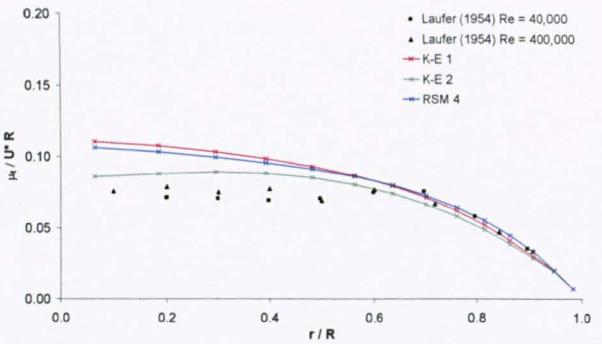

Q = 5 l/s
(Re = 72160

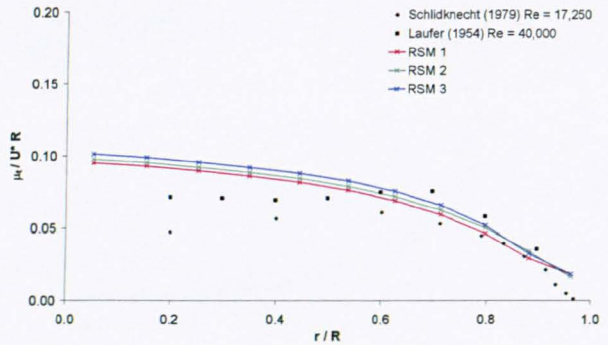

Q = 2 l/s
(Re = 29040)

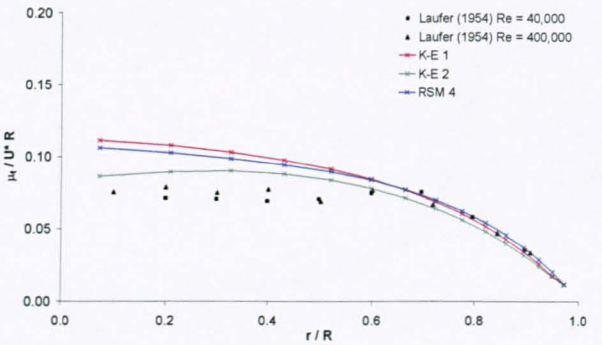

Q = 10 l/s
(Re = 144320

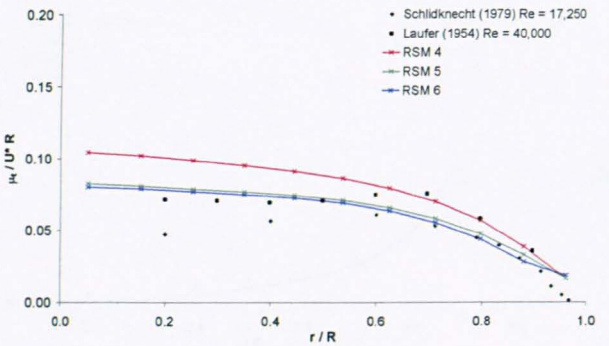

Q = 2 l/s
(Re = 29040)

Figure 5.9 Predicted and measured turbulent viscosity

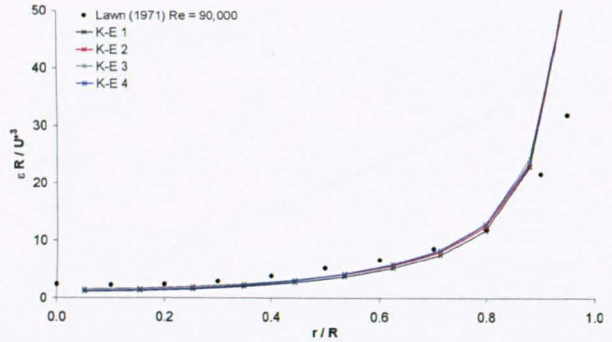

Q = 2 l/s
(Re = 29040)

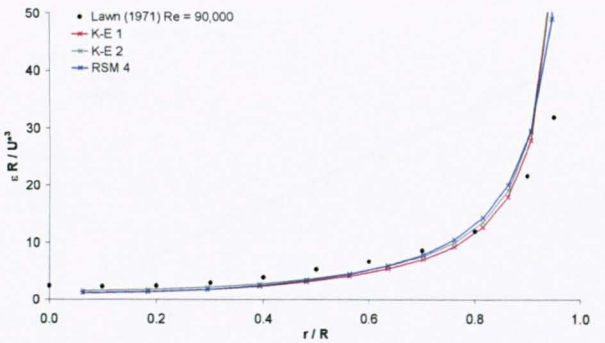

Q = 5 l/s
(Re = 72160

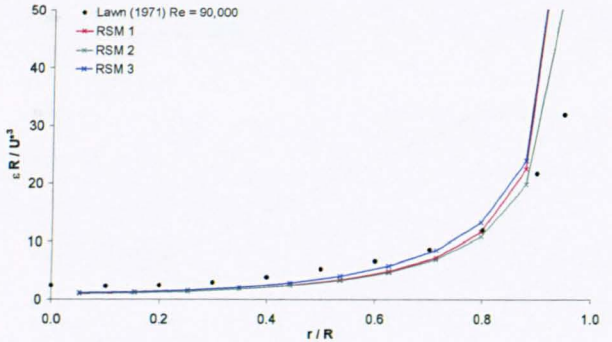

Q = 2 l/s
(Re = 29040)

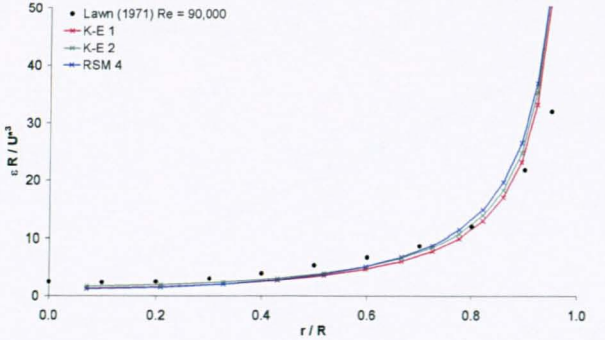

Q = 10 l/s
(Re = 144320

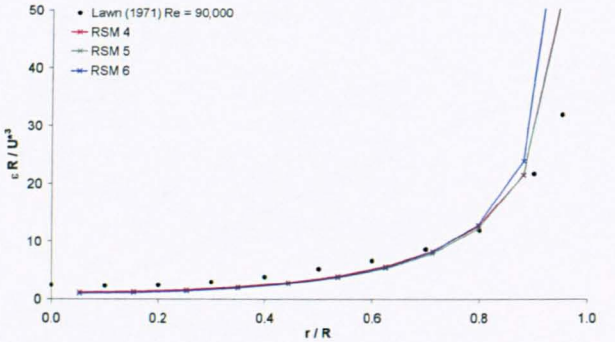

Q = 2 l/s
(Re = 29040)

Figure 5.10 Predicted and measured turbulent dissipation rate

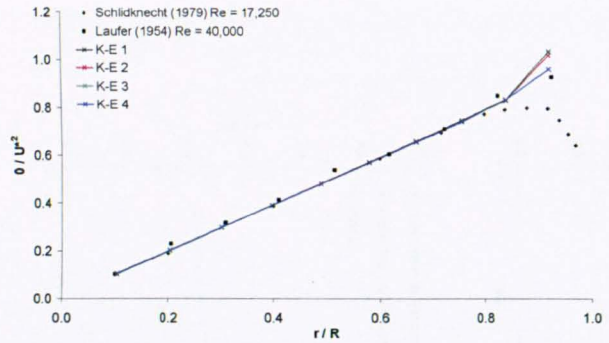

Q = 2 l/s
(Re = 29040)

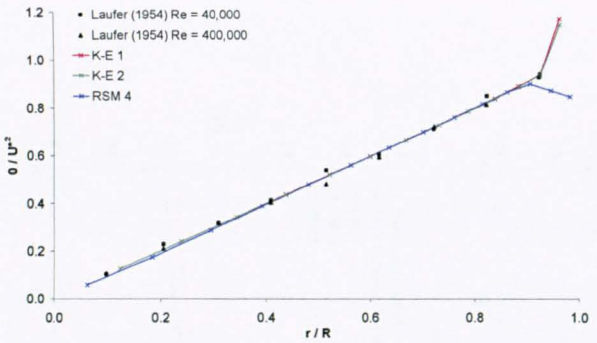

Q = 5 l/s
(Re = 72160

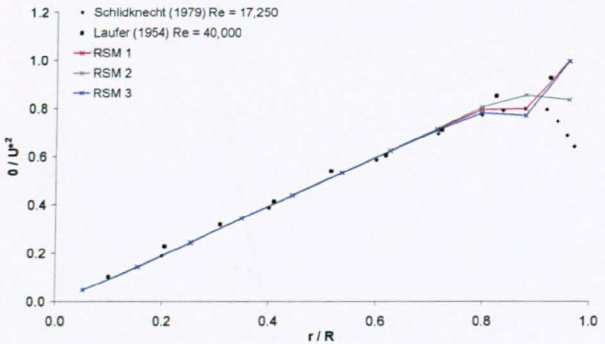

Q = 2 l/s
(Re = 29040)

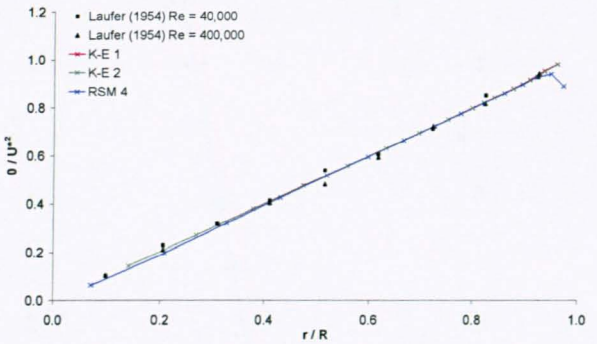

Q = 10 l/s
(Re = 144320

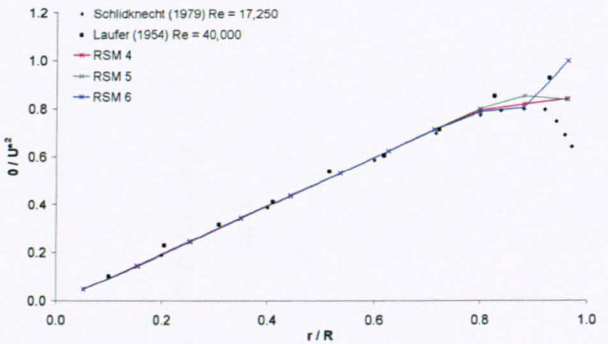

Q = 2 l/s
(Re = 29040)

Figure 5.11 Predicted and measured Reynolds shear stress

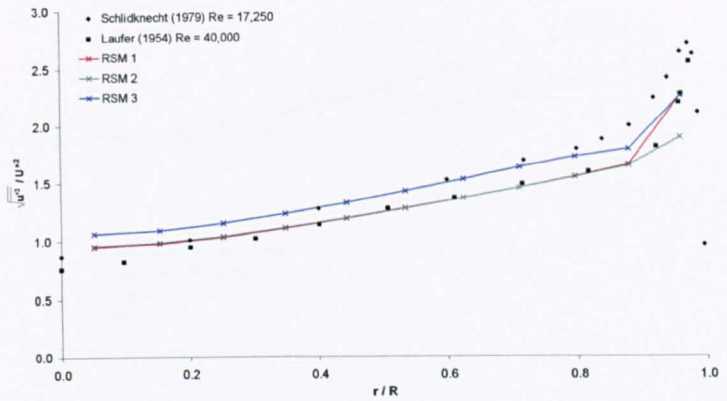

2 l/s

(Re = 29040)

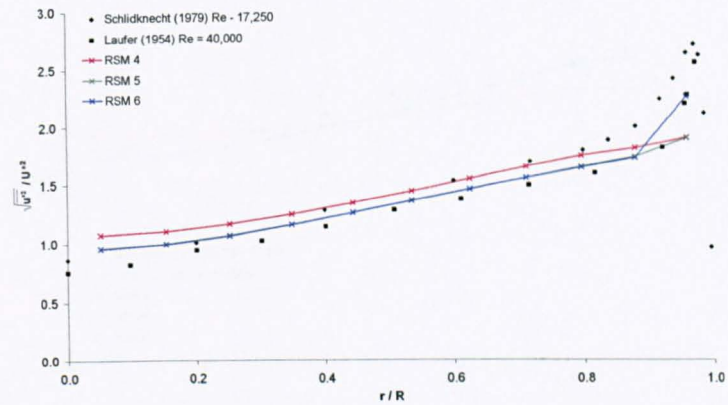

2 l/s

(Re = 29040)

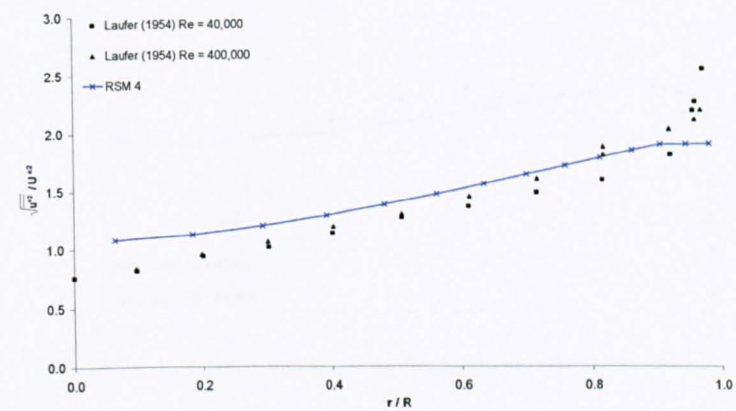

5 l/s

(Re = 72160)

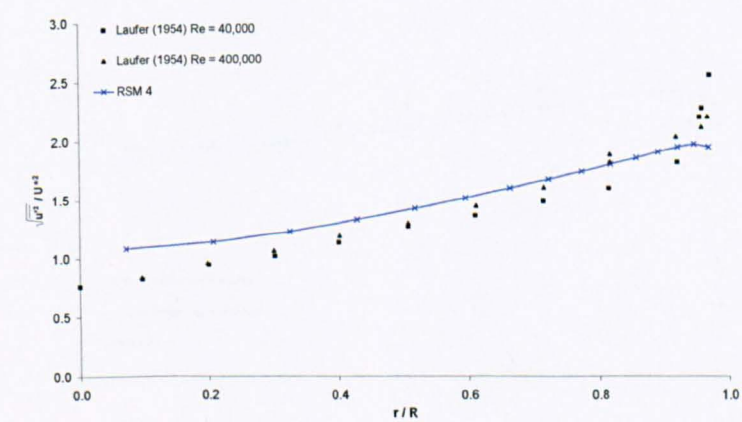

10 l/s

(Re = 144320)

Figure 5.12 Predicted and measured Reynolds axial normal stress

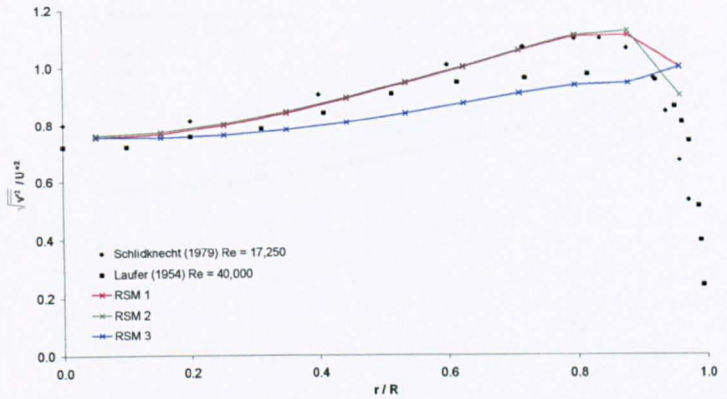

2 l/s

(Re = 29040)

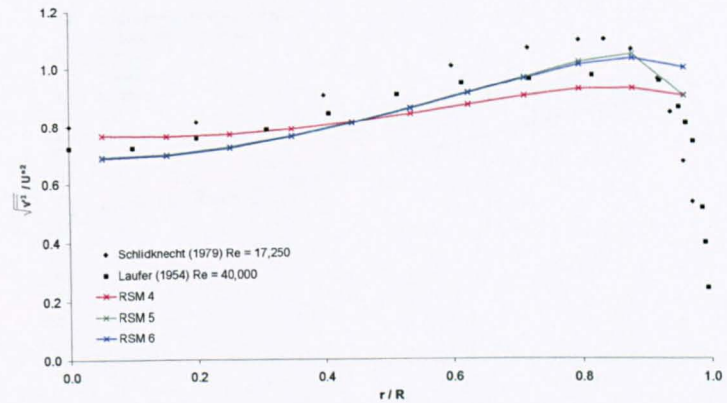

2 l/s

(Re = 29040)

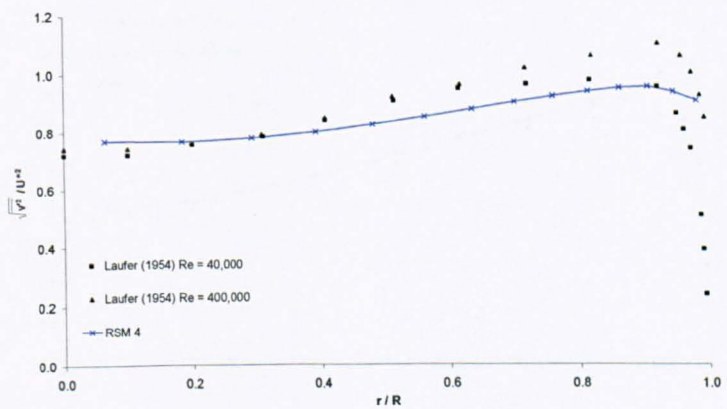

5 l/s

(Re = 72160)

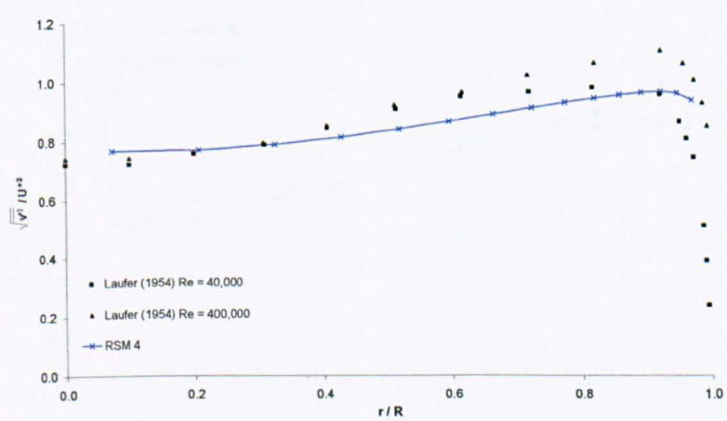

10 l/s

(Re = 144320)

Figure 5.13 Predicted and measured Reynolds radial normal stress

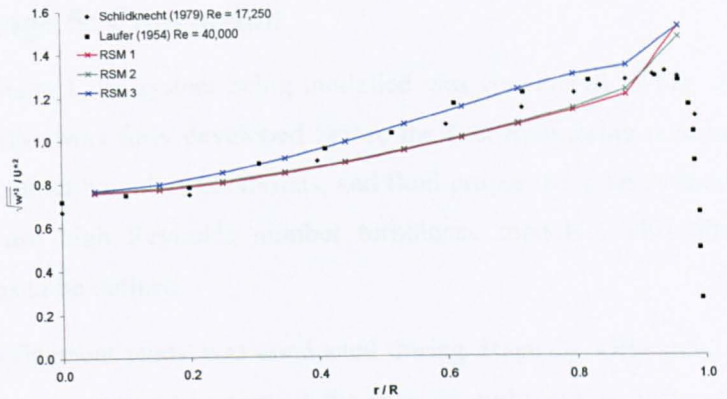

2 l/s

(Re = 29040)

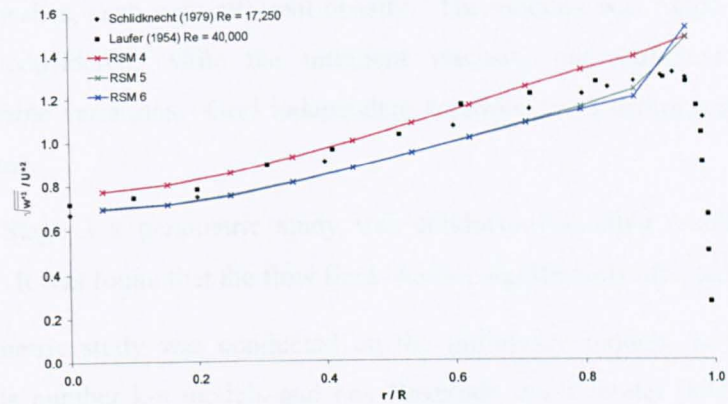

2 l/s

(Re = 29040)

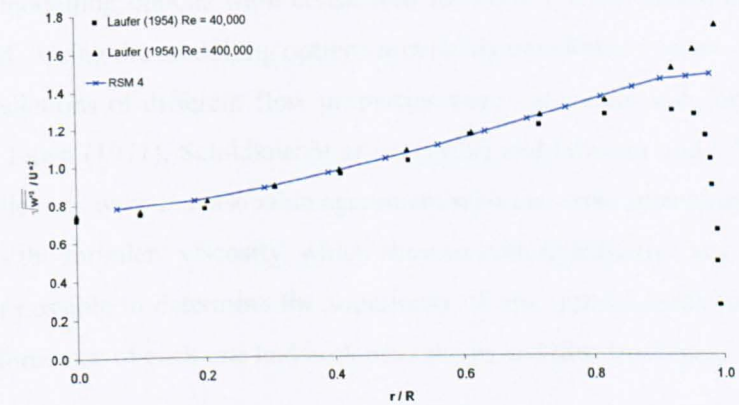

5 l/s

(Re = 72160)

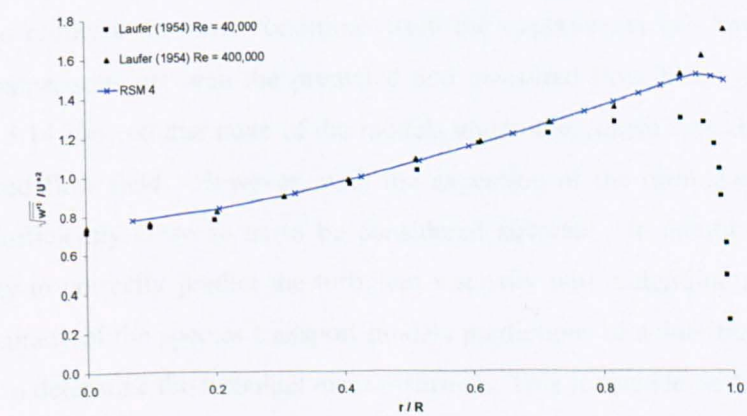

10 l/s

(Re = 144320)

Figure 5.14 Predicted and measured Reynolds tangental normal stress

5.7 Stage 5: Conclusion

During Stage 1 the system being modelled was considered. This, along with the assumption that the flow was fully developed before the first monitoring position, allowed the geometry, inlet and outlet boundary conditions, and fluid properties to be defined. The decision was made to only use high Reynolds number turbulence models. This allowed the wall boundary conditions to be defined.

A grid refinement study was conducted during Stage 2. Grid independence was assessed by considering the spatial variations in the velocity, turbulent viscosity and turbulent kinetic energy on six meshes, each with different density. The velocity was found to be insensitive to mesh density considered, while the turbulent viscosity and turbulent kinetic energy showed considerable variations. Grid independent solutions were determined for the three flow rates considered.

During Stage 3 a parametric study was conducted on eight combinations of discretization scheme. It was found that the flow field was not significantly affected by the choice of scheme.

A parametric study was conducted on the turbulence models during Stage 4. Three high Reynolds number k-ε models and one Reynolds stress model (RSM) was considered. Two further modelling options were considered for the k-ε RNG model and six further options for the RSM. Using the modelling options previously developed a series of flow fields was created. The predictions of different flow properties were compared with the measurements of Laufer (1954), Lawn (1971), Schildknecht *et al.* (1979) and Guymer and O'Brien (2000). In general the predictions were in reasonable agreement with the experimental data. The only exception to this was the turbulent viscosity, which showed both quantitative and qualitative differences. It was not possible to determine the superiority of one type of model or one individual model as the performance of each one had both advantages and disadvantages.

The aim of the study was to determine which modelling options were most appropriate to use in order to replicate the flow conditions from the experiments of Guymer and O'Brien (2000). The comparisons between the predicted and measured flow fields presented in Figure 5.7 to Figure 5.14 showed that none of the models under assessment was able to exactly replicate the measured flow field. However, with the exception of the turbulent viscosity the predictions were sufficiently close so as to be considered accurate. It should be noted that the models inability to correctly predict the turbulent viscosity will undermine any attempts to determine the accuracy of the species transport models predictions of solute transport as it is used by the model to determine the turbulent mass diffusion. This is considered further in Chapter 6.

With the exception of the turbulence models it was possible to determine the most appropriate modelling options to use. These are shown in Table 5.5 and Table 5.6. it appears that on balance the optimum model in this situation may be RSM5. This model appeared to capture the

near wall behaviour better than any other, whilst still retaining good predictions in the core of the flow. However the decision as to which models to employ for the dispersion validation presented in chapter 6 was influenced by the fact that flow fields for the two higher discharges had already been established using K-E 1, K-E 2 and RSM 4. Time constraints, coupled with the marginal differences in performance observed between the different turbulence models, meant that these three turbulence models, rather than RSM 5, were utilised in Chapter 6.

Parameter	Setting / Value
Fluid	
Density	998.2 kg/m^3
Absolute viscosity	1.003 kg/m s
Boundary conditions	
Wall	
Model	Standard wall functions
Roughness height	8 x10^{-5} m
Roughness constant	0.5
Inlet	
Q = 2 l/s	Vel = 0.33 m/s - Turb Int = 4.4 %
Q = 5 l/s	Vel = 0.82 m/s - Turb Int = 4.0 %
Q =10 l/s	Vel = 1.64 m/s - Turb Int = 3.6 %
Hydraulic diameter	0.088 m
Outlet	
Pressure	0 Pa
Turbulent intensity	As above
Hydraulic diameter	0.088 m
Discretization scheme	
Pressure	Second order
Pressure velocity coupling	SIMPLE
Momentum	Second order upwind
Turbulent kinetic energy	Second order upwind
Turbulent dissipation rate	Second order upwind
Reynolds stress	Second order upwind

Table 5.5 Determined flow field modelling options

Discharge (l/s)	Mesh	Boundary layer thickness (m)	No. of elements on radius	Spacing on the length (m)	Total No. of elements	Max. aspect ratio
2	GR 6	0.0035	12	0.0036	33336	1.07
5	GR 10	0.0015	14	0.003	46662	2.00
10	GR 15	0.0008	16	0.0023	69568	2.88

Table 5.6 Determined mesh modelling options

6 Validation of the dispersion predictions

6.1 Introduction

Chapters three and four reported on a feasibility study that was conducted to test the appropriateness of two alternative methods for simulating the transport of a solute tracer through a pipe. In chapter four it was shown that the particle tracking approach was computationally efficient and, with the exception of the mean travel time, that the predictions were robust. The mean travel time is, however, very important when considering the transport of a tracer and for this reason the approach is not given further consideration here, although the author feels the potential of the particle tracking approach remains significant. The species transport modelling approach was outlined in chapter three. The approach was shown to be sensitive to a number of the modelling options, but a robust simulation procedure was attainable. For this reason consideration is given solely to the species transport model in the sections that follow.

The accuracy of the species transport model's predictions of solute dispersion was not considered during the feasibility study. In order to assess the accuracy of the predictions it was decided to make a comparison with the measurements of solute dispersion reported by Guymer and O'Brien (2000). The numerical flow field that was mainly used in the feasibility study was based on this experimental study. It was, however, comparatively crude, having a 'reasonable' mesh and employing largely default modelling options. In chapter five a series of tests was performed to determine the most appropriate modelling options to use in order to reproduce the experimental flow field. By making a number of assumptions/simplifications, it was possible to define all modelling options except for the turbulence model. No single turbulence model resulted in predictions that were clearly superior to the others, although all the models that were evaluated were judged to produce acceptable predictions.

In Section 6.2 a comparison is made between the species transport model predictions of solute transport and the measurements of Guymer and O'Brien (2000). Although the qualitative features were similar, there were significant quantitative differences. In an attempt to determine the cause(s) of these differences, consideration was given to the appropriateness of the modelling assumptions/simplifications that were made and to the accuracy of the published data. These studies are reported in Section 6.4 to Section 6.7.

6.2 Data comparison

6.2.1 Introduction

In order to assess the accuracy of the species transport model's predictions of longitudinal dispersion, a comparison was made with the measurements of Guymer and O'Brien (2000). The comparison is reported in Section 6.2.4. In Section 6.2.2 a summary is presented of the experimental configuration and data analysis techniques used by Guymer and O'Brien (2000), while in Section 6.2.3 details are presented of the modelling options and strategy used in the numerical simulations.

6.2.2 Guymer and O'Brien (2000) dispersion study

6.2.2.1 Laboratory study

Figure 6.1 shows the main features of the experimental configuration. The tests were performed in a straight pipe with an internal diameter of 88 mm. Series 10 fluorometers (Turner Designs, 1981) were installed at two locations, 2.7 m apart. Pressure transducers were placed according to Figure 6.1.

The measurement volume of the fluorometers was modified to allow the average cross sectional concentration to be determined within the pipe. Fluorometers work by shining green light and detecting the red light emitted, with the amount of red light emitted being directly proportional to the concentration of the tracer. The system was therefore blacked out to prevent any extraneous light from entering.

During each test the tracer, Rhodamine WT, was introduced into the centre of the supply pipe at a distance of more than 100 pipe diameters upstream of the first measurement position. As the tracer passed the measured positions the fluorometers recorded the temporal change in the concentration. In total seven discharges were considered between 2 and 10.3 l/s, with typically ten repeat tests at each flow rate.

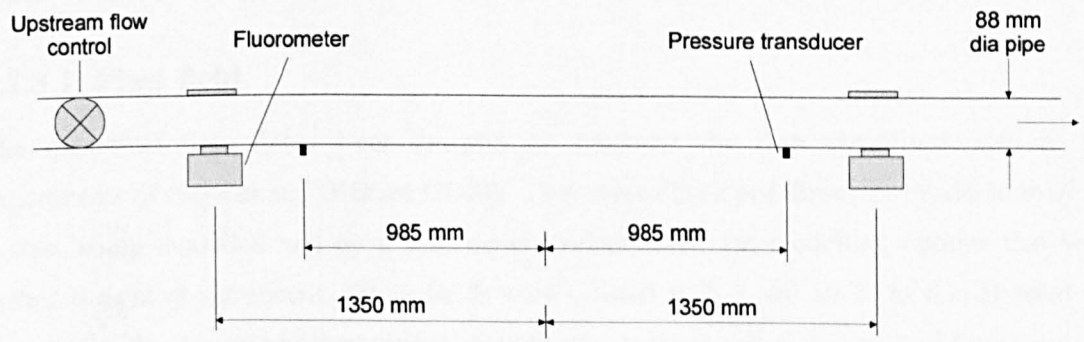

Figure 6.1 The experimental configuration

6.2.2.2 Data analysis and results

Instead of analysing the individual traces and then averaging the results, the method preferred by Guymer and O'Brien (2000) was to average the repeat readings prior to analysis. This was done through a superposition of the repeat readings for each set of tests about the peak concentration. The data was then smoothed using a low band pass filter. A previously determined calibration was used to covert the voltage readings recorded by the fluorometers into a concentration. The region where the solute concentration was greater than background was isolated to leave a discrete trace. The data was then mass balanced to remove any discrepancies that may have been caused by the calibration or by other means.

In the majority of cases the standard moment analysis described in Chapter 3 was unable to determine the most appropriate values for the longitudinal dispersion coefficient and the mean travel time. A software routine was therefore developed to optimise the fit between the measured and predicted downstream distributions. The routine refines the prediction of travel time and longitudinal dispersion coefficient to determine the values that minimise the error between the predicted and measured distributions. Details regarding the optimisation routine are presented in Dennis *et al.* (1999).

The variation in the optimised longitudinal dispersion coefficient with discharge is shown in Figure 6.2 (contained within Section 6.2.4). As would be expected, the longitudinal dispersion coefficient increases with discharge. Following the approach used by Guymer and O'Brien (2000) a linear regression equation, Equation (6.1), is presented which was developed by considering all the data points and fitting through the origin. A comparison with the measured data gives an R^2 value of 0.745.

$$K = 3.3Q \qquad (6.1)$$

where K is the longitudinal dispersion coefficient.

6.2.3 Numerical simulation

6.2.3.1 Flow field

The numerical flow fields were designed to represent the flow conditions used in the experiments of Guymer and O'Brien (2000). They were developed through consideration of the system being modelled and by a systematic evaluation of the modelling options that were regarded as most significant. Flow fields were created at 2, 5 and 10 l/s as this allowed the accuracy of the species transport model predictions to be assessed over a range of flow rates. At each flow rate three flow fields were created because it was not possible to identify one turbulence model that was clearly superior. Consideration was given to the standard k-ε model

(K-E 1), the RNG k-ε model (K-E 2) and the Reynolds stress model (RSM 4). Details regarding these turbulence models and the other flow field modelling options are presented in Chapter 5.

6.2.3.2 Species transport model

The species transport modelling options were specified according to the recommendations of the feasibility study reported in Chapter 3. In each of the tests the tracer was introduced into the pipe from the velocity inlet for one second. The tracer was then tracked through the pipe until zero concentration was left. Monitoring positions were created at the inlet, outlet and at two metre intervals along the length of the pipe to record the change in the average mass fraction of dye with time, thus creating a series of temporal profiles. Only one simulation was performed for each configuration because the species transport model does not use stochastic methods and therefore reproduces exactly

The simulations were performed using the uncoupled, or cold processing technique. The second order implicit scheme was used for the temporal discretization and the second order upwind scheme for the spatial discretization. The convergence criteria for the species transport equations were set to 1 $x10^{-3}$, with a maximum of 20 iterations per time step. For most of the time steps convergence was obtained within three iterations, with the only exceptions being when the dye initially entered the pipe, or at the end of the end of the simulation when low concentrations left the pipe. Increasing the maximum number would not have changed the solution as the residuals normally stabilised to a constant value after approximately 10 iterations. Repeat simulations were performed on each flow field using progressively smaller time steps until time step independence was reached, determined when the longitudinal dispersion coefficient changed by less than 1 %. Time step independence was reached at 0.02 s at 2 l/s, 0.005 s at 5 l/s and 0.002 s at 10 l/s.

The physical properties of the tracer were specified to be the same as the primary water phase. The molecular diffusion coefficient was specified to be 1 x 10^{-10} m^2/s and the turbulent Schmidt number was left at the default setting of 0.7 throughout the domain.

The relationship between the longitudinal dispersion coefficient and flow rate was established by undertaking an analysis of the temporal moments. The method used is reported in Chapter 3. The value presented for the coefficient in subsequent sections is the constant value obtained once the tracer had entered the equilibrium zone.

6.2.4 Comparison

The variation in numerical predictions of longitudinal dispersion coefficient with discharge is shown in Figure 6.2. Taylor's (1954) analysis demonstrates that the coefficient is dependent upon the shear velocity, U^*, which increases linearly with discharge. The coefficient should therefore also increase linearly with discharge, and is correctly reproduced in the numerical

models. The predictions made using the different flow fields are not the same, with a maximum variation of approximately 20 % at 10 l/s.

Plotted alongside the numerical predictions are the measured values and the linear regression equation proposed by Guymer and O'Brien (2000). Although the qualitative features are the same there are significant quantitative differences. At every flow rate the measured dispersion is under predicted, with an under prediction of between 41 % and 52 % between the linear regression equation and the numerical predictions at 10 l/s.

In Chapter 5 it was observed that the predictions made using the K-E 2 turbulence model were the most accurate of the three models considered here, with the predictions of axial velocity, turbulent kinetic energy and Reynolds shear stress all showing good quantitative agreement. The predictions of turbulent viscosity also showed the same qualitative trends as the experimental data, while the other models, in particular K-E 1, showed considerable quantitative and qualitative errors. The turbulent viscosity is used in the species transport equations to determine the turbulent mass diffusion. This may be the reason why the predictions of dispersion most closely represented the experimental data when they were made with the flow field developed using the K-E 2 turbulence model.

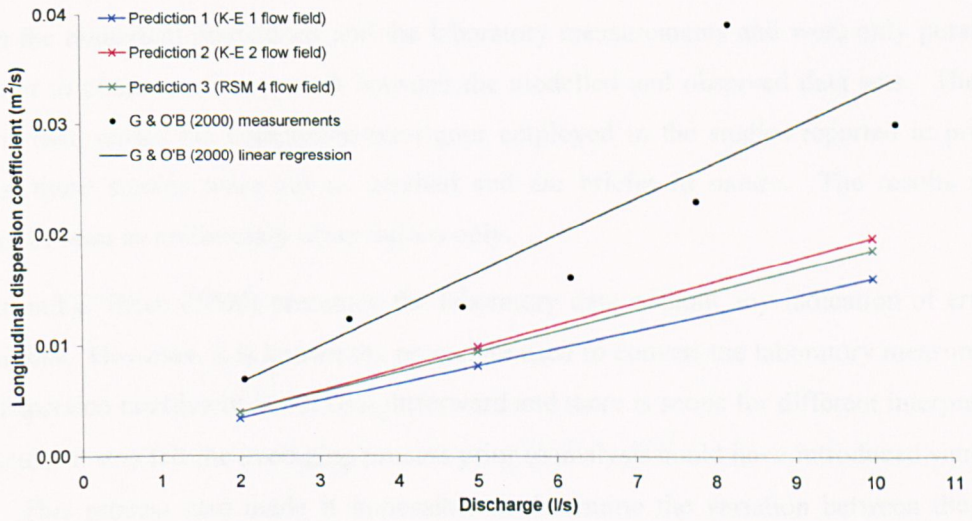

Figure 6.2 Measurements and predictions of the longitudinal dispersion coefficient

6.3 Discussion

Although the numerical predictions showed the same qualitative trends as the measurements of Guymer and O'Brien (2000) there were significant quantitative differences. Although part of this difference was due to the incorrect prediction of the turbulent viscosity in the underlying flow field it is unlikely to be the sole reason. For instance, the predictions made by Hrenya *et al.* (1998) of heat transfer in a pipe, a similar process to mass transfer, were all within 18 % of the measured values, with the underlying flow fields showing similar trends. In an attempt to

determine the cause of the additional error, consideration was given to what were believed to be the most significant modelling assumptions/simplifications that were made, and to the appropriateness of using the published data as a means of assessing the accuracy of the predictions.

The modelling assumptions/simplifications that were regarded as most likely to have caused the error were:

- The flow being fully developed before the first measurement position in the laboratory experiments.
- The use of high Reynolds number turbulence models and wall functions.
- A homogeneous value of 0.7 for the turbulent Schmidt number.

Studies that focus on each of these factors are presented in Section 6.5 to Section 6.7.

These factors were not considered previously for a number of reasons. Firstly, the ability to model the full experimental facility, or to consider more complicated turbulence models, was only made possible towards the end of the research when new computational resources became available. The second reasons is that chronologically they follow on from the comparison between the numerical predictions and the laboratory measurements and were only pursued in an attempt to obtain a closer match between the modelled and observed data sets. The third reason is that, unlike the comprehensive rigour employed in the studies reported in previous chapters, these studies were not as detailed and are briefer in nature. The results should therefore be seen as preliminary observations only.

Guymer and O'Brien (2000) presented the laboratory data without any indication of errors or uncertainties. However, it is known the procedure used to convert the laboratory measurements into a dispersion coefficient is not straightforward and there is scope for different interpretation. In particular it was felt the averaging process prior to analysis could have introduced significant errors. This process also made it impossible to determine the variation between the repeat readings, something that other studies have shown can be considerable. For these reasons the data at 2.1, 4.8 and 10.3 l/s was reanalysed using the method outlined in Section 6.4.1. In Section 6.4.2 a comparison is made between the numerical predictions reported previously and the reanalysed measurements. The theoretical equation proposed by Taylor (1954) is also presented.

6.4 Laboratory data

6.4.1 Re analysis of the laboratory data

The reanalysis of the laboratory data was conducted in three stages:

Stage 1: Removal of the background concentration

Stage 2: Isolation of the trace

Stage 3: ADE optimisation and analysis

6.4.1.1 Stage 1: Removal of background concentration

Following discussions with the author (Guymer, 2003) the original output files from the fluorometers were supplied. A visual inspection was used to identify regions where the concentration of the tracer in the flow was at a background level, Figure 6.3. In these regions the variations in the readings were solely caused by the 'noise' of the instruments. The magnitude of the background concentration was determined by averaging the voltage readings from these regions. The background concentration was then removed by subtracting the background value from every reading.

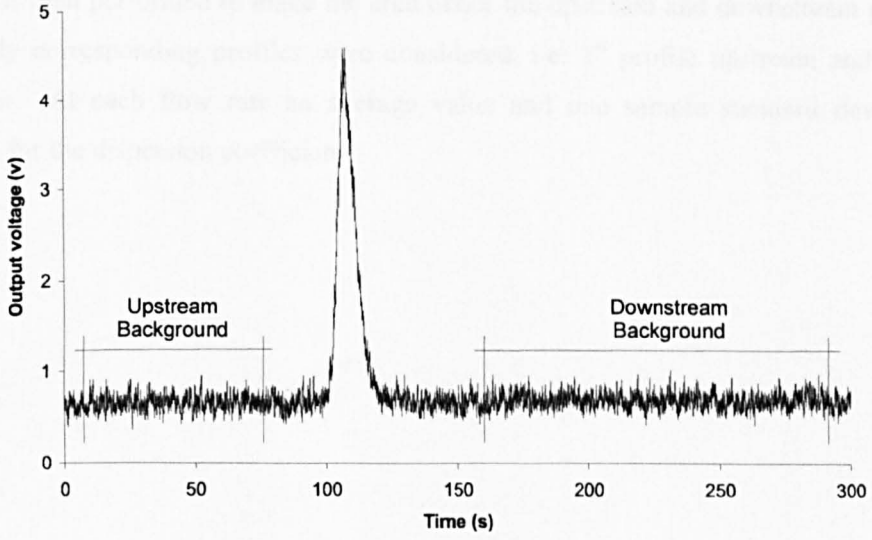

Figure 6.3 Identifying the background concentration

6.4.1.2 Stage 2: Isolation of the trace

Due to instrument noise it was not possible to identify the exact start and end of the trace. This is not normally important because these variations are white noise, which should not affect the optimisation routine. However, preliminary tests showed that the mass balance calculations were affected by the cut off location, which in turn affected the optimised predictions.

In order to assess the influence of the cut off location three different upstream and downstream profiles were considered for each trace (An example of the profiles created at each flow rate is shown in Figure 6.4). The first profile had the shortest duration. Working from either side of the peak the criteria used to define the profile was when five consecutive readings were below one percent of the peak reading. The durations of the 2nd and 3rd profiles were varied to make the relationship between the width of the main part of the trace and the total width approximately the same at each flow rate. At 2 l/s the duration of the profiles were increased by five and ten seconds either side of the first profile. At 5 and 10 l/s the duration of the main profile was less so 4 and 8, and 2 and 4 more seconds were included respectively.

6.4.1.3 Stage 3: ADE optimisation and analysis

As noted by Guymer and O'Brien (2000), it was not possible to use standard moment analysis to accurately determine the ADE parameters. Therefore, the optimisation routine of Dennis *et al.* (1999) was used to determine the mean travel time and longitudinal dispersion coefficient of each trace. The limits of accuracy adopted were 0.00001 s for the travel time and 0.00001 m^2/s for the dispersion coefficient.

Before performing the ADE optimisation the voltage readings were converted into a concentration. One volt was made equivalent to one unit of concentration. A mass balance exercise was then performed to make the area under the upstream and downstream profiles the same. Only corresponding profiles were considered, i.e. 1st profile upstream and 1st profile downstream. At each flow rate an average value and one sample standard deviation was determined for the dispersion coefficient.

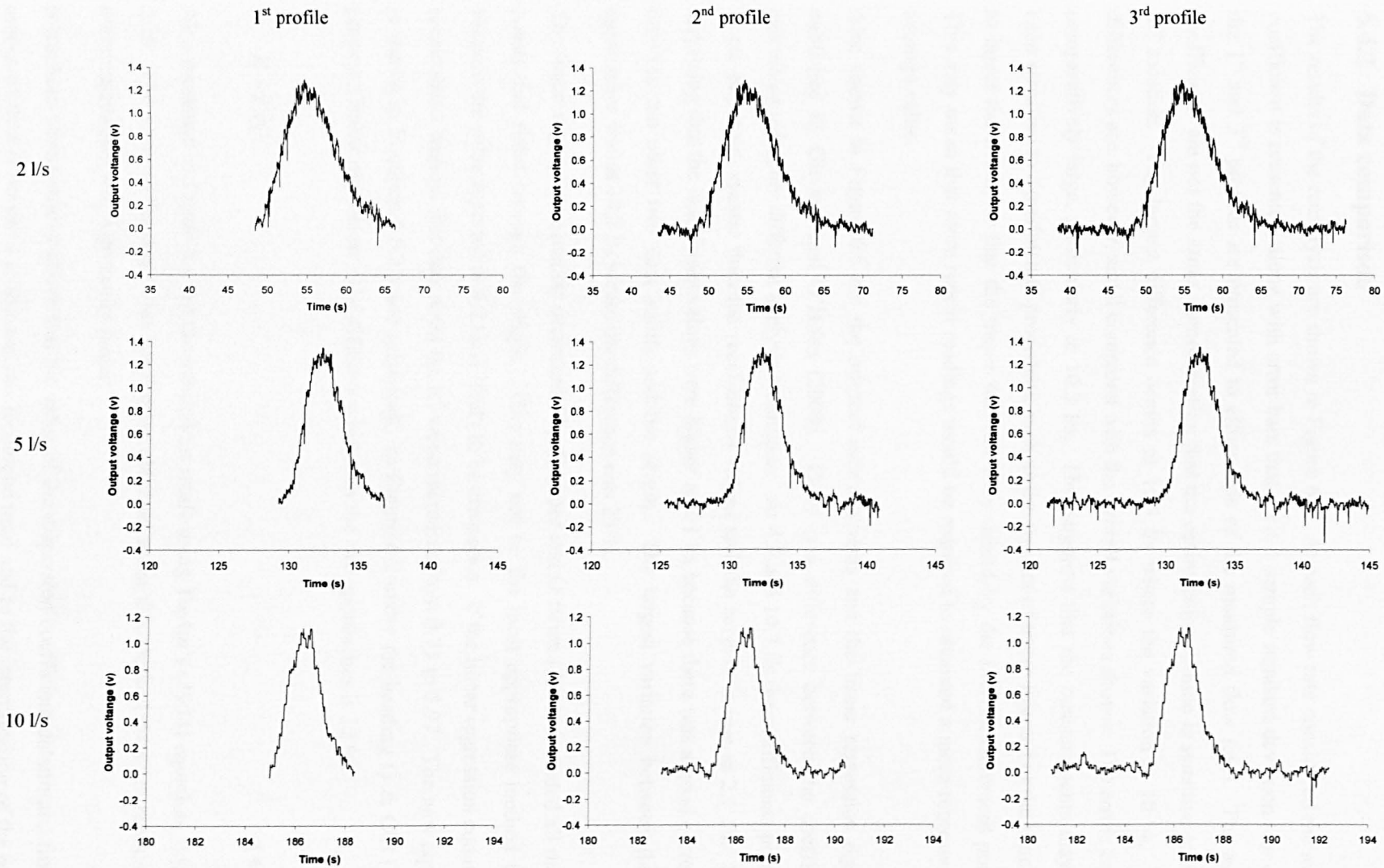

Figure 6.4 Illustration of the three profiles considered at each flow rate

6.4.2 Data comparison

The results of the reanalysis are shown in Figure 6.5. At each flow rate considered the average coefficient is presented, along with error bars that are ± 1 sample standard deviation (for clarity the 1st and 3rd profiles are presented to either side of the measured flow rate). The average coefficients are not the same, demonstrating that the optimisation routine is sensitive to the cut off location. The largest difference occurs at 10.3 l/s where the variation is 10 %. These differences are, however, small compared with the overall variations shown. The errors bars are comparatively large, particularly at 10.3 l/s. This suggests that the measurements may have been sensitive to experimental procedure, such as the amount of tracer injected or the time taken to inject the tracer, or that the tracer was not fully mixed by the first measurement position. This may mean that more repeat readings would be required to obtained a more representative average value.

Also shown in Figure 6.5 are the original measurements and the linear regression equation published by Guymer and O'Brien (2000). There is a difference between the coefficients calculated using the different analysis techniques. At 4.8 and 10.3 l/s the coefficients presented in the paper are greater than the recalculated values and the reverse is true at 2.1 l/s. It was surprising that the reanalysed values were higher at 2.1 l/s because there was a good correlation between the other two data points and the origin. The largest variation between the two approaches was at 10.3 l/s where the difference was 23 %.

The linear regression equation determined by Guymer and O'Brien (2000) included all the data points and fitted through the origin. This may not be the most appropriate method to use because the value reported at 8.2 l/s is likely to be erroneous. If the linear regression equation is recalculated without this data point the R^2 value increases from 0.75 to 0.97. The new equation is shown in Equation (6.2) and graphically in Figure 6.2 under the heading G & O'B (2000) proposed linear regression. The difference between the two approaches is 12 %.

$$K = 2.9Q \qquad (6.2)$$

Also presented in Figure 6.5 are the predictions made using Taylor's (1954) equation, Equation 2.18. The value of the dispersion coefficient obtained using this method does not replicate the other approaches and is generally larger.

It has been demonstrated above that the value of the dispersion coefficient determined from the measured data is sensitive to the analysis technique used and to the interpretation of the results. It has also been shown that there is a difference between these values and the predictions made using Taylor's equation. It is therefore not possible to categorically determine a relationship between flow rate and dispersion coefficient at this time.

Plotted alongside the above approaches are the three numerical predictions. Although the above approaches are all under predicted the quantitative difference may be more or less than first thought. It was felt by the author that the reanalysed data was the most accurate representation of the laboratory data, particularly at 4.8 and 10.3 l/s. All of the predictions fell within the imposed error bounds (i.e. one standard deviation) and in particular the predictions made using the flow field created with the K-E 2 model showed a good agreement. As it is not possible to categorically determine the relationship between dispersion coefficient and discharge at this time a more detailed comparison is not made with the predictions because it would involve too much conjecture and speculation.

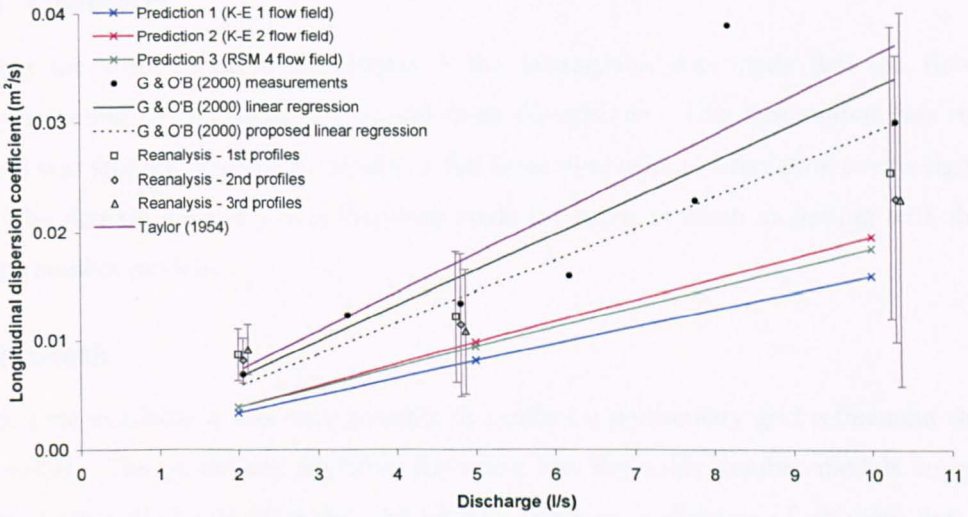

Figure 6.5 The variation in the longitudinal dispersion coefficient with discharge for the different methods considered

6.5 Low Reynolds number turbulence models

6.5.1 Introduction

The tests reported in Section 6.2 were based on flow fields that were developed using high Reynolds number turbulence models and wall functions. Low Reynolds number turbulence models were not previously considered because the extra resources required to resolve the flow field close to the wall made it impractical to run the models with the computational power available. Towards the end of the project two new computational resources became available which made it feasible to consider them on a limited basis. A series of preliminary tests were therefore performed to assess whether the use of low Reynolds number turbulence models might enhance the flow field predictions, in particular the prediction of turbulent viscosity.

A brief grid refinement study was first conducted to ensure the predictions made using the low Reynolds number models were close to being grid independent. This study is reported in

Section 6.5.3. A comparison was then made between the flow field predictions obtained using the low and high Reynolds number turbulence models and the experimental data of Laufer (1954) and Schlidknecht *et al.* (1979). This would determine whether the predictions were enhanced when using the low Reynolds number approach. This study is reported in Section 6.5.4, together with a summary of the experimental studies presented in Chapter 2. Before these studies are reported a description of the modelling options used to develop the low Reynolds number flow fields is presented in Section 6.5.2.

6.5.2 Modelling options

6.5.2.1 Geometry

Following the work reported in Chapter 3 the assumption was made that the flow field predictions would be the same in two and three dimensions. This assumption was required because it was still not possible to conduct a full three dimensional simulation over a significant reach. The domain geometry was therefore made the same as when modelling with the high Reynolds number models.

6.5.2.2 Mesh

With the time available it was only possible to conduct a preliminary grid refinement study on three meshes. The guidelines available for using low Reynolds number models suggest the boundary layer cell should be within the viscous sublayer, a distance of no more that $y^+ = 5$ from the wall (Fluent, 1998). The size of the boundary layer was therefore fixed using Equation 2.33 so that the cell extended to $y^+ = 2$, a distance of 0.0002 m. The number of cells on the length of the pipe was fixed at 10000, with a constant spacing of 0.001 m, creating a maximum aspect ratio of 5. This is just within the generally accepted range for the mesh to still be appropriate. With the computational resources available it was not possible improve the aspect ratio by considering more cells on the length as this would have created a mesh that would have been too large to have been feasibly modelled. The number of cells on the radius was varied, with the spacing between the nodes specified to ensure the ratio of any two succeeding interval lengths was constant. The details of each mesh considered is presented in Table 6.1.

In Figure 6.6 a comparison is made between Mesh FM2 and mesh used when modelling at the same flow rate with high Reynolds number models (Mesh GR 6). It is clear that a considerably finer mesh is required when using low Reynolds number models.

Mesh	Boundary layer thickness (m)	No. of elements on radius	Spacing on the length (m)	Total No. of elements	Max. aspect ratio
FM 1	0.0002	30	0.001	300000	5.0
FM 2	0.0002	40	0.001	400000	5.0
FM 3	0.0002	50	0.001	500000	5.0

Table 6.1 Details of the three low Reynolds number meshes considered during the grid refinement study

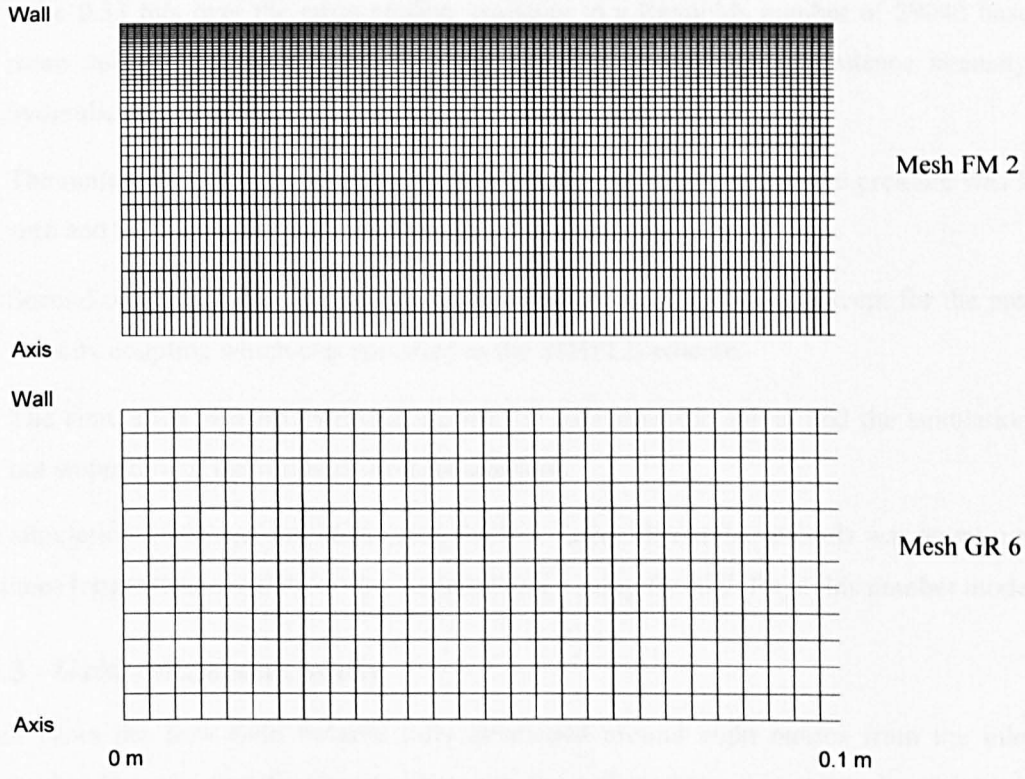

Figure 6.6 A comparison between low and high Reynolds number meshes

6.5.2.3 Flow field

Wall functions are not employed when low Reynolds number turbulence models are used. Instead the turbulence models are modified to enable the viscous affected region to be resolved with a mesh all the way to the wall. With the time available it was only possible to consider three of the low Reynolds number models supported by Fluent 5.5 (Fluent, 1998). The first two were modifications of the K-E 1 and K-E 2 modelling configurations described previously. In the fully turbulent region the same equations are applied, while in the viscous affected region the one equation model of Wolfstein (1969) is applied. The momentum and turbulent kinetic energy equations are solved in the same manner, but the turbulent viscosity and turbulent dissipation rate are solved using modified equations. The third model considered was proposed by Lam and Bremhorst (1981). This is a full low Reynolds number k-ε model in which all of the transport equations are integrated to the wall. Further information regarding the low

Reynolds number turbulence models that were considered can be obtained from the Fluent 5 User's Guide (Fluent, 1998).

The remaining flow field modelling options were based on the study reported in Chapter 5, with a brief description presented below.

- The flow was given the properties of water at 20 °C.
- The inlet to the domain was specified as a velocity inlet. The inflow velocity was specified to be 0.33 m/s over the cross section, equating to a Reynolds number of 29040 based on mean velocity and pipe diameter. The turbulence parameters, turbulence intensity and hydraulic diameter, were set to 4.4 % and 0.088 m respectively.
- The outlet from the pipe was specified as a pressure outlet. The gauge pressure was left at zero and the turbulence parameters were modelled as the velocity inlet.
- Second order spatial discretization schemes were used throughout, except for the pressure velocity coupling which was specified as the SIMPLE scheme.
- The simulation was performed using the 2D axisymmetric solver and the simulation was not stopped until the residuals became constant.

The simulation time required when using the low Reynolds number models was approximately ten times longer than simulation time required when using the high Reynolds number models.

6.5.3 Grid refinement study

In all cases the flow field became fully developed around eight metres from the inlet. A monitoring line was therefore created between the wall and the axis at this location to record variation in the flow properties over the cross section. The flow properties changed only slightly between the meshes for each of the turbulence models considered. For illustrative purposes the variation in the turbulent viscosity over the cross section for the K-E 1 turbulence model configuration is shown in Figure 6.7. Although a truly grid independent solution was not reached, all of the predictions could be considered to be within a few percent of a grid independent solution. This would be close enough to determine if the predications were sufficiently better to justify the extra computational expense.

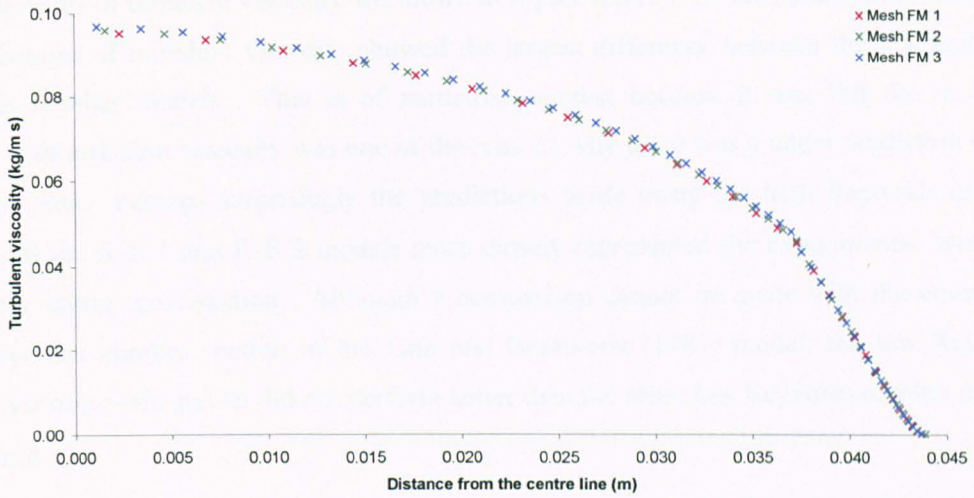

Figure 6.7 Comparison between the turbulent viscosity predictions on different meshes

6.5.4 Flow field comparison

In Figure 6.8 a comparison is made between the predictions of axial velocity, turbulent kinetic energy, turbulent viscosity and Reynolds shear stress made using the low and high Reynolds number turbulence models. Presented alongside the predictions are the measurements of Laufer (1954) and Schildknecht *et al.* (1979). These measurements were used to determine if the flow field predictions were improved when using the low Reynolds number models.

The predictions of axial velocity are shown in Figure 6.8 (a). Near to the wall, $r/R > 0.8$, the predictions made using the low and high Reynolds number versions of the K-E 1 and K-E 2 turbulence models were approximately the same. Away from the wall the predictions made using the low Reynolds number model under predicted the high Reynolds number model. When a comparison was made with the experimental measurements the predictions made using the high Reynolds number models could be considered accurate over the whole cross section, while the predictions made using the equivalent low Reynolds number models under predicted the peak experimental velocity. The prediction made using the Lam and Bremhorst (1981) model was approximately the same as the other low Reynolds number models.

The predictions of the turbulent kinetic energy are shown in Figure 6.8 (b). The predictions made using the low and high Reynolds number versions of the K-E 1 and K-E 2 turbulence models were noticeably different close to the wall and in the core of the flow. Near to the wall the predictions made using the low Reynolds number models more closely represented the experimental data, while in the core of the flow the predictions were better when the high Reynolds number models were used, although there was still an over prediction of the measurements. The prediction made using the model proposed by Lam and Bremhorst (1981) was most accurate of the models considered. Close to the wall the experimental conditions are modelled well, but there was still an over prediction in the centre of the pipe.

The predictions of turbulent viscosity are shown in Figure 6.8 (c). Of the parameters considered the predictions of turbulent viscosity showed the largest difference between the low and high Reynolds number models. This is of particular interest because it was felt the incorrect prediction of turbulent viscosity was one of the reasons why there was a under prediction of the measured data. Perhaps surprisingly the predictions made using the high Reynolds number versions of the K-E 1 and K-E 2 models more closely represented the experimental data over almost the entire cross section. Although a comparison cannot be made with the equivalent high Reynolds number version of the Lam and Bremhorst (1981) model, the low Reynolds number version of the model did not perform better than the other low Reynolds number models considered.

The predictions of Reynolds shear stress are shown in Figure 6.8 (d). Away from the wall, $r/R < 0.8$, the predictions made by the different models and the experimental measurements are approximately the same. Close to the wall the predictions made using the low Reynolds number models more closely represented the experimental data, with best predictions made when the K-E 1 model was used.

6.5.5 Conclusion

This study has shown that the flow field predictions were not the same when using low and high Reynolds number turbulence models. In some instances the predictions near to the wall were improved when the low Reynolds number models were used, but were often worse than the predictions made using the high Reynolds number models in the core of the flow. In particular the predictions of turbulent viscosity were considerably worse when the low Reynolds number models were used.

Based on this study it would appear as though the extra computational expense required to use the low Reynolds number turbulence models is not of benefit. It should, however, be once again noted that this study was limited and that other researchers have shown that low Reynolds number turbulence models do provide improved predictions (Martinuzzi and Pollard, 1989).

With the computational resources currently available it is only feasible to use the low Reynolds number turbulence models in two dimensions. This approach would therefore not be appropriate when modelling more complex engineering structures where the flow is fully three dimensional, such as combined sewer overflows (CSOs), storage tanks or manholes.

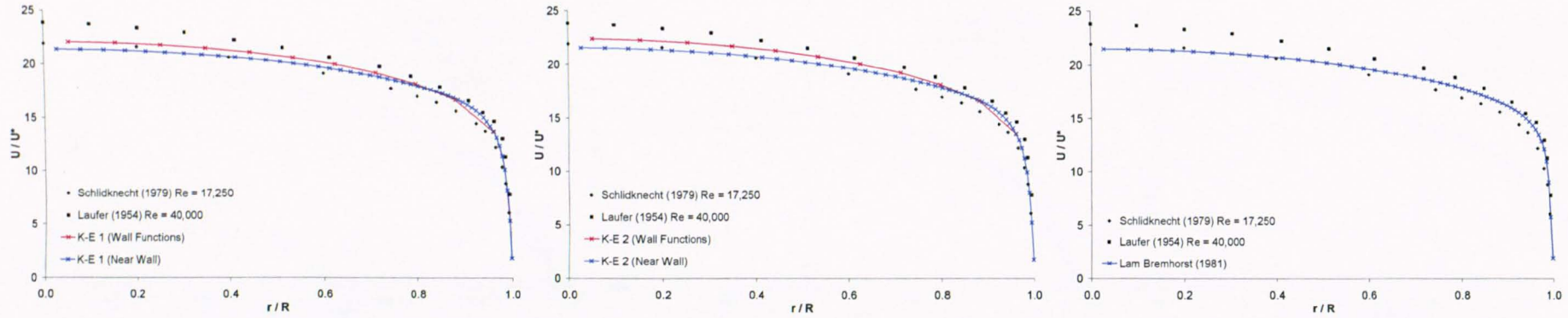

(a) Axial velocity

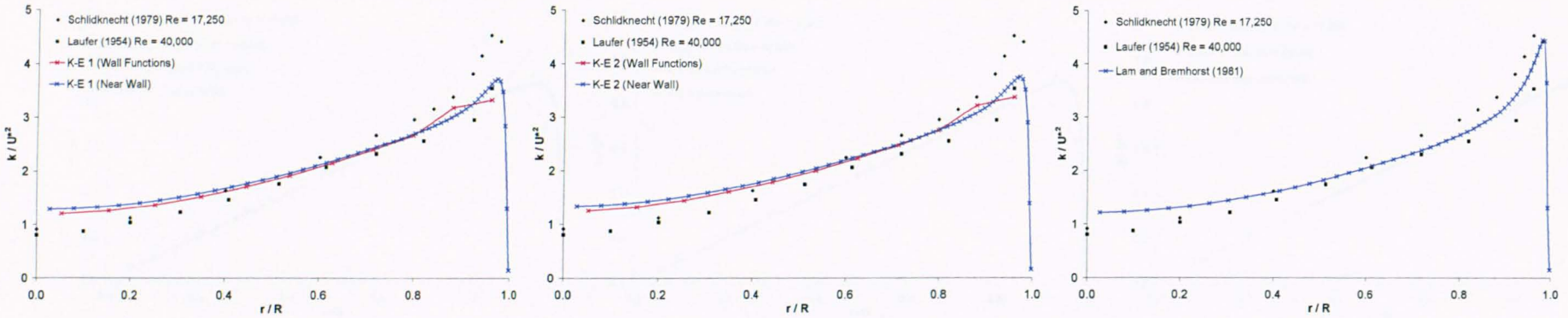

(b) Turbulent kinetic energy

Figure 6.8 Measured and predicted flow properties (continued overleaf)

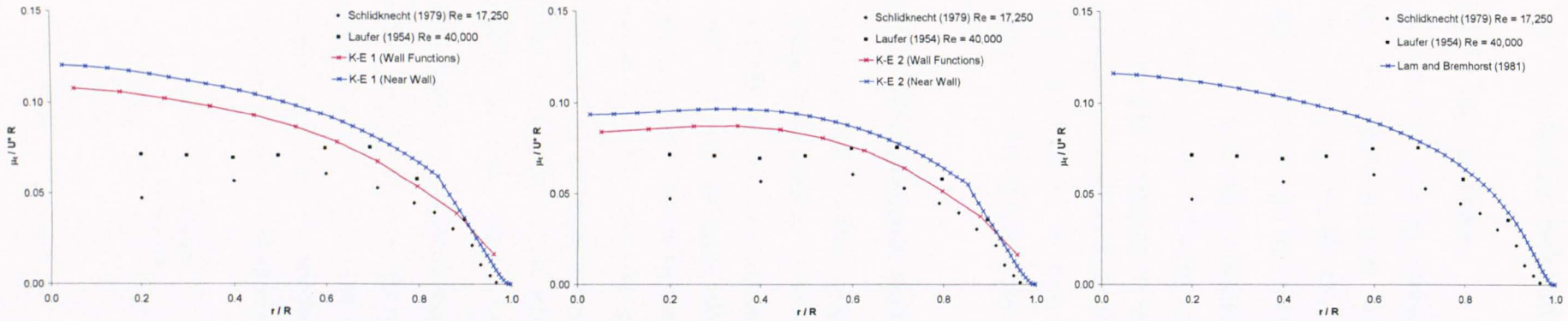

(c) Turbulent viscosity

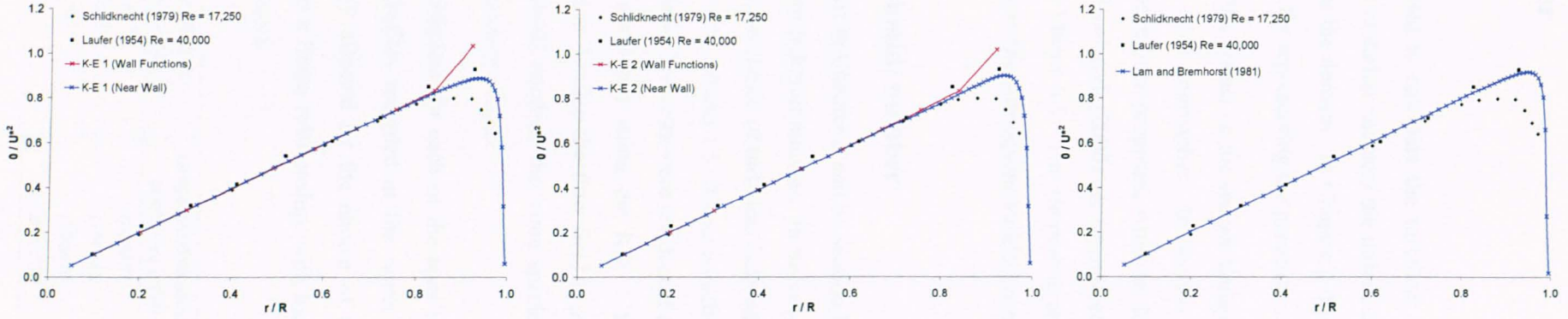

(d) Reynolds shear stress

Figure 6.8 Measured and predicted flow properties (continued from previous page)

6.6 Turbulent Schmidt number

6.6.1 Introduction

The turbulent Schmidt number, Sc_t is used to calculate the turbulent mass diffusion in the species transport equations. In the studies in earlier chapters the turbulent Schmidt number was left at the default setting of 0.7 throughout the domain. In Chapter 2 this was shown to one of many approaches that have been proposed for representing the parameter.

A series of tests were conducted to assess the impact on the species transport models predictions of solute transport of using some of the other approaches. In Section 6.6.2 consideration is given to other homogeneous values that have been proposed, while in Section 6.6.3 the spatial variations proposed by Rotta (1964) and Koeltzsch (2000) are considered. It is not possible to implement a spatial variation directly in Fluent 5.5. An alternative approach was therefore devised. A description of the approach and the subsequent validation is presented in Section 6.6.3.1

6.6.2 Homogeneous turbulent Schmidt number

The predictions of solute transport reported in Chapter 3 and in Section 6.2 were made using a homogeneous value of 0.7 for the turbulent Schmidt number. In order to assess how sensitive the predictions of solute transport were to the choice of turbulent Schmidt number three further tests were conducted using values of Sc_t = 0.5, 1.0 and 1.5. These constitute the range of values that have been proposed for this type of flow. The tests were conducted at 2 l/s and were based on the flow field that was previously developed using the K-E 1 turbulence model. A description of the modelling options used to develop the flow field is presented in Chapter 5. With the exception of the turbulent Schmidt number, the same species transport modelling options were used, these are described in Section 6.2.3.2.

The predicted longitudinal dispersion coefficient for each of the tests is shown in Table 6.2, while Figure 6.9 shows the temporal profiles recorded at the outlet from the pipe. The dispersion of the tracer was significantly affected by the choice of the turbulent Schmidt number. As would be expected there was a linear relationship, with less dispersion occurring when the turbulent Schmidt number was small.

Test No.	Turbulent Schmidt No.	Molecular diffusion coefficient (m^2/s)	Longitudinal dispersion coefficient (m^2/s)	% difference from Sch-1
Sch-1	0.7	1×10^{-10}	0.00337	-
Sch-2	0.5	1×10^{-10}	0.00245	- 27 %
Sch-3	1.0	1×10^{-10}	0.00475	+ 41 %
Sch-4	1.5	1×10^{-10}	0.00707	+ 110 %

Table 6.2 Variation in dispersion coefficient with homogeneous turbulent Schmidt number

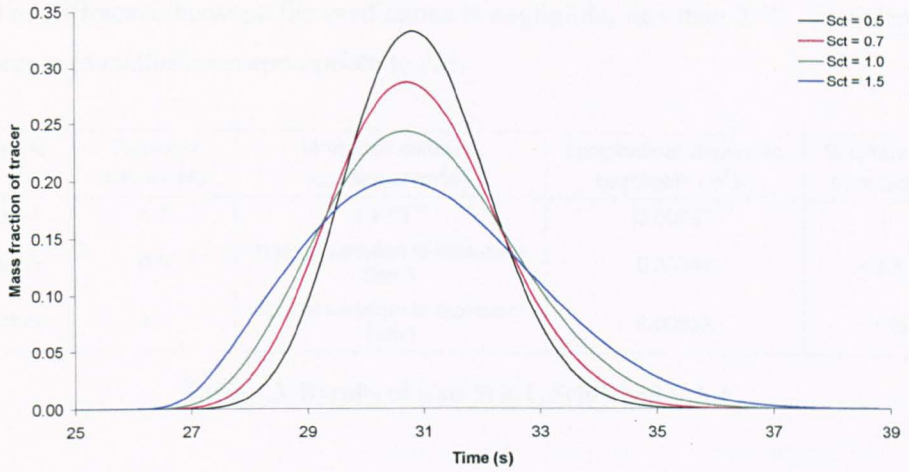

Figure 6.9 The variation in the temporal profile recorded at the outlet

6.6.3 Spatially variation in the turbulent Schmidt number

6.6.3.1 Implementing a spatial variation

By default it is only possible to define a homogenous value for the turbulent Schmidt number in Fluent 5.5. Following a personal correspondence with a member of the Fluent staff (Harwood, 2002) an approach was devised that might enable a spatial variation to be implemented. A description of the method adopted and the process of validation is presented below.

The turbulent Schmidt number and the turbulent viscosity are used to determine the turbulent mass diffusion in the species transport equation, Equation 2.35. The molecular and turbulent mass diffusion terms are then combined to give the total mass diffusion. In Fluent 5.5 it is possible to spatially vary the molecular diffusion coefficient via a user defined function (udf). It was proposed that a spatial variation in the turbulent Schmidt number could be implemented by specifying appropriate values for the spatial variation in the molecular mass diffusion term.

To confirm that the approach was appropriate two tests were performed in which the spatial variation in the molecular diffusion coefficient was defined to mimic the predictions made using a different homogeneous turbulent Schmidt number to the one specified. With the exception of the molecular diffusion coefficient and the turbulent Schmidt number the tests were conducted using the same flow field and species transport modelling options that were described in Section 6.6.2. The homogeneous turbulent Schmidt number was specified to be 0.5 and 1.0 throughout the domain. The spatial variation in the molecular diffusion coefficient was then modified to make the total mass diffusion at each cell centre equal to the total mass diffusion that would have been obtained if the turbulent Schmidt number had been specified as 0.7.

Table 6.3 compares the dispersion coefficients obtained using the above method with the predictions made using the default setting of Sch-1, which was what they were attempting to

mimic. The difference between the predictions is negligible, less than 2 %. This demonstrates that the proposed method was appropriate to use.

Test No.	Turbulent Schmidt No.	Molecular diffusion coefficient (m^2/s)	Longitudinal dispersion coefficient (m^2/s)	% difference from Sch-1
Sch-1	0.7	1×10^{-10}	0.00337	-
Sch-5	0.5	Spatial variation to represent Sch-1	0.00344	+ 2 %
Sch-6	1.0	Spatial variation to represent Sch-1	0.00332	- 1 %

Table 6.3 Results of tests Sch-1, Sch-5 and Sch-6

6.6.3.2 Test results

Two further tests were conducted to assess how the predictions of solute transport would have be affected by the use of a non homogeneous turbulent Schmidt number. The spatial variations considered were based on the proposals made by Rotta (1964) and Koeltzsch (2000). With the exception of the molecular diffusion coefficient and the turbulent Schmidt number the tests were conducted using the same flow field and species transport modelling options that were described in Section 6.6.2. These parameters were defined using the method described above.

The results of the study are shown in Table 6.4. Both of the spatial variations show a larger dispersion coefficient than the one obtained when a homogeneous value of 0.7 was used for the turbulent Schmidt number. The increase would bring the predicted dispersion coefficient very closely in line with the reanalysed Guymer and O'Brien (2000) data presented in Figure 6.5.

Test No.	Turbulent Schmidt No.	Molecular diffusion coefficient (m^2/s)	Longitudinal dispersion coefficient (m^2/s)	% difference from Sch-1
Sch-1	0.7	1×10^{-10}	0.00337	-
Sch-7	0.7	Spatial variation to represent Sc_t = Rotta (1964)	0.00414	+ 23 %
Sch-8	0.7	Spatial variation to represent Sc_t = Koeltzsch (2000)	0.00401	+ 19 %

Table 6.4 Results of tests Sch-1, Sch-7 and Sch-8

6.6.4 Conclusion

This study has demonstrated that the species transport models predictions of solute transport in a pipe are extremely sensitive to the value of the turbulent Schmidt number selected. This is unfortunate because there is not a general consensus over the form the turbulent Schmidt number should take. Depending upon the approach followed this study has shown that a closer match may be made between the predictions of solute transport and the measurements of Guymer and O'Brien (2000). However, further research would be required to categorically determine if these approaches are more appropriate to use.

Others have shown the predictions of solute transport to be less sensitive to changes in the turbulent Schmidt number when modelling flow through channels or rivers. This suggests it may be less critical to select the correct value when considering other types of large engineering structures.

6.7 Modelling the upstream conditions

6.7.1 Introduction

The final option to be considered in attempting to understand the cause of the differences between the measured and simulated dispersion coefficients was how accurately the CFD model represented the experimental test facility used by Guymer and O'Brien (2000). The pipe roughness was estimated in Chapter 2 and it was felt the value could not be improved upon by further consideration. It was also felt that the pipe diameter was modelled correctly. In the previous tests the assumption had been made that the flow was fully developed before the first measurement position. Guymer and O'Brien (2000) did not mention the upstream conditions, but more information about the test facility is presented in O'Brien (2000). Upstream of the first measurement position was a straight pipe 1.9 m or 22 D in length. Further upstream was a series of shorter pipe sections connected by 90 ° bends The assumption that the flow field was fully developed in unlikely to be correct as the distance from the first measurement position to the previous bend was less than the general accepted guidelines of at least 50 D to obtain uniform flow conditions (Massey, 1997). Three further simulations were therefore undertaken to assess the impact on the flow field (and hence the prediction of the longitudinal dispersion coefficient) of simulating part of the upstream network.

With the time available it was only possible to consider one flow rate. Due to the limitations of the available computational resources the study was conducted at 2 l/s, the lowest flow rate considered by Guymer and O'Brien (2000). Details of the flow field and species transport modelling options used in the study are presented below.

6.7.2 Modelling options

6.7.2.1 Geometry

This investigation required full 3D simulations to be undertaken. It would not have been practical to model the whole upstream network due to its size and complexity; it would also not significantly enhance the results. Focus was therefore given to the pipe sections directly upstream of the measurement positions as these will be most critical in altering the flow field. A detailed description of the upstream conditions is not presented in Guymer and O'Brien (2000) or in O'Brien (1999). An approximate description was, however, obtained through personal conversation with Saiyudthong and Osborne (2002). Details of the model geometry

used in the study are presented in Figure 6.10. As with the previous studies the diameter of the pipe was specified to be 88 mm.

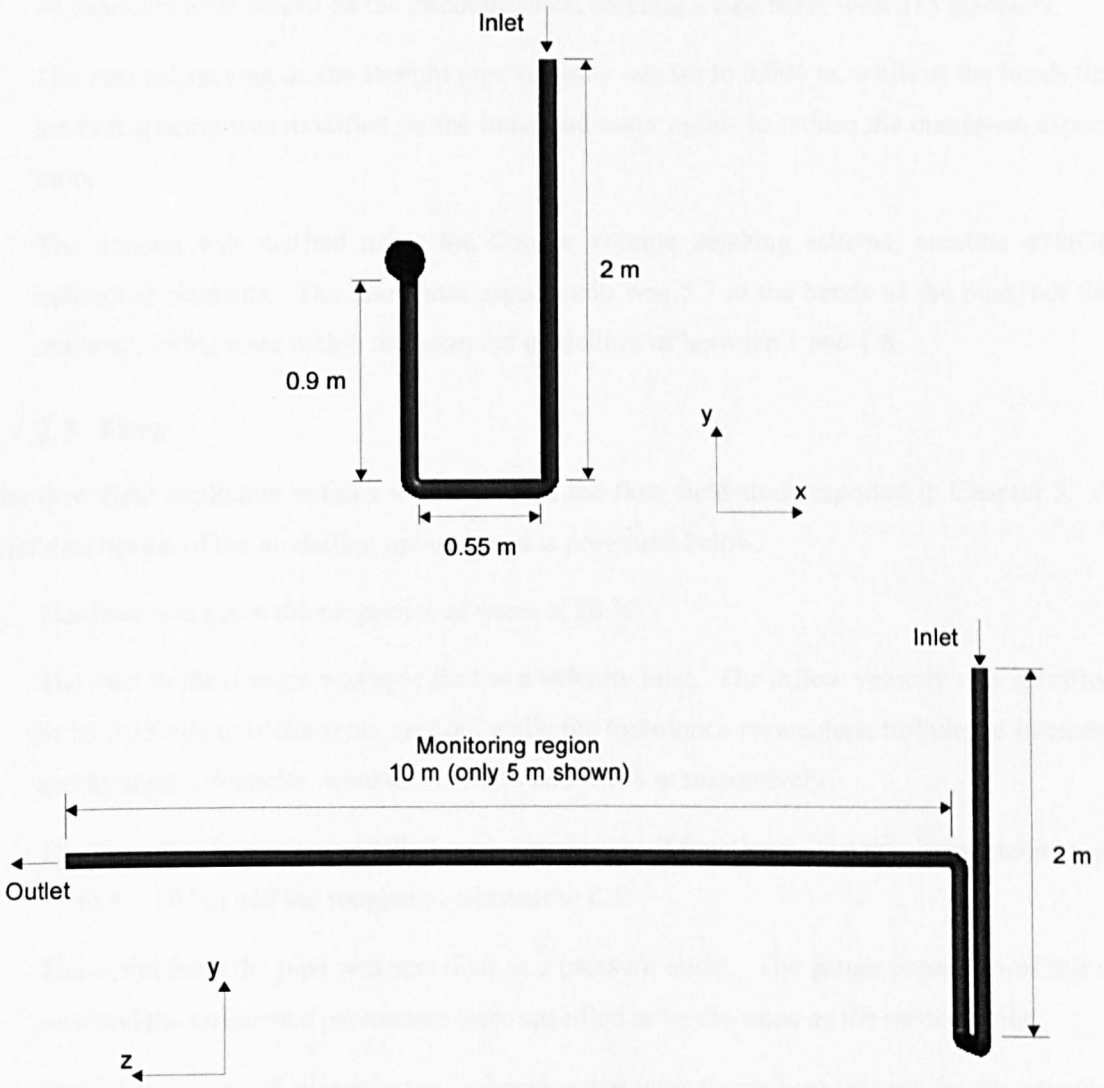

Figure 6.10 The model geometry

6.7.2.2 Mesh

The mesh was designed around the conclusions of previously reported work. In parametric test five reported in Chapter 3 the flow field and species transport predictions were the same when using the three dimensional mesh and the equivalent two dimensional mesh. The two dimensional meshes were subsequently shown to be grid independent for the fully developed flow conditions considered in Chapter 5. With the time available it was not possible to conduct a further grid refinement study for the new configuration. It was therefore decided to base the design of the new mesh configuration on the denser of the two three dimensional meshes considered, mesh number eight, as this would provide a degree of flexibility. A brief description of the modelling options used is presented below:

- The size of the boundary layer cell was fixed at 0.0035 m throughout as this produced a y^+ value of 30 in fully developed flow.
- 44 elements were placed on the circumference, creating a face mesh with 215 elements.
- The interval spacing on the straight pipe sections was set to 0.006 m, while at the bends the interval spacing was modified on the inner and outer radius to reduce the maximum aspect ratio.
- The domain was meshed using the Cooper volume meshing scheme, creating 490630 individual elements. The maximum aspect ratio was 5.7 at the bends of the pipe, but the majority, 99 %, were within the accepted guidelines of between 1 and 1.8.

6.7.2.3 Flow

The flow field modelling options were based on the flow field study reported in Chapter 5. A brief description of the modelling options used is presented below.

- The flow was given the properties of water at 20 °C.
- The inlet to the domain was specified as a velocity inlet. The inflow velocity was specified to be 0.33 m/s over the cross section, while the turbulence parameters, turbulence intensity and hydraulic diameter, were set to 4.4 % and 0.088 m respectively.
- The boundary layer was modelled using standard wall functions. The roughness height was set to 8 x 10^{-5} m and the roughness constant to 0.5.
- The outlet from the pipe was specified as a pressure outlet. The gauge pressure was left at zero and the turbulence parameters were specified to be the same as the velocity inlet.
- Second order spatial discretization schemes were used throughout, except for the pressure velocity coupling which was specified as the SIMPLE scheme.
- The same three high Reynolds number turbulence modelling configurations were considered that were used previously, namely K-E 1, K-E 2 and RSM 4.
- The simulation was not stopped until the residuals became constant.

6.7.2.4 Species transport model

In each of the tests the tracer was introduced into the pipe from the velocity inlet for 1.2 seconds. The tracer was then tracked through the domain until the concentration left in the pipe was zero. Ten monitoring positions were created at one metre intervals between z =1 m to z = 10 m, and a further position at z = 4.7 m. At each monitoring location the change in the average mass fraction of dye with time was recorded.

The simulations were performed using the uncoupled, or cold processing technique. The second order implicit scheme was used for the temporal discretization and the second order upwind scheme for the spatial discretization. The convergence criteria for the species transport equations were set to 1 $x10^{-3}$, with a maximum of 20 iterations per time step. The time step was set to 0.01 s, which was less than the value found to give time step independence.

The physical properties of the tracer were specified to be the same as the primary water phase. The molecular diffusion coefficient was specified to be 1 x 10^{-10} m^2/s and the turbulent Schmidt number was left at the default setting of 0.7 throughout the domain.

The longitudinal dispersion coefficient was calculated between each monitoring position using the temporal moment analysis reported in Chapter 3.

6.7.3 Results and discussion

Consideration was first given to assessing whether the flow properties were fully developed before the first measurement position. Five streamwise monitoring lines were created parallel to the monitoring region at the locations shown in Figure 6.11. At intervals along the line the *x*, *y* and *z* velocities were recorded.

The velocities for the flow field created using the K-E 1 turbulence modelling configuration are shown in Figure 6.12. The first measurement position in the laboratory tests was at z = 2 m. The plots suggest the flow field may not fully developed before this location, and may not have been even fully developed before the outlet, 10 m after the last bend. Similar trends are also shown for the flow fields created using the other turbulence models.

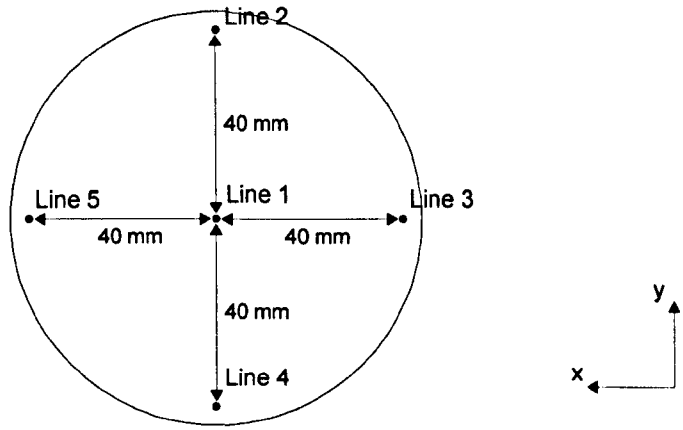

Figure 6.11 A cross section through the pipe showing the location of the monitoring lines

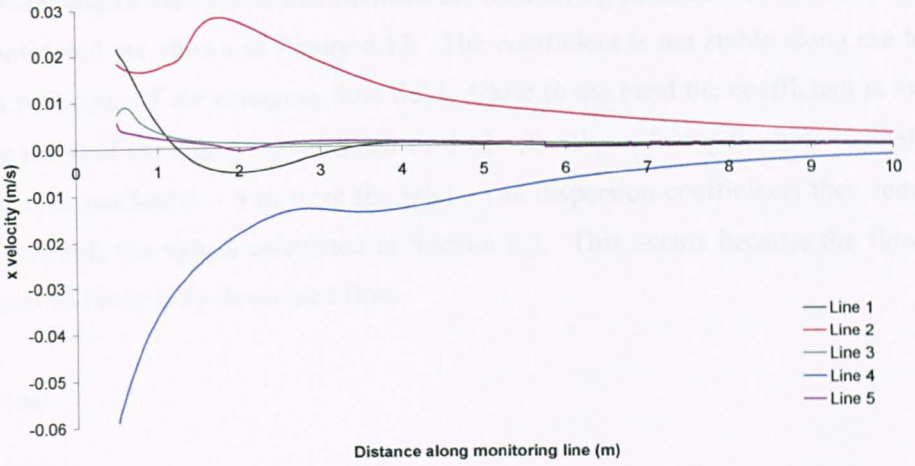

(a) x velocity

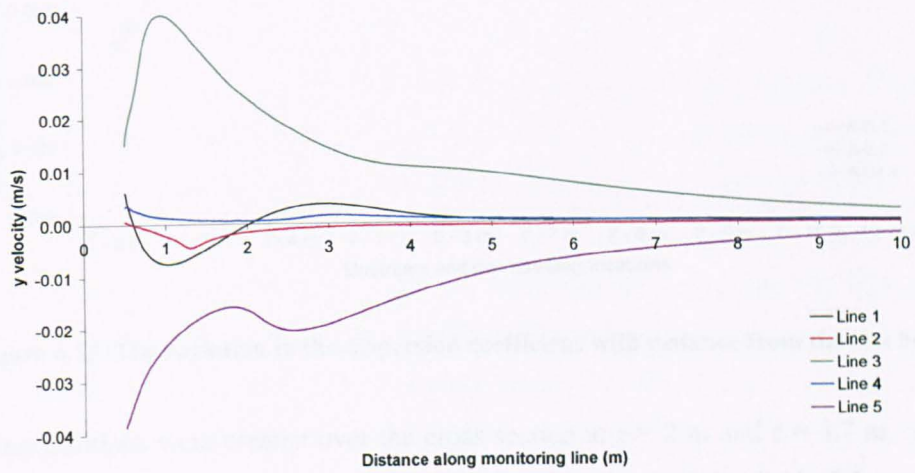

(b) y velocity

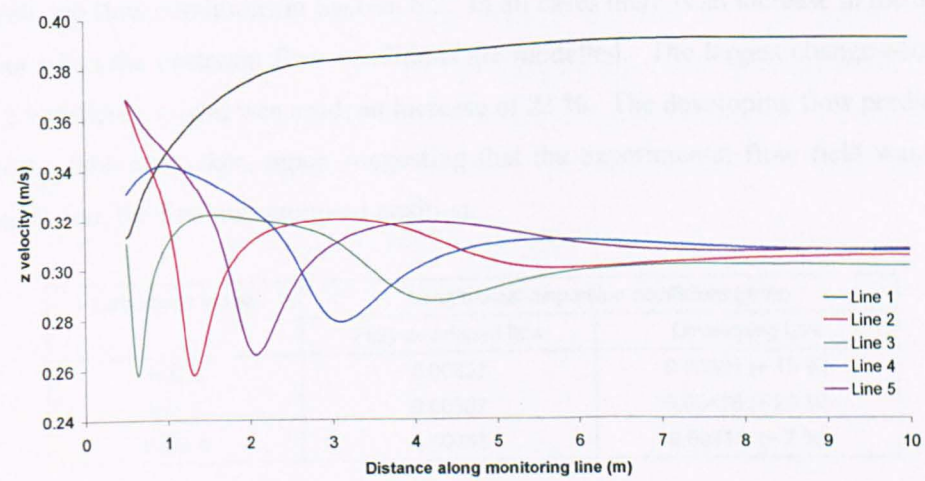

(c) z velocity

Figure 6.12 The variation in the x, y and z velocities

The dispersion coefficients calculated between the monitoring positions for the three turbulence models considered are shown in Figure 6.13. The coefficient is not stable along the length of the pipe, a reflection of the changing flow field. Close to the bend the coefficient is low. This may be the result of the high transverse and vertical velocities reducing the longitudinal mixing. A peak value is reached 3 – 4 m from the inlet. The dispersion coefficients then reduces and converges towards the values calculated in Section 6.2. This occurs because the flow field is getting closer to being fully developed flow.

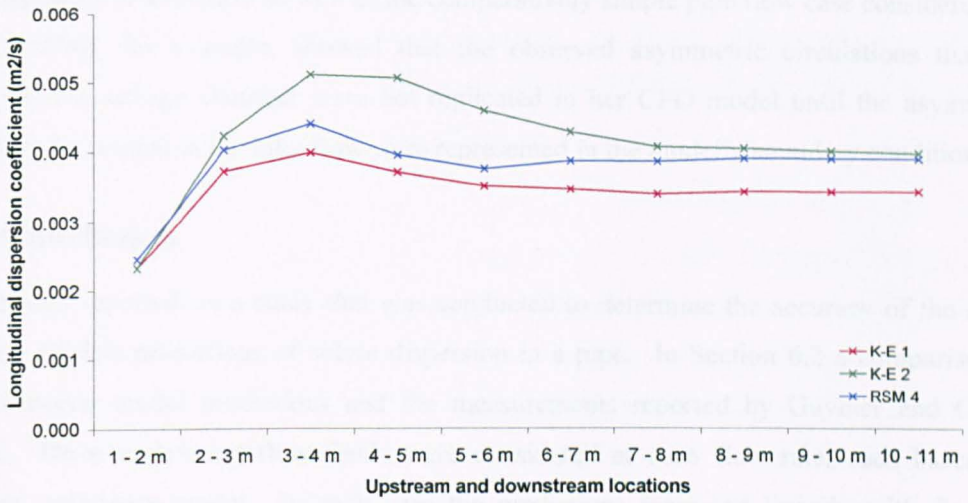

Figure 6.13 The variation in the dispersion coefficient with distance from the last bend

Monitoring positions were created over the cross section at z = 2 m and z = 4.7 m, replicating the locations used in the experiments of Guymer and O'Brien (2000). Table 6.5 compares the dispersion coefficients calculated between these locations with the coefficients calculated using fully developed flow conditions in Section 6.2. In all cases there is an increase in the dispersion coefficient when the upstream flow conditions are modelled. The largest change occurs when the K-E 2 turbulence model was used, an increase of 23 %. The developing flow predictions are closer to the laboratory data, again suggesting that the experimental flow field was not fully developed before the first measurement position.

Turbulence model	Longitudinal dispersion coefficient (m^2/s)	
	Fully developed flow	Developing flow
K-E 1	0.00337	0.00381 (+ 13 %)
K-E 2	0.00387	0.00476 (+ 23 %)
RSM 4	0.00387	0.00414 (+ 7 %)

Table 6.5 The dispersion coefficients calculated using fully developed flow conditions and the modified upstream boundary conditions

6.7.3.1 Conclusion

This study has demonstrated that the flow conditions may have not been stable by the first measurement position in the laboratory experiments, and that it would therefore be more appropriate to model the upstream conditions in future tests. However, all of the results should be viewed in the light that a full grid independence study was not conducted and that the y^+ values went beyond the recommended range of $30 < y^+ < 60$ at, and close to, the bends.

This study has highlighted sensitivities to boundary conditions that are equally valid in complex three dimensional structures as well as the comparatively simple pipe flow case considered here. Stovin (1996), for example, showed that the observed asymmetric circulations that were observed in a storage chamber were not replicated in her CFD model until the asymmetries thought to be present in the inlet flow were represented in the model's boundary conditions.

6.8 Conclusion

This chapter reported on a study that was conducted to determine the accuracy of the species transport models predictions of solute dispersion in a pipe. In Section 6.2 a comparison was made between model predictions and the measurements reported by Guymer and O'Brien (2000). Three underlying flow fields were considered at each flow rate, each based on a different turbulence model. In each case the predictions increased linearly with flow rate, demonstrating that they were robust. Although all the predictions showed the same qualitative trends as the measurements there were significant quantitative differences, with a constant under prediction when compared with the measurements.

In an attempt to understand the cause for these quantitative differences consideration was given to assessing both the accuracy of the reported values and to the appropriateness the modelling assumptions/simplifications that were made, namely the use of high Reynolds number turbulence models, a homogenous value of 0.7 for the turbulent Schmidt number and whether or not the flow was fully developed before the first measurement position. These studies were reported in Sections 6.4 to Section 6.7.

- When the measured data was reanalysed using an alternative method the dispersion coefficients obtained were not the same as those presented by Guymer and O'Brien (2000), demonstrating a sensitivity in the choice of technique. The reanalysis process also demonstrated a significant range in the coefficients obtained from the repeat tests, which was not possible to obtain from the previous method. Although the numerical predictions still under predicted the reanalysed values at 5 and 10 l/s the difference between them was less and all the predictions were within one sample standard deviation of the average value.
- A comparison was made between the flow fields predicted using the low and high Reynolds number turbulence models and the flow field measurements of Laufer (1954) and

Schildknecht *et al.* (1979). Although some improvements were shown near to the wall, the overall flow field predicted using the low Reynolds number models where not an enhancement.

- The default homogeneous value of 0.7 was used for the turbulent Schmidt number in the initial comparisons. This is just one approach that has been proposed for representing this parameter. Consideration was therefore also given to three other homogenous values, and to two spatial variations that have also been proposed. A spatially variation cannot be implemented directly into Fluent 5.5, so an alternative method was developed to do this. The predictions made of dispersion coefficient were found to be extremely sensitive to turbulent Schmidt number, and depending upon the approach chosen, the predictions were greater or less than the experimental values.
- During the initial comparison the assumption was made that the flow field was fully developed upstream of the first monitoring position. To test the appropriateness of this assumption a section upstream of the monitoring positions was simulated. This study demonstrated that the flow conditions may not have been fully developed before the first monitoring position in the laboratory experiments and that consequently the dispersion predictions were improved when the upstream conditions were correctly modelled.

Limitations in the perceived accuracy of the laboratory data set mean no absolute measure of simulation accuracy has been presented. However, the model's ability to correctly replicate the trend in dispersion coefficient as a function of discharge, and the closeness of the predicted values to the reanalysed data, both provide confidence in the use of this approach.

7 Conclusions and suggestions for further work

7.1 Introduction

The quality aspect of sewer discharges has become an important issue in recent years due to the tightening of environmental constraints. Field studies have shown that the majority of the pollutant load is transported as solutes, or as fine sediments that are in suspension. Models that predict the travel time, and in some instances the dispersion, of these pollutants are becoming increasingly used. Appropriate values need to be assigned for the different components of the urban drainage system when the dispersion is accounted for, but at present there is only limited guidance for how to do this. Laboratory and field measurements have been made, but the findings are often case specific and lack generality. It is clear that a more versatile approach would be desirable.

Previous studies have demonstrated that computational fluid dynamics (CFD) may be used to predict the transport of a solute. Most of these studies modelled the movement of a solute through relatively complex flows, with any discrepancies between the predicted and measured values being attributed to the complexity of the flow and to the simplifying assumptions that were required. The aim of this study was to determine whether CFD could be used to accurately predict the movement of a solute in a straightforward flow, specifically fully developed pipe flow.

To attain this aim, two alternative transport models were evaluated; the discrete phase model and the species transport model. In order to address the lack of validation apparent in previous studies, both the flow field and dispersion predictions were compared with published data. Detailed conclusions have already been presented at the end of each chapter. The following section therefore focuses on the key outcomes of the thesis. In Section 7.3 the modelling methodology that was developed during the study is presented, and suggestions for further work are outlined in Section 7.4.

7.2 Conclusions

- Two approaches to modelling the transport of a solute have been evaluated, namely the species transport model and the discrete phase model (also called the particle tracking model). Feasibility and parametric studies were undertaken because the guidance available

for using these models to predict the transport of a solute is limited, and in some instances, contradictory. These studies are believed to be the most comprehensive undertaken to date in the context of fully developed pipe flow.

- **Species transport model parametric study** – In this study 6 modelling options were evaluated and over 100 separate tests conducted. The predictions were found to be sensitive to the choice of the spatial and temporal discretization scheme, and to the size of the time step. However, the options that resulted in robust predictions for both the mean travel time and dispersion were identified.
- **Discrete phase model parametric study** – In this study 7 modelling options were considered during 35 tests. It was shown that the model was computationally efficient and that consistent predictions were attainable. However, the prediction of the mean travel time was inaccurate. For this reason the discrete phase model was eliminated from subsequent investigations.

- The data set of Guymer and O'Brien (2000) was identified as appropriate for validation of the species transport model's dispersion predictions. The data set contains detailed measurements of solute dispersion through a 0.088 m diameter straight pipe over a range of discharges between 2.1 and 10.3 l/s. The first part of the validation study focused on the flow field, as it was essential to demonstrate that this was accurate prior to the assessment of the species transport model.

Flow field parametric studies and validation

- The most appropriate modelling options were identified in order to represent the experimental flow conditions. This was achieved through a consideration of the system being modelled, a grid refinement study, and two parametric studies that evaluated the impact of the discretization schemes and turbulence models on the flow field.
- The Guymer and O'Brien data set was restricted to dispersion observations, with the information on the underlying flow field being too limited to facilitate validation. For this reason, three further data sets (Laufer, (1954); Lawn, (1971); Schildknecht *et al.*, (1979)) were identified for comparison with the simulation results. Comparisons were made with the measurements of axial velocity, turbulent kinetic energy, turbulent dissipation rate, Reynolds shear stress, turbulent viscosity and where appropriate the axial, radial and tangential fluctuating velocity components.
- Ten high Reynolds number turbulence model configurations were evaluated at 2 l/s, and three of the models at 5 and 10 l/s. This set of comparative simulation data is believed to be unique in the context of pipe flow modelling.

- With the exception of the turbulent viscosity, the simulated flow fields showed the same qualitative and quantitative trends as the measurements. However, the incorrect prediction of turbulent viscosity was judged to be a significant concern because the turbulent viscosity is used to calculate the turbulent mass diffusion in the species transport model. The comparisons also revealed that no one specific turbulence model was clearly superior to the others.

Validation of the species transport model's dispersion predictions

- The species transport model was utilised to predict the transport of a solute at three flowrates (2, 5 and 10 l/s). At each flow rate three different flow fields were considered, each relating to a different turbulence modelling configuration.
- The predicted variation in longitudinal dispersion coefficient with discharge showed the same linear trend as the theoretical equation proposed by Taylor (1954). However, the simulated data consistently under predicted the measured (Guymer and O'Brien) values.
- The work presented in Hrenya *et al.* (1998) suggested that the difference was not solely caused by the incorrect prediction of turbulent viscosity. Consideration was therefore given to assessing both the accuracy of the laboratory data and the appropriateness of the modelling assumptions/simplifications that were made.
    - Reanalysis of the measured data revealed that the value of dispersion coefficient obtained was sensitive to the choice of analysis technique.
    - Tests conducted using low Reynolds number turbulence models revealed that, although the near wall flow field was in some instances improved, the overall flow field predictions were not better.
    - The predictions were found to be extremely sensitive to the turbulent Schmidt number.
    - The assumption of fully developed flow in the laboratory experiments was questioned when the results of simulations incorporating a section of the upstream pipe network were evaluated.

    The reanalysis of the laboratory data, and modelling refinements highlighted above tended to align the simulation results more closely with the experimental data and justifies the use and further development of the approach.

Summary

- During the thesis it has been demonstrated that CFD may be used to accurately represent the conditions of fully developed turbulent flow in a straight pipe. It has also been demonstrated that CFD may be used to produce robust predictions of solute transport under these flow conditions. This is believed to be a unique contribution.
- The general methodology that was developed during this study is presented in Section 7.3. Highlighted below are some of the practical engineering applications to which the methodology may be applied. Suggestions for how it could be extended to other urban drainage structures are presented in Section 7.4.
    - To predict the transport of contaminants through the drinking water supply chain or sewer system.
    - To quantify the quality impacts of intermittent discharges to the sewer system, such as effluents discharged from the food industry.
    - To determine the residence time of pollutants in a variety of contexts.
    - To predict the mixing effects in tidal sewer systems.

7.3 Simulation methodology

The main practical engineering outcome from this research is a recommended methodology for which to model the transport of a solute through a pipe using CFD. The methodology is presented in the form of a flow chart in Figure 7.1. The modelling options that were found to give robust predictions are highlighted in Section 3.4 and Section 5.7.

The methodology presented in Figure 7.1 is applicable not only to a pipe flow but to flow through all types of engineering structures. The flow field and species transport modelling options that were found to be appropriate for pipe flow are, however, not universal and will require case-by-case adjustment. There is limited guidance on how to identify modelling options in a specific context, and many of the published studies have failed to explicitly document the options that were employed. Nevertheless the need to ensure grid and time step independent solutions and the need to correctly model significant flow features (e.g the upstream conditions) are relevant in all studies.

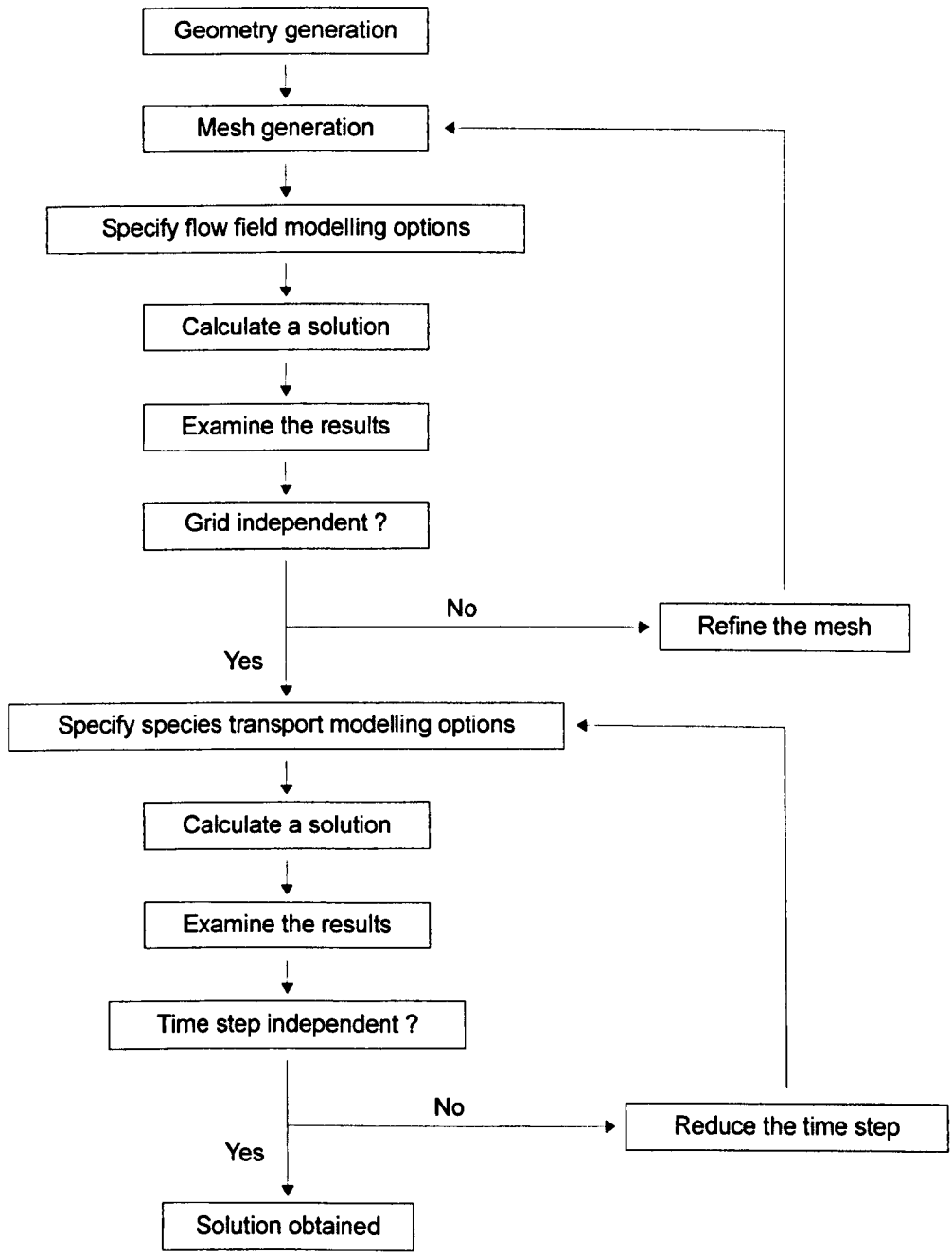

Figure 7.1 Proposed simulation methodology

7.4 Suggestions for further work

It is the author's opinion that there are two key directions for future work. The first would be to refine the current study and the second would be to apply the methodology that has been developed to other urban drainage structures. A number of topics that could be considered for further investigation are outlined below.

7.4.1 Extension of the current study

- It is not possible to determine the accuracy of the predictions of solute dispersion in a pipe with the data that is currently available. New data sets should therefore be collected in which details of the full experimental configuration are presented along with detailed measurements of key flow properties. This study also highlighted differences in the approaches used to analyse measured data. The most appropriate technique should therefore be identified and utilised.
- During the feasibility study the mean travel time of the tracer was shown to be incorrect when using the discrete phase model. This approach is, however, more computationally efficient than the species transport model and would therefore be of benefit when considering larger structures. Future work should determine why this error occurred and provide a solution.
- At this time it is not possible to identify the most appropriate value for the turbulent Schmidt number. This is of importance because it is used in the species transport model to calculate the turbulent mass diffusion. Future work should therefore be conducted to determine the spatial variation in this parameter over the boundary layer.
- The study demonstrated that, with the exception of the turbulent viscosity, the flow field predictions were reasonably accurate. Future studies should therefore try to improve the predictions of turbulent viscosity, perhaps by altering the constants used in the turbulence models or by using low Reynolds number models. This, however, may be a limitation inherent within all CFD code. It is felt that when modelling large urban drainage structures the importance of the near wall modelling and the turbulent Schmidt number may be less.

7.4.2 Application of the methodology to urban drainage structures

- This study has developed a robust methodology with which to predict the flow field and transport of solutes or fine particles though a pipe. It is proposed that a similar approach will be valid for modelling dispersion in other types of urban drainage structures. The formulation of a simulation methodology is of interest because there is only limited advice available at the current time. This aim could be achieved by using the work reported in this

thesis as a basis and progressively increasing the level of modelling complexity. Presented below is a progression of flow types and relevant urban drainage structures that the author feels it would be appropriate to use

- Flows with a free surface (e.g. partially filled pipes or channels)
- Flows in which the cross sectional area changes (e.g. storage tanks or manholes)
- Flows with multiple inlets/outlets (e.g. CSOs)

- When extending the study to consider other urban drainage structures, detailed flow field and solute transport measurements would be required. In some instances comprehensive measurements are available, such as solute transport through a manhole (O'Brien, (1999); Dennis, (2000); Saiyudthong, (in press)) whilst in others new measurements will be required.
- To date the work has been restricted to simulations in which the discharge was constant, yet the importance of transient flows in the sewerage system is well known. It would therefore be of interest to explore the impact of time varying flows, particularly in respect to optimising the design of CSOs.

7.4.3 Other points of interest

- Further work could explore the use of the dispersion coefficient as a means of validating the numerical flow field. This would be of particular benefit when no other measurements are available for validation.
- This study has highlighted the types of issues that will be relevant in any type of CFD modelling (e.g. grid independence and choice of turbulence model). The way in which the parametric studies were conducted could be used as a template for future work aimed at applying CFD in similar contexts (e.g. in sewer chemical transformations or sediment transport prediction).

REFERENCES

Abbot, M.B. and Basco, D.R., (1989). *Computational fluid dynamics – An introduction for engineers*, Longman Scientific & Technical, Harlow, UK.

Ackers, J.C., Butler, D. and May, R.W.P., (1996). *Design of sewers to control sediment Problems*, CIRIA Report 141, CIRIA, London, UK.

Adamsson, Å., Stovin, V. and Bergdahl, L., (in press). *A bed shear stress boundary condition for storage tank sedimentation,* accepted for publication in ASCE Environmental Engin. Expected July 2003.

Anderson, J.D., (1995). *Computational fluid dynamics - The basics with applications*, McGraw-Hill, USA.

Andoh, R.Y.G., (1994). *Urban runoff: Nature, characteristics and control*, J. Inst. Wat. Env. Man., Vol. 8, No. 4, 371-378.

Ashley, R.M. and Crabtree, R.W., (1992). *Sediment origins, deposition and build up in combined sewer systems*, Wat. Sci. Tech., Vol. 25, No. 8, 1-12.

Asztely, M. and Lyngfelt, S., (1996). *Three dimensional modelling of energy losses in a manhole*, Proc. 7th Int. Conf. on Urban Storm Drainage, Hanover, Germany, 647-652.

Baker, R.J. and Launder, B.E., (1974). *The turbulent boundary layer with foreign gas injection –1. Measurements in zero pressure gradients*, Int. J. Heat Mass Trans., Vol 17, 275-295.

Blom, J., (1970). *Experimental determination of the turbulent boundary layer*, Proc. Fourth Int. Heat Mass Transfer Conf., Vol 2, Elsevier, Amsterdam, Paper FC 2.2.

Boxall, J.B., Guymer, I., Shepherd, W.J. and Fox, K., (2002). *Changes in water quality parameters due to in-sewer processes*, IWA 3rd World Water Congress, Melborne, Australia.

Butler, D., May, R.W.P. and Ackers, J.C., (1996). *Sediment transport in sewers Part 1: Background*, Proc. Inst. Civ. Engrs., Wat. Marit. & Energy, Vol. 118, No. 2, 103-112.

Buxton, A.P., (in press). *The development of a computational methodology for the prediction of the sediment retention performance of invert traps in combined sewer systems*, PhD thesis, The University of Sheffield. Expected 2003.

Calabrese, R.V. and Middleman, S., (1979). *The dispersion of discrete particles in a turbulent fluid field*, AIChe J., Vol. 25, No. 6, 1025-1035.

Christodoulou, G.C., Ioakeim, I. and Ioannou, K., (1995). *Modeling of pollution from the wastewater discharge of the city of Limassol*, Wat. Sci. Tech., Vol. 32, No. 9-10, 197-204.

Crabtree, R. W., (1989). *Sediments in sewers*, J. Inst. Wat. Env. Man., Vol. 3, No., 6, 569-578.

Danish Hydraulic Institute (DHI), (1994). MOUSETRAP User Manual, version 1.00.

Datta, R., (1993). *Eddy viscosity and velocity distribution in turbulent pipe flow*, AIChe J., Vol. 39, No. 7, 1107-1112.

Dennis, P.M., Guymer, I. and Antonopoulos, C., (1999). *Optimisation of the aggregated dead zone model for solute dispersion in surcharged manholes*, 8th Int. Conf. on Urban Storm Drainage, Institution of Engineers, Australia.

Dennis, P., (2000). *Longitudinal dispersion due to surcharged manholes*, PhD thesis, University of Sheffield, Sheffield, UK.

Domgin, J.F., Huilier, D., Burnage, H. and Gardin, P., (1997). *Coupling of a Lagrangian model with a CFD code: Application to the numerical modelling of the turbulent dispersion of droplets in a turbulent pipe flow*, J. Hydraul. Res., Vol. 35, No. 4, 473-490.

Durst, F., Jovanovic, J. and Sender, J., (1995). *LDA measurements in the near-wall region of a turbulent pipe flow*, J. Fluid. Mech., Vol. 295, 305-335.

Eggels, J.G.M., (1994). *Direct and large eddy simulation of turbulent flow in a cylindrical pipe geometry*, PhD thesis, Delft University Press, Delft, Netherlands.

Eggels, J.G.M., Unger, F., Weiss, M.H., Westerweel, J., Adrian, R.J., Friedrich, R. and Nieuwstadt, F.T.M., (1994). *Fully developed turbulent pipe flow: a comparison between direct numerical simulation and experiment*, J. Fluid Mech., Vol. 268, 175-209.

Fischer, H.B., List, E.J., Koh, R.C.Y., Imberger, J. and Brooks, N.H., (1979). *Mixing in Inland and Coastal Waters*, Academic Press, New York.

Fluent, (1998). *Fluent 5 User's Guide*, Fluent Europe, Sheffield, UK.

FWR, (1998). *Urban pollution management manual*, 2nd Edition, Marlow, Buckinghamshire: FWR, FR/CL 0009.

Gambit, (1998). *Modelling Guide*, Fluent Europe, Sheffield, UK.

Geropp, D. and Odenthal, H.J., (2001). *Flow rate measurements in turbulent pipe flows with minimal loss of pressure using a defect-law*, Flow Meas. Instrum., Vol. 12, No. 1, 1-7.

Gersten, K. and Herwig, H., (1992). *Stromungsmechanik*, Vieweg-Verlag.

Gibson, M.M. and Launder, B.E., (1978). *Ground effects on pressure fluctuations in the atmospheric boundary layer*, J. Fluid Mech., Vol. 86, 491-511.

Glekas, I.P., (1995). *Application of a three dimensional model for the prediction of pollutant dispersion in Cyprus coastal waters*, Wat. Sci. Tech., Vol 32, No.'s 9-10, 179-187.

Guymer, I. and O'Brien, R., (2000). *Longitudinal dispersion due to surcharged manhole*, ASCE J. Hydraul. Eng., Vol. 126, No. 2, 137-149.

Guymer, I., (2003). Personal conversation.

Hancu, S., Ghinda, T., Ma, L., Lesnic, D. and Ingham, D.B., (2002). *Numerical modelling and experimental investigation of the fluid flow and contaminant dispersion in a channel*, Int. J. Heat Mass. Trans., Vol. 45, No. 13, 2707-2718.

Harwood, R., (1999). *Modelling combined sewer overflow chambers using computational fluid dynamics*, PhD thesis, University of Sheffield, Sheffield, UK.

Harwood, R., (2002). Personal correspondence.

Herath, S.K., Jayasuriya, L.N.N. and Hussey, C.J., (1999). *Modelling wastewater quality in sewerage systems*, Proceedings of the 8th International conference on urban storm drainage, Sydney, Australia, Australia: The institution of engineers, 179-186.

Hinze, J.O., (1975). *Turbulence – Second Edition*, McGraw-Hill, USA.

Hrenya, C.M., Bolio, E.J., Chakrabarti, D. and Sinclair, J. L., (1995). *Comparison of low Reynolds number k-ε turbulence models in predicting fully developed pipe flow*, Chem. Eng. Sci., Vol. 12, No. 12, 1923-1941.

Hrenya, C., Miller, S., Mallo, T. and Sinclair, J., (1998). *Comparison of low Reynolds number k-ε turbulence models in predicting heat transfer rates for pipe flow*, Int. J. Heat Mass Trans., Vol. 41, No. 11, 1543-1547.

Kim, S.E. and Choudhury, D., (1995). *A near wall treatment using wall functions sensitised to pressure gradient*, FED, Vol., 217, Separated and complex flows, ASME, 273-280.

Koeltzsch, K., (2000). *The height dependence of the turbulent Schmidt number within the boundary layer*, Atmos. Environ., Vol. 34, No. 7, 1147-1151.

Lam, C.K.G. and Bremhorst, K.A., (1981). *Modified form of the k-ε Model for Predicting Wall Turbulence*, ASME, J. Fluids Eng., Vol 103, No. 3, 456-460.

Laufer, J., (1954). *The Structure of Turbulence in Fully Developed Pipe Flow*, NACA Report 1174, National Bureau of Standards, Washington DC, USA.

Launder, B.E. and Spalding, D.B., (1972). *Lectures in mathematical models of turbulence*, London Academic Press, UK.

Launder, B.E. and Spalding, D.B., (1974). *The Numerical Computation of Turbulent Flows*, Comput. Methods Appl. Mech. Eng., Vol. 3, 269-289.

Launder, B.E. and Sharma, B.I., (1974). *Application of the energy-dissipation model of turbulence to the calculation of flow near a spinning disc*, Lett, Heat and Mass Trans., Vol. 1, 131-138.

Launder, B.E., Reece, G.J. and Rodi, W., (1975). *Progress in the Development of a Reynolds Stress Turbulence Closure*, J. Fluid. Mech., Vol. 68, Pt 3, 537-566.

Launder, B.E., (1976). *Heat and mass transport.* In: Bradshaw, P., Topics in applied physics, Vol. 12, Turbulence, Springer, Berlin, Germany.

Lawn, C.J., (1971). *The determination of the rate of dissipation in turbulent pipe flow*, J. Fluid Mech., Vol. 48, 477-505.

Massey, B.J. (1997). *Mechanics of Fluids,* Chapman & Hill, London, UK.

Martinuzzi, R. and Pollard, A., (1989). *Comparative study of turbulence models in predicting turbulent pipe flow.* Part 1: Algebraic stress and k-ε models, AIAA J, Vol. 27, No. 1, 29-36.

Myong, H.K. and Kasagi, N., (1990). *A new approach to the improvement of kappa-epsilon turbulence model for wall bounded shear flows*, JSME Int. J., Vol. 33, 63-72.

Nikuradse, J., (1932). *Gesetzmassigkeiten der turbulenten Stromung in glatten Rohren*, Verein deutscher Ingenieure, Forschungsheft No. 356, Berlin, Germany.

O'Brien, R., (1999). *Dispersion due to surcharged manholes*, PhD thesis, University of Sheffield, Sheffield, UK.

Patankar, S.V. and Spalding, D.B., (1972). *A calculation procedure for heat, mass and momentum transfer in three dimensional parabolic flows*, Int. J. Heat Mass Trans., Vol. 15, 1787-1806.

Patel, V.C. and Head, M.R., (1969). *Some observations on skin friction and velocity profiles in fully developed pipe and channel flow*, J. Fluid Mech., Vol. 38, 181-201.

Perry, A.E. and Abell, C.J., (1975). *Scaling laws for pipe flow turbulence*, J. Fluid Mech., Vol. 67, 257-271.

Pollard, A. and Martinuzzi, R., (1989). *Comparative study of turbulence models in predicting turbulent pipe flow*. Part 2: Reynolds stress and k-ε models, AIAA J, Vol. 27, No. 12, 1714-1721.

Quarmby, A. and Quirk, R., (1972). *Axisymmetric and non-axisymmetric turbulent diffusion in a plain circular tube at high number*, Int. J. Heat. Mass Trans., Vol. 15, 2309-2327.

Reynolds, A. J., (1975). *The prediction of turbulent Prandtl and Schmidt numbers*, Int. J. Heat Mass Trans., Vol. 18, 1055-1069.

Rodi, W., (1993). *Turbulence models and their application in hydraulics – A state of the art review*, Third edition, IAHR, Rotterdam, Netherlands.

Rotta, J. C., (1964). *Temperaturverteilungen in der turbulenten Grenzschicht an der ebenen Platte*, Int. J. Heat Mass Trans., Vol. 7, 215-228.

Rutherford, J. C., (1994). *River Mixing*, John Wiley and Sons, UK.

Saiyudthong, C. and Osborne, P., (2002). Personal conversation.

Saiyudthong, C., (in press). *Effects of changes in pipe direction across manholes on dispersion*, PhD thesis, The University of Sheffield, UK. (Expected 2003).

Salter, H.E., Ta, C.T. and Williams, S.C., (2000). *Three-dimensional computational fluid dynamic modelling of a facultative lagoon*, Wat. Sci. Tech., Vol. 42, No. 10-11, 335-342.

Sayre, W.W., (1968). *Dispersion of mass in open channel flow*, PhD thesis, Colorado State Unversity, USA.

Schildknecht, M., Miller, J. A. and Meier, G.E.A., (1979). *The influence of suction of the structure of turbulence in fully developed pipe flow*, J. Fluid Mech., Vol. 90, 67-107.

Schlichting, H., (1968). *Boundary layer theory, 6th Edition*, McGraw-Hill. New York, USA.

Schlichting, H., (1997). *Grenzschicht theorie*, Vol. 9, Springer, Berlin, Germany.

Shaw, C.T., (1992). *Using computational fluid dynamics*, Prentice Hall International Ltd, UK.

Shih, T.H., Liou, W.W., Shabbir, A. and Zhu, J., (1995). *A new k-ε eddy viscosity model for high Reynolds number turbulent flows – model development and validation*, Comp. Fluids, Vol. 24, No. 3, 227-238.

Shilton, A., (2000). *Potential application of computational fluid dynamics to pond design*, Wat. Sci. Tech., Vol. 42, No. 10-11, 327-334.

Speziale, C.G., (1991). *Analytical methods for the development of Reynolds stress closures in turbulence*, Annu. Rev. Fluid Mech., Vol. 23, 107-157.

Stovin, V.R., (1996). The prediction of sediment deposition in storage chambers based on laboratory observations and numerical simulation, PhD thesis, The University of Sheffield, UK.

Stovin, V.R. and Saul, A.J., (1996). *Efficiency prediction for storage chambers using computational fluid dynamics*, Wat. Sci. Tech., Vol. 33, No. 9, 163-170.

Stovin, V.R. and Saul, A.J., (1998). *A computational fluid dynamics (CFD) particle tracking approach to efficiency prediction*, Wat. Sci. Tech., Vol. 37, No. 1, 285-293.

Stovin, V.R., Saul, A.J., Drinkwater, A. and Clifforde, I., (1999). *Field testing CFD-based predictions of storage chamber gross solids separation efficiency*, Wat. Sci. Tech., Vol. 39, No. 9, 161-168.

Ta, C.T. and Brignal, W.J., (1998). *Application of computational fluid dynamics technique to storage reservoir studies*, Wat. Sci. Tech., Vol. 37, No. 2, 219-226.

Tannehill, J.C., Anderson, D.A. and Pletcher, R.H., (1997). *Computational fluid mechanics and heat transfer – second edition*, Taylor & Francis Ltd, UK.

Taylor, G.L., (1921). *Diffusion by continuous movement*, Proc. London math Soc., Ser. A., No. 1, Vol. 20, 196-211.

Taylor, G.I., (1953). *Dispersion of soluble matter in solvent flowing slowly through a tube*, Proc. R. Soc., Series A, Vol. 219, 186-203.

Taylor, G.I., (1954). *The dispersion of matter in turbulent flow through a pipe*, Proc. R. Soc., Series A, Vol. 223, pp 446-468.

Tennekes, H. and Lumley, J.L., (1990). *A first course in turbulence*, MIT Press, London, UK.

Thakre, S.S. and Joshi, J.B., (2001). *A low Reynolds number k-epsilon modelling of turbulent pipe flow: Flow pattern and energy balance*, Can. J. Chem. Eng., Vol. 79, No. 2, 214-226.

Turner Designs, (1981). *Operating and service manual: model 10 series fluorometers*, Turner Designs, 845 W, Maude Avenue, Sunnyvale, California, 94086.

Tyack, J.N. and Fenner, R.A., (1999). Computational fluid dynamics modelling of velocity profiles within a hydrodynamic separator, Wat. Sci. Tech., Vol. 39, No. 9, 169-176.

Yakhot, V. and Orszag, S.A., (1986). *Renormalization group analysis of turbulence: Basic theory*, Journal of scientific computing, Vol. 1, No. 1, 1-51.

Verbanck, M.A., Ashley, R.M. and Bachoc, A., (1994). *International worksop on the origin, occurance and behaviour of sediments in sewer systems: Summary of conclusions*, Wat. Res., Vol. 28, No. 1, 187-194.

Versteeg, H.K. and Malalasekera, W., (1999). *An introduction to computational fluid Dynamics - The finite volume method*, Longman, UK.

Wallingford Software, (2001). HydroWorks v7.0 on-line help file.

Weiss, M. H., (1993). *Drag reduction with riblets in pipe flow*, PhD thesis, University of Calgary, Canada.

Westerweel, J., (1993). *Digital particle image velocimetry: theory and application*, PhD thesis, Delft University of Technology, Netherlands.

White, F.M., (1991). *Viscous fluid flow – Second Edition*, McGraw-Hill Inc, New York, USA.

Wood, M.G., Howes, T., Keller, J. and Johns, M.R., (1998). *Two dimensional computational fluid dynamic models for waste stabilisation ponds*, Water Res., Vol. 32, No. 3, 958-963.